The University Of Sheffield.

Department of Civil and Structural Engineering

# Transient Mobilisation of Pipe-Wall Adhered Material in Drinking Water Distribution Systems

A Thesis Submitted for the
Degree of Doctor of Philosophy

2019

Supervised by Prof. Joby Boxall and Dr. Richard Collins

**Sally L Weston**

# Executive Summary

Discolouration, an aesthetic indicator of drinking water quality, affects approximately 6.7 million customers annually in the UK and is perceived to mask other water quality failures. Existing management techniques cannot explain all of these discolouration failures. Therefore, understanding the processes and forces that lead to discolouration is crucial. Material associated with discolouration is mobilised from the pipe wall when its adherence strength is exceeded by imposed hydraulic forces. Transient events generate significant dynamic forces, yet, there is currently little conclusive evidence exploring their influence on mobilisation of material.

This study aims to determine, for the first time, if transient forces can mobilise of material adhered to the pipe-wall, which cannot be mobilised by steady state flows at the same initial or final conditions. An innovative, rigorous laboratory experiment was designed to test this aim. Replicated adhered material was created using magnetic particles inside the pipe and an electromagnet external to the pipe, so that controlled current through the electromagnet quantified adherence force experienced by the magnetic particles. Hydraulic steady state and transient tests, for a range of flow rate and pressure conditions, were conducted to determine the current at which mobilisation occurred.

A key contribution of this research was the confirmation that valve closing and valve opening transients cause mobilisation of adhered material, where steady state cannot. This is substantial finding, particularly for valve closing transients as the steady state force reduces during the valve movement. Mobilisation must be due to the dynamic forces generated by the transient. An observationally driven analysis led to development of a function to capture the magnitude of the hydraulic force generated during transients. The one dimensional function was termed the 'Peak Dynamic Force' and begins to quantify transient induced forces that lead to mobilisation of pipe-wall adhered material.

The work presented within this thesis is unique in that it consistently isolated transient forces and quantified their mobilisation ability. This dynamic ability has theoretical and practical implications, and could ultimately lead to the development of effective management strategies for improving drinking water quality.

# Acknowledgements

This project was supported by the Research Councils UK (RCUK) and administered by the Department of Civil and Structural Engineering at the University of Sheffield. The laboratory used in these experiments was funded by the UK Engineering and Physical Sciences Research Council via Responsive mode Grant 'Contaminant Intrusion into Distribution Systems (CID)' EP/G015546/1 and Platform Grant EP/1029346/1.

First and foremost, I would like to thank my supervisors Prof Joby Boxall and Dr Rich Collins for their patience and direction over the last few years. Their academic and personal guidance has been vital, and I would like to particularly thank them for the challenge, laughter and encouragement throughout this process. Congratulations to Joby for getting better at keeping track of openings or closings. Similarly, I would like to thank members of the D106 and D105 offices for the chatter and help navigating PhD student life. A special appreciation is given to Dr Will Shepherd; I'm very grateful for your help and friendship, especially with the pipe in a pipe project. My grateful thanks are extended to the technical and support staff of Civil Engineering, particularly Paul Osbourne, Alex Cargill and Dave Callaghan for their continued help in the lab. I would like to take this opportunity to thank everyone for their support whilst I have been ill. It's not been a simple journey, but working in an environment where others go out of their way to help me function makes things easier.

I would not be where I am today with the help of my family (Joneses and Westons) and friends. I would like to extend my appreciation to Lizzie, Becky, Alex and Monday hoopers for the fun distractions and unconditional belief. Finally, special thanks have to be given to Kat and Nick. You've been an amazing team guiding me through everything PhD related, and you always encourage me to pursue my interests, but perhaps at a more realistic speed.

To my grandparents Brenda and John Neal,
who know less about hydraulics than railway engines.

To my husband Nick,
who knows me more than anyone.

# Contents

**Executive Summary** i
Acknowledgements ii
Contents iv
List of Figures x
List of Tables xvii
List of Abbreviations and Nomenclature xviii

**Chapter One Introduction**
1.1 Motivation for Improving Water Quality 1
1.2 Current Practise and Problems 1
1.3 Transients as a Cause of Water Quality Failure 2
1.4 Thesis Structure 2

**Chapter Two Literature Review**
2.1 Introduction 4
2.2 Evolution of Drinking Water Distribution Systems 4
2.2.1 Initial Implementation 4
2.2.2 The Role of Water Quality and Public Health in DWDS 5
2.2.3 What Does a DWDS Look Like Today? 8
2.2.4 "Typical" Hydraulic Conditions 8
2.3 Hydraulic Transients 10
2.3.1 Transient Fundamentals 10
2.3.2 Velocity Profiles and Unsteady Shear Stresses 11
2.3.3 Boundary Layers 13
2.3.4 Parameters Affecting Transient Wavespeed 14
2.3.4.1 Fluid Properties 14
2.3.4.2 Pipeline Properties 15
2.3.4.3 Other Properties 15
2.3.5 Methods for Determining Wavespeed 16
2.3.5.1 Utilising Fluid and Pipeline Properties 16
2.3.5.2 Comparison of Pressure Signals 17
2.3.5.3 Joukowski Equation 17
2.3.6 Other Transient Properties 18
2.3.6.1 Pipeline Period 18
2.3.6.2 Line Packing 19
2.3.6.3 Cavitation 19

2.3.7 Transient Effects and Applications 20
2.4 Water Quality and Mobilisation of Material 21
2.4.1 Discolouration 21
2.4.2 Particles Typically Linked to Discolouration 22
2.4.3 Metals and Discolouration 23
2.4.4 Do Discolouration Particles Follow Gravitational Settling Theory? 24
2.4.5 Biofilm Approach 26
2.4.6 Force Balance between Adhered Material and Hydraulic Forces 28
2.4.7 Current Discolouration Management Techniques 30
2.5 Transient Mobilisation 32
2.5.1 Drinking Water Distribution Systems 32
2.5.2 Biofilms 33
2.5.3 Vascular Trauma 34
2.5.4 Colloidal Mobilisation 35
2.5.5 Whey Protein Layers in Milk Treatments 36
2.6 Summary 37

**Chapter Three Aims and Objectives**

**Chapter Four Methodology and Methods**
4.1 Introduction 40
4.2 Methodology 40
4.2.1 Introduction 40
4.2.2 Representative Hydraulic System 40
4.2.2.1 Selecting Laboratory Experiments 40
4.2.2.2 The Laboratory Facility 41
4.2.2.3 Selecting Dynamic Events 42
4.2.3 Replicating Adhered Material 42
4.2.4 Experimental Methodology 43
4.2.4.1 Defining Mobilisation 44
4.2.4.2 Current to Quantify a Mobilisation Force 44
4.2.4.3 Mobilisation Force Relationships 44
4.2.4.4 Valve Operations 45
4.3 Methods 46
4.3.1 Introduction 46
4.3.2 Laboratory Specifications 46
4.3.2.1 Equipment 48
4.3.2.2 Software for Equipment Control and Data Collection 49

4.3.2.3 Pressure at the Electromagnet 49
4.3.3 Generating Transients 49
4.3.3.1 Rapid Valve Operations 49
4.3.3.2 Repeatability of Valve Operations 50
4.3.3.3 Location of the Transient-Inducing Valve 53
4.3.3.4 Using the Bypass for Test Conditions 53
4.3.4 Replicating Adhered Material 54
4.3.4.1 Effect of the Magnetic Field on Water 54
4.3.4.2 Temperature of the Electromagnet 55
4.3.4.3 Particle Details 55
4.3.4.4 Inserting the Particles into the Electromagnetic Field 57
4.3.5 Determination of the Mobilisation Threshold 58
4.3.6 Validation of the Mobilisation Threshold 61
4.3.7 Experimental Programme 62
4.3.7.1 Experimental Test Method 62
4.3.7.2 Testing Conditions 63
4.4 Summary 64

**Chapter Five Results**
5.1 Introduction 65
5.2 Ball Bearings as Magnetic Particles 65
5.2.1 Steady State 65
5.2.2 Valve Closing Transients 67
5.2.2.1 Complete Valve Closing Transients 67
5.2.2.2 Partial Valve Closing Transients 71
5.2.3 Valve Opening Transients 71
5.2.3.1 Complete Valve Opening Transients 71
5.2.3.2 Partial Valve Opening Transients 77
5.3 Powder as Magnetic Particles 81
5.3.1 Powder Structure 81
5.3.2 Steady State 84
5.3.3 Valve Opening Transients 85
5.3.3.1 Complete Valve Opening Transients 85
5.3.3.2 Partial Valve Opening Transients 88
5.3.4 Confirming Mobilisation of Powder 90
5.4 Summary 93

**Chapter Six Analysis of Transient Mobilisation Behaviour**


6.1 Introduction 95

6.2 Effect of Initial and Final Steady State Conditions on Mobilisation 95

6.2.1 Effect of Initial Flow Conditions 95

6.2.1.1 Effect of Initial Flow 96

6.2.1.2 Effect of Initial Flow Regime 97

6.2.1.3 Effect of Initial Particle Movements 98

6.2.1.4 Streamwise Movements Post Instigation of Mobilisation 102

6.2.2 Effect of Final Flow Conditions 105

6.2.3 Effect of Initial Pressure Conditions 106

6.2.4 Effect of Final Pressure Conditions 108

6.2.5 Effect of the Change in Flow Rate 109

6.2.6 Effect of the Change in Pressure 110

6.2.7 Summary of Steady State Conditions 111

6.3 Effect of Short-Term Conditions 112

6.3.1 When Mobilisation Was Instigated 112

6.3.1.1 Method: Synchronisation of Pressure Sensors and Camera 113

6.3.1.2 Exploring $\Delta t$ 116

6.3.2 Exploring Dynamic Surge Properties 118

6.3.2.1 Method: $\Delta P$ Quantification 121

6.3.2.2 Method: $dP/dt$ Quantification 122

6.3.2.3 Dynamic Surge Properties Comparison 123

6.3.3 Exploring $\Delta P$ 125

6.3.4 Evaluating $\Delta P$ 127

6.4 Development of a Transient Mobilisation Behaviour Function 130

6.4.1 Method: Converting $\Delta P$ into $\Delta Q$ 131

6.4.1.1 Determining Wavespeed 131

6.4.1.2 Errors in Valve Opening $\Delta Q$ 133

6.4.2 Exploring $\Delta Q$ 133

6.4.3 Peak Dynamic Force 136

6.4.3.1 PDF Variation Due To Wavespeed 139

6.4.3.2 Applying PDF to Complete Valve Closing Transients 141

6.5 Applying Peak Dynamic Force to Powder Results 142

6.6 Summary 144


**Chapter Seven Discussion**


7.1 Introduction 146

7.2 Objective One 146

7.2.1 Replication of Adhered Material 146
7.2.2 Location of the Electromagnetic System 147
7.2.3 Particle Detachment 147
7.2.4 Evidencing Transient Events 148
7.3 Objective Two 148
7.3.1 Separating Transient and Steady State Forces 148
7.3.2 Separating Accelerating and Decelerating Events 149
7.3.3 Repeated and Different Conditions 150
7.3.4 Extension to Other Industries 150
7.4 Objective Three 151
7.4.1 Particle Structures 151
7.4.2 Mobilisation Ability and Trends 151
7.4.3 Differences between the Materials 152
7.4.3.1 Material Resistive Forces 152
7.4.3.2 Applied Hydraulic Force 153
7.5 Objective Four 154
7.5.1 Structure of the Peak Dynamic Force Function 155
7.5.2 Proposed Mechanisms for Mobilisation 156
7.5.2.1 Pressure Wave Front Mechanism 156
7.5.2.2 Velocity Profile Mechanism 157
7.5.3 Applying the Pressure Wave Front Mechanism 158
7.5.4 Applying the Velocity Profile Mechanism 160
7.5.4.1 Valve Closing Transients 160
7.5.4.2 Valve Opening Transients 161
7.5.4.3 Initial Turbulence Effects 161
7.5.5 Objective Four Summary 162
7.6 Significance of This Work 163
7.6.1 Theoretical Impacts 163
7.6.2 Practical Impacts 163
7.6.3 Future Research 164
7.6.3.1 Velocity Wall Profiles 164
7.6.3.2 Impact of Organic Material 165
7.6.3.3 An Alternative Impact on Water Quality 165

**Chapter Eight Conclusions**
8.1 Thesis Overview 166
8.2 Leading Conclusions 166
8.3 Further Conclusions 166

**Chapter Nine** **References** 168

**Appendix** **Summary of Experiments Performed** 183

# List of Figures

**Figure 2.1.** Schematic example of the two peak diurnal flow pattern typical for customer use. Note the axes are not to scale. 9

**Figure 2.2.** Schematic for determining wavespeed by comparing pressure wave signals at known sensor locations. Wavespeed can be calculated by dividing the distance between sensor locations, by the time difference between the first wave crests. 17

**Figure 2.3.** Schematic of an idealised transient signifying the primary pressure surge and pressure increase due to line packing effects. 19

**Figure 2.4.** Discoloured water from a customer tap (Wazny, 2013). 21

**Figure 2.5.** a) Turbidity data collected by Boxall and Saul (2005) – inlet monitor returned a zero response confirming that all material was mobilised from within the study pipe, b) NTU scale, adapted from CamLab (Atkin, 2017). 23

**Figure 2.6.** a) Corrosion in an iron pipe (Margevicius, 2012) b) 'Black' water (Temple Water, 2015). 24

**Figure 2.7.** Photograph from inside a trunk main showing material adhesion across the internal pipe wall (Husband and Boxall, 2016). 26

**Figure 2.8.** Concept illustration showing pipe-wall adhered material accumulation during low hydraulic forces, which is then mobilised by higher hydraulic forces. 29

**Figure 2.9.** Illustration showing the endothelial layer between blood and the smooth muscle cells (Vallance & Channon, 2010). Only the endothelial cells are exposed to the shear stress generated by the blood flow. 34

**Figure 3.1.** Graphical representation of the theory investigated: steady state forces are lower than the material adhered strength thus mobilisation does not occur. Initial and final conditions of the transient do not exceed this steady state condition, yet the dynamic forces induced could surpass the material strength and cause mobilisation. 38

**Figure 4.1.** Photograph (a) and schematic (b) of ferritic particles in the pipe invert held by the electromagnet under the pipe. A camera was placed directly above the particles to record the particles. 43

**Figure 4.2.** Schematic of the magnetic force decreasing in controlled steps until the magnetic force is just lower than the hydraulic force, causing mobilisation. 44

**Figure 4.3.** Schematic of mobilisation force relationships between hydraulic force and magnetic force at the point of mobilisation. The transient relationship sits above the steady state relationship, indicating conditions where transient conditions can cause mobilisation, but steady state conditions cannot (green highlight). Linear 45

relationships are drawn as the simplest association possible, which may or may not pass through the origin.

**Figure 4.4.** Photograph of the laboratory facility with key visible features indicated. Note: the blue pipe system on the right hand side is separate and not associated with this work. 47

**Figure 4.5.** Laboratory schematic, including key features and distances from the reservoir. 48

**Figure 4.6.** Wavespeed as a function of time since start of continuous pumping. 51

**Figure 4.7.** Pressure traces of five repeats of an example valve opening transient evidencing a repeatable pressure change over 0.1 s. Each transient is aligned to the start of the first pressure drop. 52

**Figure 4.8.** Pressure traces of five repeats of an example valve opening transient evidencing a repeatable pressure change over 10 s. Each transient is aligned to the start of the first pressure drop. 52

**Figure 4.9.** Illustration showing how the bypass was used to generate a system flow rate whilst the transient valve was fully closed. 53

**Figure 4.10.** Schematic showing complete and partial a) valve closing, and b) valve opening transients. 54

**Figure 4.11.** Cumulative percentage of SAF 2507 particle diameters. 56

**Figure 4.12**. SAF 2507 particles examined using secondary electron imaging in a scanning electron microscope (SEM). 57

**Figure 4.13.** Schematic of the particle insertion method. 58

**Figure 4.14.** MATLAB code to analyse the videos; ball bearing image a) unprocessed and b) processed, powder image c) unprocessed and d) processed. 59

**Figure 4.15.** Quantified particle oscillation in the traverse and streamwise directions for a range of flow rates. 60

**Figure 4.16.** Complete valve closing example of the absolute streamwise distance changes experienced by a ball bearing due to repeated transients with decreasing current. Current and absolute streamwise distance change are scaled to the ranges tested/observed. 61

**Figure 4.17.** Complete valve opening example of the absolute streamwise distance changes experienced by a ball bearing due to repeated transients with decreasing current. Current and absolute streamwise distance change are scaled to the ranges tested/observed. 62

**Figure 4.18.** Flow chart for the steady state and transient experimental test methods. 63

**Figure 5.1.** Relationship between the current at which mobilisation occurred for ball bearings and steady state flow rates. 66

**Figure 5.2.** Streamwise tracking example of a ball bearing during a complete valve 68

closing transient transitioning from a 0.7 l/s initial flow rate to a zero final flow rate. Part a) is a selection of discrete frames taken by the camera, where the green line is the mobilisation threshold relative to the initial location of the particle centroid. Frames i, ii, vi and vii have 0.1 s spacing, where frames iii, iv, and v are selected as part of the transient surge. Part b) is the streamwise distance change of the particle centroid, relative to its initial position, determined by processing all video frames through the tracking programme. The frames presented in part a) are indicated in the continuous time series data of part b).

**Figure 5.3.** Pressure traces of complete valve closing transients that caused mobilisation of the ball bearings. Traces are normalised by subtracting initial pressure and adjusted so that the first surge commences at time zero. $Q_I$ initial flow rate, $P_I$ initial pressure, $I$ current at which mobilisation occurred. 69

**Figure 5.4.** Relationships between the current at which mobilisation occurred for ball bearings and steady state flow rate, or complete valve closing initial flow rate. 70

**Figure 5.5.** Streamwise tracking example of a ball bearing during a complete valve opening transient transitioning from a zero-initial flow rate to a flow rate of 0.49 l/s. Part a) is a selection of discrete frames taken by the camera. The frames have a 0.05 s spacing. Part b) is the streamwise distance change of the particle centroid, relative to its initial position, determined by processing all video frames through the tracking programme. The frames presented in part a) are indicated in the continuous time series data of part b). 73

**Figure 5.6.** Pressure traces of complete valve opening transients set one that caused mobilisation of the ball bearings. Traces are normalised by subtracting initial pressure and adjusted so that the first surge commences at time zero. $Q_F$ final flow rate, $P_I$ initial pressure, $I$ current at which mobilisation occurred. 75

**Figure 5.7.** Pressure traces of complete valve opening transients set one that caused mobilisation of the ball bearings. Traces are normalised by subtracting initial pressure and adjusted so that the first surge commences at time zero. $Q_F$ final flow rate, $P_I$ initial pressure, $I$ current at which mobilisation occurred. 75

**Figure 5.8.** Relationships between the current at which mobilisation occurred for ball bearings and steady state flow rate, or complete valve opening final flow rate. 76

**Figure 5.9.** Pressure traces of partial valve opening transients set one that caused mobilisation of the ball bearings. Traces are normalised by subtracting initial pressure and adjusted so that the first surge commences at time zero. $Q_F$ final flow rate, $P_I$ initial pressure, $I$ current at which mobilisation occurred. 78

**Figure 5.10.** Pressure traces of partial valve opening transients set two that caused mobilisation of the ball bearings. Traces are normalised by subtracting initial pressure and adjusted so that the first surge commences at time zero. $Q_F$ final 78

flow rate, $P_I$ initial pressure, $I$ current at which mobilisation occurred.

**Figure 5.11.** Pressure traces of partial valve opening transients set three that caused mobilisation of the ball bearings. Traces are normalised by subtracting initial pressure and adjusted so that the first surge commences at time zero. $Q_F$ final flow rate, $P_I$ initial pressure, $I$ current at which mobilisation occurred. 79

**Figure 5.12.** Pressure traces of partial valve opening transients set four that caused mobilisation of the ball bearings. Traces are normalised by subtracting initial pressure and adjusted so that the first surge commences at time zero. $Q_F$ final flow rate, $P_I$ initial pressure, $I$ current at which mobilisation occurred. 79

**Figure 5.13.** Relationships between the current at which mobilisation occurred for ball bearings and steady state flow rate, or valve opening final flow rates (complete and partial). 80

**Figure 5.14.** Powder structure that is a) dispersed, or b) condensed with observed voids. 81

**Figure 5.15.** Powder structure a) pre and b) post substructure mobilisation. 82

**Figure 5.16.** Cumulative frequency distribution of the percentage change in pixel counts between the start and end of transient tests where mobilisation did not occur. 83

**Figure 5.17.** Powder images pre (a and c) and post (b and d) transient that show an increase in pixel count. Images a) and b) have been unprocessed, where images c) and d) have had the colour threshold applied as part of the tracking programme. 84

**Figure 5.18.** Relationship between the current at which mobilisation occurred for powder and steady state flow rates. 85

**Figure 5.19.** Streamwise tracking example of powder during a complete valve opening transient transitioning from a zero-initial flow rate to a flow rate of 0.44 l/s. Part a) is a selection of discrete frames taken by the camera. The frames have a 0.1 s spacing. Part b) is the streamwise distance change of the particle centroid, relative to its initial position, determined by processing all video frames through the tracking programme. The frames presented in part a) are indicated in the continuous time series data of part b). 86

**Figure 5.20.** Pressure traces of complete valve opening transients that caused mobilisation of the powder. Traces are normalised by subtracting initial pressure and adjusted so that the first surge commences at time zero. $Q_F$ final flow rate, $P_I$ initial pressure, $I$ current at which mobilisation occurred. 87

**Figure 5.21.** Relationships between the current at which mobilisation occurred for powder and steady state flow rate, or complete valve opening final flow rate. 88

**Figure 5.22.** Pressure traces of partial valve opening transients that caused mobilisation of the powder. Traces are normalised by initial pressure and adjusted 89

so that the first surge commences at time zero. $Q_F$ final flow rate, $P_I$ initial pressure, $I$ current at which mobilisation occurred.

**Figure 5.23.** Relationships between the current at which mobilisation occurred for powder and steady state flow rate, or valve opening final flow rates (complete and partial). 90

**Figure 5.24.** Initial streamwise positions and distance moved of the powder during example sequences of transients with decreasing currents. They either show a step change in distances moved (a) or consistent distances moved (b). 92

**Figure 5.25.** Relationships between the current at which mobilisation occurred for powder and steady state flow rate, or valve opening final flow rates (complete and partial). Rejected results have been removed. 93

**Figure 6.1.** Currents at which mobilisation occurred for ball bearings, against valve opening initial flow rates. 97

**Figure 6.2.** Currents at which mobilisation occurred for ball bearings, against complete valve closing initial Reynolds numbers. The turbulent flow regime boundary is indicated at initial Reynolds number of 4000. 98

**Figure 6.3.** Currents at which mobilisation occurred for complete valve closing transients using ball bearings, against transverse movements particles in the initial flow. 99

**Figure 6.4.** Currents at which mobilisation occurred for all valve opening transients using ball bearings, against transverse movements particles in the initial flow. 100

**Figure 6.5.** Currents at which mobilisation occurred for complete valve closing transients using ball bearings, against streamwise movements particles in the initial flow. 101

**Figure 6.6.** Currents at which mobilisation occurred for all valve opening transients using ball bearings, against streamwise movements particles in the initial flow. 101

**Figure 6.7.** Streamwise tracking example of a ball bearing during a partial valve opening set three transient transitioning from 0.5 l/s to 0.7 l/s flow rate, initial pressure 34.9 m. Three downstream motions of the particle are presented at approximately 0.34 s, 0.72 s, and 1.22 s from the start of the video, and the mobilisation threshold is surpassed in the first motion. 102

**Figure 6.8.** Breakdown of transients by number of particle motions seen. 104

**Figure 6.9.** Streamwise tracking example of a ball bearing during a partial valve opening transient transitioning from 0.5 l/s to 0.7 l/s flow rate, initial pressure 39.7 m. Three downstream motions of the particle are presented at approximately 1.14 s, 1.64 s, and 1.94 s from the start of the video, and the mobilisation threshold is only clearly surpassed in the second motion. 105

**Figure 6.10.** Currents at which mobilisation occurred for ball bearings mobilised by 106

complete valve opening transients set two. The transients transitioned from zero initial flow rates to varying final flow rates, with initial pressure fixed at approximately 45 m.

**Figure 6.11.** Currents at which mobilisation occurred for complete valve closing transients using ball bearings, against initial pressure. 107

**Figure 6.12.** Currents at which mobilisation occurred for all valve opening transients using ball bearings, against initial pressure. 108

**Figure 6.13.** Currents at which mobilisation occurred for all valve opening transients using ball bearings, against final pressure. 109

**Figure 6.14.** Currents at which mobilisation occurred for ball bearings, against valve opening change in flow rates. 110

**Figure 6.15.** Currents at which mobilisation occurred for valve opening transients using ball bearings, against the absolute change in pressure between initial and final conditions. 111

**Figure 6.16.** Illustration showing the synchronisation datum linking the pressure transducer time series and the camera time series, via the trigger electric pulse. 113

**Figure 6.17.** Example of selecting the mobilisation time window using the frames captured by the camera during a complete valve closing transient, which transitioned from 1.00 l/s initial flow rate to zero final flow rate. 114

**Figure 6.18.** Pressure trace of an example complete valve closing transient, which transitioned from 1.00 l/s to zero final flow rate, synchronized with the mobilisation time window. 115

**Figure 6.19.** Pressure trace of an example complete valve opening transient, which transitioned from a zero initial flow rate to 0.50 l/s, synchronized with the mobilisation time window. 115

**Figure 6.20.** $\Delta t$ values for valve closing transients plotted against initial flow rate. 116

**Figure 6.21.** $\Delta t$ values for valve opening transients plotted against initial flow rate. 117

**Figure 6.22.** Pressure trace of an example partial valve opening transient, which transitioned from 0.30 l/s to 0.52 l/s, synchronized with the mobilisation time window. Initiation of mobilisation of the ball bearing must have occurred during this time period. This transient had the largest $\Delta t$ time observed of all experiments. 118

**Figure 6.23.** Pressure traces of partial valve opening transients set one that caused mobilisation of the ball bearings. Traces are normalised by subtracting initial pressure and adjusted so that the first surge commences at time zero. Part a) the time axis ranges between -2 s and 10 s to show the entire transient. Part b) the time axis ranges between -0.050 s and 0.025 s to highlight the varying gradients of the initial surge. 120

**Figure 6.24.** Schematic of an idealised transient signifying line packing effects. Highlighted points indicate the initial pressure, magnitude of the primary pressure surge $\Delta P$ and the pressure to which the surge changes to $P_S$. 121

**Figure 6.25.** Pressure trace of an example complete valve opening transient, which transitioned from zero initial flow rate to 0.51 l/s, with the $P_S$ value highlighted. 122

**Figure 6.26.** $dP/dt$ and $\Delta P$ values calculated for complete valve closing transients. 124

**Figure 6.27.** $dP/dt$ and $\Delta P$ values calculated for all valve opening transients. All sets of partial valve opening transients are statistically similar to the complete valve opening relationship, therefore the linear regression line given was determined for all valve openings. 125

**Figure 6.28.** Relationship between the current at which mobilisation occurred for ball bearings, and $\Delta P$ values for complete valve closing transients. 126

**Figure 6.29.** Relationships between the current at which mobilisation occurred for ball bearings, and $\Delta P$ values for valve opening transients. 127

**Figure 6.30.** Relationship between the $\Delta P$ values and complete valve closing initial flow rate, for ball bearings. 128

**Figure 6.31.** Relationship between the $\Delta P$ values and valve opening initial flow rate, for ball bearings. 129

**Figure 6.32.** Relationship between the $\Delta P$ values and valve opening initial pressure, for ball bearings. 129

**Figure 6.33.** Idealised force schematic for steady state and a partial valve opening transient. Parameters relating to these forces are indicated. $\Delta P$ pseudo instantaneous change in pressure, $Q_I$ initial flow rate, $P_I$ initial pressure, $Q$ flow rate. 130

**Figure 6.34.** Flow diagram of the method utilised to determine $\Delta Q$ for both valve closing and valve opening transients. The wavespeed from the closings is transferred to the openings. 132

**Figure 6.35.** Currents at which mobilisation occurred for ball bearings, against valve opening $\Delta Q$ values. Error bars in $\Delta Q$ are included as well as the steady state mobilisation force relationship for comparison. 135

**Figure 6.36.** Idealised flow rate schematic for a partial valve opening transient showing the peak dynamic force as a sum of the initial steady state flow rate, $Q_I$, and the pseudo instantaneous change in flow rate, $\Delta Q$. 136

**Figure 6.37.** Currents at which mobilisation occurred for ball bearings, against valve opening PDF values. Error bars in PDF are included as well as the steady state mobilisation force relationship for comparison. 138

**Figure 6.38.** Idealised flow rate schematic for a complete valve closing transient showing the peak dynamic force as a sum of the initial steady state flow rate, $Q_I$, 141

and the pseudo instantaneous change in flow rate, $-\Delta Q$.

**Figure 6.39.** $\Delta t$ values for valve opening transients tested with the powder plotted against initial flow rate. 143

**Figure 6.40.** Currents at which mobilisation occurred for powder, against valve opening PDF values. Error bars in PDF are included as well as the steady state mobilisation force relationship for comparison. 144

**Figure 7.1.** Illustration of the magnetic and self-weight forces on particles held against the pipe obvert and the pipe invert. 147

**Figure 7.2.** Mobilisation force relationships for steady state, complete valve opening and partial valve opening conditions for a) the ball bearings, and b) the powder. These results are for directly comparable hydraulic conditions. The current range is significantly smaller (0 mA to 180 mA) for the powder results than for the ball bearing results (0 mA to 450 mA). 152

**Figure 7.3.** Height into the flow of the viscous sublayer, buffer layer, ball bearings and largest SAF 2507 particles, respectively. The viscous sublayer and buffer layers vary with initial flow rate. 154

# List of Tables

**Table 2.1.** Examples of significant waterborne disease outbreaks since 1990 8

**Table 2.2.** Values of terminal fall velocity for iron particles. Density of water is given as 999.7 kg/m$^3$ for 10°C water. 25

**Table 4.1.** Laboratory equipment specifications. 48

**Table 5.1.** Maximum differences between the currents at mobilisation occurred and the currents given by the steady state regression line. 66

**Table 5.2.** Valve opening transients that exhibited a step change in the streamwise distance movements of the powder. 91

**Table 6.1.** $dP/dt$ and corresponding RMSE values calculated for partial valve opening transients (Set One). 123

**Table 6.2.** Wavespeed lookup table calculated using complete valve closing transients. Average wavespeeds (units m/s) are presented with standard deviations across ten repeats. 132

**Table 6.3.** Previous values of wavespeed and constant wavespeeds required for valve opening PDF values to be statistically similar to the steady state relationship. These values apply to ball bearing results. 140

**Table 6.4.** Wavespeeds required for complete valve closing PDF values to be equal to the steady state relationship. These values apply to ball bearing results. 142

**Table A1.** Steady State Experiments Performed Using Ball Bearings as Adhered Particles. 183

**Table A2.** Transient Experiments Performed Using Ball Bearings as Adhered Particles. 183

**Table A3.** Steady State Experiments Performed Using Powder as Adhered Particles. 184

**Table A4.** Valve Opening Transient Experiments Performed Using Powder as Adhered Particles. 184

# List of Abbreviations and Nomenclature

**Drinking Water Industry Specific Abbreviations**

| | |
|---|---|
| AWWA | American Water Works Association |
| DWDS | Drinking Water Distribution Systems |
| DWI | Drinking Water Inspectorate |
| EPA | Environmental Protection Agency |
| NTU | Nephelometric Turbidity Units |
| PODDS | Prediction of Discolouration in Distribution Systems |

**Pipeline Properties**

| | |
|---|---|
| $A$ | Cross-sectional Pipe Area |
| $E$ | Young's Modulus of Elasticity of the Pipe Material |
| ED | External Diameter |
| ID | Internal Diameter |
| MDPE | Medium Density Polyethylene |
| PE | Polyethylene |
| PVC | Polyvinyl Chloride |
| $\psi$ | Pipe Constraint Parameter |

**Hydraulic Properties**

Through this thesis, the term "pressure" is used to describe pressure head, $P/\rho g$, thus measured in metres.

| | |
|---|---|
| $Q_I$ | Initial (Pre-Transient) Flow Rate |
| $P_I$ | Initial (Pre-Transient) Pressure |
| $Q_F$ | Final (Post-Transient) Flow Rate |
| $P_F$ | Final (Post-Transient) Pressure |
| v | Cross-sectional Average Velocity |
| Re | Reynolds Number |
| $\rho$ | Fluid Density |
| $s$ | Specific Gravity |
| $K$ | Fluid Bulk Modulus of Elasticity |
| $c$ | Wavespeed |
| $\tau_w$ | Wall Shear Stress |
| $\tau_{ws}$ | Quasi-steady Wall Shear Stress |
| $\tau_{wu}$ | Unsteady Wall Shear Stress |
| $y^+$ | Non-dimension Wall Unit |
| $u_*$ | Friction Velocity |

| | |
|---|---|
| $\upsilon$ | Kinematic Viscosity |
| y | Radial Distance from the Pipe Wall |
| $\Delta P$ | Pseudo Instantaneous Change in Pressure |
| $\Delta V$ | Pseudo Instantaneous Bulk Change in Velocity |
| $\Delta Q$ | Pseudo Instantaneous Bulk Change in Flow Rate |
| $\Delta t$ | Time between the Start of the Transient and Initiation of Mobilisation |
| $dx$ | Change in Distance |
| $dt$ | Change in Time |
| $dP$ | Change in Pressure |
| $T$ | Pipeline Period, or Characteristic Time |
| $L$ | A Characteristic Length Scale |

**Magnetic Properties**

| | |
|---|---|
| $Re_m$ | Magnetic Reynolds Number |
| $\mu$ | Magnetic Permeability of the Fluid |
| $\sigma$ | Conductivity of the Fluid |

**Miscellaneous**

| | |
|---|---|
| $C_D$ | Coefficient of Drag |
| d | Particle Diameter |
| DAQ | Data Acquisition Device |
| EPS | Extracellular Polymeric Substances |
| k | Coefficient |
| p | Probability Value Derived from a Two-Tailed Statistical T-Test |
| $r$ | Radial Direction |
| SEM | Scanning Electron Microscope |
| $w$ | Terminal Fall Velocity |
| $x$ | Longitudinal Direction Along the Pipe |

**Units**

| | |
|---|---|
| A | Amps |
| g | Gram |
| $H$ | Henries |
| I | Current |
| N | Newton |
| S | Siemens |

# Chapter One

# Introduction

## 1.1 Motivation for Improving Water Quality

Poor water quality can cause outbreaks of infectious water-related diseases. These diseases can develop into serious public health hazards and cause significant economic costs due to health service burdens and lost revenue. In 2007, a waterborne outbreak of *Cryptosporidium* occurred in Ireland costing at least €19 million (Chyzheuskaya et al., 2017). In the same year, a drinking water distribution system (DWDS) in Finland was accidentally contaminated with waste water, causing an outbreak of gastroenteritis and cost approximately €2.1 m (Halonen et al., 2012). Research from the Centers for Disease Control and Prevention estimates hospitalisations from three water borne diseases (Legionnaire's disease, cryptosporidiosis and giardiasis) cost the United States $539 million each year (Water Quality and Health Council, 2010). This represents only a fraction of all water borne disease costs. Subsequently, the total global cost is likely to be much higher.

Water supply improvement and quality regulation have arguably done more to ensure public health over the past decades than medical developments (Bartram and Cairncross, 2010; Ferriman, 2007). However, degradation of water quality is still a substantial issue. Discoloured water, an aesthetic indicator of water quality, is perceived to mask other water quality failures and impacts customers' confidence in their drinking water supply. In 2015, 6.7 million people in the UK were affected by discoloured water, and water companies are regularly fined for these failings (Drinking Water Inspectorate, 2015).

Water quality degradation during distribution to consumers accounts for a substantial proportion of the documented disease outbreaks (Chambers et al., 2004; Craun & Calderon, 2001). It is essential, therefore, to identify the processes taking place in operational pipelines that could cause water quality incidents. Only when these processes are examined and explored can effective management strategies be developed to maintain safe drinking water in the future.

## 1.2 Current Practice and Problems

A water quality risk occurs when a significant concentration of undesirable particles present in the bulk flow are carried to consumers. Such particles include metals, chemical contaminants, and pathogens, for example. Organic material accumulating and growing on the pipe wall of DWDS can trap these particles and apply further adhesive forces in addition to the particles' self-weight, securing them in place. The particles are mobilised in the flow

when these adhesive forces are surpassed by competing hydraulic forces. Currently, it is assumed that, for the most part, hydraulic forces in operational networks follow a smooth flow pattern based on average customer demands. Thus existing mobilisation strategies are based on gradual changes in flow. Yet research has shown that DWDS exhibit persistent dynamic events throughout, resulting from hydraulic transients (Creasey & Garrow, 2011; Gullick et al., 2004).

Hydraulic transients, sometimes called water hammer, are generated by rapid changes in velocity and manifest as proportional oscillations in pressure. Transients are instigated by any and every rapid hydraulic change including, but not limited to, sudden flow control valves opening/closing, pump changes and burst events. These could be initiated by the system operator, be imposed by an external event, caused by a faulty component, or develop due to poor maintenance. Dynamic forces are induced due to the rapid change in velocity. These originate from the formation of complex velocity profiles, impulse wave propagation and other dynamic effects (Wylie & Streeter, 1978; Brunone et al., 2000). In the most extreme cases these forces can cause catastrophic and fatigue-like structural failures.

## 1.3 Transients as a Cause of Water Quality Failure

Significant forces induced by transients may provide the hydraulic forces necessary to mobilise adhered particles (Vreeburg et al., 2004; Wood et al., 2005). To date, previous DWDS research has alluded to this ability, yet these statements are mentioned in a general context rather than being the research focus. Ultimately, particle mobilisation caused by transient events may explain water quality issues not currently accounted for by gradual hydraulic changes. Therefore, it is imperative that further insight is gained regarding the impact of transients upon accumulated material within DWDS.

## 1.4 Thesis Structure

Chapter Two contains a review of the relevant literature. The first section focusses on drinking water distribution systems where this research is based. A detailed review of hydraulic transients and the forces they generate is given as well as material associated with water quality failures and current mobilisation strategies. The current state of knowledge of transient mobilisation of material is then described. Chapter Three presents the objectives to achieve the aims of the project.

Chapter Four describes the development of an innovative experiment designed to test mobilisation of adhered material, by both steady state conditions and pseudo instantaneous transients. The first half of the chapter focuses on the methodology taken to explore mobilisation and the second half details methods used. Chapter Five presents the

results of this experiment, evidencing repeatability and control. Analysis of the experiment is given in Chapter Six, which focuses on understanding the transient parameters that could lead to mobilisation.

Chapter Seven discusses the work performed with regard to the thesis aims and objectives. Commonalities and dissimilarities are drawn from the data and compared to current research described in the literature review. Reflections on the work performed are offered, accompanied by suggestions on how the outcomes may link to future practises. Future research questions stemming from this project are also discussed. Chapter Eight concludes the thesis by summarising the key findings.

# Chapter Two

# Literature Review

## 2.1 Introduction

In the UK, water entering DWDS has first passed through water treatment processes and is therefore typically of an exceptionally high quality. For example, in 2014 *E.coli* compliance was recorded at 99.99 % based on sampling undertaken at water treatment works (Drinking Water Inspectorate, 2015b). Deterioration during transit through the distribution systems, from treatment plant to customer taps, accounts for a significant proportion of documented disease outbreaks and water quality degradation (Chambers et al., 2004; Clark et al., 1993; Craun & Calderon, 2001; Hrudey & Hrudey, 2007). Therefore this work focuses on DWDS and the processes occurring within that can impact water quality.

This chapter presents a comprehensive review of relevant literature. The wider context of DWDS and the role they play in the health of society is introduced (section 2.2). The dynamic hydraulic conditions found in DWDS are explored (section 2.3), followed by water quality deterioration through the network and the organic adhered material that exists as a community on the pipe wall (section 2.4). Current literature is reviewed to examine a link between transient events and mobilisation of adhered material (section 2.5). The chapter concludes with a summary of the limitations of the current knowledge and highlights the research opportunities this research aims to build upon (section 2.6).

## 2.2 Evolution of Drinking Water Distribution Systems

### 2.2.1 Initial Implementation

The primary function of DWDS is to transport drinking water from source to consumers. Pipeline based systems were initially created in Minoan cities on the island of Crete in approximately 1500 B.C. (Crouch, 1993). Other civilizations had surface water canals, but the Minoan civilization was the first to develop an aqueduct system that used tubular conduits to convey water. Other cities such as Ephesus and Perge (modern day Turkey) had functioning water systems mostly consisting of clay pipes (Mays, 2000). The Romans developed their famous aqueducts, starting in 312 B.C., to transport water from great distances to their cities for public baths, latrines, fountains and households (Sanks, 2005). Originally the systems were only gravity driven using open and closed conduits, including novel lead pipes, but the advent of high-pressure water conveyance systems meant that properties on higher elevations could also benefit.

The fall of the Roman Empire and the following Middle Ages saw a drastic step-back in distribution systems. DWDS started returning in the 13th century but only in major locations: in the 13th century a 5.5 km lead pipeline was installed between Tybourne Brook and London UK (Sanks, 2005); cast-iron pipe was first installed in Dillenburg Castle Germany in 1455; the first major pipeline was built in 1664, travelling 25 km from Marly-on-Seine in France to the Palace of Versailles. In London, a crude water wheel was installed in the Thames River in 1582 to pump water driven by the flow of water in the river. By the mid-1700s this system grew to more than 50 km of water mains constructed from a mixture of wood, cast iron and lead pipe (Sanks, 2005). The first water distribution systems in the United States were in the state of Pennsylvania – records show these were built in the towns of Schafferstown and Bethlehem in 1746 and 1754, respectively (Walski, 2006).

Wood is a classic pipeline material as it remains strong when full – some wood pipes are still in service today (Walski, 2006). Bored logs and horse powered pumps were used until gradually replaced by iron pipes. The first cast iron pipes were laid in Philadelphia in 1817 and by 1892, San Francisco had nearly 125 km of wrought iron pipe (Sanks, 2005). Ductile iron was later introduced in 1948 to replace cast iron due to greater tensile strength, higher flexural strength and greater resistance to external corrosion. However, iron pipes tend to suffer from high susceptibility to corrosion and structural failures. The production of standardised polyethylene (PE) and polyvinyl chloride (PVC) in 1976 (Uni-Bell PVC Pipe Association, 2001) offered a cost-effective alternative due to their toughness, internal and external corrosion resistance, and flexibility. Subsequently, PE and PVC are the most common materials used for new installations or pipe replacements. Alternatively, iron pipes can be lined with a PE or PVC epoxy-based resin that produces plastic like wall properties.

DWDS have evolved over time to include diverse pipeline materials and advances in engineering, thus becoming complex infrastructures. Furthermore their role in society has changed. The primary function of DWDS is conveying a reliable supply of drinking water to consumers. However, water transported to consumers must also be safe for consumption, based on regulatory standards, with an aim of reducing risk to public health. It has been asserted that the provision of a safe and sustainable drinking supply is one of the hallmarks of a successful society (Allen et al., 2018).

### 2.2.2 The Role of Water Quality and Public Health in DWDS

A general understanding of the need to protect drinking water systems from contamination is shown in historical documents, such as the Bible, and is reflected in the design of ancient major cities, which were equipped with a separate waste discharge system (Szewzyk et al. 2000). John Snow's famous epidemiological study in 1853 (Snow, 1857) shifted the focus from local atmospheric conditions to water contamination as the cause of

disease outbreaks. Moreover, a 1919 typhoid fever outbreak in Pforzheim, Germany resulted in the establishment of protected areas as sources for drinking water production, but also in the decontamination of treated water to kill or remove as many remaining bacteria as possible.

Further research since these outbreaks has irrefutably established the presence of microbial pathogens and other contaminants (such as metals, pharmaceuticals, and toxins) within DWDS. These pathogens are linked to the spread of important infectious and parasitic diseases such as cholera, typhoid, dysentery, hepatitis, giardiasis, guinea worm and schistosomiasis (Esrey et al., 1991). There is huge potential for contaminated water, potentially intruded into the DWDS, to quickly transmit microbial diseases to numerous populations in a short space of time (Szewzyk et al., 2000). Furthermore, the availability of international travel means that diseases could spread across borders making water quality associated public health a global issue.

In developed countries, high standards of drinking water quality are regulated by national agencies to avoid such spread of disease. National agencies include the Drinking Water Inspectorate (DWI) in the UK and the Environmental Protection Agency (EPA) in the USA. These standards are monitored and any violations are heavily penalised. It has been argued that water supply improvements and regulations have done more to ensure public health than medical developments (Bartram and Cairncross, 2010; Ferriman, 2007). For example, the occurrence of diarrhoeal disease has reduced by 25-33%, and trachoma, a bacterial infection that can cause irreversible blindness, has decreased by 27% with the potential to prevent 1.4 million deaths a year in children alone (Esrey et al., 1991). Despite these modern developments, outbreaks of water-related illness can still occur and become a public health hazard, see Table 2.1.

**Table 2.1.** Examples of Significant Waterborne Disease Outbreaks Since 1990

| Location | Type of Study or Event | Key Findings | Publication Author and Year |
|---|---|---|---|
| Montreal, Canada | Controlled operational system experiment | Estimated 35% of the reported GI illnesses among tap water drinkers were water related and preventable | Payment et al., 1991; Payment et al., 1997 |
| Uggelose, Denmark | Contamination by waste water Nov 1992-Feb 1993 | 1,400 cases of gastroenteritis and secondary spread | Laursen et al. 1994 |
| Milwaukee, WI, USA | Contamination by waste water Mar-Apr 1993 | 403,000 cases of cryptosporidiosis, estimated 104 deaths Largest waterborne disease outbreak in documented United States history | MacKenzie et al. 1994 |
| Gideon, MO, USA | Contaminated water supply Dec 1993 | 600 cases of salmonellosis, 15 hospitalisations and 7 deaths | Clark et al. 1996 |
| North Battleford, Canada | Contaminated water supply Apr 2001 | 1,900 cases of cryptosporidiosis | Stirling et al. 2001 |
| USA | Meta data analysis 1971-1998 | 113/619 disease outbreaks caused by water contamination: 21,000 cases of illness, 498 hospital and emergency appointments, 13 deaths | Craun & Calderon 2001 |
| Wales and Northwest England | Self-report questionnaire study Feb 2001-May 2002 | Positive correlation between occurrence of cryptosporidiosis and disrupted water supply (mainly result of pipe bursts) | Hunter et al. 2005 |
| Walkerton, Canada | Water well contamination due to farm runoff | *E.coli* contamination caused gastroenteritis in 2,300 people, 27 people developed a serious kidney ailment and 7 deaths | Hrudey et al., 2003 |
| North Gwyneed, Wales | Ultra-violet treatment not active at water treatment works | Exposure to cryptosporidium via contaminated water: ~66,000 people in 2005 and ~70,000 people in 2008 | DWI, 2005 and 2008 |

The disease outbreaks presented in Table 2.1 were caused by significant incidents or persistent contamination. Yet low-level or 'background' disease transmission can occur, particularly gastrointestinal illnesses or cryptosporidiosis, depending on the type and amount of contamination (Tinker et al., 2009). Even if a small percentage of infected people act upon their water-induced illness, this can have substantial economic consequences due to health visits (general practitioner, emergency departments) and missed days of work. A meta-data study by Roberts et al. (2003) stated the average cost per case of salmonella was £606 (data collected between August 1993 and January 1995 in the UK). In total the estimated cost of infectious intestinal disease in England for this time period was £743 million in 1994/1995 prices, which in 2018 prices would be £1375 million. Moreover, research from the Centers for Disease Control and Prevention estimates hospitalisations from three water borne diseases

(Legionnaire's disease, cryptosporidiosis and giardiasis) cost the United States $539 million each year (Water Quality and Health Council, 2010). Collier et al. conducted a similar analysis but included two more water borne diseases; otitis externa, and non-tuberculous mycobacterial infection (Collier et al., 2015). They evidenced a higher cost of $970 million per year, corresponding to over 40,000 hospitalizations.

### 2.2.3 What Does a DWDS Look Like Today?

DWDS are complex networks comprising of extensive pipelines, which ensure a reliable supply to customers. An American Water Works Association (AWWA) distribution survey in 2002 estimated a US distribution pipe inventory of 980,000 miles – 11% more than the 880,000 miles reported in 1992 (Grigg, 2005). In England and Wales, the total length of DWDS pipe is approximated at 347,500 km (~ 216,000 miles) (Drinking Water Inspectorate, 2015b). In addition, there are numerous devices to control flow and pressure (e.g. pumping stations, valves, storage reservoirs and surge relief devices).

Distribution systems constantly evolve due to failures, maintenance, and expansion. Consequently, older pipes are gradually being replaced or retrofitted by more modern equivalents. In the UK almost a third of pipes have been in place for 30 years or more, yet centenarian pipes still exist (pipes aged a hundred years or more) (UKWIR, 2003). Similarly, PVC and PE pipes and linings are steadily being introduced (Husband and Boxall, 2010) but the majority of existing pipelines are still iron based since their introduction two centuries ago.

Pipes are generally sized to meet consumers' demand and provide emergency firefighting flow to any location in the network. Most pipes are circular and come in a variety of diameters. In the UK 73% of city/urban pipes have an internal diameter of 100-150 mm. In urban/rural areas 50% have an internal diameter of 100-150 mm, and 27% have a smaller internal diameter of 50-80 mm, which is typical of older systems (Twort et al., 2000). Consequently through DWDS there is a vast range of surface area-to volume ratios. This ratio has been estimated to be 11 $m^2/m^3$ in the UK (Fish et al., 2016) and 26 $m^2/m^3$ in the US (National Research Council, 2006).

### 2.2.4 "Typical" Hydraulic Conditions

Water demands vary due to numerous factors, including population size, usage (commercial/industrial/domestic), day, season, use of water efficient devices, and firefighting. Typically for domestic use, a two peak diurnal flow pattern exists, as illustrated in Figure 2.1; the flow significantly peaks between 7 am and 9 am as people get ready for work, then a second smaller peak occurs in the early evening as people return from work. Overnight there

is a minimum night flow to account for customer night use, burst events and background losses such as leaks and water theft. The diurnal demands seen in all distribution systems can vary up to a factor of three times the annual average daily demand depending on the size of the population area (Twort et al., 2000).

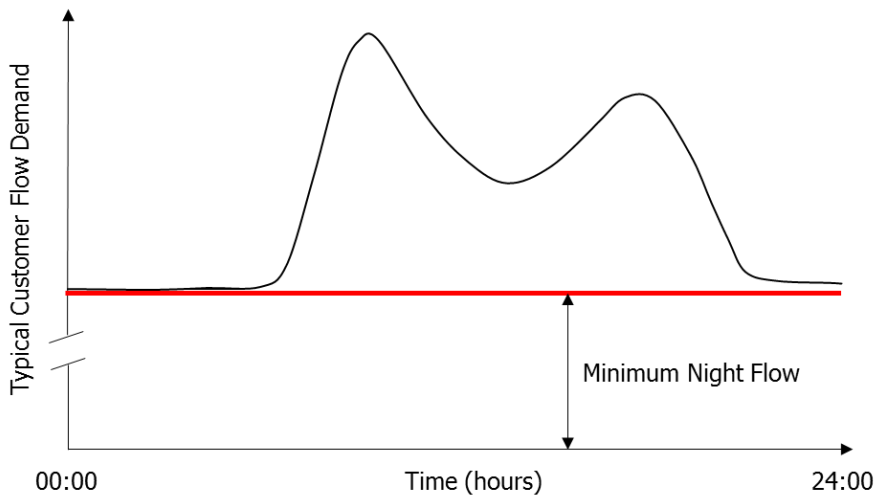


**Figure 2.1.** Schematic example of the two peak diurnal flow pattern typical for customer use. Note the axes are not to scale.

Average flow rate for UK water distribution systems is reported as 0.3 l/s for pipes of 75-100 mm internal diameter (Husband et al., 2008), equivalent to 0.04 m/s to 0.07 m/s. In the US average velocities are reported as an order of magnitude higher, 0.3 m/s to 0.9 m/s (Boyd et al., 2004). Systems in the Netherlands exhibit velocities in the range of a few centimetres per second but there is a daily peak velocity of 0.4 m/s to encourage 'self-cleaning' networks (Vreeburg et al., 2009). UK Regulation BS 6700:2006 requires the maximum velocity not to exceed 3 m/s (British Standard Institution, 2006). Although there is no set minimum velocity, some flow is usually desirable to avoid stagnation.

Pressure is also a key component of DWDS hydraulic conditions. Water pressure is supplied by pumps and the topography of the network and is regulated by pressure relief valves where necessary. A positive pressure is maintained to drive water through all branches of the network and to ensure there is sufficient flow at 'take-off' points, i.e. customer taps. Low pressure is considered detrimental as negative pressure has the potential to draw untreated particles into the clean water through a leakage point (Lindley and Buchberger, 2002). The minimum water pressure guaranteed to customers in the UK is 7 m at the point of use. However, systems are designed so that static pressure in the buried pipe in the street does not fall below 20 m, the typical pressure required to serve buildings up to three storeys high (British Standard Institution, 2006). Conversely, high pressures are also designed against (without regulation) as this increases pipe burst potential and the volume of water lost

through leakage. Water companies reduce water pressure overnight with an aim to meet leakage targets but still maintain the regulated minimum pressure (Twort et al., 2000).

## 2.3 Hydraulic Transients

DWDS are classically interpreted as steady state systems with gradual hydraulic changes in flow and pressure. Yet, emerging research is beginning to challenge this interpretation by showing these networks frequently experience dynamic conditions (Creasey & Garrow, 2011; Starczewska et al., 2015). These events are known by multiple names, usually depending which country the user is from, including water hammer, pressure surge, hydraulic shock, and hydraulic transient (the most common). In this work, the simple term "transient" will be used.

### 2.3.1 Transient Fundamentals

Transient events are instigated by any and every change in velocity that occurs over a relatively short time period. If there is an increase in velocity, the flow accelerates. Likewise, a decrease in velocity, the flow decelerates. These changes may be generated during standard operating procedures or accidental events. Primary sources of frequently occurring transients are valve operations, and pump failure (Bosserman II et al., 2008; Chaudhry, 2014; Karney and McInnis, 1992; Nerella and Venkata Rathnam, 2015; Starczewska et al., 2015). Other transient sources, which are comparatively uncommon, include flow demand changes, controlled pump shutdown, pump start-up, and infrastructure breakages (Bosserman II et al., 2008; Chaudhry, 2014).

Irrespective of source, transients transform the DWDS environment from one set of steady state conditions to another. Therefore, typical descriptors are pre-transient (initial) and post-transient (final) steady state conditions, and the changes between them. These robust parameters, for both flow and pressure, act as boundary conditions for the dynamic event. Flow rate (or velocity) is the more commonly used hydraulic parameter, but both are necessary for numerical simulations (Covas et al., 2004). A 'special case' exists for transients where there is no net change in flow, i.e. the initial flow rate and final flow rate are both zero (Collins et al., 2012). This scenario occurs when there are three sequential closed valves forming two sections of fluid as a closed system. If the two sections have different initial pressures, a transient will form when the central valve is rapidly opened. There will be an overall change in pressure but, due to the closed system, there would not be a change in steady state flow rate.

There are several distinct characteristics of transient events that distinguish them from other hydraulic events. Firstly, velocity and pressure are linearly related during the first

stages of the transient (Collins et al., 2012). Therefore, when a transient is induced, the change in velocity causes an associated pressure change, known as the pressure surge. This pressure change has the inverse sign of the velocity change so that when there is an increase in velocity, the pressure decreases proportionally (downsurge), and vice versa (upsurge). Secondly, equal and opposite pressure waves are created that transmit along the pipeline, travelling from zones of high pressure to zones of low pressure. The wave reflects off infrastructure features (such as pumps, reservoirs, closed values) and can transmit to the source causing the system pressure to oscillate between high and low values. How pressure waves propagate and reflect can be found in most transient textbooks (Chaudhry, 2014; Wylie and Streeter, 1978). Thirdly, transient effects are short lived; typical duration is in the order of a few seconds before the transient is damped by friction (Gullick et al., 2004).

### 2.3.2 Velocity Profiles and Unsteady Shear Stresses

Velocity profiles can change radically during transients. Experimental and numerical studies have been undertaken to measure the velocity profiles induced during transients, usually across the whole pipe or from the pipe centreline to the pipe wall. However, emerging research emphasises significant differences between steady and instantaneous velocity profiles taking place, particularly in the zone close to the pipe wall (Brunone and Berni, 2010).

The most dramatic example of these differences is for rapid valve closing transients that transition to zero final flow. Multiple studies have shown that these transients are capable of producing inverted near wall velocity profiles (Brunone et al., 2000; Brunone and Berni, 2010; Riasi et al., 2009; Silva-Araya and Chaudhry, 1997; Zidouh, 2009). Significantly, within the first stages of the decelerating transient, the flow direction near the wall is reversed but the core of the flow is still in the downstream direction. Consequently, the mean velocity can be a positive value (biased by the large core), yet there is increased dynamic shear stress due to the near wall velocity inversion. This is most clearly evidenced in Brunone and Berni's physical research using ultrasonic Doppler velocimetry techniques to measure velocity profiles (Brunone and Berni, 2010). This technique is non-invasive and utilises ultrasonic pulses reflecting from particles in the flow.

Naser and Karney (2008) observed that literature studying velocity profiles during transient events was biased to valve closing events. Thus, there are few studies focusing on near wall velocity profiles during valve opening events. As an indication of this bias, Brunone et al. (2000) stated that they tested both valve closing and valve opening actions to generate transients, yet only presented valve closing velocity profiles. Bergant et al. (2002) stated that the models for valve closing transients do not always transfer well to valve opening transients; suggesting separate approaches are necessary. Though, it should be noted that this study did not experimentally test instantaneous transients. The existing, if narrow,

research investigating valve opening transients agrees that the near wall profile is steeper at the beginning of the transient than the final velocity profile (Naser and Karney, 2008; Zidouh and Elmaimouni, 2013). Moreover, the velocity at the pipe wall accelerates before the velocity in the centre of the pipe (Agolom et al., 2018).

As the velocity profile changes in complex ways, the corresponding shear stress also changes. Conventionally, it is assumed that steady state expressions for shear stress, such as Darcy-Weisbach and Hazen-Williams, hold at every instant during a transient (Ghidaoui et al., 2005). Any discrepancy between the steady state condition and what happens during the transient is attributed to unsteady components. Therefore, transient analysis formulas frequently use the addition of a steady term to an unsteady term for wall shear stress, see Equation 2.1.

$$\tau_w(t) = \tau_{ws}(t) + \tau_{wu}(t) \qquad \text{Equ. 2.1}$$

Where $\tau_w$ is wall shear stress, $\tau_{ws}$ is quasi-steady wall shear stress, and $\tau_{wu}$ is unsteady wall shear stress.

Over the last 75 years, different authors have attempted to formulate unsteady wall shear stresses in numerous ways (Bergant and Simpson, 2001; Daily et al., 1945; Vardy and Brown, 2004; Zielke, 1968). An excellent review paper was given by Ghidaoui et al. (2005). Yet, further developments in technology, even in the last decade, mean that models of unsteady wall shear stress are constantly progressing.

Broadly, unsteady wall shear stress models can be split into two categories. In the first category, derived from Daily's research (Daily et al., 1945), unsteady shear stress is proportional to the instantaneous changes in fluid velocity. Thus, $\tau_{wu}$ should be positive for accelerating flows, and negative for decelerating flow. The most widely used model in this category is by Brunone et al. (1995), due to its simplicity and reasonable agreement with experimental data (Ghidaoui et al., 2005). In the second category, unsteady shear stress is based on flow history and involves weighting functions that depend on the frequency of changes in flow rate and pressure. This category describes the degree of attenuation of pressure waves and their shape evolution. Models by Zielke (1968) and Vardy and Brown (2004, 2003) fit into this category.

To determine wall shear stress in an experimental system (non-numerical), studies have either measured velocity profiles and then applied a shear stress model (e.g. Brunone and Berni, 2010; Durst et al., 1996), or directly measured the wall shear stresses. There are limited methods/studies that fit into this second group. Typically, experimental studies directly measuring shear stress either use flows accelerating or decelerating at uniform rates, thus are limited in extrapolation to fast transients (He et al., 2011).

One method of non-intrusively measuring local shear rate is known as the 'electrochemical technique' (Hanratty and Campbell, 1983). This technique was used by Zidouh (2009) to show for valve closing transients, the unsteady wall shear stress was

consistently higher than quasi-steady values obtained from velocity profiles. Moreover, the shear stress during the transient could exceed the shear stress from the initial conditions (Zidouh, 2009). Their experimental system, however, was unable to resolve the short time scales necessary to compare to existing numerical models, due to a short pipe and high wavespeed. Another means of measuring wall shear stress is using hot-film anemometry (Sundstrom and Cervantes, 2017). A thin metal wire or film with a high induced temperature is placed in the water. Shear stress is then calculated based on the temperature difference between the hot metal and the cooler water flow. This technique is normally applied to turbulent flows and is yet to be conclusively used to determine wall shear stress during rapid transient events.

### 2.3.3 Boundary Layers

This section describes the hydraulic boundary layers that exist in the immediate vicinity of the pipe wall in steady state flow. How these layers change during transients is not a straight forward process and there is very little literature on the topic.

Within the near wall boundary layers, viscosity is significant. The thin viscous sublayer is the closest layer to the pipe wall (Nowak, 2002; Pope, 2000). Within this layer, the velocity profile is nearly linear, thus the flow is considered to be laminar. Above the viscous sublayer is the buffer layer, in which turbulent effects start to play a role, but the flow is still dominated by viscous effects. The next layer is the transition layer where turbulence effects are much more significant. This layer is also known as the developed turbulent layer (Zarzycki et al., 2011). Above this, the turbulent outer layer or "core" exists.

A non-dimensional radial scale exists called 'wall units', which is used to compare across different studies. A wall unit, $y^+$, can be calculated using Equation 2.2.

$$y^+ = \frac{u_* \, y}{\upsilon} \qquad \text{Equ. 2.2}$$

Where $u_*$ is friction velocity (related to wall shear stress and fluid density), y is radial distance from the wall and $\upsilon$ is kinematic viscosity of the fluid. The inner layer of the pipe wall exists up to 200 wall units and constitutes the following layers; viscous sublayer $0 < y^+ < 5$, buffer layer $5 < y^+ < 30$ wall units, and transition layer $30 < y^+ < 200$ wall units (Pope, 2000).

Vardy and Brown (1995) developed a simplified transient model where there is a turbulent core region of flow and an annular region, which acts as the shear layer. However, they appear to overestimate the thickness of the shear layer at 10 % of the pipe diameter. In a later paper, these authors emphasise the need for detailed experimental data to support their numerical approach (Vardy and Brown, 2004).

### 2.3.4 Parameters Affecting Transient Wavespeed

Transient events generate a pressure wave that propagates along the system. The speed at which the wave travels is affected by fluid and pipeline properties. These are explored here.

#### 2.3.4.1 Fluid Properties

Wavespeed is impacted by the fluid elasticity (describing compressibility) and the mass density. Both of these factors depend on the type of fluid (this work focuses on water distribution systems), the temperature, the pressure and the presence of entrained gas or air.

Buried DWDS pipes experience some thermal variation during the year. Husband et al. (2008) recorded temperatures between 4 and 14 ºC in UK systems, where European cities tend to fluctuate more between 3 and 25 ºC (Prest et al., 2016). Pearsall (1965) stated that wavespeed changes on the order of 1 % per 5 ºC. Applying this ratio to the temperature fluctuations means that wavespeed should only vary by 4.4 % during the year in Europe. It is worth noting this paper does not inform how wavespeed values were determined.

Pressure effects are negligible on wavespeed except at very high pressures (Pearsall, 1965). Using the data presented in Pearsall's paper (1965), the wavespeed between static pressures of 20 m and 200 m (typical range for DWDS, section 2.2.4) would vary by less than 0.2 %. Higher pressures than this would be difficult to test in operational networks due to the pressure rating of pipeline materials; therefore sea water is used as further example of the relationship between pressure and density (thus wavespeed). Sea water is slightly denser than drinking water due to the salt content; at 10 ºC the density of drinking water is 0.999 g/cm$^3$, where sea water is 1.028 g/cm$^3$ at zero depth (Encyclopædia Britannica, 2018). At a depth of 1,000 m the density of sea water changes by less than 0.5 % when compared to zero depth; similarly, at a depth of 10,000 m the density changes by only 4.2 %. Therefore, it can be seen that wavespeed will change with temperature and pressure, although temperature effects will dominate. However, both factors do not cause wavespeed to vary significantly over typical DWDS conditions.

Gases can be present in operational DWDS. These gases can be either entrained air or dissolved gases that come out of the solution when the pressure is reduced, even when it remains above vapour pressure (Boyd et al., 2004; Chaudhry, 2014). The presence of gas in the pipeline can severely reduce wavespeed. Pearsall (1965) showed that as little as 1 part of air in $10^4$ parts of water by volume (0.1 %) causes wavespeed to halve. On the other hand, there is also a complex variation in pressure interaction as the pressure waves reflect off the gas 'cavities' (Lee, 1998). Consequently, the presence of gas can dampen transient pressure oscillations (Boyd et al., 2004; Chaudhry, 2014). Deaeration devices may be used to minimise the air content (Lee and Pejovic, 1996), yet some air will still remain in the fluid system.

Models for determining wavespeed either assume there is no free air or gas in the pipeline, or include a modified bulk fluid modulus of elasticity and an air fraction content coefficient (Lee, 1998).

#### 2.3.4.2 Pipeline Properties

Wavespeed is impacted by pipeline properties, including pipe size, wall thickness, pipe material, constraints in the longitudinal (streamwise) direction. These parameters combine to influence pipe elasticity, a measure of the material's flexibility. The pipe's elasticity means that as the transient propagates, the material stretches radially due to differential water pressures, i.e. the cross-sectional area of the pipe can alter (Ghidaoui et al., 2005). If the energy of the fluid is used to stretch the pipe material, there is less energy to drive the wave along the pipe. Consequently, a rigid pipe tends to exhibit a much higher wavespeed than for a flexible pipe (Pearsall, 1965; Twyman, 2016). Moreover, elastic pipe materials tend to dampen the transient wave more than in rigid pipes (Pearsall, 1965).

Of the aforementioned pipeline properties, pipe material is the primary factor of transient wavespeed, due to its dominance over material elasticity. For example, a copper pipe with Young's modulus of elasticity 1100 GPa will exhibit transient wavespeeds around 1300 m/s (Bergant et al., 2002; Riasi et al., 2009; Zielke, 1968). On the other end of the spectrum, a polyethylene pipe with Young's modulus of elasticity 0.8 GPa will exhibit transient wavespeeds between 240 m/s to 425 m/s (Grann-Meyer, 2005)

The behaviour of a viscoelastic pipe material, like polyethylene, can vary due to mechanical stresses. In a DWDS, these stresses typically come from the water pressure (Covas et al., 2005, 2004). High pressure causes time-dependent changes in the material's elasticity. For example, Janson (1995) found that high density polyethylene pipes may have a short-term Young's modulus of elasticity of 1 GPa, but a long-term modulus of 0.7 GPa. The pipe material deforms and increases the cross-sectional area of the pipe, thus changing the wavespeed. Material creep depends on the material and temperature, but also on pipe constraints (axial and circumferential) and the stress-time history of the system (Covas et al., 2005, 2004).

#### 2.3.4.3 Other Properties

Wavespeed is a dynamic process and decreases with distance, and consequently time (Covas et al., 2004). Initially the generated wave front is sharp but the steepness of the front slope disperses considerably in time due to unsteady friction and fluid inertial effects (Covas et al., 2004; Tijsseling et al., 2006). Tijsseling et al. showed that the wave front can spread up to approximately ten pipe diameters in length (2008). Damping actions eventually reduce the wave until the system stabilises at its new conditions (Boulos et al., 2005).

Another factor affecting wavespeed is the condition on the pipeline. Random variations along the pipe, for example internal pipe corrosion, could result in random reflections and damping of the pressure wave (Duan, 2017). This effect is known as wave scattering. Recent studies have demonstrated that wave scattering significantly influences the speed of wave propagation, more so than friction effects (Duan et al., 2017, 2014).

### 2.3.5 Methods for Determining Wavespeed

Several methods are utilised for determining the wavespeed of a pressure surge. These are presented here as well as their advantages and disadvantages. Wavespeed is typically denoted by either $a$ or $c$. In this work the later will be used for consistency.

#### 2.3.5.1 Utilising Fluid and Pipeline Properties

The first method for calculating wavespeed combines the fluid and pipeline properties discussed in sections 2.3.4.1 and 2.3.4.2, into one encompassing equation, Equation 2.3. This equation was proposed by Halliwell (1963), though is sometimes referred to as the 'Korteweg formula', and can be found in most transient textbooks (Chaudhry, 2014; Wylie and Streeter, 1978).

$$c = \sqrt{\frac{K}{\rho\left[1 + \frac{K}{E}\psi\right]}} \qquad \text{Equ. 2.3}$$

Where $c$ is wavespeed, $\rho$ is fluid density, $K$ is fluid bulk modulus of elasticity, $E$ is Young's modulus of elasticity of the pipe material, and $\psi$ is a constraint parameter. This later parameter is non-dimensional and depends on the elastic properties of the pipe, such as longitudinal movements, ratio of wall thickness to diameter, and Poisson's ratio.

This equation is particularly useful for modelling purposes. The parameters used are standard values so can be commonly identified in established literature, e.g. the specific Young's modulus for the pipe material. This approach avoids necessitating field measurements, which would be particularly beneficial for modelling a section of DWDS that cannot easily be fitted with sensors.

The wavespeed equation utilises fluid and pipeline properties that take other factors into consideration, such as temperature via fluid density and pipe constraints via $\psi$. Yet, not all factors are accounted for in the idealised Equation 2.3. This equation assumes there is no free gas or air in the system (Twyman, 2016). As discussed in section 2.3.4.3, wavespeed varies due to factors such as distance travelled, friction, and dispersion, suggesting an equation for wavespeed should require temporal and spatial dimensions.

Suo and Wylie (1990) extended Equation 2.3 to include a complex function of Young's modulus of elasticity of the pipe material. This function tries to capture the dynamic effect of the pipe wall viscoelasticity on wave propagation. The numerical results presented

appear to correspond well with experimental data. Yet, this paper does not appear to account for the steady state strain experienced by the pipe prior to the transient effects; a main distribution pipe that is transmitting high pressure water will experience a different strain when it is transmitting low pressure water.

#### 2.3.5.2 Comparison of Pressure Signals

A second method for calculating wavespeed is simply determining how far the wave travels in a particular time, i.e. speed equals distance over time. This could be determined by comparing, say, the crest of the wave between pressure time series data at known locations along a pipeline. This is represented in Figure 2.2.

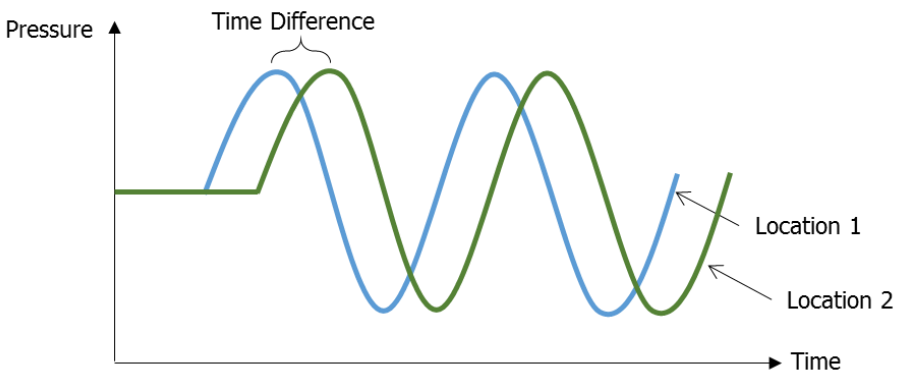


**Figure 2.2.** Schematic for determining wavespeed by comparing pressure wave signals at known sensor locations. Wavespeed can be calculated by dividing the distance between sensor locations, by the time difference between the first wave crests.

This method may seem more representative than the previous method as it is using the signal in situ, thus the fluid and pipeline properties are intrinsically incorporated. However, Rezaei et al. (2015) found that separation of sudden pressure fluctuation profiles was complex due to noise from other profiles. It is typical in operational systems for wave signals to be noisy as the signal can be affected by structural properties such as leaks, material changes, obstructions (Misiunas et al., 2005). This noise could add large uncertainties into selecting the same point for comparison between sensor locations.

#### 2.3.5.3 Joukowski Equation

Joukowski, also known as Joukowsky, (1904) conducted extensive measurements in the Moscow water distribution system. He derived an equation based on these measurements and his theoretical interpretation (Equation 2.4). The Joukowski equation is best known as the "fundamental equation of water hammer".

$$\Delta V = \pm \frac{g}{c} \Delta P \qquad \text{Equ. 2.4}$$

Where $\Delta V$ is the pseudo instantaneous bulk change in velocity, $g$ is the gravitational constant, $c$ is wavespeed, and $\Delta P$ is the pseudo instantaneous change in pressure.

If pressure and velocity data can be measured accurately with high temporal resolution, this equation can be rearranged to calculate a wavespeed. Similar to the comparison of pressure signals method, if these measurements are taken in situ, the resulting wavespeed will be highly representative. There are limitations introduced by using this equation. These are well described in Walters and Leishear (2018), and are summarised here. Firstly, it assumes one dimensional flow, i.e. bulk conditions, so does not account for two dimensional effects, e.g. wavespeed dispersion. Secondly, it is only valid for the first 'pass' of the transient response. This is useful for pseudo instantaneous dynamics, but this equation cannot be used to determine wavespeed for the entire duration of the transient. Finally, this equation is a simple first approximation ideal for uncomplicated linear systems. It does not account for transient and system complexities (such as junctions, pipe diameter changes).

### 2.3.6 Other Transient Properties

In section 2.3.1, three key transient characteristics were outlined. These were the associated pressure surge when there is a velocity change, the generation of pressure waves, and the short duration of transient events. In this section, further transient properties are described, including the pipeline period, line packing effects and cavitation.

#### 2.3.6.1 Pipeline Period

The pipeline period, sometimes called the characteristic time, is the time required for a pressure wave to travel from the transient source to a major reflection point and back to its source (Bergant et al., 2006; Karney & Ruus, 1985; Pothof & Karney, 2012). These major reflection points could be a pump, valve, dead-ends or reservoir (Misiunas et al., 2005). For a simple pipeline, the equation for this period is given in Equation 2.5.

$$T = \frac{2L}{c} \qquad \text{Equ. 2.5}$$

Where $T$ is the pipeline period, $L$ is the length from the transient source to the major reflection location, and $c$ is wavespeed.

This time period becomes the natural time scale for velocity and pressure changes in the system (Pothof and Karney, 2012). Transients are defined as 'rapid' when the operation time is less than the pipeline period (American Water Works Association, 2004; Karney and

Ruus, 1985; Nerella and Venkata Rathnam, 2015). Within this period, the previous pressure surge dominates and the velocity changes relate linearly with pressure changes (Collins et al., 2012). Beyond this period, pressure waves reflecting from different sources could interact with one another, either cancelling or superimposing depending on the boundary conditions (Bergant, 2006).

#### 2.3.6.2 Line Packing

In valve closing transients, a phenomenon known as line packing takes place (Bong et al., 2007; Chaudhry, 2014; Walters and Leishear, 2018). The flow is stopped at the valve, pressure at the valve instantly increases and the corresponding pressure surge propagates upstream as a wave. The pipe wall expands and the water continues to be compressed. An increase in storage capacity of the pipeline continues and the pressure increases beyond the magnitude of the original surge, illustrated in Figure 2.3. Line packing is affected by the length of the pipeline; as a function of the length, the pressure rise due to line packing may be several times greater than the pressure surge (Bong et al., 2007; Chaudhry, 2014). Covas et al. (2004) performed transient experiments in a laboratory facility made of polyethylene pipeline of length 271.5 m. They found that line packing pressure constituted 5 % to 10 % of the first pressure surge.

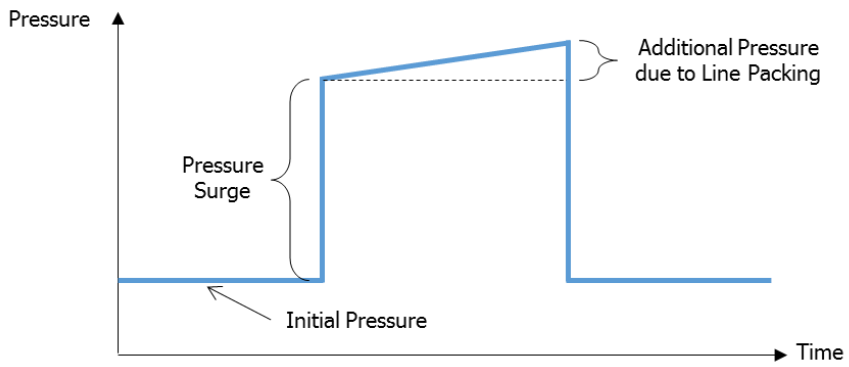


**Figure 2.3.** Schematic of an idealised transient signifying the primary pressure surge and pressure increase due to line packing effects.

#### 2.3.6.3 Cavitation

In severe transients, there is a possibility of cavitation occurring. Negative pressures induced during the transients could surpass vapour pressure, approximately -10 m (Collins et al., 2012). Once below this pressure, bubbles in the water can expand; above the vapour pressure, the bubbles become unstable and collapse violently (nucleation). Cavitation microjets are extremely small and short lived. In particularly extreme transients, the cavitation process can occur more than once within a couple of seconds (Bergant et al., 2006). This process cannot be controlled or managed (Boulos et al., 2005).

There is potential for damage to ensue during the cavity collapse as the nucleation emits as a large shock wave in the water, which can be heightened by the collective collapse of many bubbles (Caupin and Herbert, 2006). Nucleation could delaminate sensors (Minsier and Proost, 2008). Furthermore, if a pipeline section experiencing vapour pressure collides with a positive pressure section, a large and nearly instantaneous rise in pressure takes place (Bergant et al., 2006). This large pressure spike could surpass material strength for pipelines and supporting structures, potentially causing a break in the infrastructure, i.e. a pipe burst.

Cavitation is generally not considered to be a common occurrence in DWDS. It is actively designed against, for example air relief valves are installed in appropriate locations (Boulos et al., 2005). A range of normal water distribution system operations can result in negative pressures (Gullick et al., 2004). Yet, severe cavitation-inducing events are rare. Complete valve closings in particular would require large initial velocities and low initial pressures to cause cavitation. There is little evidence of cavitation events in operational systems. This could be due to the scarcity of these extreme operational conditions. Furthermore, cavitation occurs over such a short time period that it cannot be detected with typical low temporal resolution pressure data. As cavitation in DWDS is relatively rare and the focus of this work is more common dynamic events, cavitation was designed against in this research.

### 2.3.7 Transient Effects and Applications

Severe transients induce extreme dynamic pressures that can exceed the strength of some pipeline components (Bong et al., 2007; Rezaei et al., 2015; Zidouh and Elmaimouni, 2013). Generated bursts can range in size from those that are too small to be detected to violent events. Consequences can be potentially life threatening, for example shrapnel material could cause injury and damage. However, more typical consequences include service interruption, road closures, repair costs, and lost water (Misiunas et al., 2005). Transients in DWDS, therefore, have negative associations with severe structural failures and water companies aim to design systems to avoid such damaging events. Transient research has also focused on providing information on secondary structural aspects of pipelines. These include but are not limited to: leak and burst detection, identification of obstruction locations, pipe wall assessment, and revealing enclosed air pockets (Walters and Leishear, 2018).

Historically, destruction and detection of structural aspects have dominated transient research. Yet attention is beginning to be paid to be water quality implications of transients, mainly contaminant intrusion (e.g. Besner et al., 2011; Gullick et al., 2004; Lechevallier et al., Gullick et al., 2003; Walski & Lutes, 1994). Lindley and Buchberger (2002) theoretically showed that negative pressures induced during some transients could provide a driving force for an external contaminant to enter the pipeline through a pathway, such as a leak, flooded

air valve, or badly fitted joint. This was later evidenced in an experimental study performed by Fox et al. (2014) and quantified by Jones et al. (2019). Having entered the flow the contaminant could then be carried downstream to customers, affecting water quality and posing a health risk.

## 2.4 Water Quality and Mobilisation of Material

Water quality deterioration during travel through the distribution system occurs due to various factors, such as contaminant intrusion, corrosion by-products, or the release of material accumulated in the distribution system (National Research Council, 2006). To monitor public safety, chemical and biological tests are normally performed on water samples in ISO-certified laboratories (International Organisation for Standardization, 2006). Due to standard tests being time intensive, discolouration is typically used as a quick, easy, physical observation of water clarity, as shown in Figure 2.4. Furthermore, it is believed that when water is discoloured enough to be seen, the water will most likely fail other chemical and biological parameters (Husband et al., 2016).

**Figure 2.4.** Discoloured water from a customer tap (Wazny, 2013).

### 2.4.1 Discolouration

A large proportion of UK water quality complaints to drinking water suppliers are regarding discoloured water. In 2015 this amounted to a third of significant incidents and affected 6.7 million people, despite ongoing investment by water companies (Drinking Water Inspectorate, 2015a). Self-reporting by customers can bring about inherent issues with consistency due complex factors, such as expectations from previous incidents, differences in opinion and other social factors. Yet this is the parameter water companies are judged against and fined for poor performance. Recently Southern Water was fined £480,000 plus

£50,000 additional costs for discolouration due to a burst main – section 70 offence for supply of water unfit for human consumption (Gaines, 2017). Though this is indicative of all water companies (Drinking Water Inspectorate, 2017a).

Discoloured water incidents greatly affect customer's confidence in tap water quality as discolouration is perceived to be associated with health issues (Vreeburg and Boxall, 2007). Conceptually 'dirty' water is more likely to contain particles connected to disease, i.e. pathogens and toxins. Multiple studies have linked outbreaks of gastrointestinal illness to incidents in which turbidity exceeded acceptable limits (Centers for Disease Control and Prevention, 1994; Fox & Lytle, 1996; Kent et al., 1988; Levy et al., 1998; Mac Kenzie et al., 1995; Morris et al., 1996; Schuster et al., 2005; Schwartz et al., 1997). Many of these papers have investigated this relationship with good general agreement, but some of these studies have been faulted for poor quality. For example, the EPA concluded that the study by Schwartz et al. (1997) was invalid due to flaws in turbidity measurement and analysis techniques (Sinclair and Fairley, 2000). Mann et al. (2007) performed a systematic critical review of all literature (over 22,000 papers) linking drinking water turbidity to gastrointestinal illness. They stated there is likely to be an association between these factors, but only in some settings or over a certain range of turbidity. Therefore, discoloured water is not a guarantee of illness but is a suitable indicator of potentially poor-quality water.

There is an industry drive to understand the processes leading to incidents of discoloured water, to reduce consumer complaints and improve compliance with public health regulations (Drinking Water Inspectorate, 2017b). Discolouration, as an aesthetic factor, has been typically relatively hard to study as incidents tend to be short lived and their occurrence difficult to predict. Technical advances and the urgency to reduce customer contacts has led to the development and deployment of continuous instrumentation in networks.

### 2.4.2 Particles Typically Linked to Discolouration

Discolouration occurs when dissolved or suspended particulate materials accumulate in the water (Boxall et al., 2003; Polychronopolous et al., 2003; Seth et al., 2004). Discolouration is most commonly measured by turbidity as a broad indicator of the particles in the bulk water. Turbidity is the cloudiness of a fluid and is quantified by performing light scattering techniques (Davies-Colley and Smith, 2001). It is a complex function of the particle suspension, dependent on a combination of factors including: obscuration, reflection, refraction, diffraction, and scatter (Boxall and Saul, 2005). The light reflected off particles in the fluid can be detected using nephelometric (90 degrees scatter) techniques measured in Nephelometric Turbidity Units (NTU). The higher the NTU value, the higher the turbidity of the sample, as indicated by Figure 2.21 b). Discolouration events all have the same key

characteristic curve – a sharp rise in turbidity due to initial release that reduces within a few hours as it dilutes, see Figure 2.5 a).

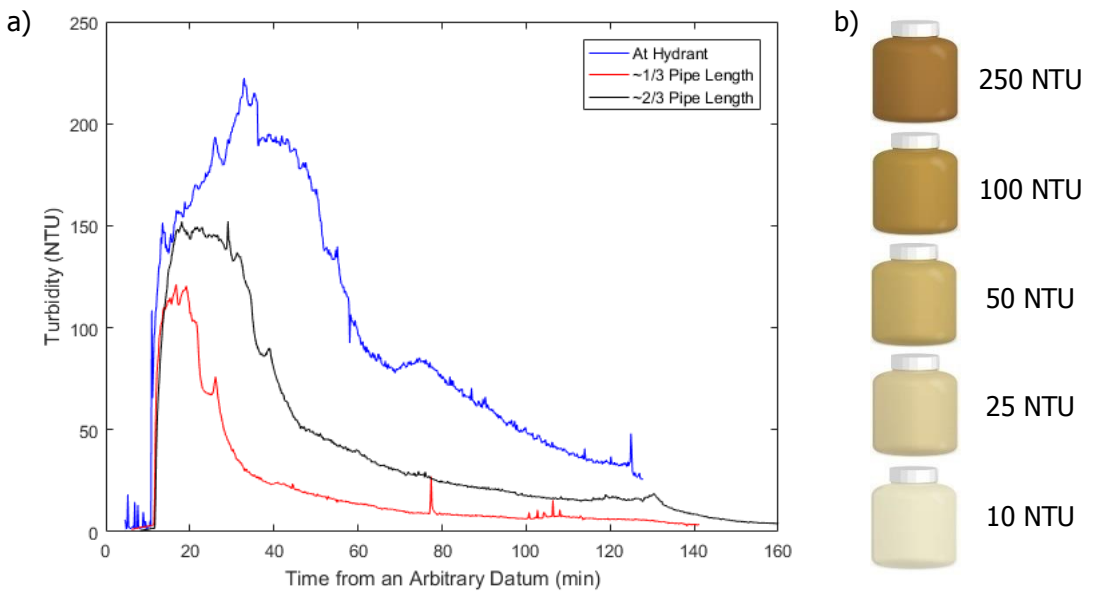


**Figure 2.5.** a) Turbidity data collected by Boxall and Saul (2005) – inlet monitor returned a zero response confirming that all material was mobilised from within the study pipe, b) NTU scale, adapted from CamLab (Atkin, 2017).

In the UK turbidity is regulated such that water leaving treatment plants should not exceed 1 NTU and "endpoint" water, i.e. at customer taps, should be less than 4 NTU (Drinking Water Inspectorate, 2010). Turbidity compliance in English and Welsh water treatment plants in 2014 was recorded at 99.98 % (Drinking Water Inspectorate, 2015b). However, there have been incidents where water quality deteriorated further than 4 NTU through the DWDS, as seen in the above data. These events demonstrate the role of networks in governing final water quality, as the networks interact with the water during transportation.

Boxall et al. (2001) collected discoloured water samples from systems with different pipe materials, source water, pipe age, and water qualities. Analysis of the particles showed that the majority of particles were less than 50 µm in diameter and a significant number were less 5 µm. An average diameter of 10 µm was determined. A relatively small variation in size distribution between site samples suggested consistency, i.e. the particles occurring in discoloured water are irrespective of the origin system.

### 2.4.3 Metals and Discolouration

Metal particles are the main component of discolouration samples (Seth et al., 2004). Such metals include aluminium, copper, iron, zinc, lead, manganese, and phosphorus. Iron is

the dominant metal found in discoloured water (Boxall et al., 2003), though manganese particles have often been observed (Sly et al., 1990). These metals give water its discoloured appearance when significant concentrations are mobilised into the bulk flow; iron particles relate to 'red' water and manganese particles relate to 'black' water. These colours can be seen in Figure 2.6. Since 2010, sampled iron and manganese levels have failed regulatory limits on average 122 times per year and 25 times per year in England, respectively (Drinking Water Inspectorate, 2015b). The water treatment plant can unintentionally add such particles into the water, such as alum or iron flocs, or the particles can originate from the distribution system itself (Vreeburg and Boxall, 2007). Iron particles, as the dominant metal, will be focused on from here on out.

a) 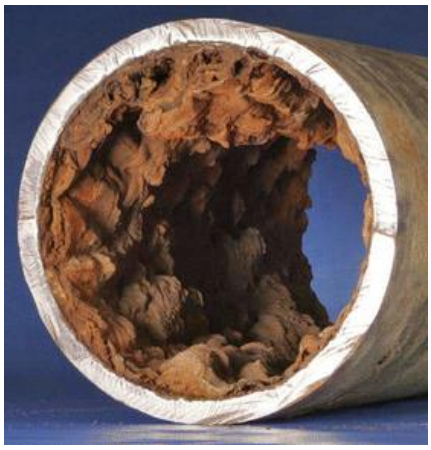 b) 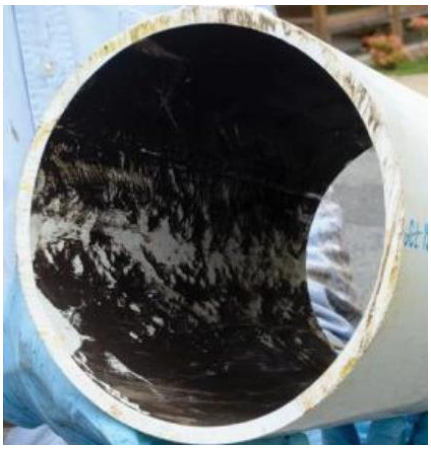

**Figure 2.6.** a) Corrosion in an iron pipe with a red appearance (Margevicius, 2012) b) Accumulated manganese particles with a black appearance (Temple Water, 2015).

Iron particles resulting from corroding metal pipes and fittings are thought to be an important contributor to discolouration (Wagner, 1994). The corrosion reactions produce ferrous hydroxide, which is then oxidized to ferric hydroxide (Naser et al., 2008; Seth et al., 2004). These iron constituents may remain at the pipe wall level or transported into the bulk fluid, which may then accumulate in other non-ferrous pipes (Boxall et al., 2003; Seth et al., 2004). This supports field collections by Friedman et al. (2003) where multiple pipelines were flushed across twelve utilities from United States, United Kingdom and Australia. They showed iron was the primary constituent measured regardless of pipe material.

### 2.4.4 Do Discolouration Particles Follow Gravitational Settling Theory?

When a discoloured water sample is left to stand for a period (>24 hours), particles settle under their own self-weight forming a deposit (Vreeburg and Boxall, 2007). Consequently it is reasonable to believe that the metal particles in pipelines act as heavy sediment and travel along the invert as in river channel sediment. The theory of how particles

settle is well established and validated, reviews can be found in most textbooks. Balancing submerged self-weight forces and drag forces means that the speed at which particles descend through the water, the terminal fall velocity, can be calculated using Equation 2.6.

$$w = \left[\frac{4}{3}\frac{1}{C_D}\, d\, g\, (s-1)\right]^{\frac{1}{2}} \qquad \text{Equ. 2.6}$$

Where $w$ is terminal fall velocity, $C_D$ is the drag coefficient (typically 0.47), $d$ is particle diameter, $g$ is acceleration due to gravity, and $s$ is specific gravity.

Metals found in discoloured water tend not to be simple heavy elements, instead oxides and hydroxides with lower specific gravities (Seth et al., 2004). The specific gravity of three example iron oxides and hydroxides are: $Fe_2O_3$ 5.24, $Fe(OH)_3$ 4.25, and $Fe(OH)_2$ 3.4 (Patnaik, 2003). Terminal fall velocities were calculated for various iron particles with an average diameter of 0.01 mm (Boxall et al., 2001), see Table 2.2.

**Table 2.2.** Values of terminal fall velocity for iron particles. Density of water is given as 999.7 kg/m$^3$ for 10°C water.

| | **Iron** | **Iron (III) Oxide** | **Iron (II) Hydroxide** |
|---|---|---|---|
| Chemical formula | $Fe$ | $Fe_2O_3$ | $Fe(OH)_2$ |
| Specific gravity | 7.87 | 5.25 | 3.4 |
| Density (kg/m$^3$) | 7874 | 5250 | 3400 |
| Density in water (kg/m$^3$) | 6874 | 4250 | 2400 |
| Terminal fall velocity (m/s) | 0.044 | 0.034 | 0.026 |

Boxall et al. (2001) showed that the terminal fall velocities of particles associated with discolouration are less than the boundary turbulence induced by the lowest flows within UK DWDS. In the example used in their work, Boxall et al. (2001) calculated a boundary shear velocity of 0.15 m/s for a 0.1 l/s discharge through an old cast iron main. This value is approximately an order of magnitude greater than the values calculated in Table 2.2. Therefore, the particles should not be able to settle and accumulate in operational DWDS under gravitational settling forces alone. In conclusion, sediment or gravitational settling theory is not dominant for discolouration particles in operational networks. Only particles and processes not governed by gravitational settling theory will be considered further in this work.

These calculations are supported by in situ observations of material accumulation. There is a lack of distinct invert deposit but rather a uniform circumference of metal particles on the pipe wall. This can be clearly seen in Husband and Boxall's paper, which is presented here in Figure 2.7 (Husband and Boxall, 2016). Particles can be transported from the bulk water to the less turbid regions near the pipe wall, via processes such as turbophoresis and Saffman lift force (Thienen et al., 2010). The particles are then adhered to the pipe wall by

forces greater than gravity, i.e. particles transported to the obvert of the pipe do not simply 'fall off' but are instead held against gravity.

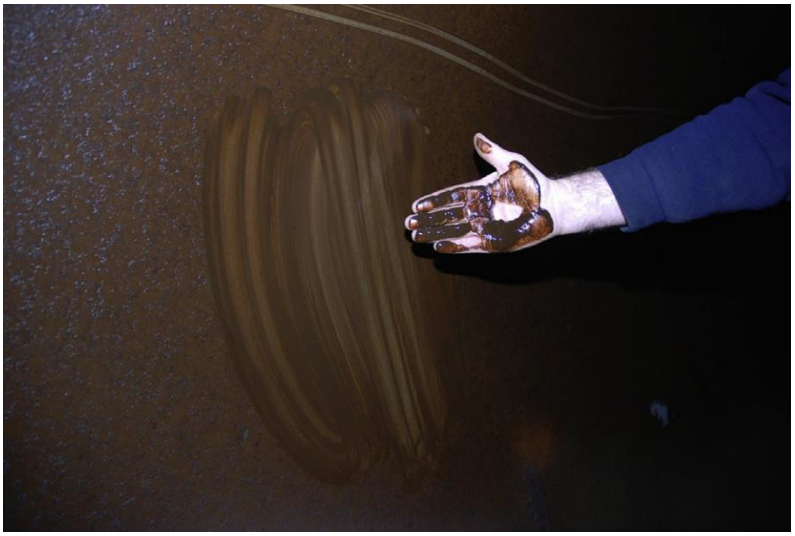

**Figure 2.7.** Photograph from inside a trunk main showing material adhesion across the internal pipe wall (Husband and Boxall, 2016).

Metha and Lee (1994) observed that particles of the size range associated with discolouration normally exhibit adhesive properties. Sources of such adherence forces include complex and interconnected physical, chemical and biological processes that, in general, are poorly understood. One proposed source of adherence force originates from DWDS biofilm research and will be explored here as the 'biofilm approach' to particle adherence forces.

### 2.4.5 Biofilm Approach

Specific gravity of discolouration material has been reported as between 1 and 1.3, irrespective of factors such as location, pipeline material, water source, and water age (Boxall et al., 2001; Seth et al., 2004). Conversely, Friedman et al.'s study (2003) measured an average specific gravity of 2.9 across twelve utilities over three countries (UK, USA, and Australia). These values are considerably lower than the specific gravity of the iron constituents described in the previous section. Consequently metals like iron and manganese must only be a component of the material associated with discolouration. Gauthier et al. (2001) showed that organic matter represents the most important fraction of suspended solids in distributed water, from 40 to 76%. This organic matter includes microbial biomass, which can comprise of up to 10 % of suspended solids (Gauthier et al., 1999). The vast majority (95 %) of microbial biomass is attached to the pipe wall (Flemming et al., 2002), creating biofilms.

Biofilms are defined as a complex assemblages of microorganisms bound together and adhered to an organic or inorganic surface, such as a pipe wall. Biofilms produce a matrix of extracellular polymeric substances (EPS) that act like a scaffolding system for the microorganisms. It provides organisation, mechanical and chemical stability making it an essential element without which the biofilm would not exist (Branda et al., 2005; Flemming & Wingender, 2010). Intertwining the EPS are interstitial voids or cavities and extensive channels that circulate nutrients and oxygen for aerobic bacteria (De Beer et al., 1994). Various properties of the pipeline system, such as pipe material and source water, may influence the presence, structure and composition of the microbial biofilms, and vice versa. The two systems impose on each other, interacting in intricate and sophisticated manners, which are yet to be fully understood. Factors affecting biofilm attachment, growth and maturity are many and highly complex. This thesis will focus on the more mechanical aspects of biofilm structure and detachment, rather than the microbial science involved with biofilm study.

The majority of biofilms are less than 1 mm in height from the pipe surface (Cowle et al., 2014; Paul et al., 2012) and exist as a complete film or small patches of biomass (Menaia and Mesquita, 2004). Biofilm structures can described as 'cell clusters' or 'streamers', where 'streamers' are structures that taper towards the downstream direction (Stoodley et al., 1998). Some streamers have been observed to oscillate in the flow. It is established that biofilms do not have a single uniform strength, but rather a stratification of strengths with weaker layers near the fluid-biofilm interface and stronger layers closer to the biofilm-pipe interface (Ohashi and Harada, 1994; Paul et al., 2012; Peyton, 1996; Zhang and Bishop, 1994). Furthermore, this strength can vary depending on the conditions the biofilm is exposed to, such as nutrients and chemicals (Douterelo et al., 2016). Accordingly, various apparent values of biofilm elastic modulus values have been measured: Stoodley et al (1999) report values in the range of 17 to 240 $N/m^2$ for biofilm in a tensile state, where Körstgens et al. (2001) experimentally determined vales of 6,500 ± 500 $N/m^2$ from uniaxial compression tests.

The adhesive nature of biofilms means that particles transported to the biofilm/water boundary can be trapped within the EPS structure. A variety of biofilm factors affect this ability such as permeability, heterogeneity, and internal structure (Billings et al., 2016), but the overall effect is for particles to harbour in the biofilm, i.e. the biofilm acts as a trap or reservoir. These particles can include metals, contaminants, viruses, pathogens, carbon and sand particles, fungi, toxins and other suspended solids (Peyton and Characklis, 1992; Vreeburg and Boxall, 2007; Wingender and Flemming, 2011). If the particles are entrapped in the biofilms, then they are not present in the bulk water, which conceptually is good for customers. Nevertheless, there can be considerable consequences. For example, iron, the primary constituent of discolouration material, can be biosorped by biofilms and lead to

excessive growth of iron oxidising bacteria. Such bacteria include many *Legionella* species, known for causing Legionnaire's disease (Lau and Ashbolt, 2009; Rathsack, 1997; Shen et al., 2015). If these bacteria are then detached, a potential health risk is posed. For example, the release of biofilm-entrapped oocysts was suggested as the cause of a cryptosporidiosis outbreak in Lancashire, England (Howe et al., 2002). It is vital, therefore, to understand the mechanisms leading to biofilm detachment in order to minimize any risk to users.

Biofilm detachment occurs when the bonds are broken and the separated cells are carried away by the flow (Bakke, 1986; Stoodley et al., 1999). Biofilm detachment can be broadly categorised as either erosion or sloughing, although not all authors recognise this distinction (Stewart, 1993). Erosion is used to describe a continuous natural process where small quantities of cells are released into the bulk water causing 'background' contamination (Stoodley et al., 2001). Furthermore it is assumed to be effective over the entire biofilm surface. In contrast, sloughing refers to more significant detachment events that occur in an ephemeral manner. Cell clusters in these events can be as large as approximately 1600 cells (Stoodley et al., 2001) and can be a comparable size to the biofilm itself (Morgenroth and Wilderer, 2000). Released aggregates affect biofilm architecture. Spatial heterogeneity is increased (Telgmann et al., 2004), i.e. the biofilm can increase in "patchiness" (Stewart, 1993). Furthermore organisms within the biofilm can be redistributed (Morgenroth and Wilderer, 2000), and water biostability deteriorates. Sloughing events are, therefore, more likely to generate microbiological regulatory failures through considerable release of trapped particles and should be viewed as 'worst case' events.

### 2.4.6 Force Balance between Adhered Material and Hydraulic Forces

It has been well recognised that a balance exists between the hydraulic forces in a network and the resistive forces of the particulates associated with discolouration (Boxall et al., 2001; Prince et al., 2003; Walski, 1991). The particles are held by their own self-weight and any additional forces that come from the pipe wall, including the adhesive forces of cohesive material such as biofilm. When the hydraulic force exceeds these forces, the particles are released into the bulk flow, as illustrated in Figure 2.8. Undesirable material (e.g. trapped contaminants, bacteria, fungi) could be mobilised and consumed by customers, therefore inducing a potential health risk, without necessarily causing a discolouration failure. Discolouration only occurs when enough material is mobilised to be visually seen with the naked eye.

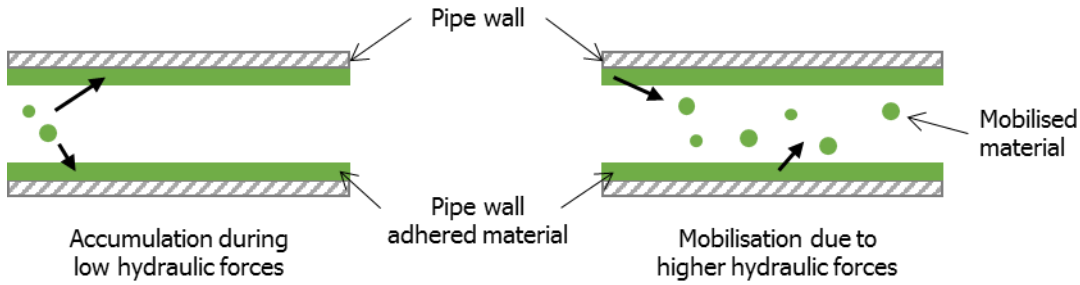


**Figure 2.8.** Concept illustration showing pipe-wall adhered material accumulation during low hydraulic forces, which is then mobilised by higher hydraulic forces.

An established relationship exists between the hydraulic forces and the material's adhesive strength (Boxall et al., 2001). The hydraulic regime imposes shear stresses on the material, which, in turn, conditions the strength of the EPS (Fish et al., 2015). If the DWDS material exists in cohesive layers as suggested by Boxall et al. (2001), aligning with biofilm research, it is believed that the layers would vary in strength and discolouration potential, i.e. the ability for the material to be mobilised. As the layers become deeper (approaching the pipe wall), there is an increase in the material's adhesive strength and decrease in discolouration potential. The minimum material strength required for a stable structure is the daily maximum hydraulic force, as any weaker biofilm will be eroded by the frequent shear. Any irregular forces, greater than the daily occurrences and equivalent conditioned material adhesion strength, pose a risk of more significant mobilisation, i.e. a sloughing event.

A semi-empirical model offered by Boxall et al. (2001) proposed that the stored turbidity volume, i.e. the volume of material capable of being mobilised, is related to the amount of applied shear stress greater than the conditioned shear strength of the material. This relationship can be seen in Equation 2.7:

$$\Delta C_e = \Delta t \, P \, (\tau_a - \tau_s')^n \qquad \text{Equ. 2.7}$$

Where $\Delta C_e$ is the amount of material removed in a time step, $\Delta t$ is the time step, $P$ and $n$ are coefficient and exponent values for a given system, $\tau_a$ is the magnitude of applied shear stress, and $\tau_s'$ is the material's shear strength. This later component varies based on the material layer exposed to the hydraulic force. The model, known as Prediction of Discolouration in Distribution Systems or *PODDS*, has been validated on many systems both in the UK (Boxall and Saul, 2005; Husband and Boxall, 2010) and abroad (Boxall and Prince, 2006). The model relies on the simple theory that adhered material is mobilised when the applied hydraulic shear stress is greater than the conditioning shear stress, Equation 2.8:

$$\tau_{applied} > \tau_{conditioning} \qquad \text{Equ. 2.8}$$

The *PODDS* model was generalised to non-specific cohesive material, yet it has been shown to effectively describe the development and strength behaviour of biofilms (Husband et al., 2016). Biofilm-specific models, including a 2-D model by Picioreanu et al. (2001), have been based on the same underlying concept. Furthermore, biofilm laboratory studies have shown that biofilm detachment is dependent on the change in applied shear stress, rather than the absolute value of shear stress (Bakke and Olsson, 1986; Peyton and Characklis, 1992; Telgmann et al., 2004).

These models do not consider the applied speed of the hydraulic shear; they are limited to gradual changes in hydraulic shear. Choi and Morgenroth (2003) suggested that dynamic changes in flow rate are more important in controlling biofilm thickness than the magnitude of the shear. Laboratory experiments performed by Husband et al. (2008) and Fish et al. (2017) tested the effects of two peak diurnal flow patterns as illustrated in Figure 2.1. These patterns describe variable flow which gradually changes over a 24 hour period. No simple, linear relationship was found between hydraulic variability and discolouration potential. The biofilms grown, however, did differ across several biological parameters for steady state and variable conditions, which would affect any mobilisation opportunities. This research implies that mobilisation of adhered material is affected by not only the magnitude of applied shear stress but also by the time period in which it acts.

### 2.4.7 Current Discolouration Management Techniques

It is believed that biofilms can never be fully removed from drinking water pipelines (Batté et al., 2003). A strongly adhered base layer of material is always present that is more cohesive and denser than other layers (Paul et al., 2012). Irrespectively, water companies are bound to perform DWDS cleaning to avoid the spread of disease and improve water quality for customers (Drinking Water Inspectorate, 2017b). One cleaning approach is to mechanically mobilise and remove the adhered material through controlled techniques. The frequency of cleaning necessary depends on the technique(s) used and its efficiency, and the priority of the section in the network. Current UK techniques include unidirectional flushing, pigging, water or air scour, and chemical dosing (Twort et al., 2000). There is little awareness of common operational conditions which produce the highest efficiency (Vreeburg, 2007).

The most common and longest applied method for cleaning networks in the UK is water flushing (Friedman and Holt, 2003; Seth et al., 2004). Flushing is predominately carried out as a reactive measure to areas where discolouration is already a problem. The technique uses the principles described in the previous section, i.e. when high flow is applied, more adhered material is mobilised. Additional flow is most commonly induced by opening a hydrant and 'blowing off' the extra water into the nearest sewer system entry point (Boxall et al., 2001). Customers can see this volume as an inconvenience and a waste of water

(Vreeburg, 2007). Occasionally there are increased customer complaints concerning discoloured water during and immediately after the flushing (Drinking Water Inspectorate, 2015a), thus flushing can have a negative operational image (Vreeburg, 2007). For example almost half of sampled iron levels that failed regulatory standards in 2014 were due to short-term, local network flushing events (Drinking Water Inspectorate, 2015b).

Usually pipes selected for flushing operations experience high turbidity levels when the hydrant is opened. The high velocities are maintained until the turbidity level measured through the hydrant reduces to a pre-selected level. This level varies greatly between water companies giving little uniformity in operations. Derived from Shield and Stokes equations, which have been shown to not apply to discolouration particles (section 2.4.4), the theoretical minimum velocity used in flushing should be 1.5 m/s (Brashear, 1998; Slaats et al., 2003). Actual velocities used by most operators tend to be significantly higher than normal daily maximum velocities and easy to achieve with standard hydrants. However the velocities used are typically flexible, inconsistently applied and difficult to monitor in the field.

As an alternative to these infrequent flushing velocities, networks in the Netherlands installed since 1999 have adopted 'self-cleaning' velocities and consequently scaled pipe diameter (van den Boomen and Vreeburg, 1999). These networks experience a designed hydraulic condition of at least 0.4 m/s on a regular basis in an attempt to re-suspend particles and prevent particles from accumulating (Vreeburg et al., 2009). Measurements have shown that this technique produces a cleaner system than conventional networks; however it is unclear as to what the actual velocity required for resuspension is and how often the self-cleaning must occur (Blokker et al., 2010).

Further highlighting the inconsistent nature of cleaning operations, whilst the above recommendations are velocity-based, others are shear-stress based. Velocity thresholds are more practical for operators, yet shear stress is more accurate if certain pipe conditions are known (Armand et al., 2015). Husband and Boxall (2010) suggested that different flushing shear stresses may be appropriate as a function of pipe material, for example they recommended a value of ~ 1.2 $N/m^2$ for plastic pipes. On the other hand, Cook and Boxall (2011) saw no further discolouration above a shear stress of 0.7 $N/m^2$ in plastic pipes. Ackers et al. (2001) advised a shear stress of 1 $N/m^2$ for recent weakly adhered material and 2.5 $N/m^2$ for older deposits. However, this larger value is based on design principles for sewer systems and may not be suitable for distribution systems.

Water companies have been investing significantly in management techniques to reduce the number of customer complaints regarding discoloured water, yet there are still 6.7 million people affected each year. Hence, an improved understanding of the factors controlling discolouration events, i.e. mobilisation of adhered material, is vital.

## 2.5 Transient Mobilisation

Previous DWDS research has alluded to the ability of hydraulic transients to mobilise adhered and cohesive material, thus causing a risk to water quality. These studies have stated that high intensities of shear are generated during transient events and may cause biofilm sloughing and particle resuspension (Boulos et al., 2005; Brunone et al., 2000; Wood et al., 2005). Yet an accurate link between pressure transients and water quality changes has not yet been established (Besner et al., 2007). These statements are mentioned in a general context rather than being the research focus.

This section reviews current literature investigating the ability of hydraulic transients to mobilise adhered material. This is explored in several contexts: drinking water distribution systems (section 2.5.1), biofilm research (section 2.5.2), and other structure-fluid based industries (medical field, geotechnical engineering and food industry) (sections 2.5.3 to 2.5.5). Although the generation and definition of hydraulic transients may be different to those described in the water industry, in these other industries dynamic effects are believed to be produced but are not evidenced.

### 2.5.1 Drinking Water Distribution Systems

Grayman et al. (1988) first proposed the use of dynamic hydraulic models as a subsequent input to water quality models. Successive transient models (Naser & Karney, 2008; Aisopou et al., 2010) simulated dynamic shear stresses and turbidity, using the discolouration model proposed by Boxall et al. (2001). These models were then compared to the results of field hydrant turbidity data drawn from Boxall et al. (2003) with inconclusive results. There are a number of possible reasons for this; most notably no high temporal resolution pressure data was collected during the field work to confirm the occurrence of a transient (Boxall and Saul, 2005). It was most likely that the valve was not rapidly opened as assumed in the modelling studies. Furthermore there were likely to be non-cohesive sediments, i.e. deposits resulting from gravitational settling, besides cohesive material as the pipeline was not flushed before the test. However, Aisopou et al. (2010) do recognise the need to investigate the physical processes underlying the interaction between the transient and mobilised material. Pothof and Blokker (2012) applied a water hammer model to sedimentation in a DWDS in the Netherlands. They found that the water hammer model did not result in essentially different flow distribution patterns compared to rigid column and quasi-steady models; only an additional velocity oscillation of approximately 0.02 m/s was generated. However, the model was not verified with sufficient flow measurements and the critical shear stresses generated were compared to non-cohesive particulate using Soulsby's

model (Soulsby, 1997), where the material typically found in active DWDS exhibits cohesive properties.

Physical transient mobilisation trials were performed by Mustonen et al. (2008) in a pilot scale DWDS where valves were rapidly closed for 5 seconds before being rapidly opened creating pressure shocks. Aisopou et al. (2012) similarly monitored a pump trip (rapid decrease then increase in flow rate) in an operational system. In both trials, concentrations of materials and turbidity increased after the dynamic events suggesting transient mobilisation. Again, no high temporal resolution pressure data was presented to confirm that a transient did occur. Furthermore these studies do not exclude steady state forces as the cause of particle mobilisation or separate effects due to opening or closing transients.

Karney and Brunone (1999) performed a valve closing transient in a distribution system in Recanati (Italy). An automatic control valve was used to generate the dynamic event in a steel pipe. Here, the pressure data verifying a transient is presented and the 'rusty crust' material was able to resist mobilisation by the initial flow rate. Poor water quality was observed after the end of the testing programme. Furthermore the water company received discolouration complaints by customers approximately six hours after testing. This research is highly suggestive of the ability for valve closing transients to cause mobilisation. However, as the authors do not evidence any repetition, it could be considered a chance occurrence.

### 2.5.2 Biofilms

Biofilm research has experimentally explored biofilm detachment due to rapid increases in shear stress. Choi and Morgenroth (2003) grew biofilms in an annular reactor and rapidly increased the applied hydraulic shear stress by increasing the rotation speed of the reactor. They found that rapidly increasing the shear stress caused a significant increase in effluent suspended solids concentration and average particle size, i.e. biofilm detachment. Bakke (1986) reported similar instantaneous detachment events for increasing rotation of a tubular reactor. In addition, Mathieu et al. (2014) grew biofilms on glass and plastic surfaces placed in a rotating disc reactor where the shear stress was also increased with rotation. Similar to Choi and Morgenroth (2003), they reported pipe-wall biofilm cell counts decreasing by 56 % on average, i.e. detachment of 44 %.

These studies provide consistent results, yet are restricted in respect to the concept of transient mobilisation. Two fundamental limitations exist. Firstly, the authors do not evidence detachment levels due to gradually increasing the shear to the same value as the rapid increases. Therefore it cannot be conclusively stated that the increases seen were due to dynamic forces rather than gradual increases. Secondly, the time taken for the shear (rotation) to increase is of a longer scale when compared to DWDS and cannot be described as "instantaneous". For example, Mathieu et al. (2014) reported increasing the rotational

speed in less than ten seconds. The biofilms grown could exhibit similar properties to those found in DWDS by being supplied with drinking water as a source. On the other hand, the use of rotating systems contrasts the more linear DWDS pipelines, possibility affecting the hydraulic force-biofilm interaction.

### 2.5.3 Vascular Trauma

The blood circulation system is similar to DWDS in that it follows a distribution system from a pump (heart) and is pressurised. In fact, the field of hydraulic transients originated in part from investigating the flow of blood in arteries by Euler in 1775 (Chaudhry, 2014). Blood vessels, arteries or veins, are lined by a thin layer of flattened cells called the endothelium made of endothelial cells, illustrated in Figure 2.9. These cells are influenced by two hemodynamic forces; cyclical strain due to transmural pressure, and the shear stress generated by blood flow passing through the vessels. Typical shear stresses range between less than 1 dyne/cm$^2$ to 80 dyne/cm$^2$ (0.1 to 8 N/m$^2$) but can increase to greater than 600 dyne/cm$^2$ (60 N/m$^2$) at different sites within the same vessel due to curvature and configuration (Ballermann et al., 1998). Therefore, akin to DWDS, there is adhered material on the "pipe" that experiences shear.

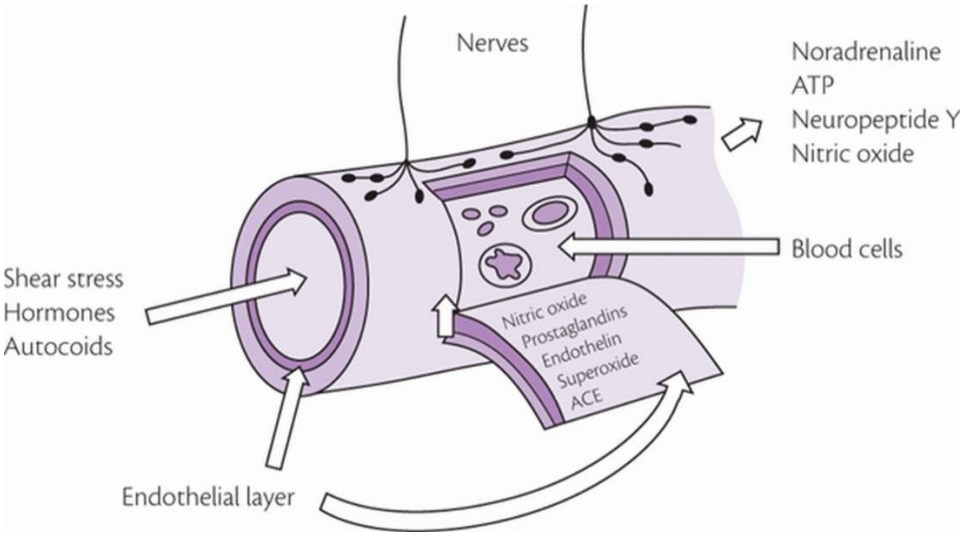


**Figure 2.9.** Illustration showing the endothelial layer between blood and the smooth muscle cells (Vallance and Channon, 2010). Only the endothelial cells are exposed to the shear stress generated by the blood flow.

Blood vessels can be injured via being crushed, punctured or severed (analogous to a pipe closure or burst). These actions are likely to provide acute shear stresses. Vascular trauma can lead to fatal complications such as thrombosis (a clot forms and interrupts blood flow to an organ or extremity) or bleeding. Gill et al. (2001) performed a study analysing the stresses of vascular trauma and found that rapid mobilisation of the endothelium occurs.

Vascular endothelial growth factor cells and circulating endothelial precursor cells are released. The first six to twelve hours after injury saw an almost 50-fold increase in these cells. Similarly Padfield et al. (2014) found an early appearance of $CD34^{+}CD45^{-}$ cells in circulation following vascular perturbation. They believe that the mechanical injury caused the $CD34^{+}CD45^{-}$ cells to be released from the coronary artery directly, thus the cells can be used as a measure of vascular injury.

Other experiments have monitored endothelial cells response to acute shear stress resembling those observed during endothelium injury. These experiments have shown that rapid mobilisation of $Ca^{2+}$ ions occurs from intracellular stores (Geiger et al., 1992), which then in turn causes secondary activation of $K^{+}$ ions. Many other chemicals are activated from membranes upon instigation of shear stress: inositol 1,4,5-trisphosphate, diacylglycerol, arachidonic acid, phospholipase A2, nitric oxide, prostacyclin, monocyte chemoattractant protein-1 (Bhagyalakshmi et al., 1992; Padfield et al., 2014).

The precise mechanisms of mechanical-chemical coupling are not fully understood, but these findings suggest that the acute shear stresses generated by blood vessel injury cause rapid mobilisation of cells. This aligns with the concept of transient mobilisation, i.e. a dynamic event can cause significant material mobilisation. Dynamic forces are not measured in the presented work, but the blood vessel events described are likely to be pseudo instantaneous, akin to valve operations in DWDS.

### 2.5.4 Colloidal Mobilisation

A colloid is a two-phase material in which microscopic (<1 μm) insoluble particles of one substance are dispersed throughout another substance. The colloidal particles are sufficiently small that they do not settle, or would take a very long time, because attractive van der Waals forces exist that are greater than gravity forces on individual particles. In geotechnical engineering, saturated clays are typical colloid substances.

It is established in geotechnical engineering that the mechanical energy of moving water imposes hydraulic shear forces that can surpass the van der Waals forces between particles. Increases in velocity will result in the release of colloidal particles (Shang et al., 2008). Saiers and Lenhart (2003) observed that at a given flow rate, only a limited amount of colloids could be released in column experiments. However, subsequent increases in flow rate led to further releases. Shang et al. (2008) also support this finding by testing step-wise increases in incoming flow rate. This behaviour is relatable to the hydraulic-adhered material force balance seen in DWDS.

Zhuang et al. (2007) examined mobilisation for single continuous infiltration and multiple infiltration pulses (three or four sequential events) for in situ colloidal sediments. Here transient flow was defined as 'temporal variability in water content and pore water

velocity', representing multiple abrupt events such as thunderstorms. The time period of these events is not given, therefore it is unknown how "rapid" these events are. The observed colloid concentrations in the effluent collected indicated that transient flow mobilised more colloids than the steady-state flow. This occurred both in the primary peak event and as a cumulative mass over the entire testing period; on average the multiphase infiltration liberated ~30% more colloids than the single-pulse infiltration. This corresponds with a study by El-Farhan et al. (2000) who also investigated mobilisation during transient infiltration events. Correspondingly they found peak particle concentrations near the rising and falling limbs of the hydrographs were two to six times higher than plateau concentrations. Zhuang et al. concluded that a pulse of transient flow is similar to a "hydrological activator"; colloids that are persistently held under steady-state conditions overcome the associated "energy barrier" for mobilisation. Nonetheless, their study is only preliminary in describing the exact mechanisms of colloid mobilisation under transient flow in porous media.

Fundamentally a DWDS pressure transient cannot be extrapolated to geotechnical engineering as the material does not experience rapid, oscillating pressures in the same constrained manner. However, these results imply that a dynamic increase in force can mobilise material not affected by steady state conditions, which does align with the aforementioned DWDS research.

### 2.5.5 Whey Protein Layers in Milk Treatments

The food industry is particularly analogous to drinking water systems as both systems necessitate stringent quality and hygiene regulations for consumption. In the dairy industry, milk and milk products are treated thermally. The increased temperature results in the breakdown of some proteins, minerals and fats, that adhere to the pipe surface forming fouling layers. These layers, known as whey protein layers, can decrease the thermal efficiency of equipment as they increase resistance to heat transfer. Cleaning is time consuming and expensive, thus optimising the cleaning process is strongly desired.

Several studies have tested the impact of flow pulsations, imposed on the steady flow by a pulsator, on the mobilisation of whey protein layers (Augustin & Bohnet, 1999; Bode et al., 2007; Gillham et al., 2000). The pulsations enhance shear stresses on the adhered layers and caused material mobilisation. Bode et al. (2007) showed the two parameters that influenced the cleaning process were maximum velocity and 'waviness', the intensity of the pulsation which causes flow reversal at the pipe wall. Increasing the maximum velocity reduces the time taken to clean the material layers (measured by fouling resistance). Increasing the 'waviness' ratio also cuts the cleaning time. Combined, these two effects can shorten the overall cleaning time by two and a half times (Bode et al., 2007; Gillham et al.,

2000). Bode et al.'s (2007) study determined the waviness as the dominant factor and recommended that operating conditions include pulsed flow with reversal effects.

Föste et al. (2011) performed transient computation fluid dynamic simulations and experimental tests on this pulsed flow approach. These were compared to the waviness-cleaning-time data collected from Bode et al.'s experiment. Both results followed the same characteristic curve; the total cleaning time is nearly constant when there is no flow reversal ($0<W<1$) but the cleaning time decreases suddenly when flow reversal occurs. Using the validated simulation, Föste et al. (2011) were able to predict the local enhancement of cleaning efficiency using pulsed flow.

Compared to the other environments examined, these situations are most comparable to DWDS pressure transients. Although not evidenced, the pulsator was expected to act on a similar time scale to transient-inducing valve operations and generate oscillating pressures. The dynamic events were shown to detach material (increasing cleaning efficiency), where the steady state conditions could not. Furthermore, flow reversal as a dominant factor in material mobilisation agrees with valve closing transient research that shows significant induced shear stresses due to near-wall velocity profiles (Brunone and Berni, 2010). However, these studies do not detail the properties of the whey protein layers for comparison to adhered DWDS material.

## 2.6 Summary

Extensive literature has shown that in DWDS there are unwanted particles, such as metals, contaminants, and pathogens, which can adhere to the pipe wall. These particles are possibly trapped by the microbial biofilms growing on the internal pipe surfaces. These particles remain adhered until they are mobilised into the bulk flow. Entrained particles can lead to water quality failures, like discolouration, and potentially public health risks if significant material is released. Understanding the hydraulic forces that cause mobilisation of adhered material is key in managing water quality.

For water quality purposes DWDS are currently modelled as steady state systems with gradual changes in hydraulic force. However, emerging research is showing that transients frequently occur throughout the network and DWDS should be considered as dynamic. Previous transient research has suggested that forces induced during transient events may mobilise adhered material, otherwise not be impacted by steady state forces. Nevertheless, a pronounced finding from this review is the scarcity of research into this linking the two fields of adhered particle mobilisation and dynamic hydraulic events, in both drinking water contexts and other industries. Whilst some studies are suggestive, there is a significant absence of conclusive data principally evidencing the occurrence of transients with high speed pressure data. Besner et al. (2007) stated that an accurate link between pressure

transients and water quality changes has not yet been established. Furthermore, there is little attention focusing on how transients induce mobilising forces, i.e. the mechanisms for mobilisation.

Rigorous investigation of the impact of transient dynamics on mobilisation of adhered material is vital as existing techniques are not adequately reducing discolouration failures. Combining this with knowledge of the adhered material present will challenge the historically structural based applications of transient research and potentially open a new field of enquiry.

# Chapter Three

# Aims and Objectives

Literature has shown that for wall-bound adhered material to be mobilised, hydraulic forces must exceed the material's adhesive strength. In steady state environments, if the material is conditioned by a high flow, a lower steady state flow will not cause mobilisation. A transient induced by rapidly transitioning between two steady state conditions could theoretically induce short-duration oscillating dynamic forces. If these forces are greater than the conditioned adhered material strength, then material will be mobilised by the transient and not by steady state conditions. This theory is graphically represented in Figure 3.1. Research testing this theory is necessary as dynamic mobilisation of material into the bulk flow could lead to drinking water quality issues not currently anticipated.

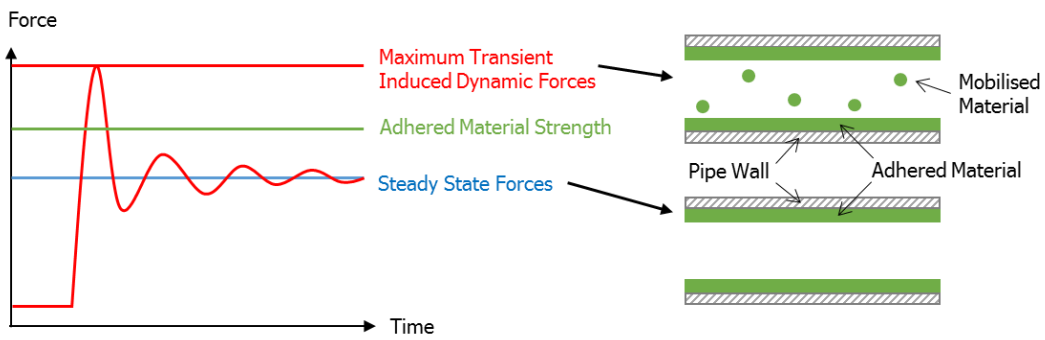


**Figure 3.1.** Graphical representation of the theory investigated: steady state forces are lower than the material adhered strength thus mobilisation does not occur. Initial and final conditions of the transient do not exceed this steady state condition, yet the dynamic forces induced could surpass the material strength and cause mobilisation.

The aim of this research was to investigate if transient forces can cause mobilisation of adhered material that cannot be mobilised by steady state flow at the same initial or final conditions. Then to investigate what aspects of transient behaviour could drive mobilisation. This study had four main objectives:

1. To develop an investigative technique in order to address the aim of this research. This technique would necessitate control, repeatability and reliability.
2. To determine, for sets of trials across a wide range of conditions, if transient induced forces can mobilise adhered material where steady state flow conditions cannot.
3. To compare mobilisation of replicated adhered materials, becoming more representative of operational DWDS.
4. To understand and interpret the relative significance of transient forces that might contribute to material mobilisation.

# Chapter Four
# Methodology and Methods

## 4.1 Introduction

Previous research investigating transient mobilisation of adhered particles in DWDS suggests that there is increased mobilisation of material after a dynamic event has occurred. The limitations of these studies, however, mean that there is an absence of conclusive evidence demonstrating mobilisation due to transients, rather than a change in steady state forces. This chapter will present experiments that aim to examine this phenomenon. The first half of this chapter will describe the development of the experiments, and the second half will describe the methods taken.

## 4.2 Methodology

### 4.2.1 Introduction

This methodology is broken down into three sub-sections. The first examines why laboratory experiments were used to generate a representative hydraulic system (section 4.2.2). The second section explains why cohesive material was replicated for this work and how the system to achieve this was developed (section 4.2.3). Experimental methodology is reported in the last section to show how the two systems (hydraulic and material) were used together (section 4.2.4).

### 4.2.2 Representative Hydraulic System

#### 4.2.2.1 Selecting Laboratory Experiments

There are multiple ways to explore the concept of transient mobilisation. Quantitative studies can include numerical simulations, physical experiments performed in the field, or laboratory studies. Previous work to demonstrate transient mobilisation, section 2.5, included all three of these approaches, and there are advantages and disadvantages to each.

Numerical simulations, or computer modelling, can be a useful way of testing a complicated scenario. Researchers can explore extreme cases in a systematic one-factor-at-a-time manner with no risk. This is highly beneficial when testing water quality as there is no risk of physical repercussions, such as discoloured water reaching customers or causing damage to infrastructure. However, there is currently no conclusive base knowledge or experimental data set for a numerical simulation to validate and verify against.

A physical alternative is field work, i.e. testing in operational drinking water networks. Whilst this may be the most realistic option in testing transients and organic systems in situ, there are several disadvantages. Firstly, complete control over the system is rare. There are many uncontrollable factors that can alter the system and affect the experimental outcome. For example, a pipe may burst causing the transient response to change, or instrumentation could only be installed in certain locations due to limited entry to the pipeline under a busy road. Furthermore, the ability to perform repeats is significantly limited in operational networks, as no two sections have the same infrastructure (e.g. pipe diameter, material) and organic material (e.g. structure, strength). Without this ability, it becomes challenging to conclusively demonstrate verification of the results collected. However, probably most critical for water companies, there is a risk to water quality and DWDS infrastructure.

Physical laboratory experiments offer several advantages. Representative and extreme experiments can be tested in a systematic manner to provide a thorough exploration of the processes occurring. Furthermore, there is increased, but not complete, control over the system compared to field studies. Instrumentation, for example, can be installed in different locations to measure different effects. Laboratory experiments can never fully simulate the intricacies of an operational network, for example laboratory pipelines do not tend to experience the same degree of corrosion and wear; hence there will be an element of artificiality in any model. Interpretation and scaling of results would be required as the intricacies of an operational network cannot be fully accounted for, as well as time taken for appropriate facility design. Yet, any risk to operational networks and customers is bypassed.

Consequently, laboratory experiments were chosen for this work. Strict control can be placed over the system so that rigorous experiments can be tested in a systematic manner to provide a thorough grounding of the processes occurring. With good design and operation, laboratory facilities can allow the study of subtle phenomena that could be overshadowed by temporal and spatial variability in an operational system.

#### 4.2.2.2 The Laboratory Facility

The laboratory facility used in this research needed to be representative of operational networks. The pipeline necessitated a modern DWDS material, a typical pipeline diameter, and hydraulic conditions that encompass the typical values discussed in sections 2.2.3 and 2.2.4, as well as more extreme events. The facility used is based at the University of Sheffield and was selected as it met these requirements. It consists of a reservoir, pump and pipeline configured as a recirculating system. The pipeline is made of medium density polyethylene (MDPE) and has an internal diameter of 50 mm. Furthermore the flow rates and pressures can range up to approximately 4.50 l/s and 47 m, respectively.

#### 4.2.2.3 Selecting Dynamic Events

In operational networks, transients can be produced by a variety of sources, including but not limited to; valve operations, pump trips, flow demand and burst events. These were discussed in section 2.3.1. Valve operations are the most common instigators of dynamic events, and the resulting transients are representative of most transients recorded in operational systems. For example, a pump trip can be recreated via a rapid valve closure followed by a rapid valve opening. Consequently, valve operations were selected to generate all transients induced in the laboratory experiments. These actions included valve openings and valve closings for a variety of initial and final conditions.

### 4.2.3 Replicating Adhered Material

An important component of this research was to design an experimental setup to replicate the significant features of pipe-wall adhered organic material whilst being repeatable and controllable. Organic material is extremely variable and time consuming to accumulate and test. Comparing the effect of different hydraulic forces on organic material with a high level of certainty can therefore be problematic, as the variation in material properties could be greater than the variability in hydraulic forces.

From reviewing literature, see section 2.4.5, several key features of organic material emerged that are consistent across their complexities. These features are adherence to the pipe surface where this adherence force is greater than the material's self-weight, variable adherence strength, and material structure. A key requirement of this research was to design an analogue to replicate these features with high repeatability and control.

An innovative solution was developed using an electromagnet. When ferritic particles enter an electromagnetic field they experience an attractive force towards the electromagnet, greater than the particle's self-weight. This force can be controlled and quantified by applying different magnitudes of current through the electromagnet. In this work, an electromagnet was placed flush against the outside of the pipe and magnetic particles placed on the pipe invert, see Figure 4.1. Current was, therefore, used as a quick, controllable, and repeatable method of quantifying the pipe-wall adhesion force the particles experienced.

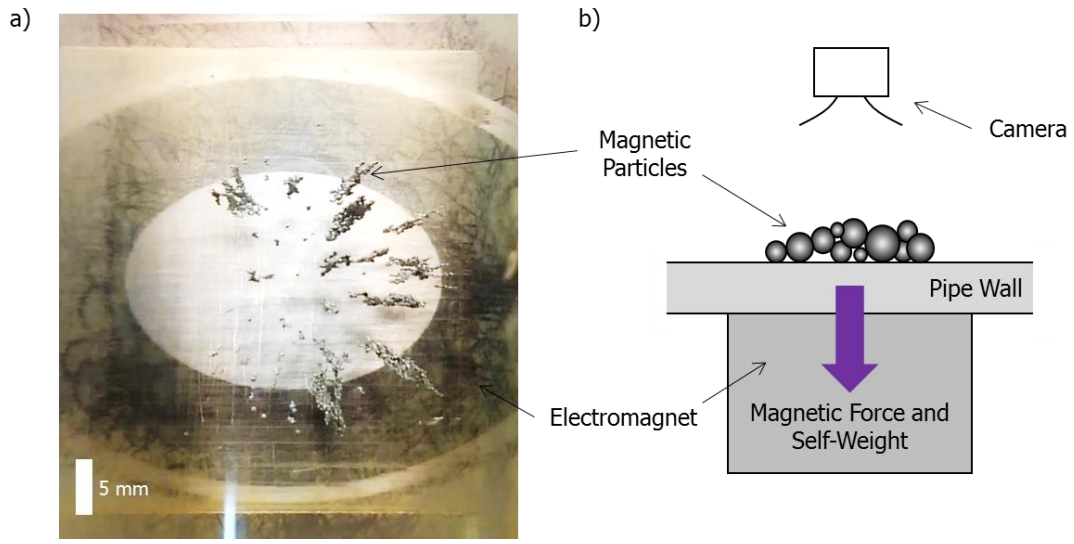


**Figure 4.1.** Photograph (a) and schematic (b) of ferritic particles in the pipe invert held by the electromagnet under the pipe. A camera was placed directly above the particles to record the particles.

Two types of magnetic particles were selected to represent the pipe-wall adhered material structure. To understand ideal behaviour, the first set of particles were 500 µm spherical ball bearings (Simply Bearings, 2015) used individually. These particles were highly repeatable and had a basic structure, thus their behaviour would be the simplest case to understand the hydraulic effects. To replicate cohesive layers of organic material, i.e. more representative of operational DWDS, the second set of particles were 35 – 145 µm more irregular particles (Sandvik, 2013) used as a powder. The steel alloy grade for the powder was SAF 2507, thus these particles will be called SAF 2507 particles from here on out. The particles would normally exhibit some degree of interlocking under their own self-weight. However, when placed in the electromagnetic field, these particles became magnetised and experienced additional magnetic bonds between themselves, replicating the cohesive forces of typical organic material.

Together the electromagnet and particles created a quick, repeatable and controllable system to replicate the key organic material features identified. Critically this magnetic analogue was developed so that adhesion force from the electromagnet was the dominant force, rather than the particle's self-weight.

### 4.2.4 Experimental Methodology

The first objective of this work was to design a system where hydraulic conditions and replicated adhered material can be tested simultaneously. This was achieved by installing the electromagnet into the laboratory facility. Here, experimental methodology is outlined in

to show how the aim of this research was addressed; to conclusively demonstrate the ability of transients to cause mobilisation of adhered particles, where steady state conditions cannot.

#### 4.2.4.1 Defining Mobilisation

When hydraulic forces surpass the resistive forces of an adhered material, weaker bonds of the material can irreversibly break causing fragments to be entrained in the flow. This is described in section 2.4.5. It is therefore reasonable to describe such an event as streamwise movement from the original location, or mobilisation of the fragment. In this work, mobilisation of the magnetic particles was defined in an equivalent manner; particles were mobilised if they were carried further than a distance-based threshold in the streamwise direction. Determination of this threshold is discussed in section 4.3.5.

#### 4.2.4.2 Current to Quantify a Mobilisation Force

To cause mobilisation in operational systems the hydraulic force is increased to overcome the strength of the adhered material (section 2.4.6). In the laboratory facility, whilst the hydraulic forces were well controlled, the use of replicated material meant that greater control was placed over the adherence (magnetic) force. This was due to the magnetic force being controlled and quantified via current through the electromagnet. Thus, the experimental methodology was reversed: the hydraulic force was established and the magnetic force slowly reduced in steps until the particles just mobilised, see Figure 4.2. At the point of mobilisation, the magnetic force created by the electromagnet must be slightly lower than the hydraulic force for mobilisation to occur. Therefore, the current at which mobilisation occurred for that particular hydraulic force became, effectively, a mobilisation force for those hydraulic conditions.

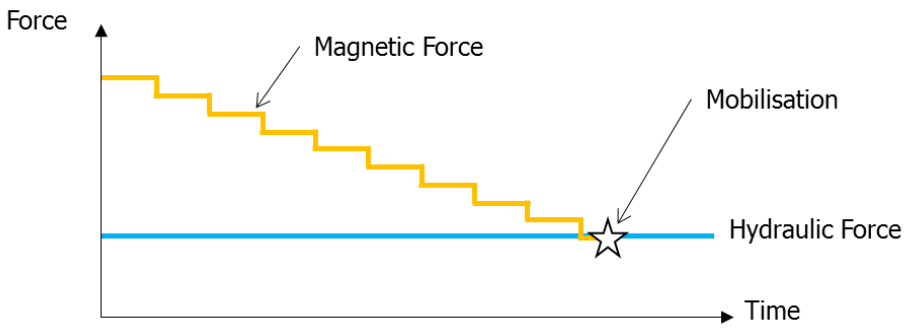


**Figure 4.2.** Schematic of the magnetic force decreasing in controlled steps until the magnetic force is just lower than the hydraulic force, causing mobilisation.

#### 4.2.4.3 Mobilisation Force Relationships

The experimental approach taken was to develop mobilisation force relationships: hydraulic forces and magnetic forces at the point of mobilisation, for a variety of hydraulic

conditions. Comparison of these relationships for different steady state and dynamic hydraulic conditions would determine if transient tests can cause mobilisation where steady state cannot.

Figure 4.3 presents a schematic of possible transient and steady state mobilisation force relationships. Linear relationships are drawn as the simplest association possible, which may or may not pass through the origin. The area above each relationship indicates that the magnetic forces are too high for mobilisation to occur due to the hydraulic force. The area below each relationship indicates the magnetic forces are too low, thus mobilisation would occur due to the hydraulic force. If transient relationships sat above the steady state relationship, as illustrated in Figure 4.3, an area would exist where the transients can cause mobilisation but steady state cannot (green highlight).

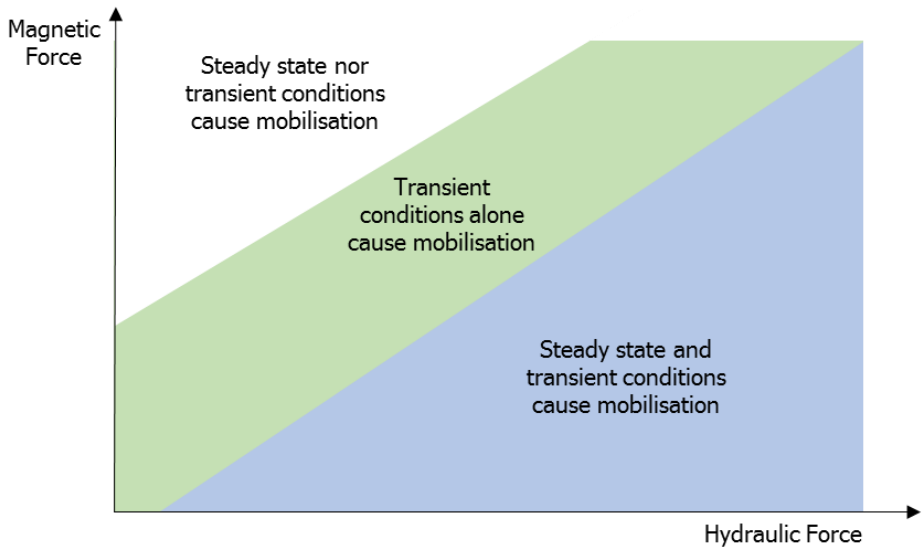


**Figure 4.3.** Schematic of mobilisation force relationships between hydraulic force and magnetic force at the point of mobilisation. The transient relationship sits above the steady state relationship, indicating conditions where transient conditions can cause mobilisation, but steady state conditions cannot (green highlight). Linear relationships are drawn as the simplest association possible, which may or may not pass through the origin.

#### 4.2.4.4 Valve Operations

To test the simplest and most convincing case of transient mobilisation, valve closing transients were performed first. For these transients, the flow transitions from an initial flow rate to lower final flow rate, i.e. there is decelerating flow. The adherence forces acting upon the particles must be able to resist the initial flow rate. If the valve were closed gradually the hydraulic force would slowly decrease and the particle would stay in its initial position. However, if the valve were closed rapidly, any possible mobilisation of the particle can only be due to the dynamic forces generated.

To test accelerating flow, valve opening transients were performed. For these transients, the flow transitions from an initial flow rate to higher final flow rate. These are more complex than the closing transients as there is an inherent increase in steady state hydraulic force, in addition to any potential dynamic forces. Therefore, the adherence forces acting upon the particles must be able to resist the final flow rate. Comparison of mobilisation due to the valve opening transients and mobilisation due to steady state would separate these two effects.

## 4.3 Methods

### 4.3.1 Introduction

The second half of this chapter describes the methods undertaken. It is broken down into six sub-sections. The first details laboratory specifications including facility infrastructure, equipment and data collection (section 4.3.2). The second outlines how transients generated were rapid and repeatable (section 4.3.3). The following sub-section builds on the previous development of the electromagnetic system to show how the repeatable adhered particles were managed (section 4.3.4). The distance-based threshold (sections 4.3.5 and 4.3.6) and the experimental programme (section 4.3.7) are then detailed.

### 4.3.2 Laboratory Specifications

An experimental facility at the University of Sheffield was utilised in this work. It was designed for transient testing in viscoelastic pipes, funded by EPSRC grant EP/G015546/1. The laboratory consists of a single 141.4 m pipeline of 12 bar rated MDPE pipe (PE80). The nominal internal diameter (ID) is 50 mm and external diameter (ED) is 63 mm. The pipeline was constructed in an elliptical manner, see Figure 4.4, so that there are eight long loops from beginning to end held by supports which allow minimal longitudinal movement.

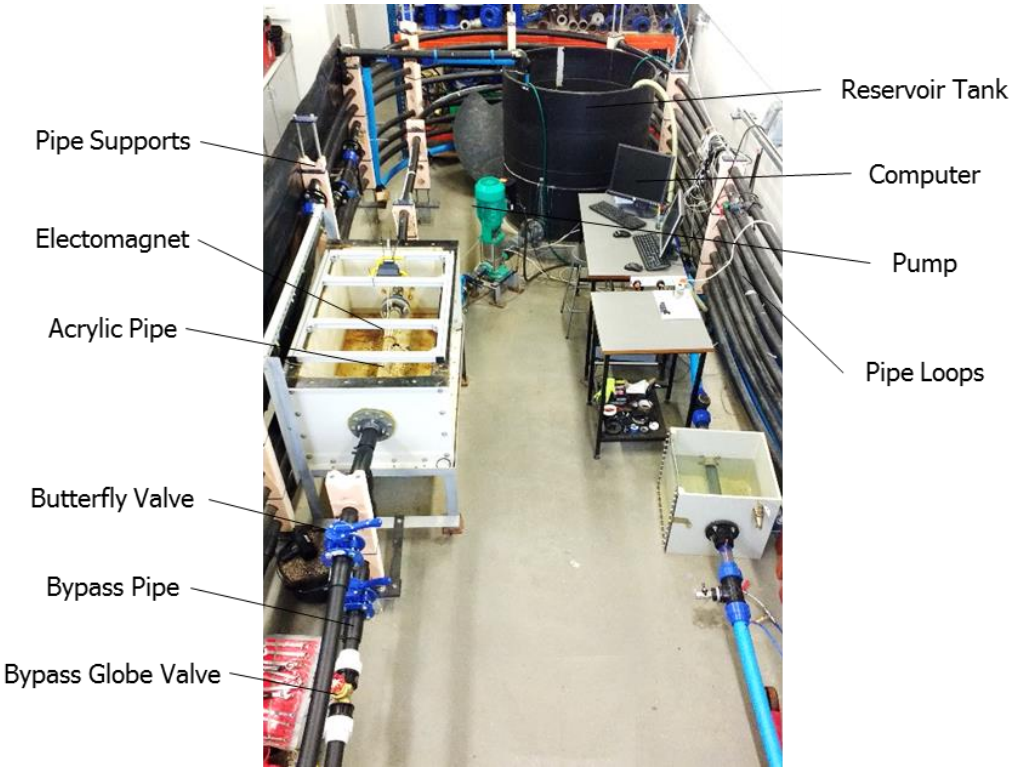


**Figure 4.4.** Photograph of the laboratory facility with key visible features indicated. Note: the blue pipe system on the right hand side is separate and not associated with this work.

The system is fed from a reservoir tank, volume ~1 $m^3$, configured as a recirculating system using drinking water from the local network supplied via a standard plumbing tap. To control microbial growth, the system was dosed with 24 ml of Rodolite H (sodium hypochlorite solution, < 16% free chlorine) every 14 days. Flow rate was controlled via two manual globe valves; one installed on a parallel bypass pipeline and the second manual downstream. Pressure was controlled by an upstream 3.5 kW Wilo MVIE variable speed pump. The bypass comprised of the same MDPE pipe for consistency. Sections of the pipe could be isolated by the globe valves and three quarter turn butterfly valves, the locations of which are outlined in Figure 4.5.

The electromagnet was installed at 82.48 m from the pump on a straight section of the pipeline. To see the magnetic particles, a 750 mm long section of transparent acrylic pipe (equal ID of 50 mm and ED of 63 mm) replaced the opaque MDPE pipe. This can be seen in Figure 4.4. The acrylic section was aligned so that the electromagnet was central.

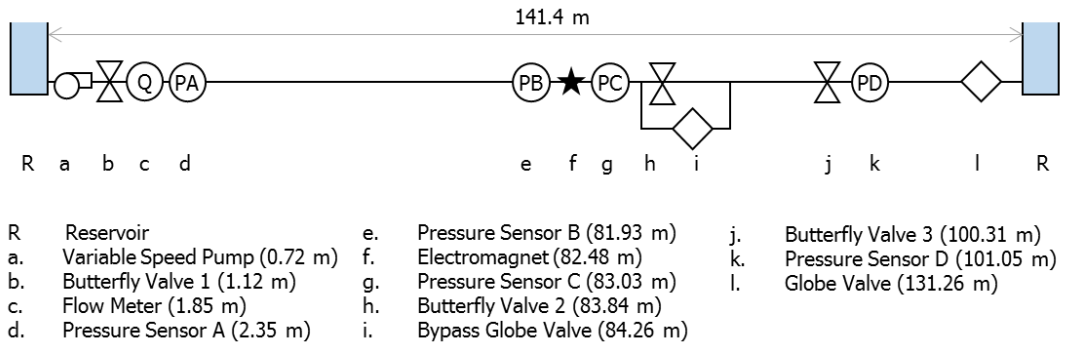


**Figure 4.5.** Laboratory schematic, including key features and distances from the reservoir.

4.3.2.1 Equipment

Online monitoring of pressure and flow was achieved using a data acquisition device (DAQ). The specifications of all laboratory equipment used can be found in Table 4.1. The equipment was regularly calibrated against independent measures to ensure accuracy. High speed (2000 Hz) pressure sensors were used. A high speed flow meter sampling at the same frequency for one-to-one pressure/flow mapping would ideally have been used. However, such a highly specialised instrument was unobtainable in this work. As the flow rate parameters of interest were steady state based (pre and post transient), a low frequency flow meter was used instead.

**Table 4.1.** Laboratory equipment specifications.

| Parameter | Instrument | Manufacturer | Range | Sampling Frequency | Resolution |
|---|---|---|---|---|---|
| Flow | Flow Systems Model 910E Electronic Flow Meter | Roxspur, U.K. | 0.1 to 5000 l/s | ~3 Hz | ± 0.001 l/s |
| Pressure | Gems 2000 series Pressure Sensors | Gems Sensors and Controls, U.S.A. | Vacuum to 24 bar | 2000 Hz | ± 0.16m |
| Flow and Pressure | USB-6009 DAQ | National Instruments, U.S.A. | -10 to 10 V | 2000 Hz | 7.73 mV |
| Adhesion | Electro-holding Magnet | Eclipse Magnets, U.K. | 0 to 425 mA | N/A | ± 1 mA |
| Mobilisation | High-Speed Camera Model X2-X7 | Mega Speed, U.S.A. | N/A | 393.6 fps ± 0.9 fps | Up to 1920 x 1080 pixels |

The electromagnet chosen was a circular magnet 40 mm in diameter, as seen in Figure 4.1 a). This size of magnet was chosen for two reasons. Firstly, for practical reasons, the magnet needed to be smaller than the external pipe diameter (63 mm). Secondly, the 40 mm electromagnet had the largest magnetic field strength (H-field) when compared to other diameters of electromagnet from the same manufacturer, thus was likely to produce a greater range of results. The electromagnet used was an electro-holding magnet, which means that it is magnetised when direct current is applied. The higher the current, the higher the magnetic (adhesive) force.

#### 4.3.2.2 Software for Equipment Control and Data Collection

LabVIEW software (National Instruments Corporation, 2015) was used to extract the relevant data for flow and pressure from the acquisition device. This information was visually displayed in real time on the computer, as well as being stored for later analysis. LabVIEW was also used to specify and control the current through the electromagnet. The changes in wire resistance due to thermal effects were controlled by a variable resistor connected to the electromagnet. A current resolution of 1 mA was set through the LabVIEW software, but the accuracy is likely to be significantly higher.

Mega Speed Camera Control software (Mega Speed, 2017) managed the high-speed video camera, which is discussed in section 4.3.5. Again, this information was visually displayed in real time on the computer, as well as being stored for later analysis.

#### 4.3.2.3 Pressure at the Electromagnet

Four pressure sensors were distributed across the system as illustrated in Figure 4.5. They monitored the pressure in different sections of the pipeline; upstream "PA", near the electromagnet "PB" and "PC", and downstream "PD". This was designed so that when sections of the pipeline were isolated via valve operations, the pressures in the different sections could still be known. The critical pressure needed was the pressure at the electromagnetic system, as it was the most representative of the pressure experienced by the magnetic particles. The two pressure sensors "PB" and "PC" were used either side of the acrylic pipe as, due to their close proximity, the pressure responses were extremely similar. This created a fail-safe in case one of the sensors broke during testing. In this work, any pressure values given were collected from "PC" unless stated otherwise.

### 4.3.3 Generating Transients

#### 4.3.3.1 Rapid Valve Operations

Transients are typically described as 'instantaneous' or 'rapid' when the valve operation time is less than the pipeline period (section 2.3.6.1). Butterfly valves were used in

the system as they are known for quick operation; a controlling lever can be manually turned from one position to another in one swift movement. To determine if the butterfly valves met the pipeline period criteria, high speed videos were recorded of example transient-inducing valve operations. The videos showed that the operation times achieved were 0.19 s ± 0.04 s. For the butterfly valve at a distance of 84 m from the pump, the pipeline wavespeed would have to be greater than 880 m/s for these transients to not be instantaneous. Typical wavespeeds for polyethylene are 240 m/s to 425 m/s (Grann-Meyer, 2005), therefore valve operations in this facility produced instantaneous transients according to the pipeline period criteria.

#### 4.3.3.2 Repeatability of Valve Operations

Two methods were deployed in the laboratory facility to increase transient repeatability. Firstly, the manual valve operations were always conducted as quickly as possible and within the first pipeline period. Secondly, section 2.3.4.2 showed that transient features are affected by the viscoelastic property of polyethylene pipes. The material's elasticity means that as the transient propagates, the cross-sectional area of the pipe can alter due to differential water pressures, affecting wavespeed and damping effects. Therefore, to increase transient repeatability, the creep effects of the pipe were controlled to reduce variability in cross-sectional area.

Preliminary testing aimed to determine the conditions necessary to produce negligible creep effects for this laboratory system. The pump was run with continuous operation, to increase temperature and applied hydraulic stresses, over four days with wavespeed measured every 15 minutes during the day. Determination of wavespeed is detailed in section 6.4.1. Figure 4.6 shows the wavespeed decay over time, normalised by maximum wavespeed experienced. It can be seen that the wavespeed rapidly changes over the first 10 hours then plateaus, or 'conditions', at lower valve.

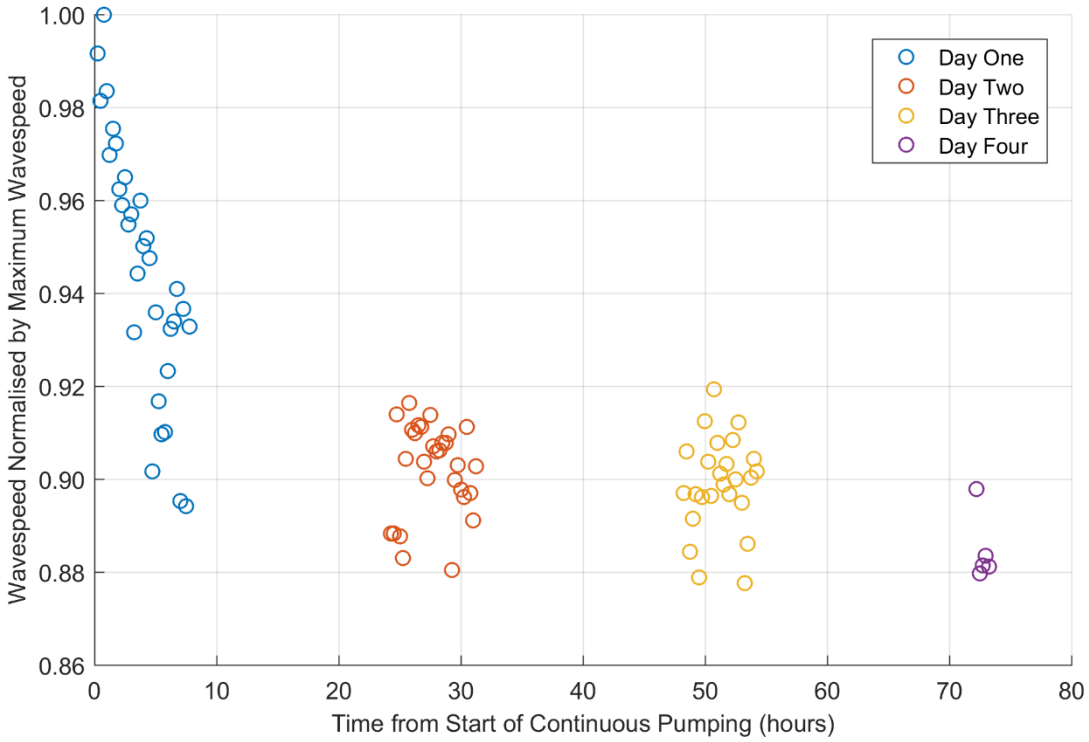


**Figure 4.6.** Wavespeed as a function of time since start of continuous pumping.

Based on this finding, the laboratory was run for three days before all experimental testing was conducted so that the pipeline produced repeatable wavespeeds and, therefore, transients. This was further reflected in the experimental programme. For example, if the applied water pressure had been reduced for five minutes then reapplied, testing would not commence for a following five minutes so that the pipe could return to its conditioned strain.

Figure 4.7 shows five repeats of an example valve opening transient for the first 0.1 s of the transient response. Each transient is aligned to the start of the pressure drop as the start of the transient response. Visually these are very similar and emphasise the repeatability of inducing the first dynamic surge. Figure 4.8 presents these same example valve opening transients over a longer period of 10 s. It can be seen that this repeatability continues over the entire period of the transient. To quantify, each repeat was compared to the 'average transient' to produce RMSE values of 0.19 m or less. These RMSE values are less than the standard deviation of initial steady state pressure data, suggesting that the transients generated are highly repeatable. However, this method could be biased by aligning the transients to the start of the pressure response.

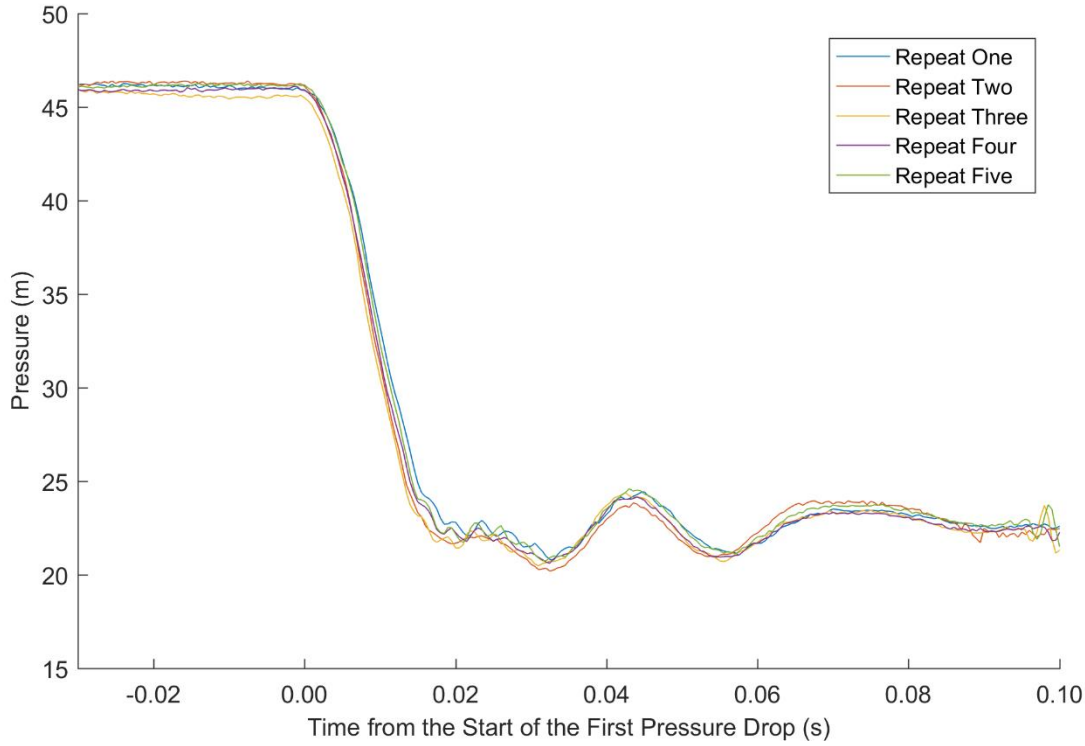


**Figure 4.7.** Pressure traces of five repeats of an example valve opening transient evidencing a repeatable pressure change over 0.1 s. Each transient is aligned to the start of the first pressure drop.

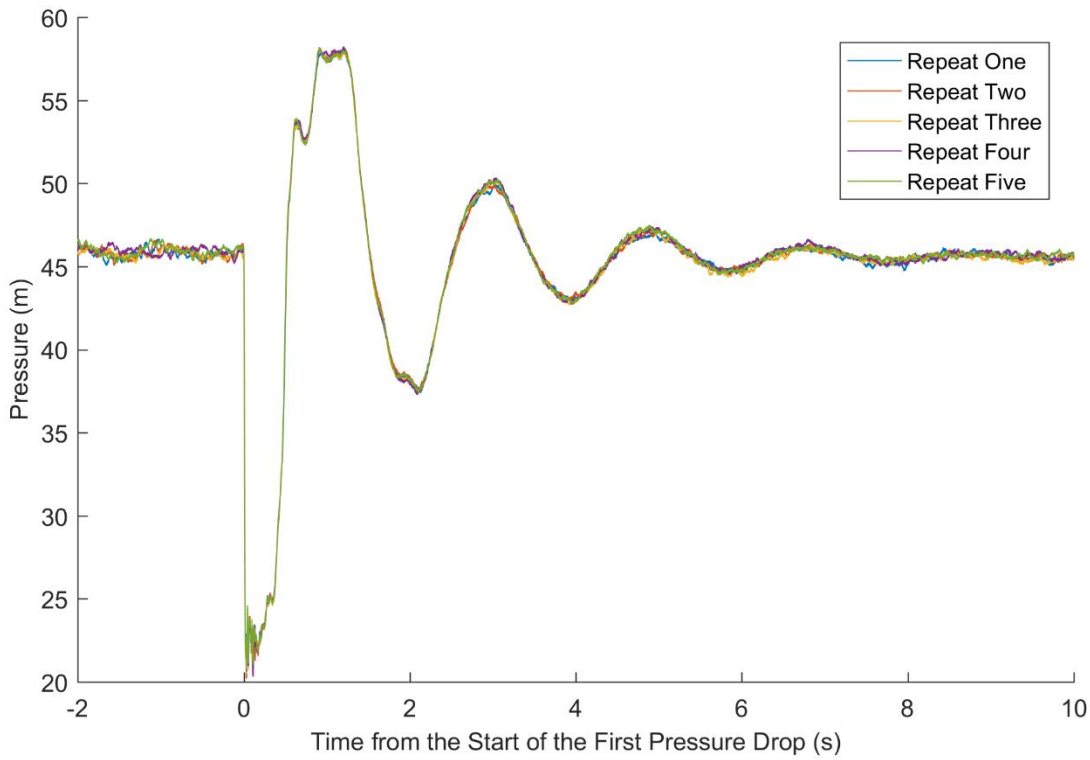


**Figure 4.8.** Pressure traces of five repeats of an example valve opening transient evidencing a repeatable pressure change over 10 s. Each transient is aligned to the start of the first pressure drop.

#### 4.3.3.3 Location of the Transient-Inducing Valve

The valve chosen in the facility to be the 'transient valve', i.e. only valve used to generate transients, was butterfly valve 2, see Figure 4.5 h). This valve was located 1.36 m downstream of the electromagnet. This valve was chosen as the dynamic effects experienced by the magnetic particles would be greatest compared to transients generated by the valves further away, i.e. less damping would occur for a closer valve. However, this also meant that the manual valve operations could transfer force from the valve to the acrylic pipe and cause the particle to mobilise.

To determine if structural forces were a factor to consider in mobilisation, preliminary tests were performed where the ball bearing particles were placed in the pipeline with minimal flow (0.1 l/s) and no magnetic force. The transient valve was then repeatedly struck with a mallet to simulate structural forces generated by the valve operations. The ball bearings did not mobilise, even when the valve was struck with considerable force. Thus, the valve operations were unlikely to transfer enough force through the pipeline to be a factor in mobilisation.

#### 4.3.3.4 Using the Bypass for Test Conditions

To test consistent physical movements and repeatable hydraulic forces, the transient valve was only used with full valve movements, i.e. the valve was moved from fully open to fully closed and vice versa. To increase the range of conditions that could be tested, a bypass with installed around the transient valve. The bypass allowed water could still flow round the system when the transient valve was fully closed, illustrated in Figure 4.9. The globe valve was used to control this flow rate.

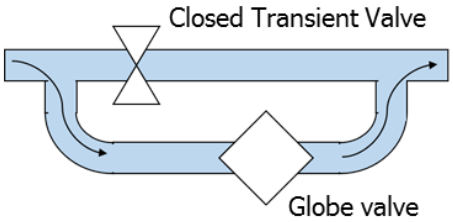


**Figure 4.9.** Illustration showing how the bypass was used to generate a system flow rate whilst the transient valve was fully closed.

For valve opening transients, without the bypass the only initial flow rate that could be generated was zero as the transient valve was fully closed. With the bypass, any initial flow rate could be generated using the bypass globe valve whilst the transient valve was fully closed. In either case, once the transient valve was opened, the downstream globe valve could be manipulated to cause any final flow rate.

For valve closing transients, the opposite scenario is true. Without the bypass, only zero final flow rates were permitted to the transient valve moving from fully open to fully closed. With the bypass, any final flow rate could be generated.

Transients were split into two sub categories based on whether the initial (valve opening) or final (valve closing) flow rates were zero or non-zero. If these respective conditions were zero, the transients were labelled as 'complete', i.e. no flow went through the bypass. If these respective conditions were non-zero, the transients were labelled as 'partial', i.e. some flow went through the bypass. Figure 4.10 demonstrates a) valve closing and b) valve opening transients that have complete and partial conditions.

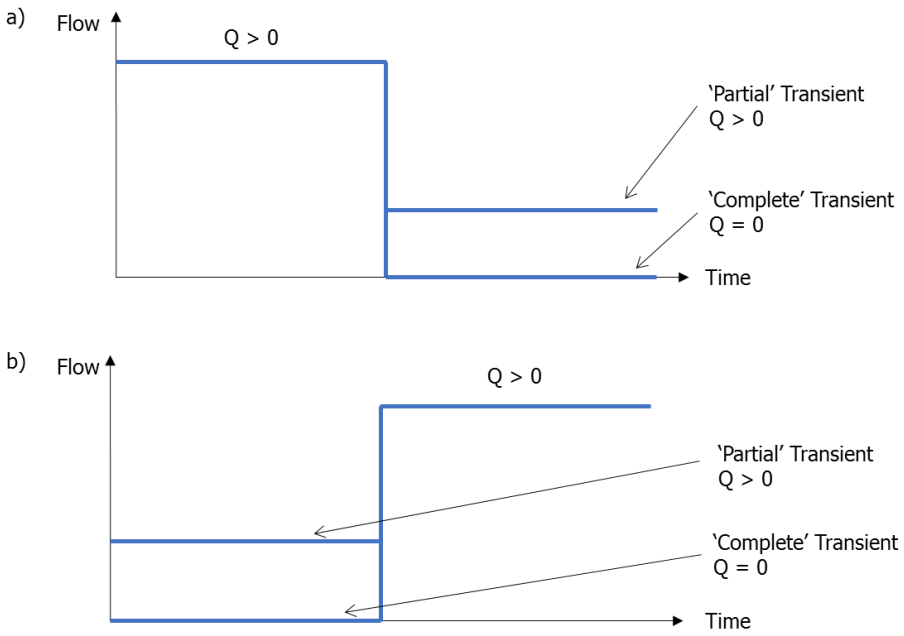


**Figure 4.10.** Schematic showing complete and partial a) valve closing, and b) valve opening transients.

### 4.3.4 Replicating Adhered Material

An important component of this research was to design an experimental setup to replicate the significant features of adhered material whilst being repeatable and controllable. This section will further detail management of the electromagnet and the magnetic particles previously introduced.

#### 4.3.4.1 Effect of the Magnetic Field on Water

Water is dipolar, meaning that that it can be affected when passing a magnetic field. The study of this effect is called magnetohydrodynamics and it forms the basis for magnetic flow meters (Davidson and Belova, 2002). Magnetohydrodynamics was briefly considered in this work to determine if the magnetic field of the electromagnet was interacting with the

local water conditions. A parameter known as the magnetic Reynolds number, $Re_m$, was calculated to quantify this interaction. The equation for this parameter is given in Equation 4.1.

$$Re_m = \mu \, \sigma \, v \, L \qquad \text{Equ. 4.1}$$

Where $\mu$ is the magnetic permeability of water (1.26 x $10^{-6}$ H/m), $\sigma$ is the conductivity of water (0.05 S/m), $v$ is cross-sectional average velocity, and $L$ is a characteristic length, usually pipe diameter in distribution systems. For the range of flow rates generated in this laboratory, the magnetic Reynolds number was on the order of $10^{-9}$. For scale, the magnetic Reynolds number of the Earth is on the order of $10^3$. As $Re_m$ was significantly less than one, magnetohydrodynamics was not a factor that needed to be considered.

#### 4.3.4.2 Temperature of the Electromagnet

The temperature of the electromagnet could have impacted the magnetic field generated. As the applied current increases, the temperature also increases. Consequently, the coil resistance also increases, affecting the current passing through the wires and potentially impacting the magnetic field. Discussed in section 4.3.2.2, the electromagnet control system was utilised that any temperature fluctuations were adjusted for, thus maintaining a constant field. Furthermore the electromagnet used had a limited current range so that the temperature generated was not significant enough to cause any variation in the magnetic field.

#### 4.3.4.3 Particle Details

The ball bearings and powder were outlined in section 4.2.3. The ball bearings were Grade 10 AISI 52100 particles, where the powder was SAF 2507 particles. Both sets were professionally manufactured and made of chrome-steel. The particles were therefore significantly dense, 7.83 g/cm$^3$, compared to around 1.3 g/cm$^3$ for discolouration material (Boxall et al., 2001). The high corrosion resistance of the chrome-steel ensured that the particle volume did not change when in the pipe, i.e. the water did not degrade the shape of the particles. This was an advantage for repeatable controllable experiments. However, the individual metallic particles cannot deform elastically as organic material can. Whilst this may limit direct comparison between the magnetic particles used here and the adhered material in DWDS, the effects would be consistent across the experiment.

The ball bearings were 500 µm ± 0.25 µm in diameter and highly spherical. The SAF 2507 particles were more irregular, see Figure 4.12. A laser diffraction particle size analyser, Malvin Mastersizer 3000 (Malvern Instruments Limited, 2013), was used to measure the size of the particles; 95 % were measured as between 31 – 144 µm in diameter. Figure 4.11 presents a size distribution of the particles showing the cumulative percentage of measured diameter bins. The value above the bars is the cumulative percentage value. These particles,

as well as the ball bearings, are larger than typical particle sizes in discoloured water (less than 50 µm in diameter, see section 2.4.2). However, the particle sizes are similar to the height of adhered material (Cowle et al., 2014).

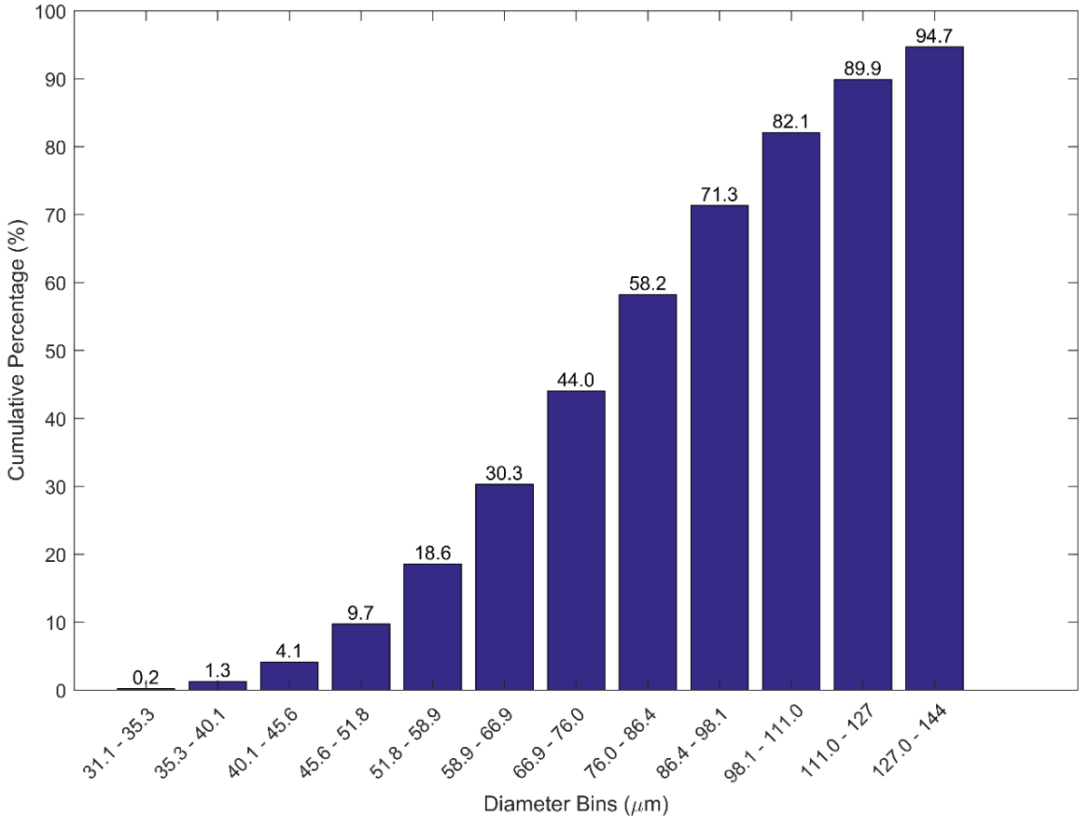


**Figure 4.11.** Cumulative percentage of SAF 2507 particle diameters.

Figure 4.12 shows two photographs of SAF 2507 particles mounted on an adhesive carbon dot and examined using secondary electron imaging in a scanning electron microscope (SEM). In this case the magnetic field could not be applied due to inference with the microscope. When the particles experience a magnetic field, they are more likely to coalesce or interlock due to the magnetic forces induced between them. This effect is analogous the EPS generated in biofilms, discussed in section 2.4.5.

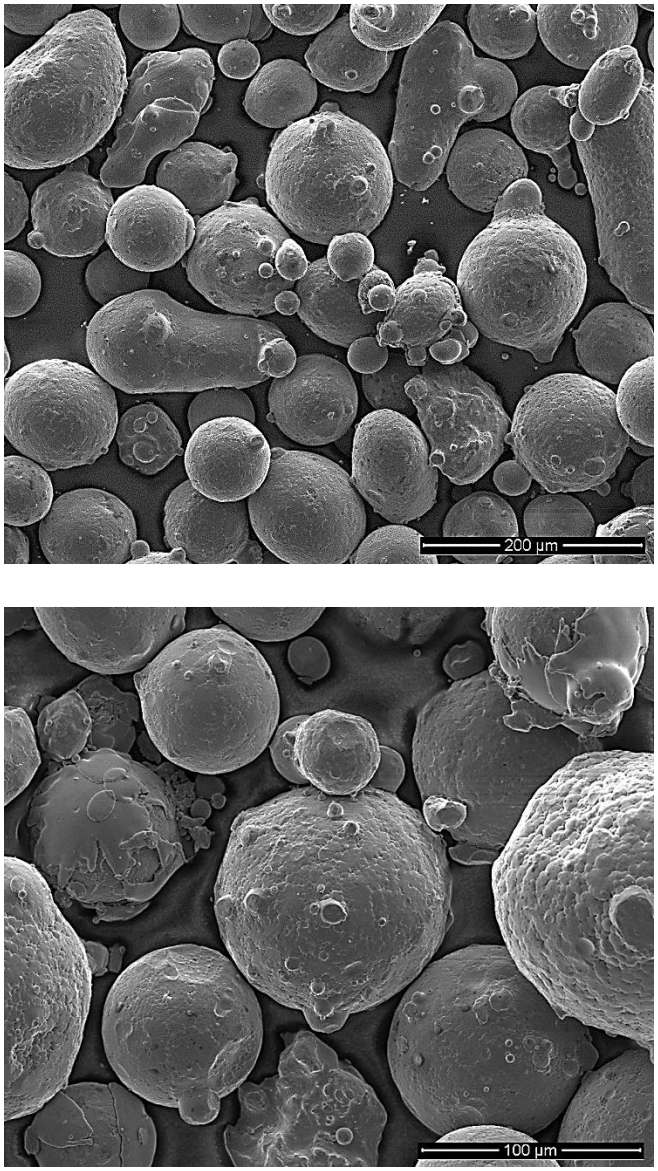


**Figure 4.12**. SAF 2507 particles examined using secondary electron imaging in a scanning electron microscope (SEM).

4.3.4.4 Inserting the Particles into the Electromagnetic Field

To transfer the particles from outside the pipe to the pipe invert in a systematic manner, pipettes were used as consistent volumes of material could be taken. Each ball bearing, 0.00051 g, was pipetted using a 150 µl pipette. For tests using the SAF 2507 particles, 0.0049 g ± 0.0016 g was pipetted using an 80 µl pipette.

To insert the particles (prepared using the pipettes) into the electromagnetic field, all valves in the laboratory were slowly closed and the section containing the electromagnet (valve 1 to the transient valve) was depressurised using a small valve on the top of the acrylic pipe. By only depressurising this section, the rest of the pipeline remained at its conditioned state, see section 4.2.3.2 regarding creep effects. This small valve was then

disconnected resulting in the connector creating an entry point into the pipeline. The particles were deposited by inserting the tip of the respective pipette into a thin non-ferritic metal tube, and passing this tube through the entry point onto the invert above the electromagnet. This is shown in Figure 4.13.

To obtain similar magnetic forces on the particles, this metal tube and a grid placed between the external surface of the pipe and the electromagnet were used to consistently place the particles in the same place in the magnetic field. That is to say the metal tube directed the particles into the same grid space, as observed through the high speed video camera. The particles were held by the electromagnet (current at maximum) and the tube and pipette withdrawn. The closed valve was then reconnected and the pipeline fully opened and repressurised ready for testing.

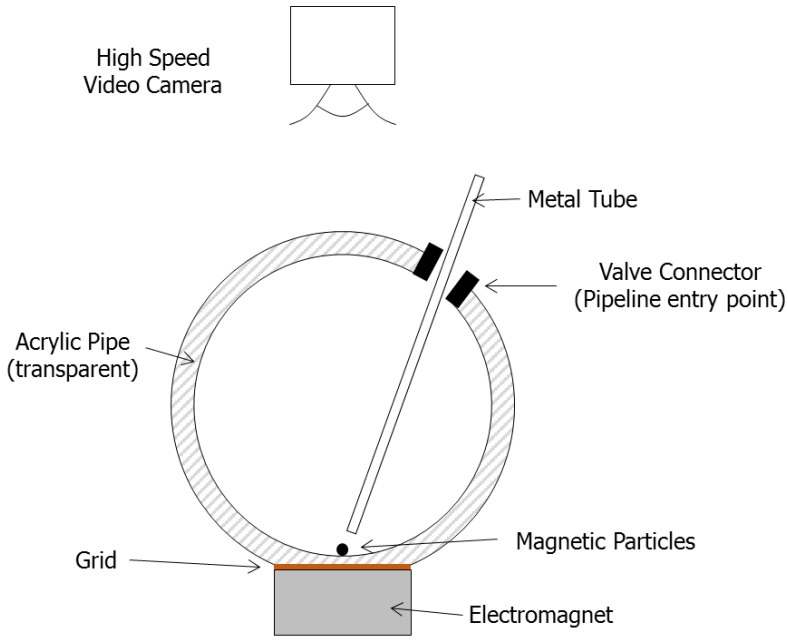


**Figure 4.13.** Schematic of the particle insertion method.

### 4.3.5 Determination of the Mobilisation Threshold

In this work mobilisation was defined by the particles surpassing a distance-based threshold in the streamwise direction. This definition was outlined in section 4.2.4.1. To determine if the particle surpassed the threshold during testing, a high speed video camera (described in Table 4.1) was installed directly above the electromagnet to view the particles in plan, aided by a local light source. Videos taken by the camera during testing would then be analysed to track the streamwise location of the particles.

A bespoke MATLAB (MathWorks, 2016) code was written to analyse the high speed videos. The code selected each frame of the video and processed them in turn. The particles were isolated by filtering out background pixels using a colour threshold manually optimised

to reduce as much visual noise as possible. The centroid of the remaining pixels was then selected using the MATLAB image processing toolbox, whether it was a single ball bearing or a mass of powder. The centroid point, indicated by the red symbols in Figure 4.14 b) and d), could then be tracked from frame to frame. The resulting location-time series data was then used to determine if the particles passed the distance-based threshold during the video. The light source was managed to minimise shadow effects of the powder as much as possible, however the shadows could not be completely removed. Therefore, in some cases the area of powder particles was overestimated.

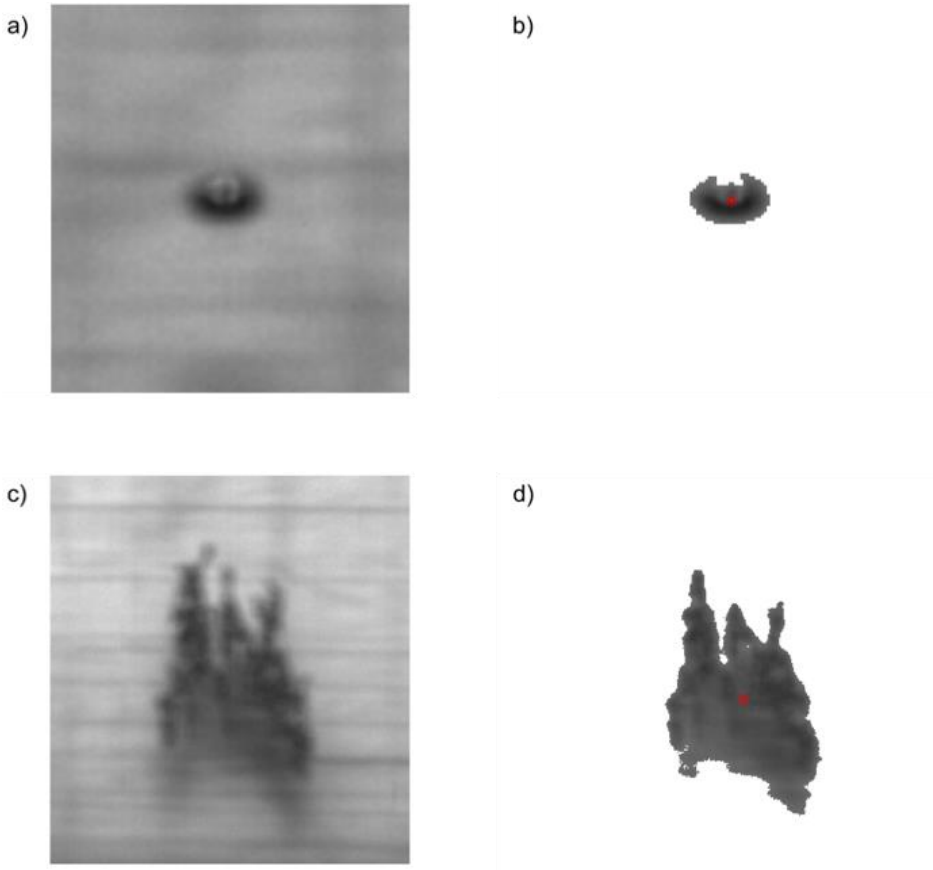


**Figure 4.14.** MATLAB code to analyse the videos; ball bearing image a) unprocessed and b) processed, powder image c) unprocessed and d) processed.

As the two types of material, ball bearings and powder, differed in structure, separate threshold distance values were necessary. In either case, the distances would have to be large enough to clearly distinguish the mobilisation event from other streamwise movements.

Preliminary testing showed that the bearings were naturally slightly mobile whilst in the flow, i.e. they were not stationary in the streamwise and circumferential direction. To quantify these oscillations, the particles were tracked during three seconds of high speed video at different flow rates and the standard deviation of these oscillations was calculated in both directions. The higher the flow rate, the greater the oscillation, see Figure 4.15. This

correlation is most likely due to turbulent structures acting upon the particle, however these were not measured. The combination of the electromagnet, curvature of the pipe and flow structures resisted motion in the dominant streamwise direction. Consequently these streamwise oscillations are smaller in general.

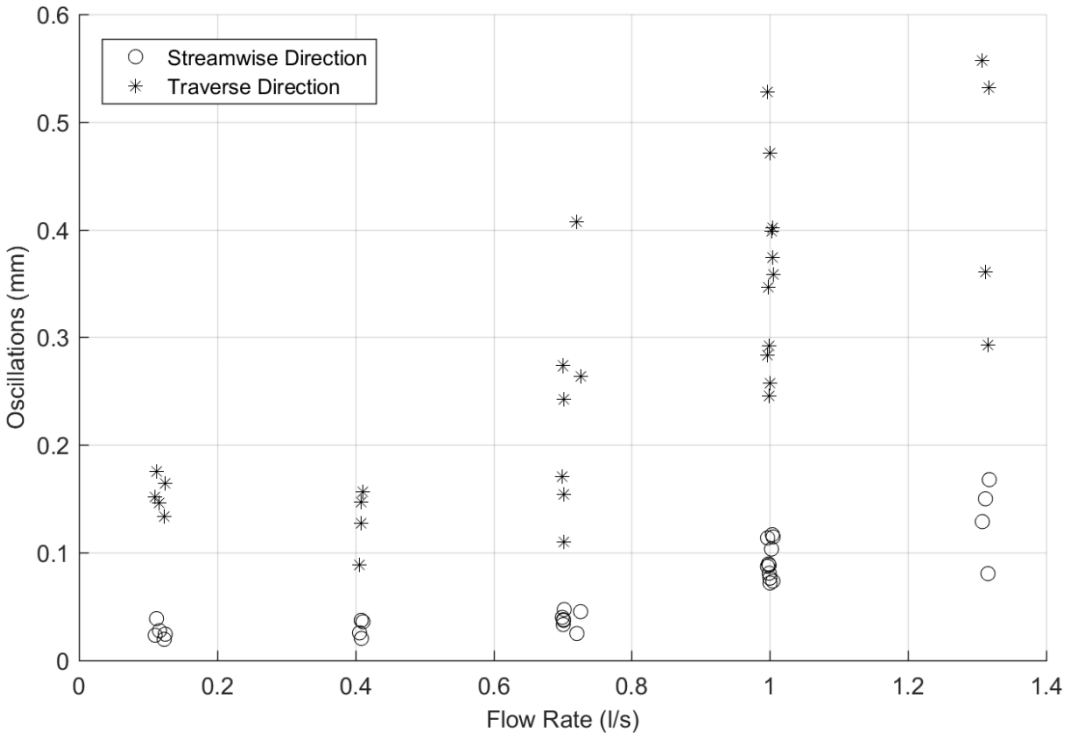


**Figure 4.15.** Quantified particle oscillation in the traverse and streamwise directions for a range of flow rates.

The maximum streamwise and traverse oscillations were 0.168 mm and 0.557 mm, respectively. The streamwise distance threshold for ball bearings was therefore set at 1 mm, as this value is significantly greater than any oscillations, i.e. a factor of safety approaching two. This threshold distance was applied irrespective of streamwise direction. That is to say mobilisation occurred if the particle travelled 1 mm in the upstream or downstream direction from its original position.

The powder was also able to oscillate in the flow, yet movements were not quantified in the same manner as preliminary testing showed that the structure of the powder was too variable. Therefore the streamwise distance based threshold was taken as when all powder particles left the view of the camera, i.e. the greatest measureable distance. This distance was greater than the 1 mm threshold used for the ball bearing results. The camera was positioned so that the downstream edge of the frame along the downstream edge of the electromagnet. Consequently when the particles left the field of view, they were mobilised from the plan area of the electromagnet and did not return.

### 4.3.6 Validation of the Mobilisation Method

Preliminary experiments showed that as the applied current through the electromagnet decreased, the ball bearings moved in the streamwise direction from their original position. These movements were relatively small (less than the 1 mm distance threshold) and the particles returned to their original position when the system was 'reset' for the next test. At the current at which mobilisation occurred, however, much larger streamwise distance changes were witnessed where the bearings surpassed the distance based threshold.

Figures 4.16 and 4.17 present two example cases of particle movements changing with decreasing current; a complete valve closing transient with initial flow rate of 0.1 l/s (Figure 4.16), and a complete valve opening transient with no initial flow rate (Figure 4.17). Both transients had an initial pressure of 45 m. To compare between then, the axes are scaled between the minimum and maximum values of current (x axis) and absolute streamwise distance change (y axis). In both cases as current approaches the current at which mobilisation occurred (scaled as zero), the absolute streamwise distance changes are low before a step change occurs at the point of mobilisation.

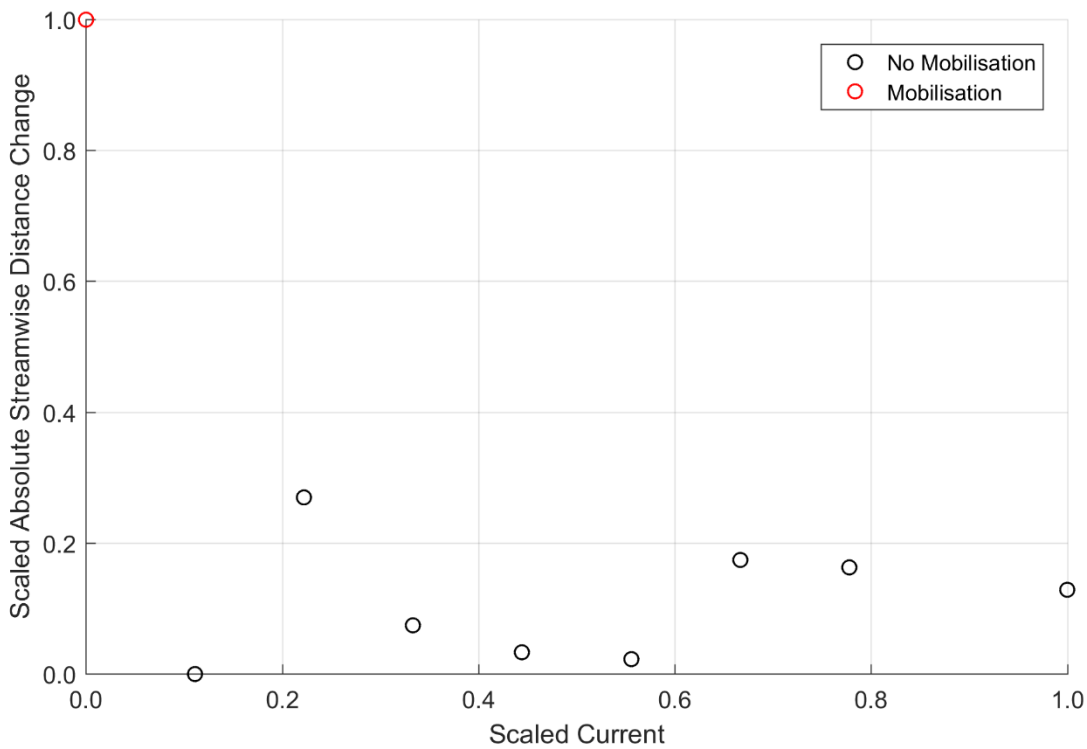


**Figure 4.16.** Complete valve closing example of the absolute streamwise distance changes experienced by a ball bearing due to repeated transients with decreasing current. Current and absolute streamwise distance change are scaled to the ranges tested/observed.

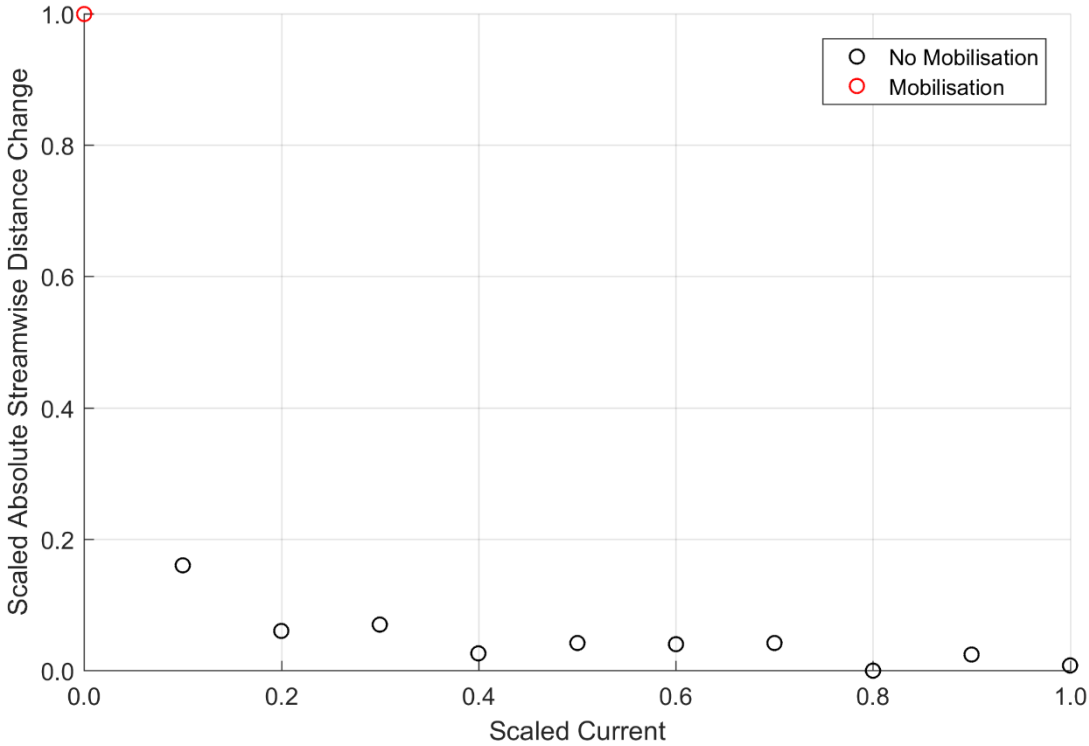


**Figure 4.17.** Complete valve opening example of the absolute streamwise distance changes experienced by a ball bearing due to repeated transients with decreasing current. Current and absolute streamwise distance change are scaled to the ranges tested/observed.

This observed behaviour suggests that the current at which mobilisation occurred is not a by-product of the preceding small streamwise movements, but rather a clear and consistent phenomenon is captured by this experimental method.

### 4.3.7 Experimental Programme

The experimental approach, defined in section 4.2.4.2, was to establish the hydraulic conditions and reduce the magnetic force until the distance-based threshold was met. This produced a current at which mobilisation occurred for that particular hydraulic condition. Repeating this method for different hydraulic conditions would then produce mobilisation force relationships (hydraulic conditions against current). This section will detail the test method used and the overall experimental programme.

#### 4.3.7.1 Experimental Test Method

Firstly, the particles were inserted (section 4.2.4.4) with the current at maximum. Hydraulic conditions of flow and pressure were then established by adjusting the system pump and globe valves. These conditions could have been steady state or initial transient conditions.

In steady state cases the conditions remained whilst the current through the electromagnet was slowly decreased in 1 mA steps, via the LabVIEW software, until the particles mobilised past the threshold. In transient cases, the initial hydraulic conditions were set with the transient valve at the appropriate location; for valve closing transients it was at the 'open' position, for valve opening transients it was at the 'closed' position. The valve was then rapidly changed to the alternate position to generate the respective transient. If the particle did not meet the criteria for mobilisation, the butterfly valve was slowly turned to the original position to "reset" the initial conditions. The current was decreased by 1 mA and the process repeated until the particle passed the mobilisation threshold. Once this happened, the current at which mobilisation occurred was recorded for that particular hydraulic condition. Figure 4.18 presents flow charts of the steady state and transient test methods used.

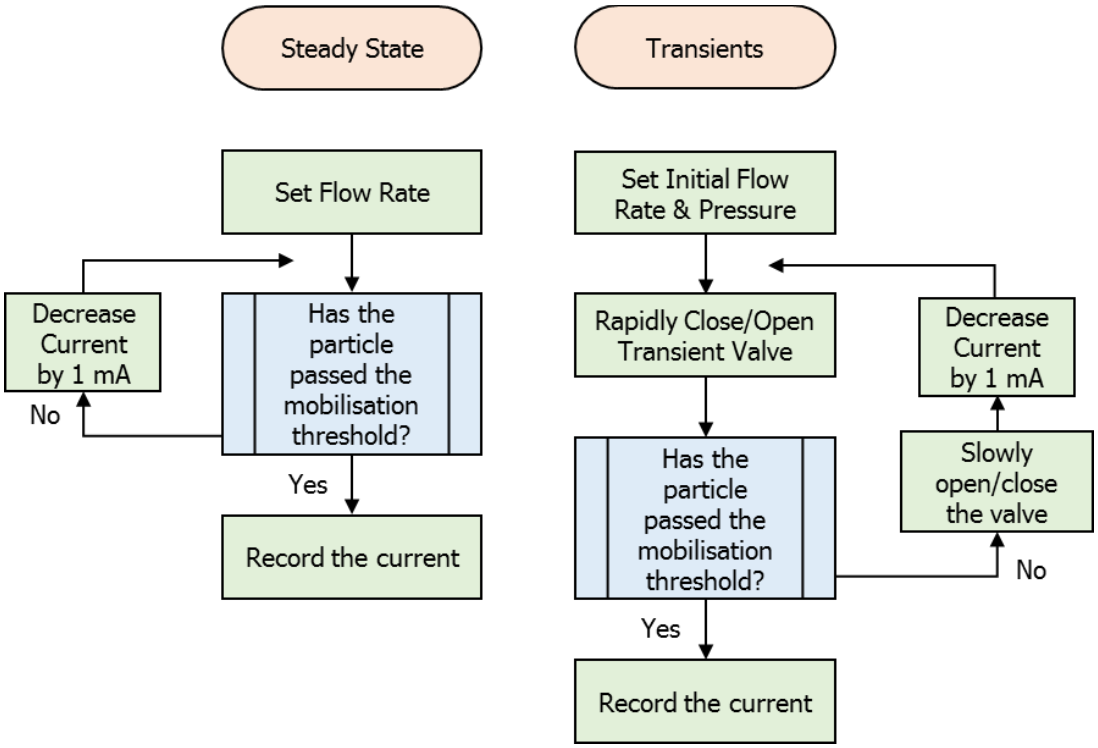


**Figure 4.18.** Flow chart for the steady state and transient experimental test methods.

4.3.7.2 Testing Conditions

Mobilisation force relationships between hydraulic conditions and the current at which mobilisation occurred were established first for ball bearings to examine idealised behaviour, then for powder to examine replicated adhered material. Within each material, the hierarchy of hydraulic tests performed was: steady state, valve closing transients then valve opening transients. This order was justified in sections 4.2.4.4. The 'complete' transients were considered the most extreme cases as they had the biggest changes in flow conditions, where 'partials' had smaller changes in flow. Therefore, 'complete' transients were tested before

'partial' transients, for both valve closing and valve opening transients. However, valve closing transients were not performed for the powder as preliminary tests showed that the mobilisation threshold was too large in the upstream direction. A lower mobilisation threshold would not have be able to separate initial powder movements from a clear step change in streamwise distance changes.

Preliminary steady state testing aimed to determine the maximum flow rate capable of mobilising a ball bearing from the electromagnetic system at maximum current. The resulting flow rate of 1.48 l/s consequently became the upper limit of the flow rates tested. The lower limit was the minimum flow rate resolvable by the flow meter, 0.1 l/s. In this pipeline, turbulent regimes (Re > 4000) were created by a minimum flow rate of 0.127 l/s, therefore the majority of flows tested were turbulent. The only exception was a flow rate of 0.1 l/s which was a transitional regime (Re 3180). These conditions are realistic of typical operational DWDS in the UK, see section 2.1.4. Pressure conditions ranged from 25 m to ~46 m to also recreate typical values. Systems are designed for a minimum mains pressure of 20 m, see section 2.1.4, with no maximum pressure, hence the maximum pressure of the pump was used as the upper limit. These limits of flow and pressure were applied to all test conditions, irrespective of steady state or transient, bearing or powder. A summary of the tests performed can be found in Appendix A.

## 4.4 Summary

This chapter presents the development of a bespoke experiment to explore mobilisation of replicated pipe-wall adhered material due to steady state and hydraulic transients. Repeatable and controllable transients were generated via rapid valve operation. Organic material is inherently too variable to repeatedly test and evaluate, thus a suitable analogue was established. The bespoke electromagnetic system with magnetic particles replicated key organic material characteristics of pipe surface adhesion, variable strength and structure.

The approach taken for experiment was to decrease the magnetic force until the particle was mobilised against the hydraulic force. At the point of mobilisation the magnetic force can be quantified by the electromagnetic current and effectively becomes an indicator of the force for those hydraulic conditions. The steady state mobilisation force relationship was tested first to act as a 'base line', followed by transient tests. The comparison of these relationships would address the aim of this research – to demonstrate the ability of transients to cause mobilisation where steady state conditions cannot.

# Chapter Five

# Results

## 5.1 Introduction

The aim of this work was to demonstrate whether transients can mobilise adhered particles where steady state conditions cannot. The laboratory experiments conducted to address this aim consisted of replicating adhered particles using magnetic particles held against the pipe wall by an electromagnet. The electromagnet provided controllable adherence strength quantified by current. Different hydraulic tests were performed, steady state and transient, to determine the current at which mobilisation of the particles occurred for each. The comparison of these values would then answer the aim.

This chapter presents the results of these experiments. The first section presents experiments conducted with ball bearing particles (section 5.2). The second section presents experiments conducted with SAF 2507 particles as a powder (section 5.3). The final section is the summary of all findings (section 5.4).

## 5.2 Ball Bearings as Magnetic Particles

Ball bearings were used to replicate idealised behaviour of adhered particles. The following hydraulic conditions were tested: steady state, valve closings (complete and partial), and valve opening (complete and partial). For each, the current at which mobilisation occurred was determined when the ball bearings surpassed the streamwise distance threshold described in section 4.3.5.

### 5.2.1 Steady State

To produce a base line to directly compare to dynamic results, the mobilisation force relationship was first determined for steady state. Figure 5.1 presents the current at which mobilisation occurred for the range of steady state flow rates tested. The regression line shows a positive linear relationship – gradient of 353.55 mA per l/s, offset -97.88 mA, coefficient of determination 0.996. The region below this relationship indicates the magnetic forces are too low, thus mobilisation would always occur due to steady state.

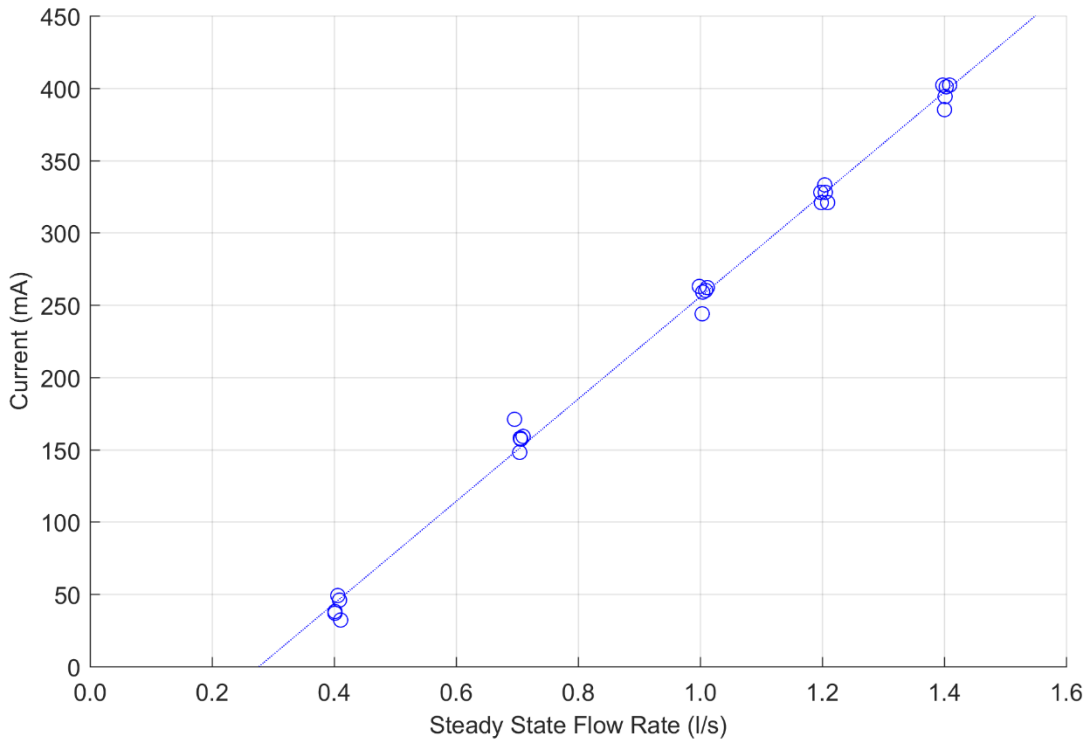


**Figure 5.1.** Relationship between the current at which mobilisation occurred for ball bearings and steady state flow rates.

Experimental control and repeatability of the ball bearings within the electromagnetic system is demonstrated by the clustering seen in Figure 5.1. During subsequent experiments, additional repeats were periodically performed to ensure the stability of this relationship, at least one additional repeat for each of the five flow rates tested. Table 5.1 quantifies the maximum absolute difference between the currents at which mobilisation occurred, and the currents given by the regression line. These values for the additional repeats are comparable to those from the experiment. Therefore, the additional repeats did not exhibit any variation from the primary relationship, i.e. the steady state relationship did not change.

**Table 5.1.** Maximum differences between the currents at mobilisation occurred and the currents given by the steady state regression line.

| Steady State Flow Rate (l/s) | Max. Current Difference from the Regression Line (mA) | |
|---|---|---|
| | Experiment | Additional Repeats |
| 0.4 | 15 | 2 |
| 0.7 | 23 | 7 |
| 1.0 | 13 | 10 |
| 1.2 | 9 | 13 |
| 1.4 | 12 | 5 |

### 5.2.2 Valve Closing Transients

The aim of these experiments was to determine if valve closing transients can cause mobilisation of a single ball bearing, where steady state cannot. Complete valve closings were performed first as the most likely case for extreme dynamic effects, i.e. the largest instantaneous decrease in flow rate. Then partial valve closing transients were performed that had smaller instantaneous decreases in flow rate. In either case the greatest flow rate pre or post transient was the initial flow rate, thus this was the parameter compared to steady state results.

#### 5.2.2.1 Complete Valve Closing Transients

The high-speed video camera was used to track the ball bearings, as described in section 4.3.5. For convention, the upstream direction is taken as negative distance changes.

Figure 5.2 shows an example of the particle's location changing, leading to mobilisation, during a complete valve closing transient commencing at an initial flow rate of 0.7 l/s. Part a) of the figure shows a selection of discrete frames of the video recording, i.e. snap shots of the particle location collected by the camera. Frames i, ii, vi and vii have 0.1 s spacing, where frames iii - v are selected as part of the transient surge. Part b) of the figure shows the streamwise distance change of the particle, relative to its initial position, determined by processing all video frames through the tracking programme. The frames presented in part a) are indicated in the continuous time series data of part b). In this example, the corresponding distance change was 1.60 mm; greater than the threshold of 1 mm, therefore, mobilisation did take place. There appears to be a sinusoidal wave in the post transient streamwise location of the particle, see Figure 5.2 b). This is a by-product of the video camera setup; the camera was held by a mechanical arm that resonated at ~480 Hz due to energy transference of the rapid valve operation.

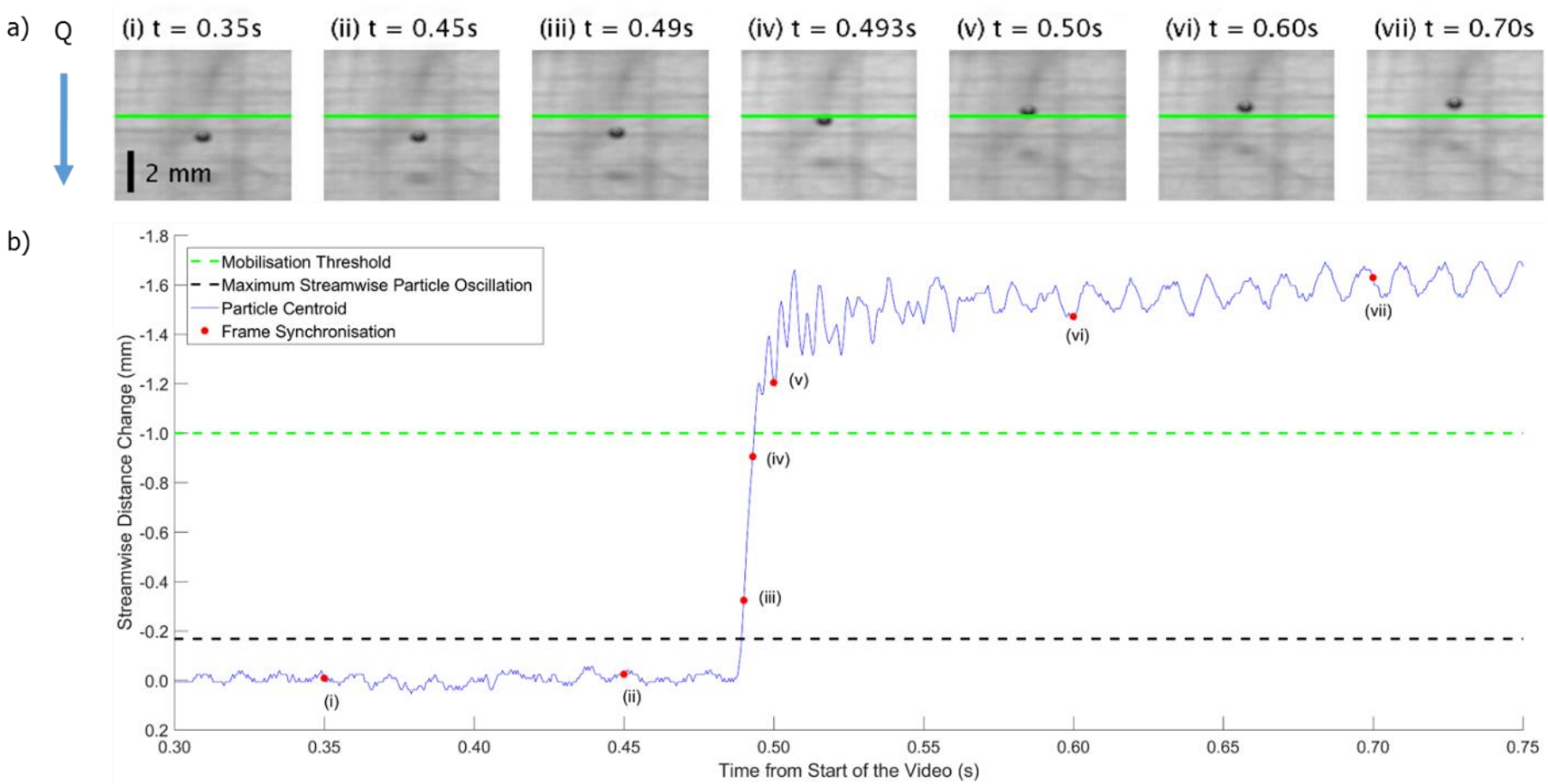


**Figure 5.2.** Streamwise tracking example of a ball bearing during a complete valve closing transient transitioning from a 0.7 l/s initial flow rate to a zero final flow rate. Part a) is a selection of discrete frames taken by the camera, where the green line is the mobilisation threshold relative to the initial location of the particle centroid. Frames i, ii, vi and vii have 0.1 s spacing, where frames iii, iv, and v are selected as part of the transient surge. Part b) is the streamwise distance change of the particle centroid, relative to its initial position, determined by processing all video frames through the tracking programme. The frames presented in part a) are indicated in the continuous time series data of part b).

The example presented in Figure 5.2 demonstrates that complete valve closing transients can mobilise a ball bearing particle past the established threshold. It was seen that the particles were held by the adhesion force during the initial flow rate and mobilisation occurred only after the testing valve was rapidly closed. This confirms that the particles would only mobilise under transient conditions.

Figure 5.3 presents pressure data collected for complete valve closing transients that caused mobilisation. The pressure data is normalised by subtracting the initial pressure (pre-transient) from the pressure data and the time is adjusted so that the first surge commences at time zero. This was done for ease of comparison to emphasise the difference in dynamic conditions generated. Only one transient per set of hydraulic conditions tested is included here for clarity. Acronyms used are: $Q_I$ for initial flow rate, $P_I$ for initial pressure, $I$ for current at which mobilisation occurred. This format for presenting transient pressure data will be used again during this chapter.

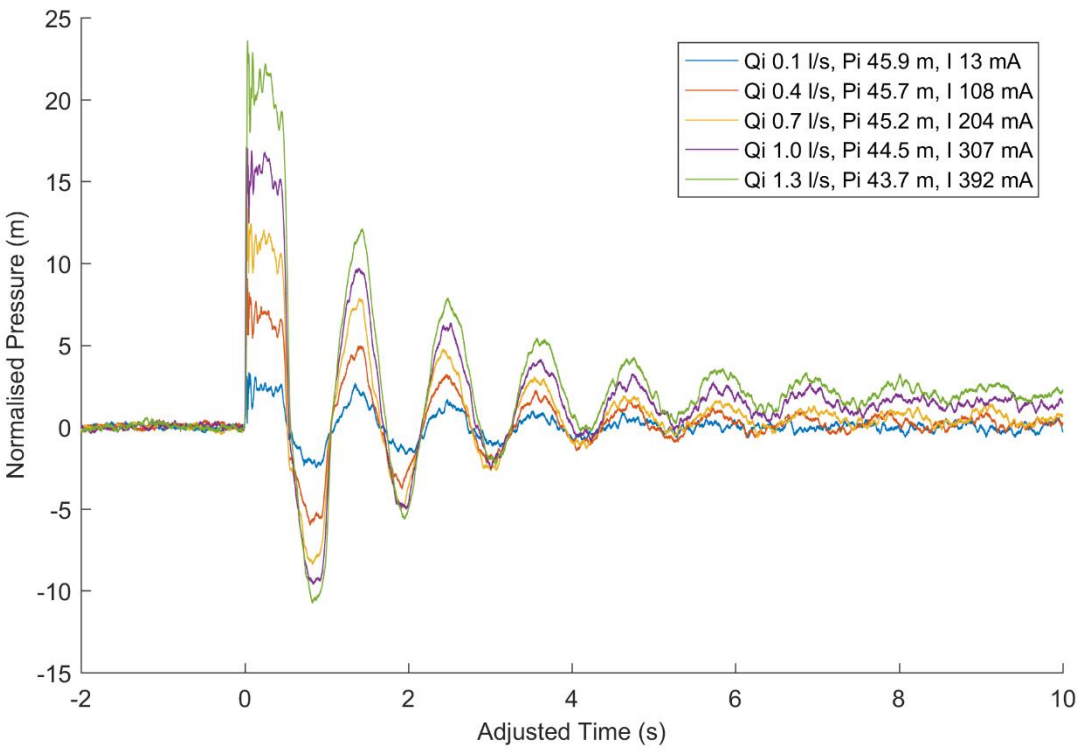


**Figure 5.3.** Pressure traces of complete valve closing transients that caused mobilisation of the ball bearings. Traces are normalised by subtracting initial pressure and adjusted so that the first surge commences at time zero. $Q_I$ initial flow rate, $P_I$ initial pressure, $I$ current at which mobilisation occurred.

Figure 5.3 shows that as the initial flow rate increased, the magnitude of the pressure changes increased, i.e. the transients appear to be stretched parallel to the vertical pressure scale. These transients then correspond to the currents at which mobilisation occurred; the

greater the pressure changes, the greater the current. Relating these currents to the initial flow rate of the complete valve closing transients produced a positive linear relationship – gradient of 320.91 mA per l/s, offset -21.82 mA, coefficient of determination 0.998. These are presented in Figure 5.4 for all repeats tested. Closing transients must have been able to resist the initial steady state flow rate, yet steady state results are included here to visually demonstrate the additional current induced by the transients. Experimental control and repeatability of the ball bearings within the electromagnetic system is demonstrated by the clustering seen.

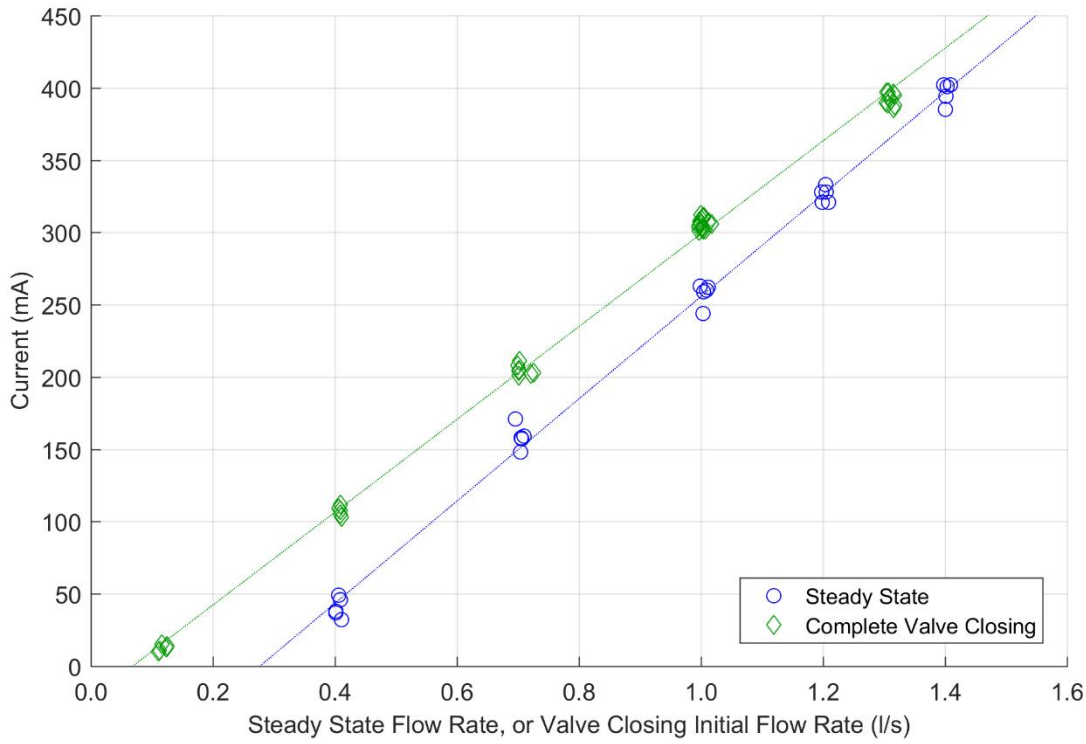


**Figure 5.4.** Relationships between the current at which mobilisation occurred for ball bearings and steady state flow rate, or complete valve closing initial flow rate.

The complete valve closing mobilisation force relationship sits above the steady state relationship, which means that there are situations where complete valve closings from an initial flow rate can cause mobilisation where steady state does not. For example, a steady state flow rate of 0.4 l/s will mobilise the particle at an average current of 44 mA, yet rapidly closing the valve at this same initial flow rate will mobilise at a higher average current of 107 mA. Therefore, a particle held at a current between these values will be mobilised by the transient and not by steady state.

Figure 5.4 shows that as the flow rate increases, the difference in the average current at which mobilisation occurs between the mobilisation force relationships decreases, i.e. the regression lines appear to converge. For example, the difference in average current at flow

rate of 0.4 l/s is 64 mA, where at a higher flow rate of 1.0 l/s the difference is 42 mA. The two lines would converge, if the relationships were to be extrapolated, at conditions of flow rate of 2.22 l/s and current of 685 mA. There is not a clear immediate reason for these specific values and they cannot be tested due to the limits of the electromagnet.

#### 5.2.2.2 Partial Valve Closing Transients

Partial valve closing transients were tested with a range of initial flow rates, and a constant final flow rate was 0.1 l/s, the lowest non-zero resolvable flow rate in the system. The particles did not mobilise under the transient conditions, i.e. when the transient was generated. The particles were mobilised in the downstream direction when the current was decreased to the same value as the current at which mobilisation occurred for the steady state initial flow rate. This occurred under the complete range of initial flow conditions tested. Partial valve closing transients with higher final flow rates were not studied as transients generated would have had less dynamic forces.

### 5.2.3 Valve Opening Transients

The aim of these experiments was to determine if valve opening transients can cause mobilisation of a single ball bearing, where steady state cannot. Akin to the previous closings, complete transients were performed first, followed by partial valve opening transients.

#### 5.2.3.1 Complete Valve Opening Transients

Two sets of complete valve opening transients were tested. The first set had variable final flow rate and variable initial pressure, at five combinations of conditions. The second set had also had variable final flow rate, but fixed initial pressure. Only three final flow conditions were selected.

Preliminary results showed that the particles mobilised downstream when the butterfly valve was rapidly opened, i.e. when the transient was induced. Figure 5.5 shows an example of the particle's location changing, leading to mobilisation, during a complete valve opening set one transient resulting in 0.49 l/s. Part a) of the figure shows a selection of discrete frames of the video recording, i.e. snap shots of the particle location collected by the camera. The frames are equally spaced (0.005 s spacing), except for the final frame. Part b) of the figure shows the streamwise distance change of the particle, relative to its initial position, determined by processing all video frames through the tracking programme. The frames presented in part a) are indicated in the continuous time series data of part b). As there is no initial flow rate, the particle is initially stationary before being carried downstream past distance threshold. The particle travelled at an average speed of 0.092 m/s, determined by the gradient of the post-mobilisation tracking. This is the product of the final (post

transient) flow rate. For complete valve opening transients, the average speed of the mobilising particles ranged from 0.054 m/s to 0.116 m/s.

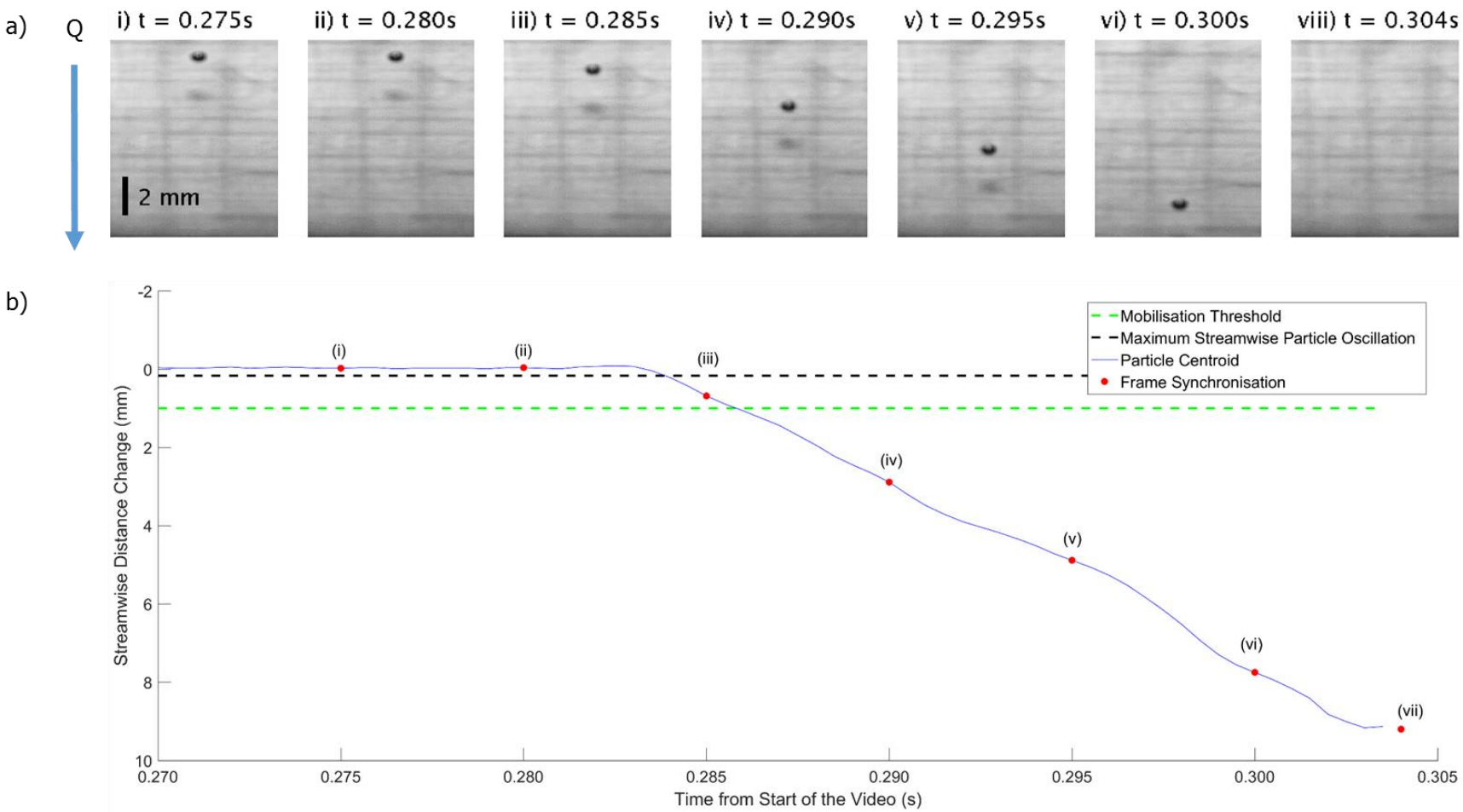


**Figure 5.5.** Streamwise tracking example of a ball bearing during a complete valve opening transient transitioning from a zero-initial flow rate to a flow rate of 0.49 l/s. Part a) is a selection of discrete frames taken by the camera. The frames have a 0.05 s spacing. Part b) is the streamwise distance change of the particle centroid, relative to its initial position, determined by processing all video frames through the tracking programme. The frames presented in part a) are indicated in the continuous time series data of part b).

The example presented in Figure 5.5 demonstrates that complete valve opening transients can mobilise a 500 μm particle past the field of view. Figures 5.6 and 5.7 present pressure data collected for complete valve opening transients that caused mobilisation, for sets one and two, respectively. The same format is applied as described previously in Figure 5.3. However, instead of $Q_I$ denoting initial flow rate, $Q_F$ is used to denote final flow rate.

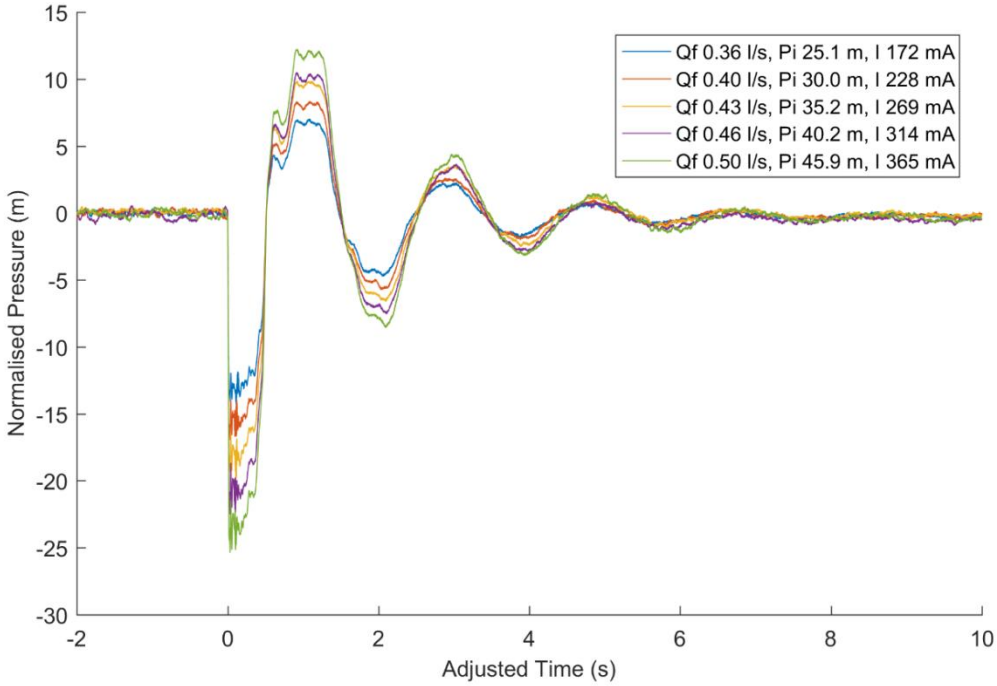


**Figure 5.6.** Pressure traces of complete valve opening transients set one that caused mobilisation of the ball bearings. Traces are normalised by subtracting initial pressure and adjusted so that the first surge commences at time zero. $Q_F$ final flow rate, $P_I$ initial pressure, $I$ current at which mobilisation occurred.

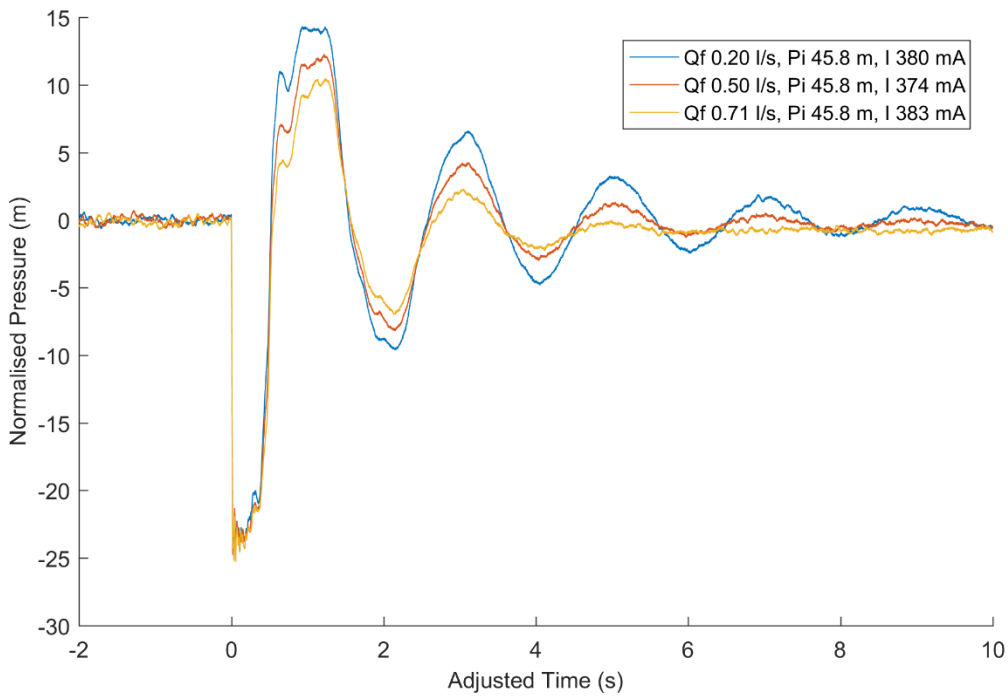


**Figure 5.7.** Pressure traces of complete valve opening transients set one that caused mobilisation of the ball bearings. Traces are normalised by subtracting initial pressure and adjusted so that the first surge commences at time zero. $Q_F$ final flow rate, $P_I$ initial pressure, $I$ current at which mobilisation occurred.

Figure 5.6 shows, for complete valve opening set one transients, as the final flow rate and initial pressure were increased, the magnitude of the pressure changes increased, i.e. the transients appear to be stretched parallel to the vertical pressure scale. These transients then correspond to the currents at which mobilisation occurred; the greater the pressure changes, the greater the current. Figure 5.7 shows, for complete valve opening set two transients, as the final flow rate increased, the transient experienced more damping. This is evidenced by the crests and peaks of the transient approaching the final pressure more quickly. However, it can also be seen that the magnitude of the first pressure change is similar for these transients with the same final pressure.

Figure 5.8 relates the currents at which mobilisation occurred to the final flow rates, for all complete valve opening transients. Complete valve opening set one transients produced a positive linear relationship – gradient of 1377.37 mA per l/s, offset -0.32 mA, coefficient of determination 0.980. Complete valve opening set two transients produced a positive linear relationship – gradient of 15.31 mA per l/s, offset -371.80 mA, coefficient of determination 0.234. Steady state results are also given for comparison.

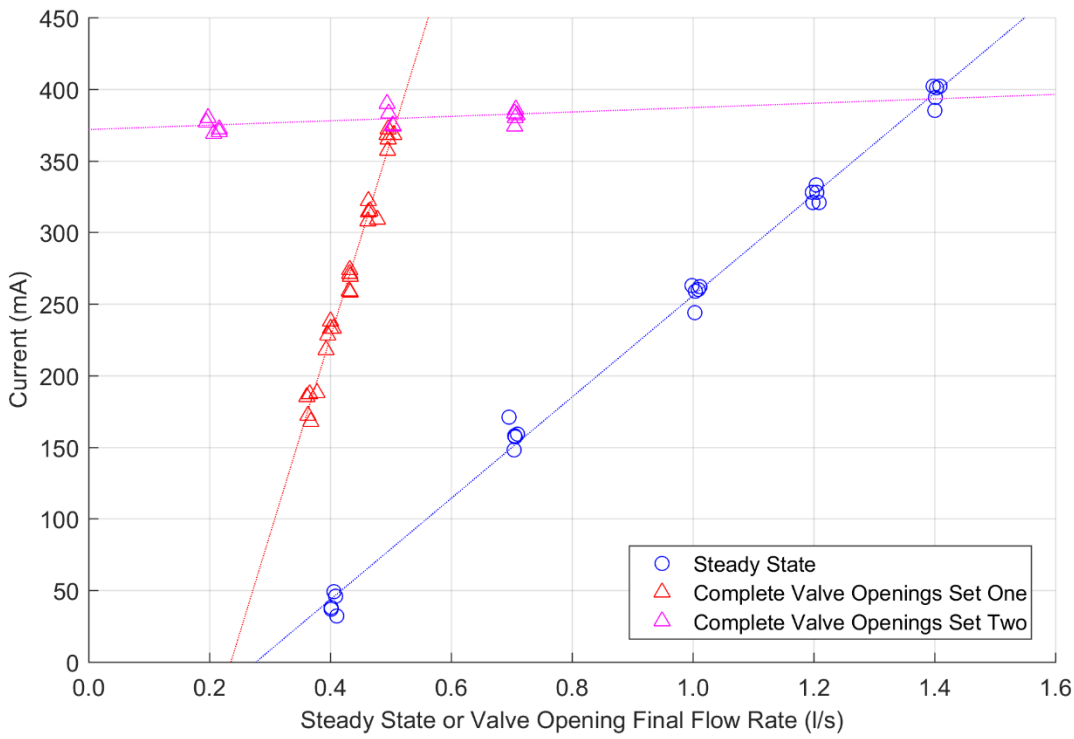


**Figure 5.8.** Relationships between the current at which mobilisation occurred for ball bearings and steady state flow rate, or complete valve opening final flow rate.

Both complete valve opening mobilisation force relationships tested sit above the steady state relationship, which means that there are situations where complete valve openings can cause mobilisation and steady state cannot. For example, a steady state flow

rate of 0.4 l/s will mobilise the particle at an average current of 44 mA, yet rapidly opening the valve to this same final flow rate (set one) will mobilise at a higher average current of 227 mA. Therefore, a particle held at a current between these values will be mobilised by the transient and not by steady state.

#### 5.2.3.2 Partial Valve Opening Transients

Four sets of partial valve opening transients were tested. As the complete transients would be the most dynamic case and steady state would characteristically be the least dynamic case, the partial valve openings were designed to sit between the two, effectively describing the space between them. All sets had varying initial pressure head conditions but differed in initial and final flow rates. The first set had a fixed initial flow rate of 0.1 l/s and the same final flow rates as for the complete valve openings set one. The other three sets had fixed initial flow rates and fixed final flow rates that increased in 0.2 l/s steps. That is set two 0.3 to 0.5 l/s, set three 0.5 to 0.7 l/s and set four 0.7 to 0.9 l/s.

For all partial valve opening transients tested, the particles were mobilised past the 1 mm threshold. Videos collected that exhibit this mobilisation occurring are not offered here as they showed no difference to the images (camera frames) presented in Figure 5.5 a). Figures 5.9 to 5.12 present pressure data collected for partial valve opening transients that caused mobilisation (sets one to four). The same format is applied as described previously in Figure 5.5.

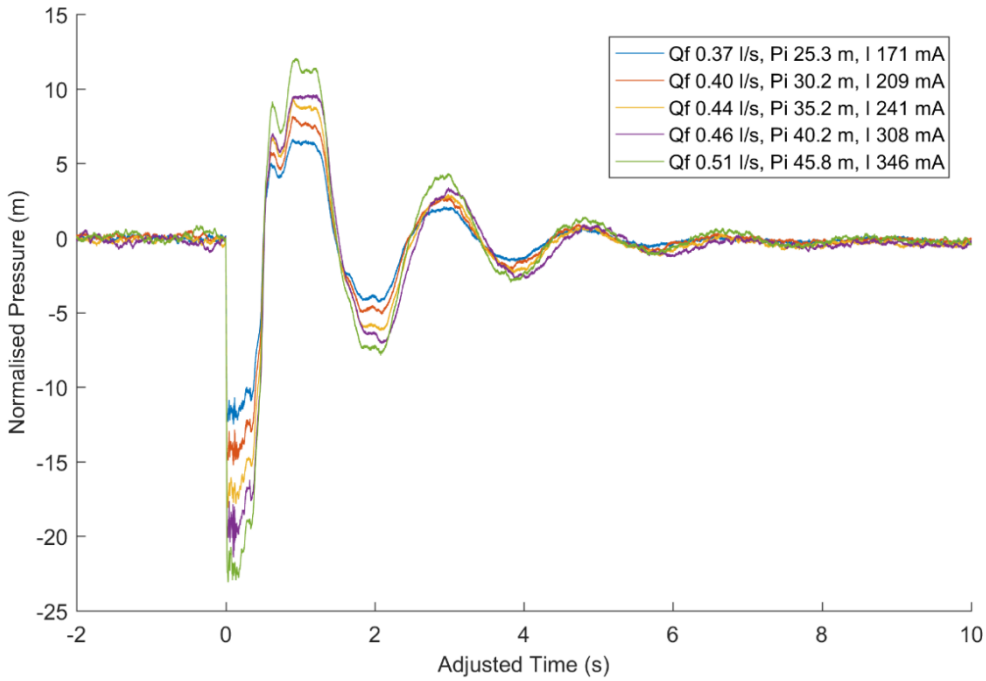


**Figure 5.9.** Pressure traces of partial valve opening transients set one that caused mobilisation of the ball bearings. Traces are normalised by subtracting initial pressure and adjusted so that the first surge commences at time zero. $Q_F$ final flow rate, $P_I$ initial pressure, $I$ current at which mobilisation occurred.

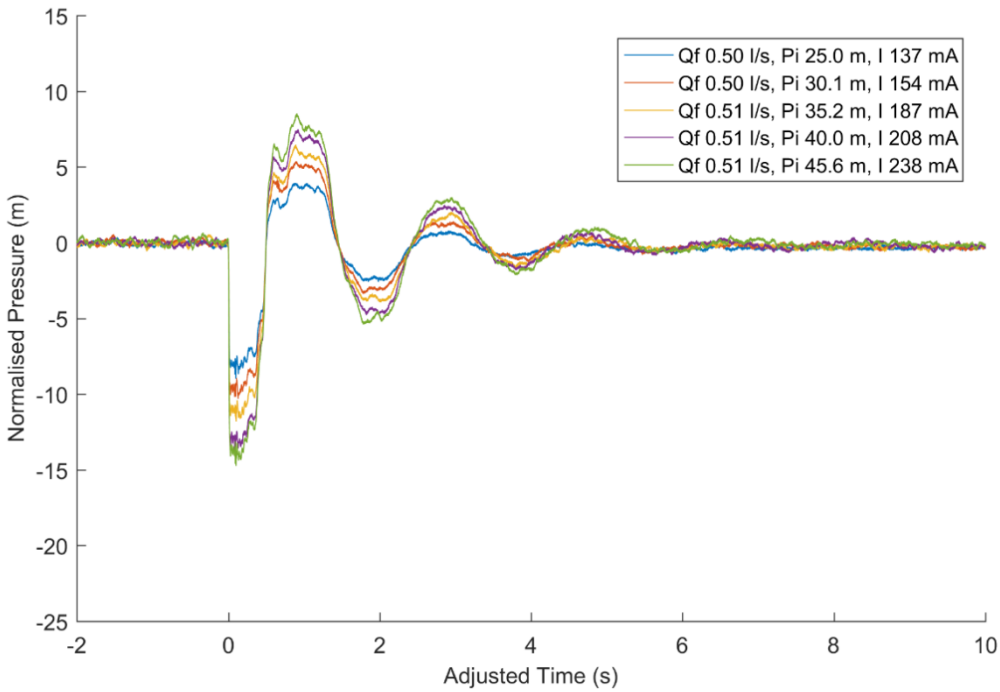


**Figure 5.10.** Pressure traces of partial valve opening transients set two that caused mobilisation of the ball bearings. Traces are normalised by subtracting initial pressure and adjusted so that the first surge commences at time zero. $Q_F$ final flow rate, $P_I$ initial pressure, $I$ current at which mobilisation occurred.

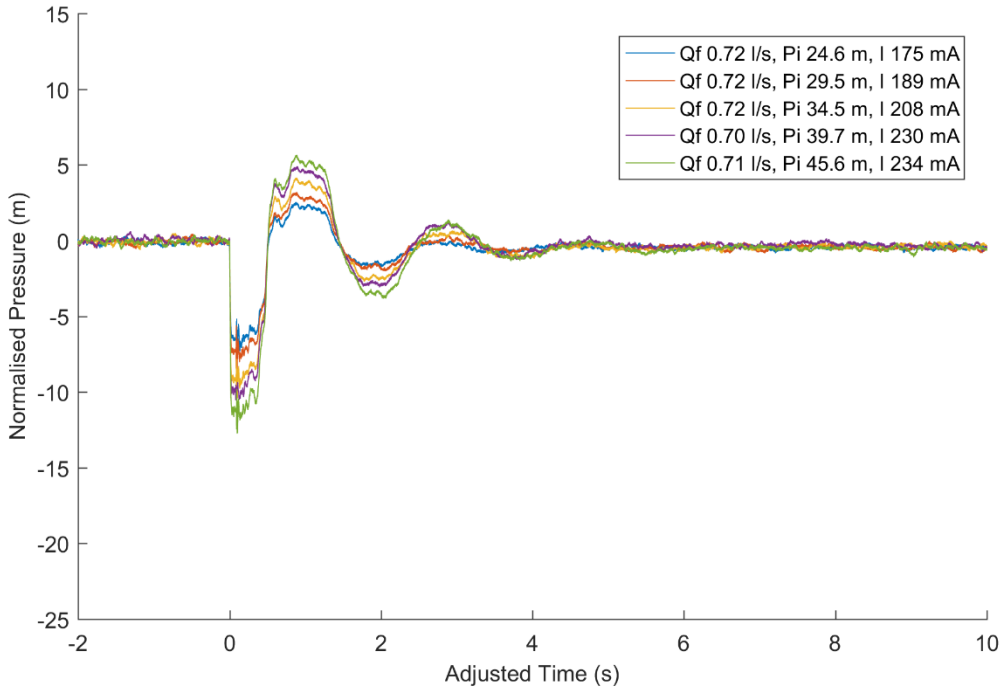


**Figure 5.11.** Pressure traces of partial valve opening transients set three that caused mobilisation of the ball bearings. Traces are normalised by subtracting initial pressure and adjusted so that the first surge commences at time zero. $Q_F$ final flow rate, $P_I$ initial pressure, $I$ current at which mobilisation occurred.

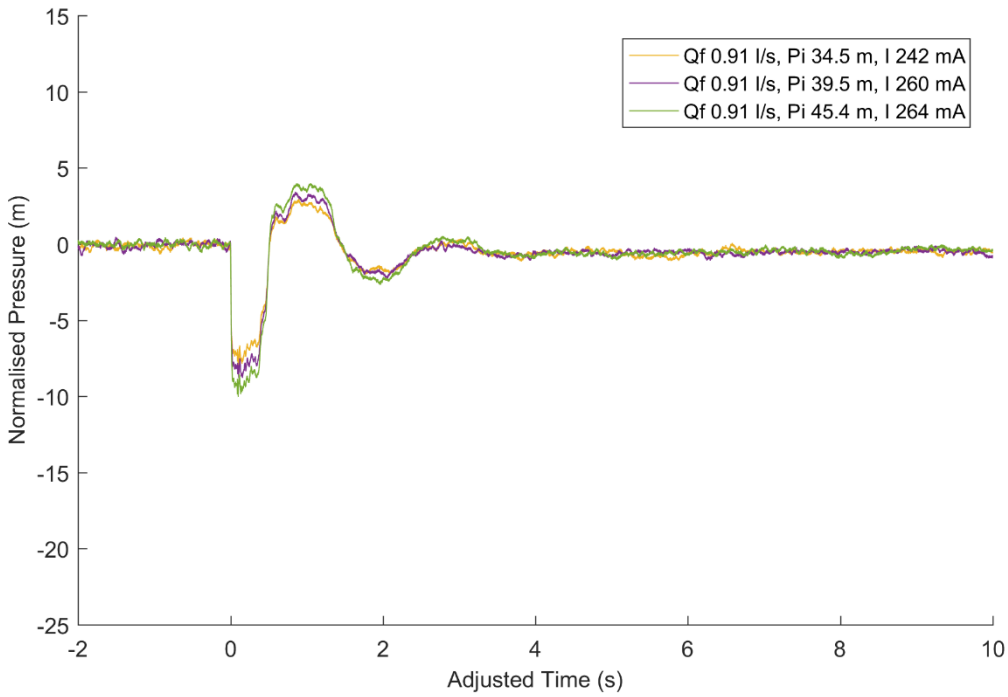


**Figure 5.12.** Pressure traces of partial valve opening transients set four that caused mobilisation of the ball bearings. Traces are normalised by subtracting initial pressure and adjusted so that the first surge commences at time zero. $Q_F$ final flow rate, $P_I$ initial pressure, $I$ current at which mobilisation occurred.

Pressure traces in Figures 5.9 to 5.12 show that as the final flow rate and/or initial pressure were increased, the magnitude of the pressure changes increased and corresponded to the currents at which mobilisation occurred. This is consistent with the complete valve opening results shown in Figure 5.6.

Comparing across the figures (moving from Figures 5.9 to 5.12), as the final flow rate of the transients increased, the range of pressure changes seen decreased. This can be seen in the transients reaching lower pressures in the first surge. For example, when comparing transients with initial pressures of ~ 45 m, for a final flow rate of 0.51 l/s the initial surge decreases to approximately - 23 m, whereas for a final flow rate of 0.91 l/s this value is only - 10 m. Furthermore the transients have fewer crests and peaks at the higher final flow rates (i.e. Figure 5.12). This is most likely due to having greater friction and damping effects.

Figure 5.13 shows the currents at which mobilisation occurred for the four sets of transients described, as well as steady state and complete valve opening cases for comparison. These mobilisation force relationships sit above the steady state relationship, demonstrating that there are situations where partial valve openings can cause mobilisation and steady state cannot.

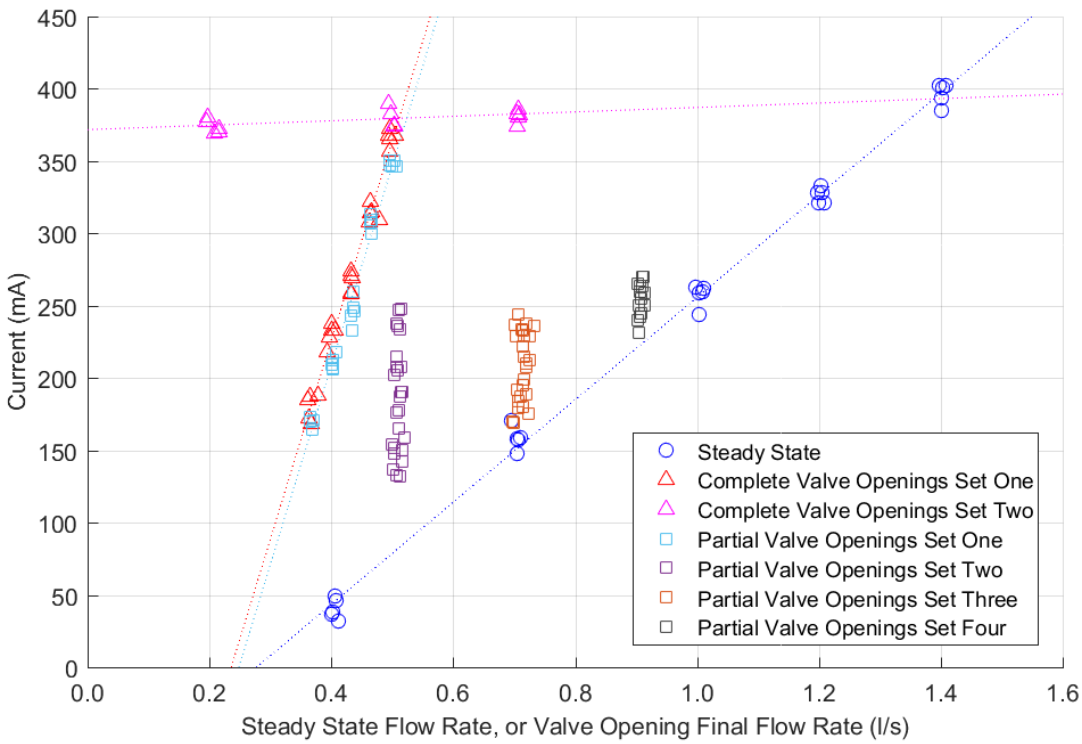


**Figure 5.13.** Relationships between the current at which mobilisation occurred for ball bearings and steady state flow rate, or valve opening final flow rates (complete and partial).

## 5.3 Powder as Magnetic Particles

SAF 2507 particles were used as a powder to replicate cohesive layers of adhered particles. Details of the particles were included in section 4.3.4.3. The following hydraulic conditions were tested: steady state, and valve opening (complete and partial). For each, the current at which mobilisation occurred was determined when all the particles surpassed the streamwise distance threshold, see section 4.3.5. The number of initial conditions performed within each transient set was less for the powder than the ball bearings due to time limitations. Initial conditions were chosen so that the same hydraulic ranges were covered for both materials. For example, in complete valve opening bearing tests the initial pressures were approximately 25 m, 30 m, 35 m, 40 m, and 45 m. In corresponding powder tests, the initial pressures were 25 m, 35 m, and 45 m.

### 5.3.1 Powder Structure

Videos collected during the experiments showed that when flow was applied to the powder, different structures were observed. Two variants are presented in Figure 5.14. In part a) the structure was dispersed into several substructures aligned with the magnetic field lines, whereas in part b) the structure was more condensed yet with some observed voids. All powder structures formed during the preliminary experiments displayed aspects of these behaviours. No relationship was seen between the structures observed and the applied current or initial hydraulic conditions.

a) b)

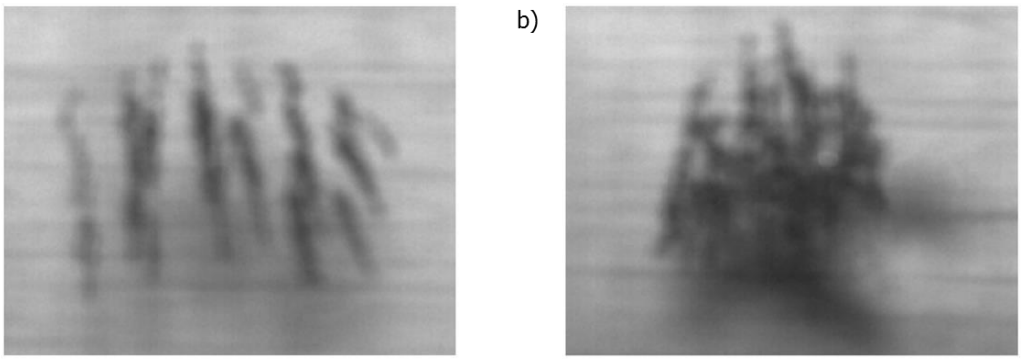

**Figure 5.14.** Powder structure that is a) dispersed, or b) condensed with observed voids.

Throughout the experiments (steady state and transient), the observed structures were not static and displayed variable configurations. Some substructures would separate from the main body and were either entirely lost from the field of view or could be seen reattaching at a new location. A likely cause of this action was small increases in hydraulic forces that were sufficient to detach parts of the powder but insufficient to mobilise the entire structure outside the distance threshold. An example of a complete valve opening transient

where one or more fragments of the powder mobilised can be seen in Figure 5.15. Here, two side substructures were completely mobilised and the central fragment, an X-like structure, condensed slightly. This observed behaviour of substructure mobilisation was not quantified in this research as the experiment was based on mobilisation of the entire powder.

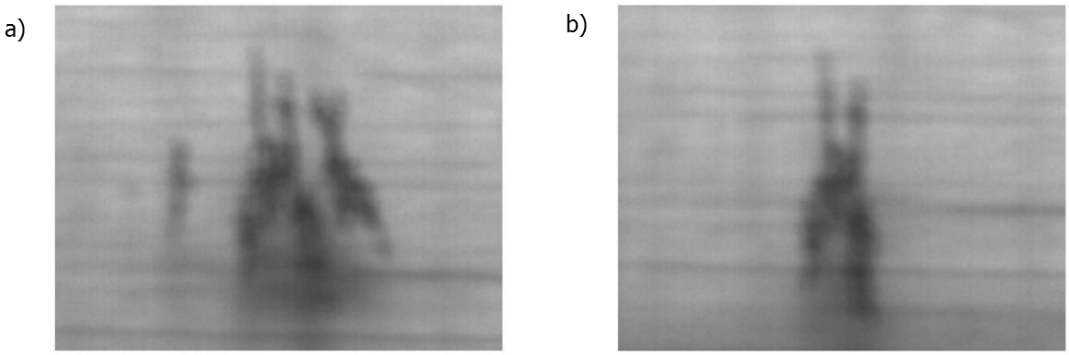


**Figure 5.15.** Powder structure a) pre and b) post substructure mobilisation.

To quantify the variable powder structure, changes in pixel count pre to post transient were determined. This was calculated, using the tracking programme, by averaging the pixel count of the final 300 video frames and subtracting the average of the initial 300 video frames. Percentage increases were then determined by dividing this change in pixel count by the initial count. Figure 5.16 shows that during 57 % of the 103 transients performed, the pixel count of the powder decreased as expected. Conversely, it increased during 43 % of transients tested. In most of these cases (72 % of all increases), the percentage increase was less than 20%. Yet in a few of these cases, the percentage increase was considerably higher.

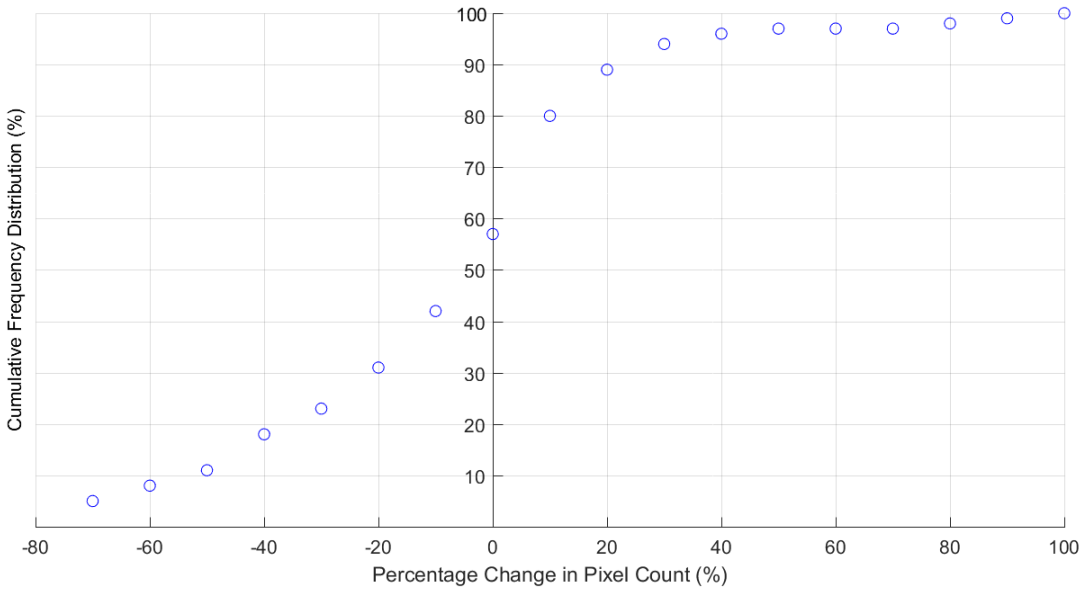


**Figure 5.16.** Cumulative frequency distribution of the percentage change in pixel counts between the start and end of transient tests where mobilisation did not occur.

Initially this may appear impossible as the powder cannot grow or expand. However, these pixel increases could be attributed to two factors. Firstly, the powder could have changed its vertical profile so that the powder intruded less into the flow and spread out along the pipe surface. This would only appear as an increased plan area in the tracking programme as the experiment was unable to resolve the powder height. Secondly, the particles could have moved in such way that the effect of shadowing was more pronounced. This is most evident in the transient videos where the pixel count increases were largest. It was not possible to separate pixels deemed to be shadow and those deemed to be powder using the tracking programme. These two processes could have occurred in isolation or in combination.

Figure 5.17 shows example images of the powder pre and post transient where there was an increase in pixel count. Visually inspecting the unprocessed images (parts a and b) there appears to be some condensing of the powder that should reduce the global plan area. However, after the tracking is applied (parts c and d), the percentage increase in pixel count between these two frames is 32 %. This was most likely due to the shadow created in the bottom right side.

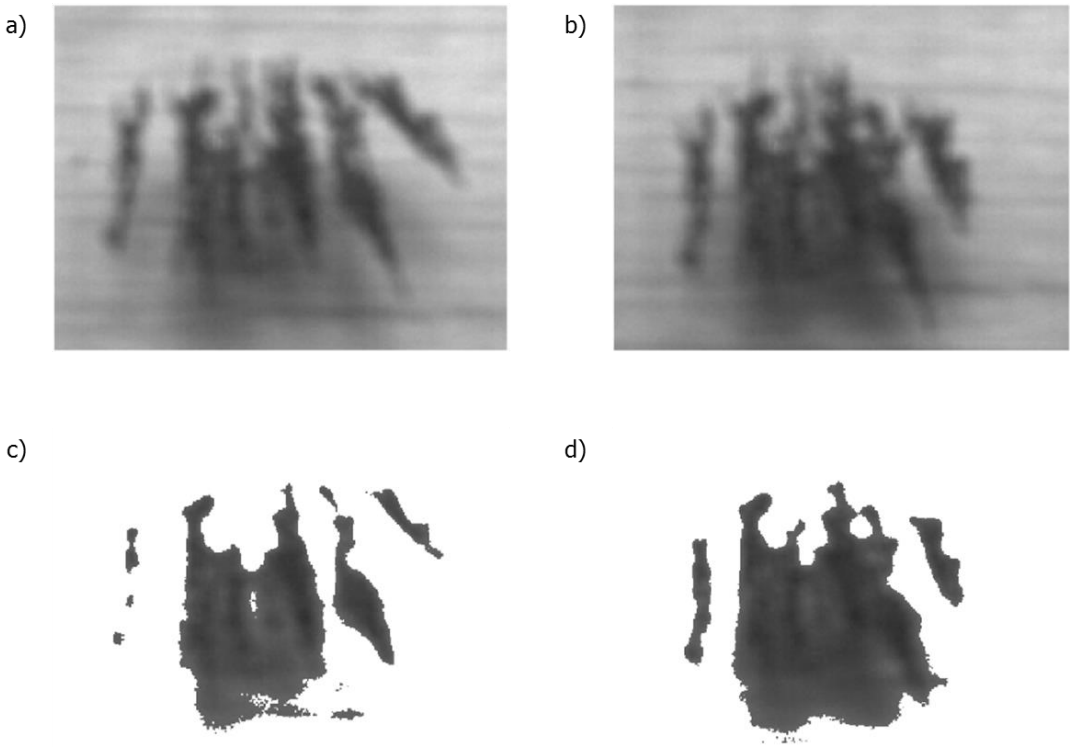


**Figure 5.17.** Powder images pre (a and c) and post (b and d) transient that show an increase in pixel count. Images a) and b) have been unprocessed, where images c) and d) have had the colour threshold applied as part of the tracking programme.

### 5.3.2 Steady State

Akin to the ball bearing experiments, to produce a base line to directly compare to dynamic results, the first mobilisation force relationship determined was for steady state. Figure 5.18 presents the current at which mobilisation occurred for the range of steady state flow rates tested. The regression line shows a positive linear relationship – gradient of 154.04 mA per l/s, offset -79.83 mA, coefficient of determination 0.970. The region below this relationship indicates the magnetic forces are too low, thus mobilisation would always occur due to steady state.

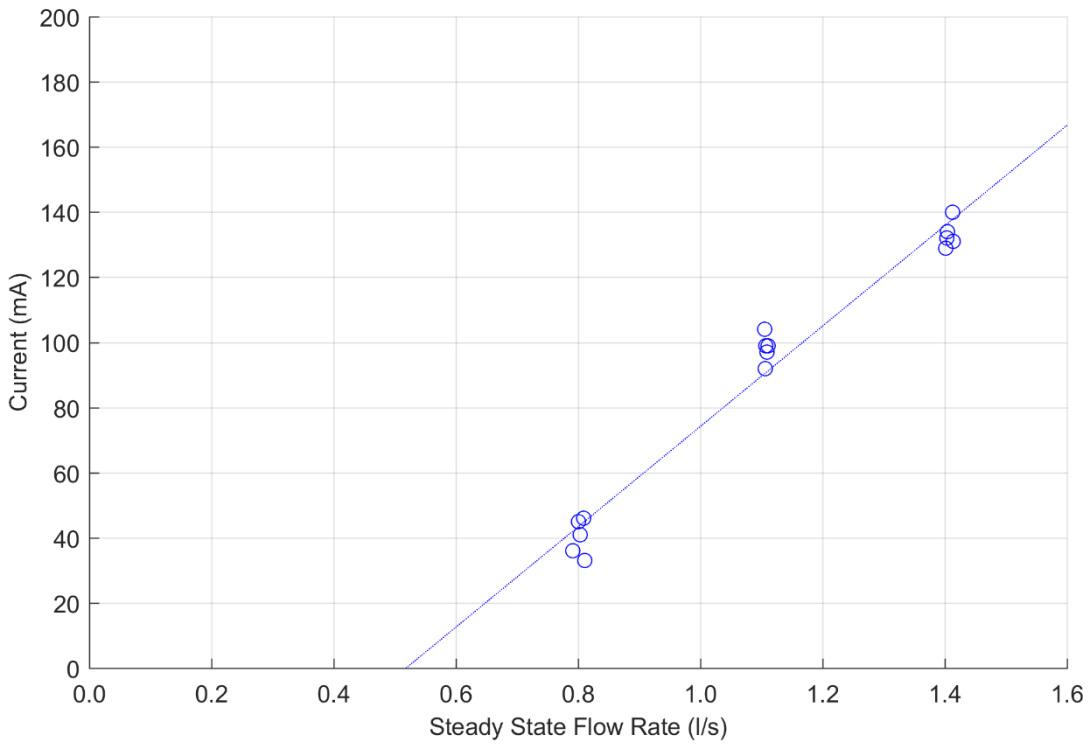


**Figure 5.18.** Relationship between the current at which mobilisation occurred for powder and steady state flow rates.

### 5.3.3 Valve Opening Transients

The aim of these experiments was to determine if valve opening transients can cause mobilisation of the powder, where steady state cannot. Complete transients were performed first, followed by partial transients. The final flow rate was the parameter compared to steady state results.

#### 5.3.3.1 Complete Valve Opening Transients

The powder mobilised downstream when the butterfly valve was rapidly opened, i.e. when the transient was induced. Figure 5.19 shows an example of the powder's location changing, leading to mobilisation, during a complete valve opening transient resulting in 0.44 l/s. Similar to Figures 5.2 and 5.5, part a) of this figure shows discrete frames of the video recorded, and part b) shows the streamwise distance change of the particle, relative to its initial position, determined by processing all video frames through the tracking programme. The frames presented in part a) are indicated in the continuous time series data of part b).

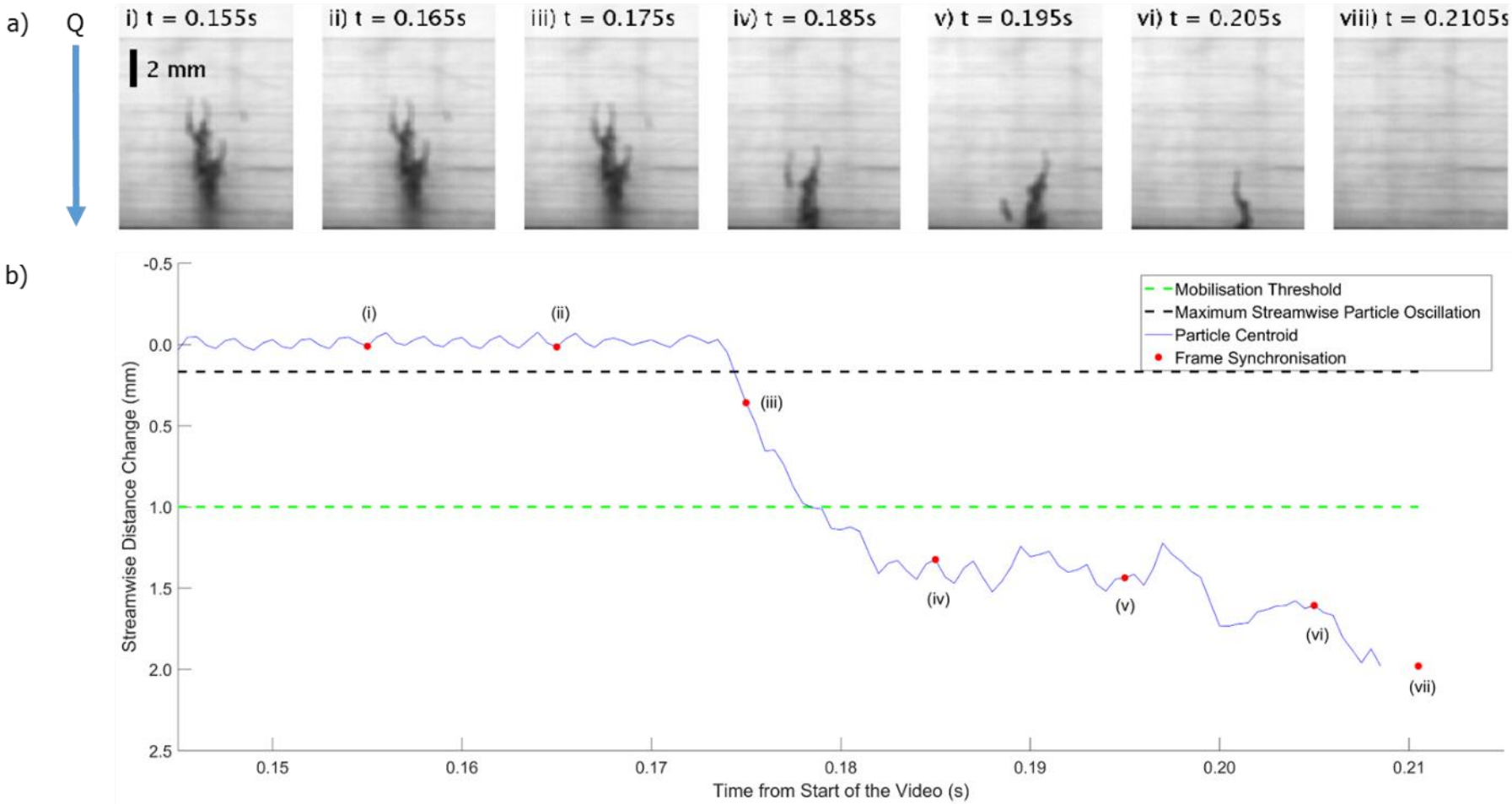


**Figure 5.19.** Streamwise tracking example of powder during a complete valve opening transient transitioning from a zero-initial flow rate to a flow rate of 0.44 l/s. Part a) is a selection of discrete frames taken by the camera. The frames have a 0.1 s spacing. Part b) is the streamwise distance change of the particle centroid, relative to its initial position, determined by processing all video frames through the tracking programme. The frames presented in part a) are indicated in the continuous time series data of part b).

The example presented in Figure 5.19 demonstrates that complete valve opening transients can mobilise the powder past the field of view. Figure 5.20 presents pressure data collected for complete valve opening transients that caused mobilisation. The same format is applied as described previously in Figure 5.5.

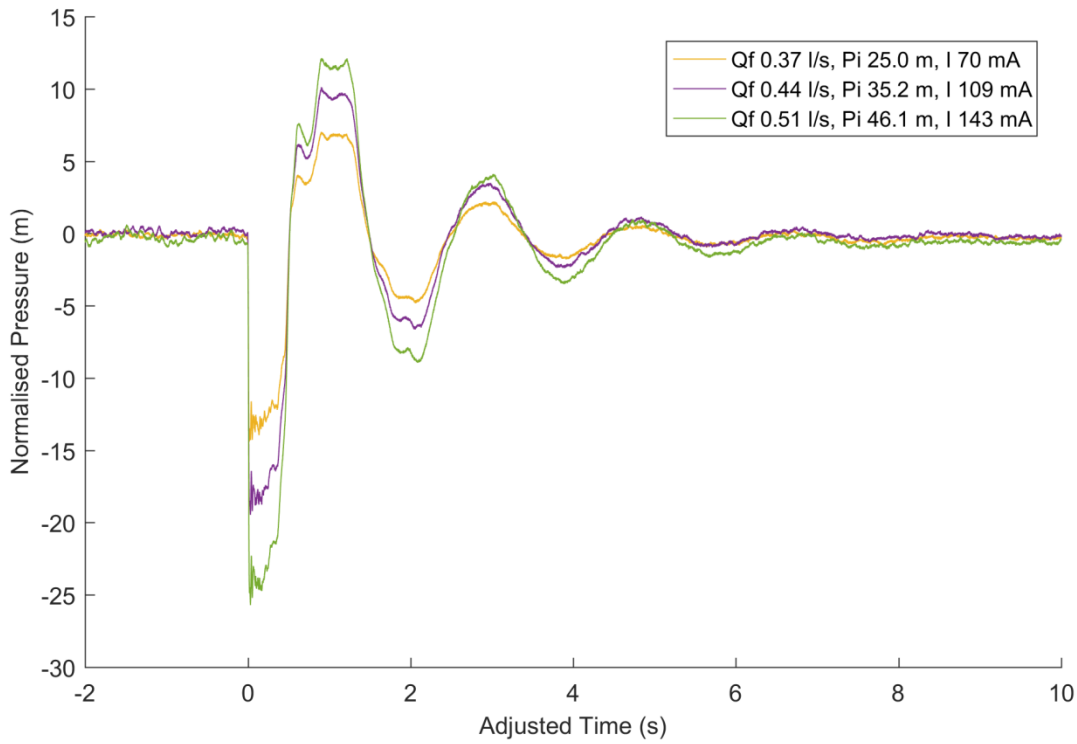


**Figure 5.20.** Pressure traces of complete valve opening transients that caused mobilisation of the powder. Traces are normalised by subtracting initial pressure and adjusted so that the first surge commences at time zero. $Q_F$ final flow rate, $P_I$ initial pressure, $I$ current at which mobilisation occurred.

Figure 5.20 shows that as the final flow rate and initial pressure were increased, the magnitude of the pressure changes increased, i.e. the transients appear to be stretched parallel to the vertical pressure scale. These transients then correspond to the currents at which mobilisation occurred; the greater the pressure changes, the greater the current. Relating these currents to the final flow rate of the complete valve opening transients produced a positive linear relationship – gradient of 572.20 mA per l/s, offset -144.40 mA, coefficient of determination 0.917. These are presented in Figure 5.21 for all repeats tested, along with steady state results.

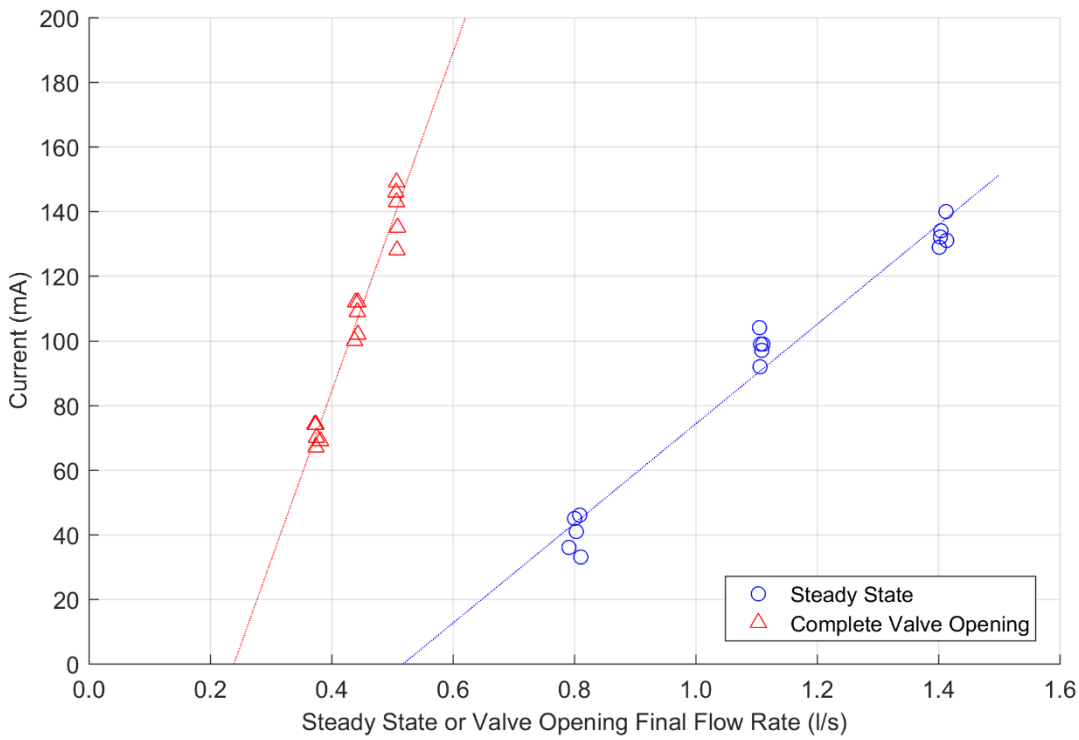


**Figure 5.21.** Relationships between the current at which mobilisation occurred for powder and steady state flow rate, or complete valve opening final flow rate.

The complete valve opening mobilisation force relationship sits above the steady state relationship, thus confirming complete valve openings can cause mobilisation and steady state cannot for powder. For example, a minimum steady state flow rate of 0.518 l/s is necessary to mobilise the particles (self-weight only), yet rapidly opening the valve to this flow rate balances a particle held with 152 mA of additional force. Therefore, particles held at a current at 152 mA or less will be mobilised by the transient and not by steady state.

5.3.3.2 Partial Valve Opening Transients

One set of partial valve opening transients was tested with the powder material. It was decided to repeat a set of the ball bearing partial valve opening transients for direct comparison between materials. The conditions chosen were initial flow rate of 0.5 l/s and final flow rate of 0.7 l/s (ball bearings set three) to span between the steady state and complete valve opening results.

For these partial valve opening transients tested, the particles were mobilised past the 1 mm threshold. Videos collected that exhibit this mobilisation occurring are not offered here as they showed no difference to the images (camera frames) presented in Figure 5.18 a). Figure 5.22 presents pressure data collected for partial valve opening transients that caused mobilisation. The same format is applied as described previously in Figure 5.5.

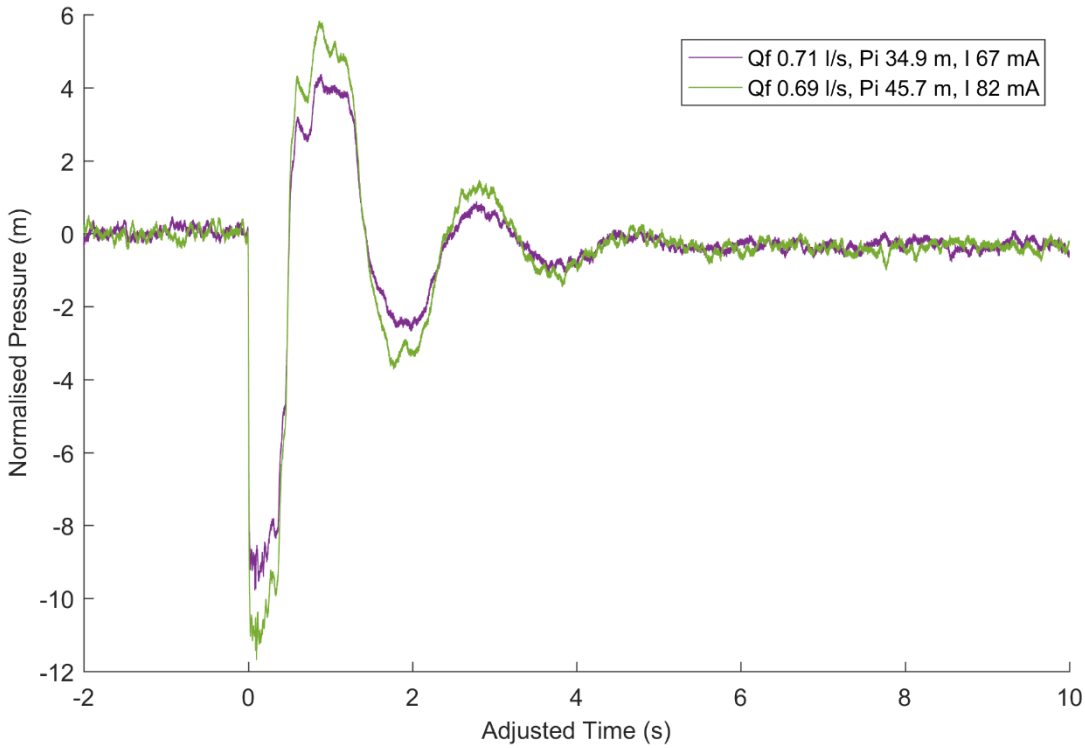


**Figure 5.22.** Pressure traces of partial valve opening transients that caused mobilisation of the powder. Traces are normalised by subtracting initial pressure and adjusted so that the first surge commences at time zero. $Q_F$ final flow rate, $P_I$ initial pressure, $I$ current at which mobilisation occurred.

Figure 5.22 shows that as the initial pressure was increased, the magnitude of the pressure changes increased. These transients then correspond to the currents at which mobilisation occurred; the greater the pressure changes, the greater the current. Figure 5.23 shows the currents at which mobilisation occurred against the final flow rate of these partial valve opening transients, for all repeats tested. Steady state and complete valve opening results are also plotted for ease of comparison. The mobilisation force relationship sits above the steady state relationship, demonstrating that there are situations where partial valve openings can cause mobilisation and steady state cannot.

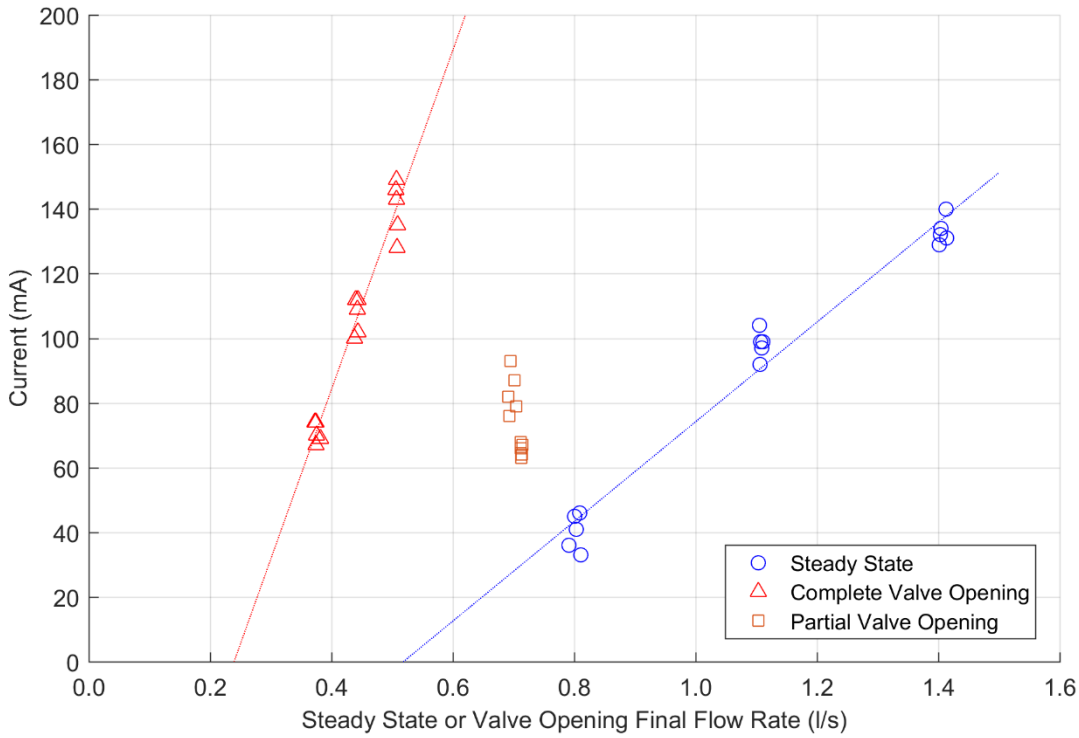


**Figure 5.23.** Relationships between the current at which mobilisation occurred for powder and steady state flow rate, or valve opening final flow rates (complete and partial).

### 5.3.4 Confirming Mobilisation of Powder

In section 4.3.6, the ball bearings were shown to exhibit a significant step change in particle movements as the current was decreased during transient testing. This showed that the method used to determine the current at which mobilisation occurred captured a consistent and distinctive phenomenon. The aim of this section is to determine if the same step change occurred in the powder results.

Of the 25 powder transient tests performed, 19 (76 %) exhibited a distinct step change in streamwise distance movements at the current at which mobilisation occurred. These results were consequently accepted. The remaining six transients did not display a significant variation in streamwise distance movements at the mobilisation current. Therefore, they were examined further.

Table 5.2 indicates the transients that showed this step change (✓) and the transients that did not (cross). This behaviour did not vary with initial flow rate, but did correlate with initial pressure. As the initial pressure increased, more transients exhibited step changes in movements.

**Table 5.2.** Valve opening transients that exhibited a step change in the streamwise distance movements of the powder.

| Valve Opening Type | Repeat Number | Initial Pressure | | |
|---|---|---|---|---|
| | | 25 m | 35 m | 45 m |
| Complete Initial Flow Rate 0.0 l/s | 1 | ✓ | ✓ | ✓ |
| | 2 | × | ✓ | ✓ |
| | 3 | × | × | ✓ |
| | 4 | × | ✓ | ✓ |
| | 5 | × | ✓ | ✓ |
| Partial Initial Flow Rate 0.5 l/s | 1 | | ✓ | ✓ |
| | 2 | | ✓ | ✓ |
| | 3 | | ✓ | ✓ |
| | 4 | | × | ✓ |
| | 5 | | ✓ | ✓ |

All transients performed showed that the powder's initial position varied in the streamwise direction between tests. Examination of the videos recorded for the six transients, however, revealed that at the current which mobilisation occurred the powder was in a much lower streamwise initial position (closer to the edge of the field of view). Therefore, the distance from this lower position to the edge was not dissimilar to previous non-mobilising currents.

Figure 5.24 presents two sets of repeated transients tested with the powder. For both, the initial position of the powder is plotted for the decreasing currents tested, and a downstream arrow indicating the streamwise distance change during the transient. Part a) is from a complete valve opening transient with initial pressure 45 m that shows a significant streamwise distance movement at the mobilisation current of 135 mA. The figure illustrates this with a large arrow. Part b) is from a complete valve opening transient with initial pressure 35 m. In this example the streamwise distance movement at the mobilisation current of 102 mA (1.36 mm) is no larger than the previous movements (0.03 mm to 1.52 mm).

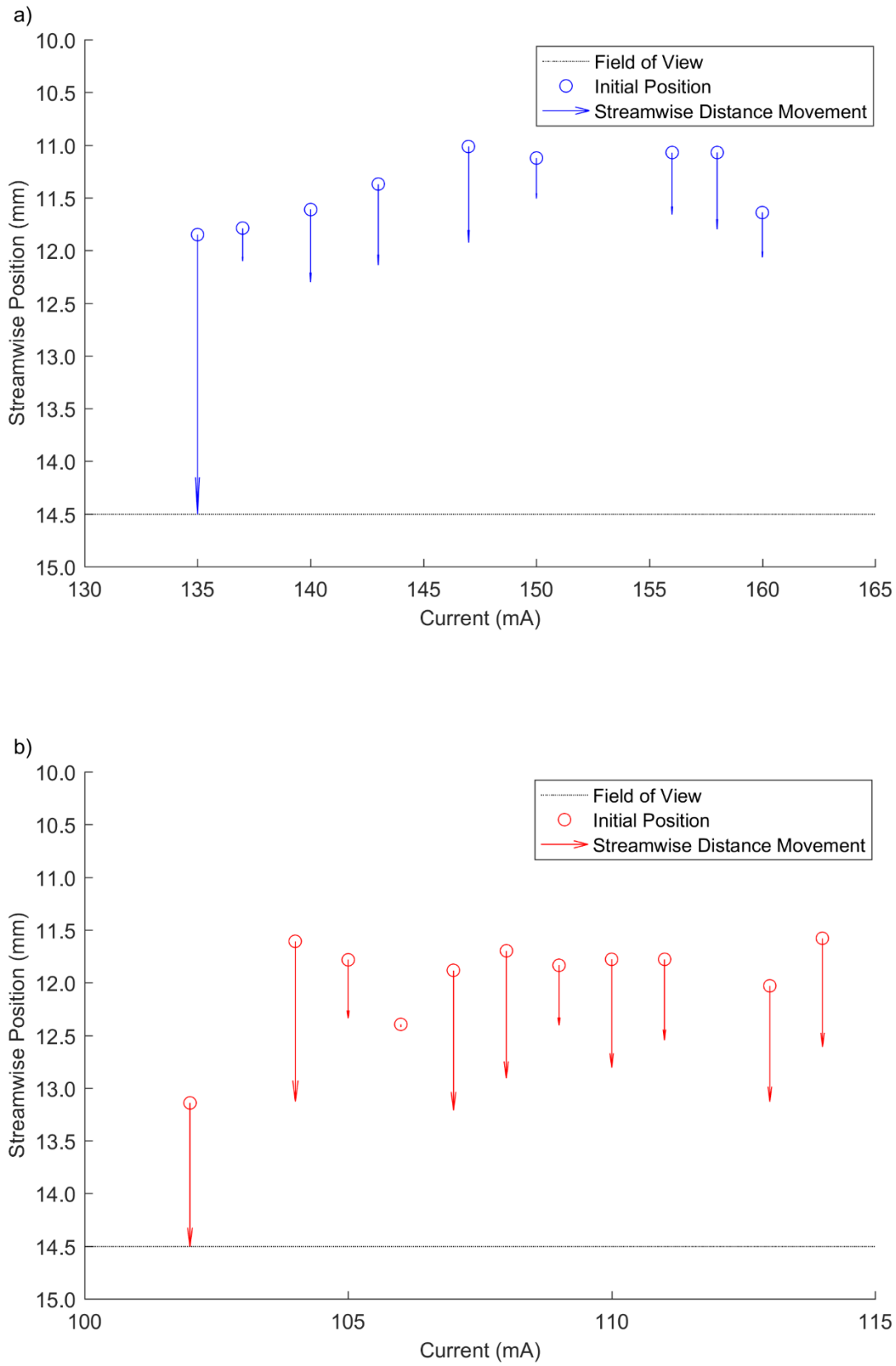


**Figure 5.24.** Initial streamwise positions and distance moved of the powder during example sequences of transients with decreasing currents. They either show a step change in distances moved (a) or consistent distances moved (b).

A significant movement of the powder over the mobilisation threshold could have occurred in the second example sequence of transients. Yet the increased proximity of the powder to the edge of the field of view meant this potential movement could not be distinguished from the previous movements. In conclusion, the six transients in question may or may not have demonstrated the same phenomena as the other 19 transients. These results were consequently rejected. Figure 5.25 presents the results originally given in Figure 5.23, but with the rejected results removed.

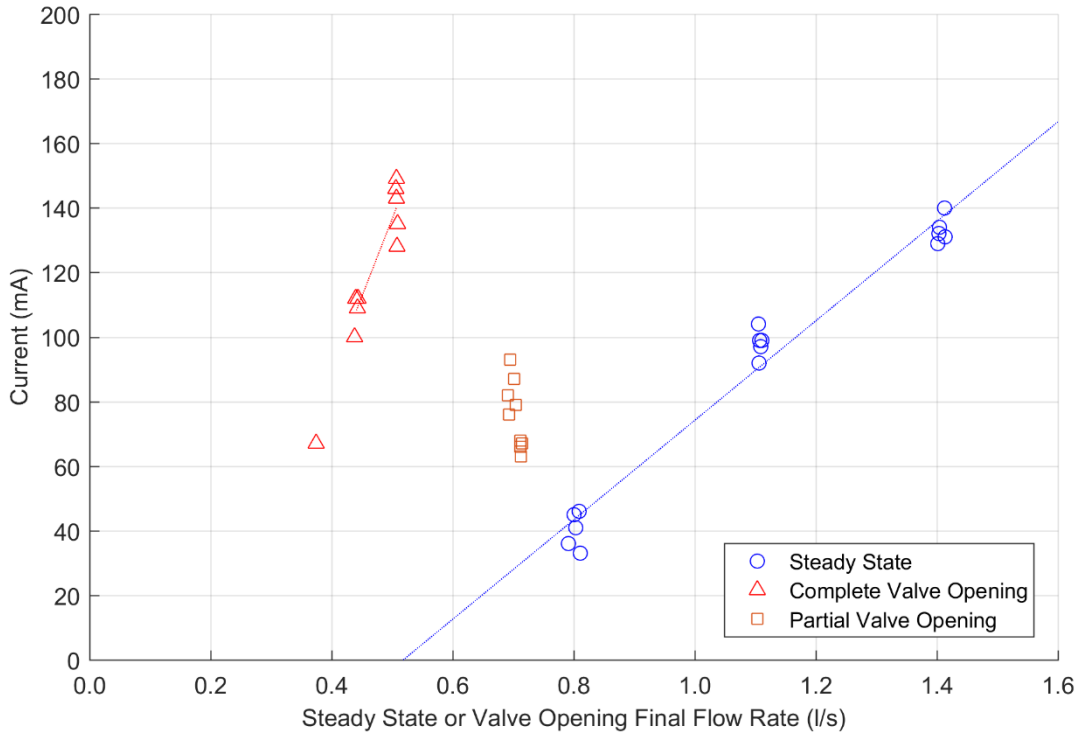


**Figure 5.25.** Relationships between the current at which mobilisation occurred for powder and steady state flow rate, or valve opening final flow rates (complete and partial). Rejected results have been removed.

## 5.4 Summary

Results presented in this chapter demonstrated the ability of transients to mobilise adhered particles where steady state cannot. This was repeatedly evidenced by transient mobilisation force relationships sitting above the steady state mobilisation force relationship, for both ball bearings and powder structures. Furthermore the results showed that this finding was consistent across multiple hydraulic conditions and different types of transient (complete valve closing, complete valve opening, partial valve opening). Of particular importance are the complete valve closing results as under typical steady state approaches the particles would not have been able to mobilise. These findings, however, must be

considered for only the transients generated in this work and cannot be extrapolated to all possible conditions.

# Chapter Six

# Analysis of Transient Mobilisation Behaviour

## 6.1 Introduction

Chapter Five demonstrated the ability of transients to mobilise adhered particles where steady state flow rate did not. Hence, an objective of this work was to determine how transients caused mobilisation. Particularly, identifying parameters describing the transient to understand how they relate to mobilisation. To achieve this objective, results from the ball bearing experiment will be analysed in detail, as the simplest and most idealised cases of mobilisation. Any knowledge derived from exploring the ball bearing results will then be applied to results from the powder experiment. This approach will demonstrate the transferability of the analysis to a more representative material.

Steady state conditions pre and post dynamic event are typically used to describe transients (section 2.3.1). These robust parameters, for both flow and pressure, act as boundary conditions to the dynamic event. Therefore, the first section of this chapter compares various steady state conditions to currents at which mobilisation occurred, to determine if these parameters correlate with mobilisation. Any further effects of these conditions are also examined. The conditions studied are: initial flow rate (section 6.2.1), final flow rate (section 6.2.2), initial pressure (section 6.2.3), final pressure (section 6.2.4), change in flow rates (section 6.2.5) and change in pressures (section 6.2.6). A summary of these findings is then given (section 6.2.7). Secondly, short-term or dynamic parameters that occur between the steady state initial and final conditions are examined (section 6.3). The following section then aims to develop a function to describe transient mobilisation behaviour to compare to steady state mobilisation behaviour (section 6.4). These sections use the ball bearing results. Section 6.5 then applies knowledge derived from the ball bearing analysis to the powder mobilisation results. Finally, a chapter summary is given (section 6.6).

## 6.2 Effect of Initial and Final Steady State Conditions on Mobilisation

### 6.2.1 Effect of Initial Flow Conditions

Initial conditions are needed to compute transient conditions as they act as the starting point for the transient. Flow rate was explored first as this is the most common parameter for describing operational conditions in DWDS. This section addresses different aspects of initial flow conditions on the particle's behaviour. It is broken into four sub sections. The first aimed to determine if initial flow rate correlated with the currents at which

mobilisation occurred. The following sub sections then explore other observations seen with regard to this parameter, including the effect of initial flow regime, initial particle transverse movements, and streamwise movements (pre and post mobilisation).

#### 6.2.1.1 Effect of Initial Flow

Complete valve closing transient results presented in Figure 5.4 demonstrated a relationship between the initial flow rate and the current at which mobilisation occurred. This was a positive linear relationship – gradient of 319.91 mA per l/s, offset -21.08 mA, coefficient of determination 0.998. Therefore, for valve closing transients, the initial flow rate was most likely a dominant factor for mobilisation.

Valve opening transients were performed at discrete initial flow rates of zero flow rate (complete), 0.1 l/s (partial set one), 0.3 l/s (partial set two), 0.5 l/s (partial set three), and 0.7 l/s (partial set four). Figure 6.1 presents the currents at which mobilisation occurred for the initial valve opening flow rates. In contrast to valve closing transients, there is not a simple linear relationship in these cases. This is most easily observed in complete valve opening transients where, for the same zero initial flow rate, almost the full range of currents (168 mA to 390 mA) were produced. However, there appears to be a quadratic relationship – squared term coefficient 785.67 mA per $(l/s)^2$, linear term coefficient -622.79 mA per l/s, offset 310.96 mA, coefficient of determination 0.444. This suggests that for valve opening transients initial flow rate does play a role in transient mobilisation, but it is not the only dependent factor. The scatter seen in each data set is explored later.

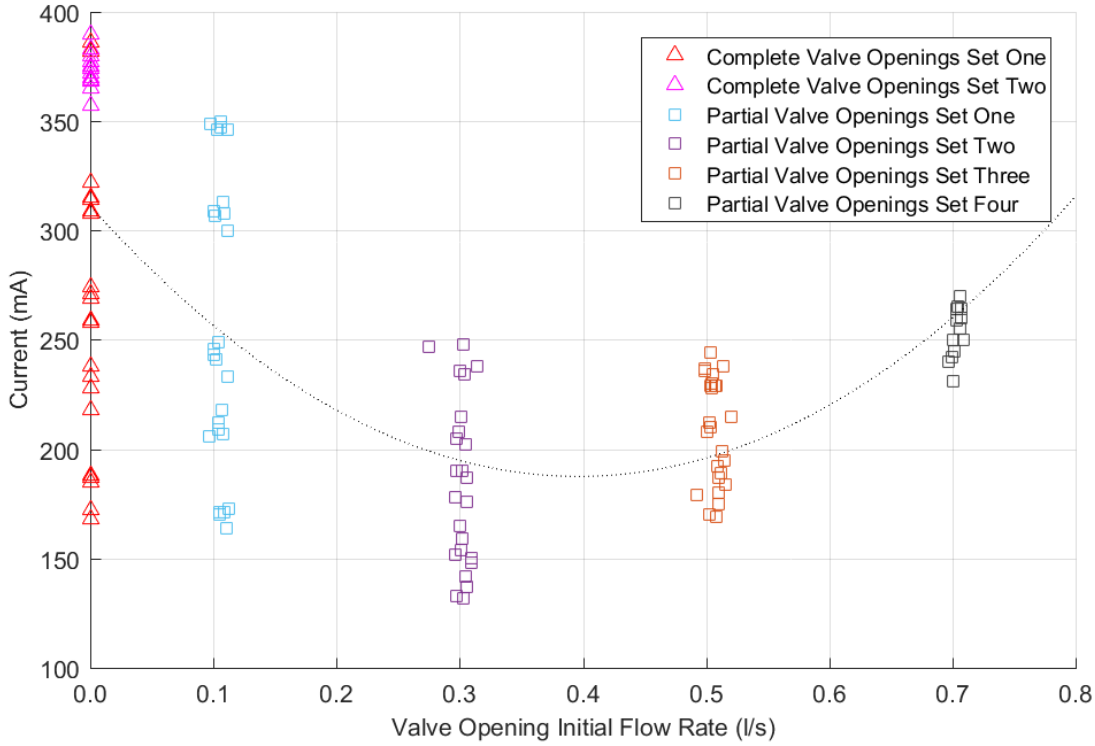


**Figure 6.1.** Currents at which mobilisation occurred for ball bearings, against valve opening initial flow rates.

6.2.1.2 Effect of Initial Flow Regime

Turbulent flow induces complex flow behaviour, including eddies, near the pipe wall, whereas in transitional flow the boundary layer is laminar (described in section 2.3.3). These eddies during turbulent initial steady state flow could affect the transient forces, and, thus, the current at which mobilisation occurred. To explore the effect of flow regime, transients with varying initial flow rates, across two flow regimes, were analysed to compare the currents at which mobilisation occurred.

Two sets of valve opening transients were performed with non-turbulent initial flow rates (completes and partials set one). For these data sets, the change from initial to final flow rates was varied. Other valve opening transients with turbulent initial flow rates (partials sets two to four) had constant changes in flow rates. Two parameters, initial flow regime and change in flow rate, were altered across these results. Therefore, initial flow regime cannot be independently examined here for valve opening transients. Only complete valve closing transients met this criterion.

A group of complete valve closing transients were performed at initial flow rate 0.102 l/s ± 0.003 l/s, Reynolds numbers 3200 ± 110, which are therefore in the transitional range. Other valve closing tests were fully turbulent with Reynolds numbers greater than 13000. This can be seen in Figure 6.2.

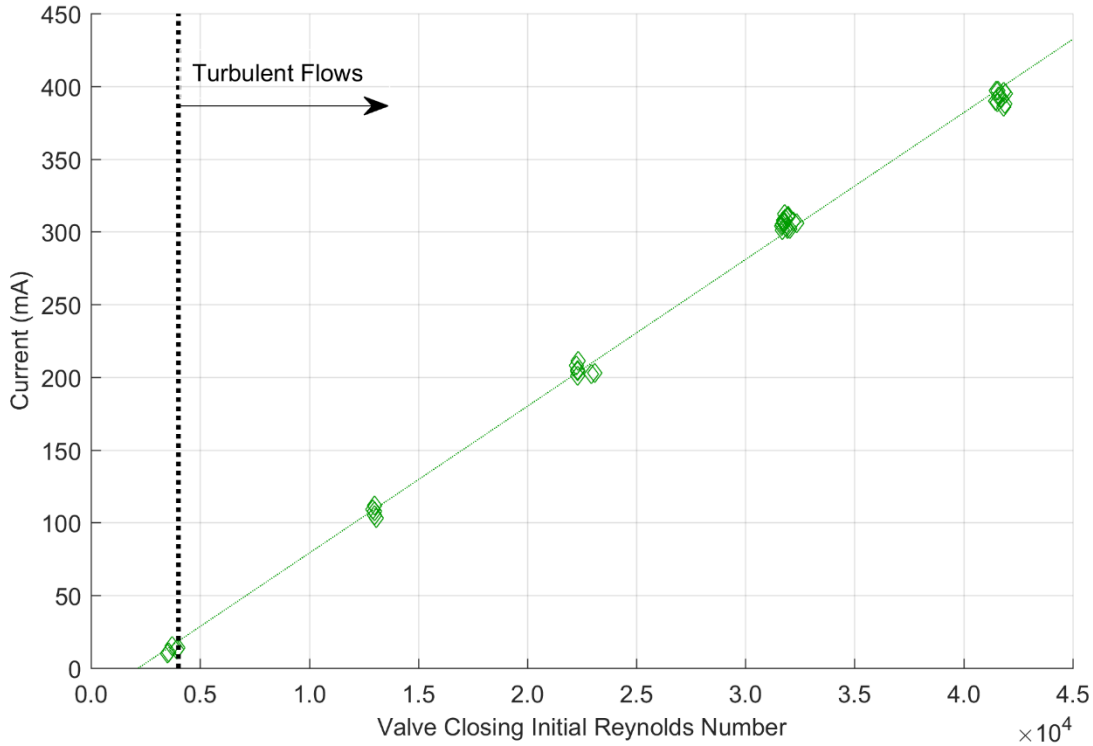


**Figure 6.2.** Currents at which mobilisation occurred for ball bearings, against complete valve closing initial Reynolds numbers. The turbulent flow regime boundary is indicated at initial Reynolds number of 4000.

The complete valve closing mobilisation force relationship was determined for all initial flow rates tested. A second relationship was determined for only turbulent initial flow rates, i.e. it excluded the tests performed at initial flow rate 0.102 l/s ± 0.003 l/s. The two relationships are not statistically different (p-value > 0.05). It, therefore, appears that the transitional flow regime did not affect the currents at which mobilisation occurred. Yet, as there is only one group of complete valve closing transients with high transitional initial flow rates, this finding is not conclusive.

#### 6.2.1.3 Effect of Initial Particle Movements

As shown in section 4.3.5, the particles made small movements prior to mobilisation. These movements occurred in the transverse (across-pipe) and streamwise (along-pipe) directions, and these movements increased with greater flow rates. To explore how the transverse and streamwise movements affected mobilisation, the movements were quantified (standard deviation of locations) during initial pseudo steady state flow and compared to the currents at which mobilisation occurred. Transverse movements were analysed first as these were consistently the larger of the two movements seen, therefore most likely to have the greatest effect. It is worth noting that complete valve opening set two transients were not recorded due to a software error, so initial particle movements for these transients were not available.

Transverse particle movements broadly correlate with mobilisation (Figure 6.3). As the initial transverse particle movements increase, the current at which mobilisation occurred also increased. However, values of mobilisation current can relate to multiple values of transverse particle movements. Initial flow rate also positively correlated with transverse particle movements (Figure 4.14) and is a factor in mobilisation (Figure 5.4). Any correlation, therefore, between initial transverse movements and mobilisation current is misleading as initial flow rate is the common dependent parameter.

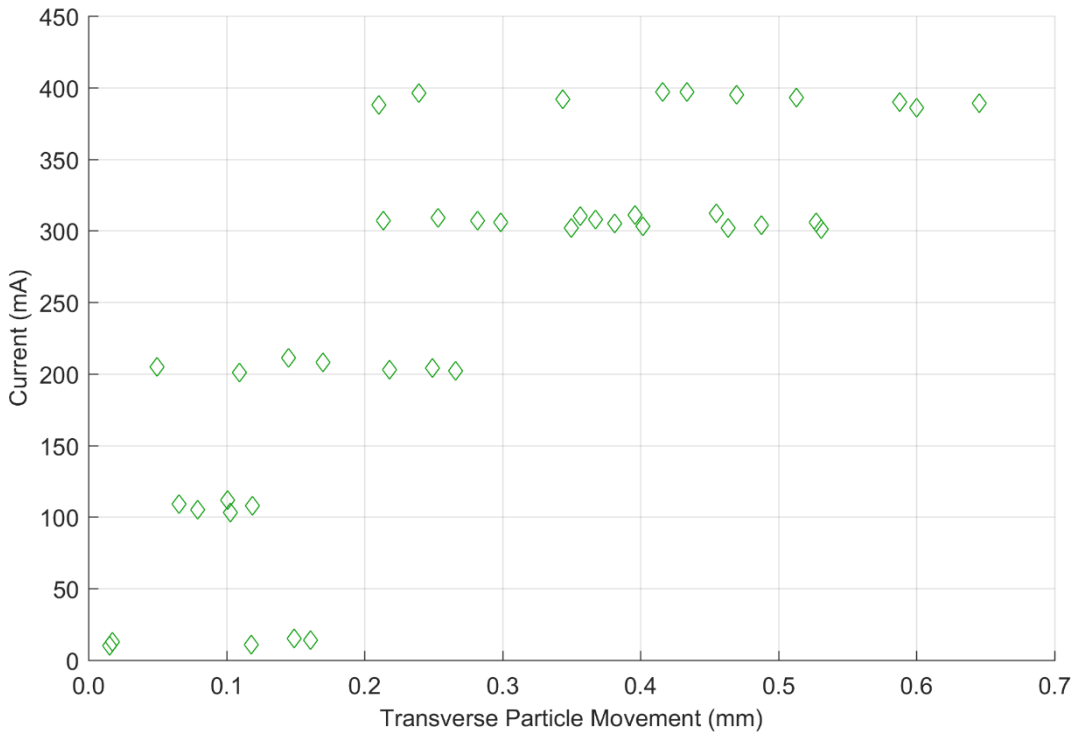


**Figure 6.3.** Currents at which mobilisation occurred for complete valve closing transients using ball bearings, against transverse movements particles in the initial flow.

Figure 6.4 presents the currents at which mobilisation occurred plotted against initial transverse movements, for all valve opening transients. The majority (90.4 %) of transverse movements were less than 0.1 mm and do not correlate with mobilisation (Figure 6.4). The only conditions where transverse particle movements were greater than 0.1 mm were partial valve opening set four transients that transitioned from 0.7 l/s initial flow rate to 0.9 final flow rate, i.e. the largest flow conditions. However, these values did not correlate with current.

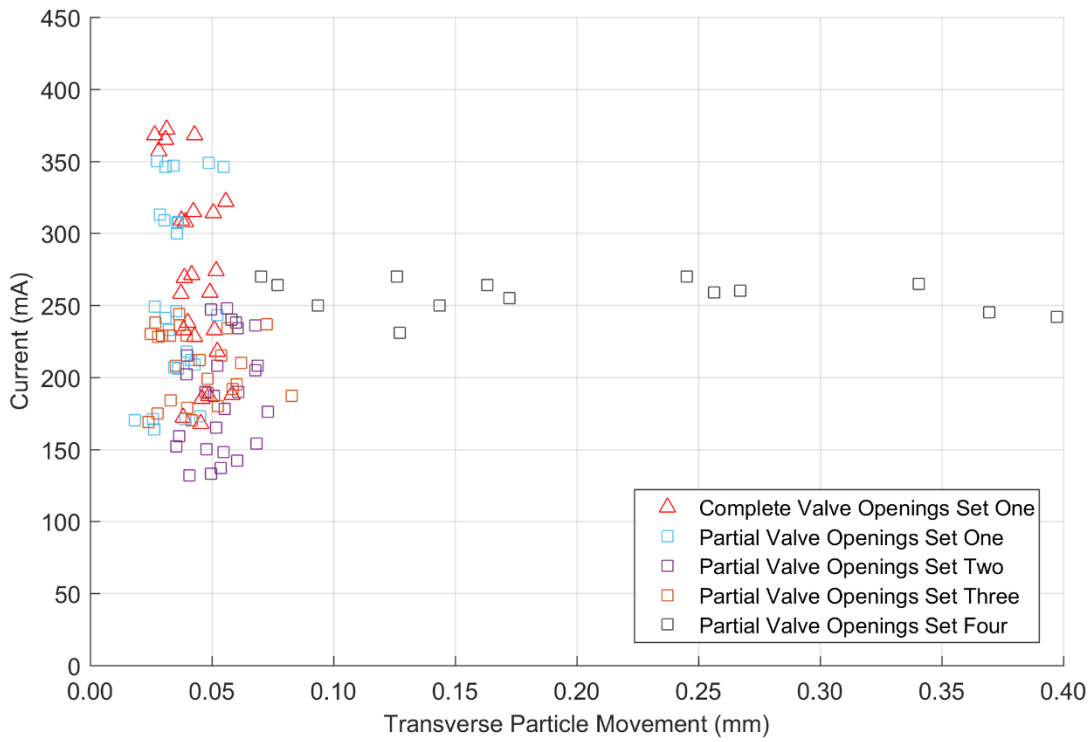


**Figure 6.4.** Currents at which mobilisation occurred for all valve opening transients using ball bearings, against transverse movements particles in the initial flow.

In a similar manner, the initial streamwise movements are consistently smaller than in the transverse direction, up to approximately 20 times smaller (Figures 6.5 and 6.6). Analysis of valve closing transients (Figure 6.5) showed that streamwise particle movements broadly correlate with mobilisation. However, in the same manner as for transverse direction, values of current can relate to multiple values of streamwise particle movements. For example, a test resulting in mobilisation current 388 mA exhibited initial streamwise movements of 0.020 mm, the third lowest value seen. Yet a repeat of the same test, which resulted in mobilisation current 392 mA, exhibited the largest value of initial streamwise movements, 0.149 mm. It is believed that initial flow rate is likely to cause streamwise particle movements (Figure 4.14) and be a factor in mobilisation (Figure 5.4). Any correlation between initial streamwise movements and mobilisation current is, therefore, misleading as initial flow rate is the common dependent parameter, consistent with observations of initial transverse movements.

Analysis of valve opening transients (Figure 6.6) shows that the few higher values of streamwise movements (greater than 0.03 mm) occurred at the highest final (and initial) flow rates. However, there is not a correlation between streamwise particle movements and currents at which mobilisation occurred. This is also consistent with observations of initial transverse movements.

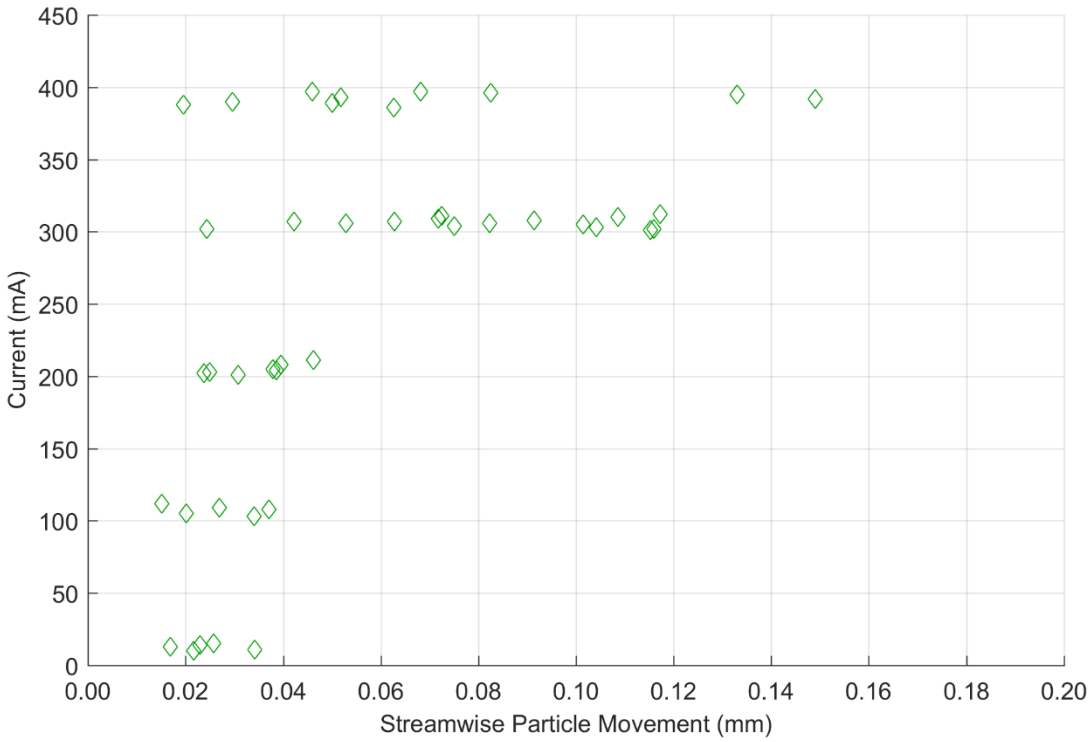


**Figure 6.5.** Currents at which mobilisation occurred for complete valve closing transients using ball bearings, against streamwise movements particles in the initial flow.

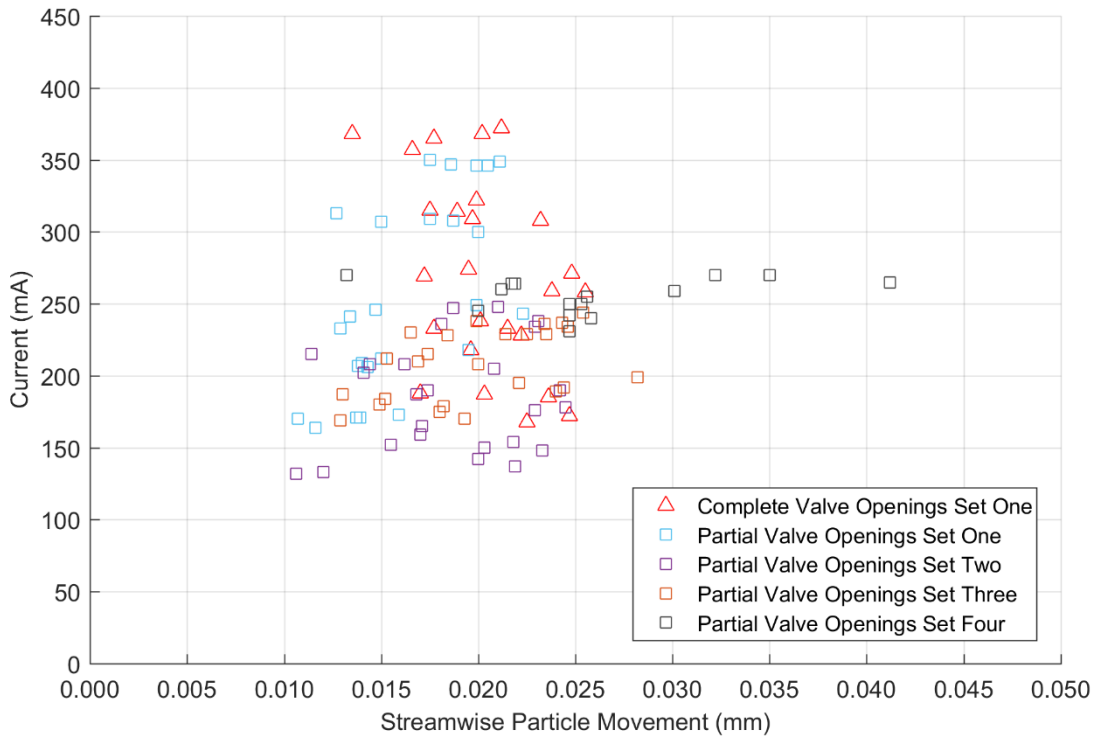


**Figure 6.6.** Currents at which mobilisation occurred for all valve opening transients using ball bearings, against streamwise movements particles in the initial flow.

6.2.1.4 Valve Opening Streamwise Movements Post Initiation of Mobilisation

Particle motion after the initial of mobilisation is part of the mobilisation process and is of interest due to a possible link to the induced transient forces. This section explores streamwise movements after mobilisation is initiated, to determine if they relate to initial flow rates and/or currents at which mobilisation occurred.

During complete valve opening transients, the ball bearings were mobilised downstream from their initial position in one motion; the ball bearing started to move and continued downstream out of the field of view. This was demonstrated in Figure 5.5 b). Particle tracking revealed that out of the total 115 valve opening transients (complete and partial), 64 % of tests exhibited this same response.

In other cases, the ball bearing was carried a small distance downstream (a "motion"), the ball bearing would stay at this new location, then be carried again (a second "motion") and so on. The particle tracking programme produced stepped tracks of the streamwise position comprised of up to five motions. Figure 6.7 presents a streamwise tracking example of a ball bearing during a partial valve opening transient transitioning from 0.5 l/s to 0.7 l/s flow rate. This example exhibits three motions at approximately 0.34 s, 0.72 s, and 1.22 s from the start of the video, surpassing the mobilisation threshold during the first motion.

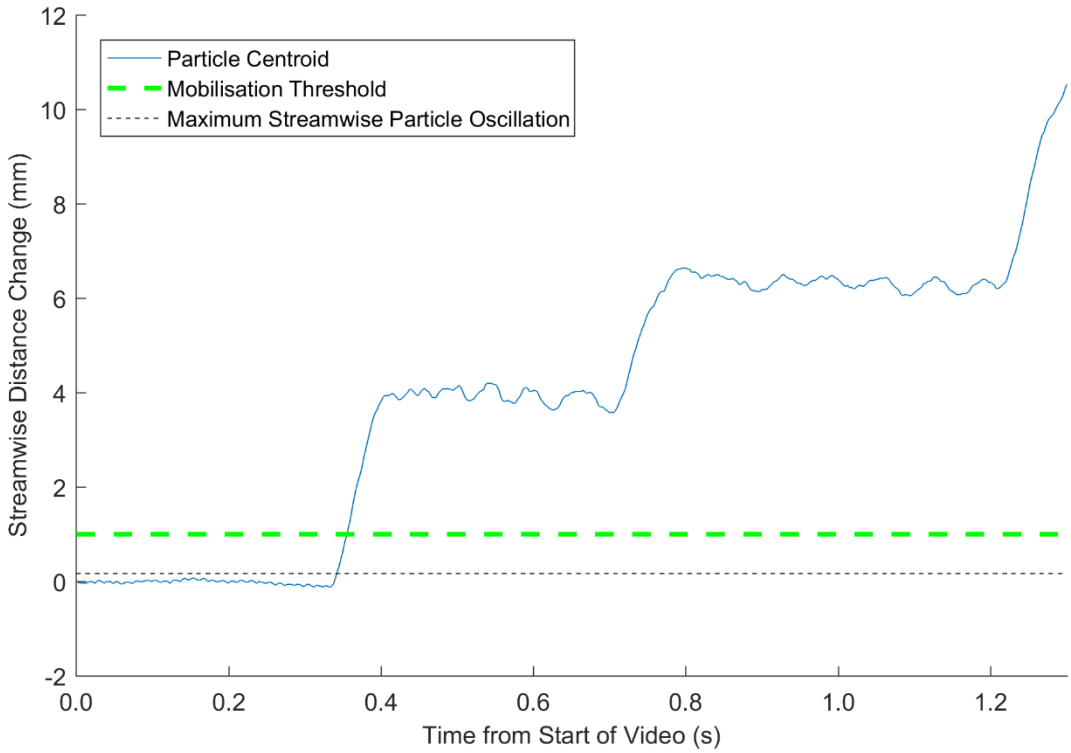


**Figure 6.7.** Streamwise tracking example of a ball bearing during a partial valve opening set three transient transitioning from 0.5 l/s to 0.7 l/s flow rate, initial pressure 34.9 m. Three

downstream motions of the particle are presented at approximately 0.34 s, 0.72 s, and 1.22 s from the start of the video, and the mobilisation threshold is surpassed in the first motion.

The number of travel motions did not correlate with the initial pressure, final flow rate or current at which mobilisation occurred. Furthermore, there was no consistency between repeats. For example, the five repeats of partial valve openings with initial conditions of 0.5 l/s and 40 m exhibited 1, 2, 2, 3, and 4 motions. There does, on the other hand, appear to be a connection between the transient initial flow rate and the number of motions seen. Figure 6.8 presents the breakdown of the transients by number of motions occurred, for each set of valve opening transients ordered by the initial flow rate. For transients where the initial flow rate is zero or has a transitional Reynolds number (complete valve openings and partial valve openings set 1), all transients were mobilised in one motion. Transients where the initial flow rate was turbulent (0.3 l/s and above) exhibited stepped series of motions during mobilisation. Once in this flow regime, there does not appear to be a relationship between number of motions and the flow rate, e.g. the maximum number of motions seen (five) does not occur in the greatest flow rate tested (0.7 l/s).

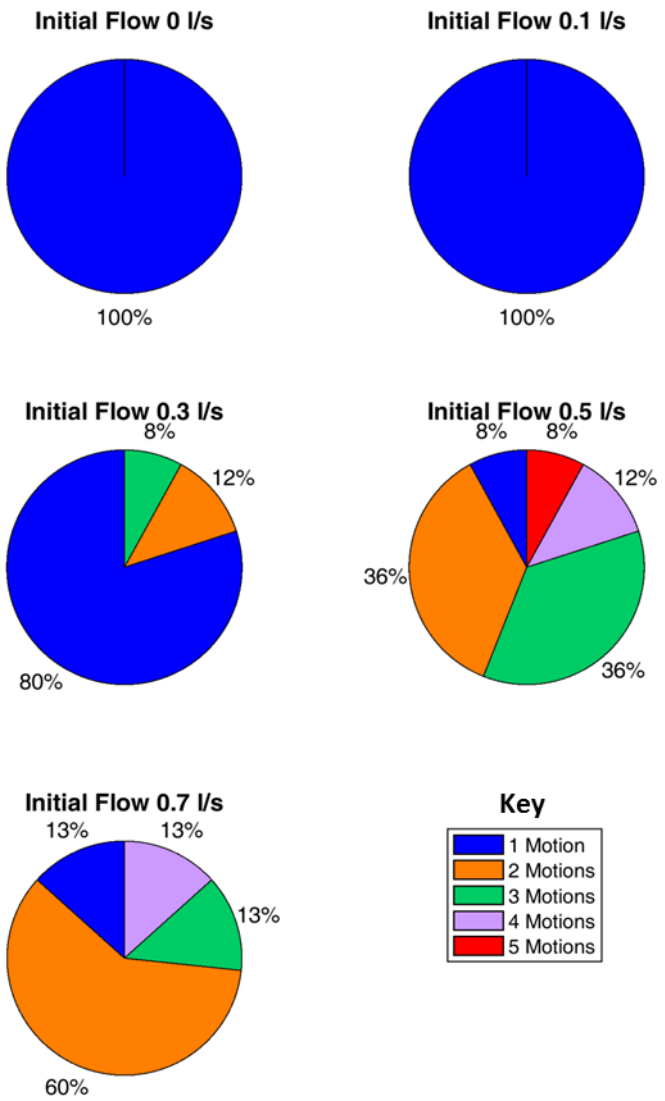


**Figure 6.8.** Breakdown of transients by number of particle motions seen.

Further examination of the multiple-motion streamwise distance tracks shows that in 80 % of cases, the first motion was greater than the mobilisation threshold, as seen in Figure 6.7. This was irrespective of the number of consecutive motions. In the other 20 % of cases, the mobilisation threshold was only clearly exceeded by the second motion, as seen in Figure 6.9. These later transients (20 % of the multiple-motion cases, but only 8 out of the total 115) varied in initial conditions and did not exhibit any dissimilarity in mobilisation current from the single motion transients.

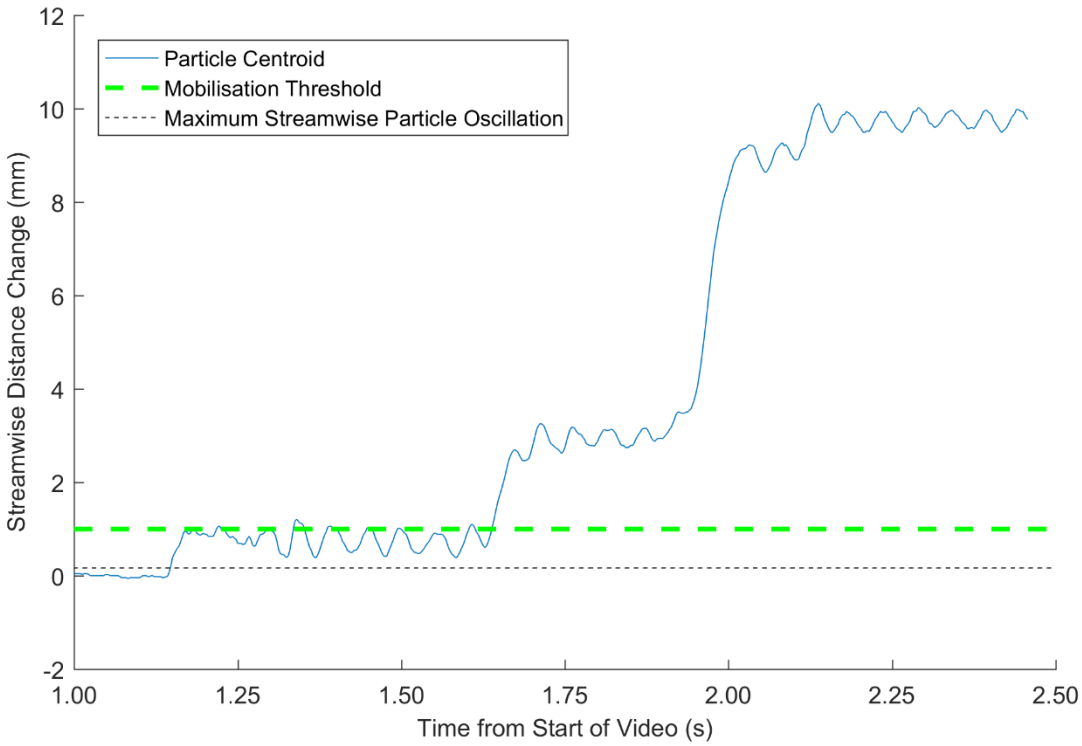


**Figure 6.9.** Streamwise tracking example of a ball bearing during a partial valve opening transient transitioning from 0.5 l/s to 0.7 l/s flow rate, initial pressure 39.7 m. Three downstream motions of the particle are presented at approximately 1.14 s, 1.64 s, and 1.94 s from the start of the video, and the mobilisation threshold is only clearly surpassed in the second motion.

In summary, the initial flow regime of valve opening transients affected whether the ball bearings mobilised in a single motion or in several. Multiple downstream motions were only found when the transient has turbulent initial flow conditions. However, these movements did not appear to correlate with the current at which mobilisation occurred.

### 6.2.2 Effect of Final Flow Conditions

Initial flow rate was previously investigated as the boundary condition for the start of a transient. Here, the opposing boundary condition is addressed; the hydraulic environment that the transient transitions into. To investigate the effect of final flow rates on currents at which mobilisation occurred, the second set of complete valve opening transients were examined, as the final flow rate was the controlled independent parameter. For these transients the initial flow rate and pressure were constant at 0 l/s and 45m, respectively. Currents at which mobilisation occurred were determined for three different final flow rates; 0.2 l/s, 0.5 l/s and 0.7 l/s. Figure 6.10 represents these results, originally shown in Figure 5.8.

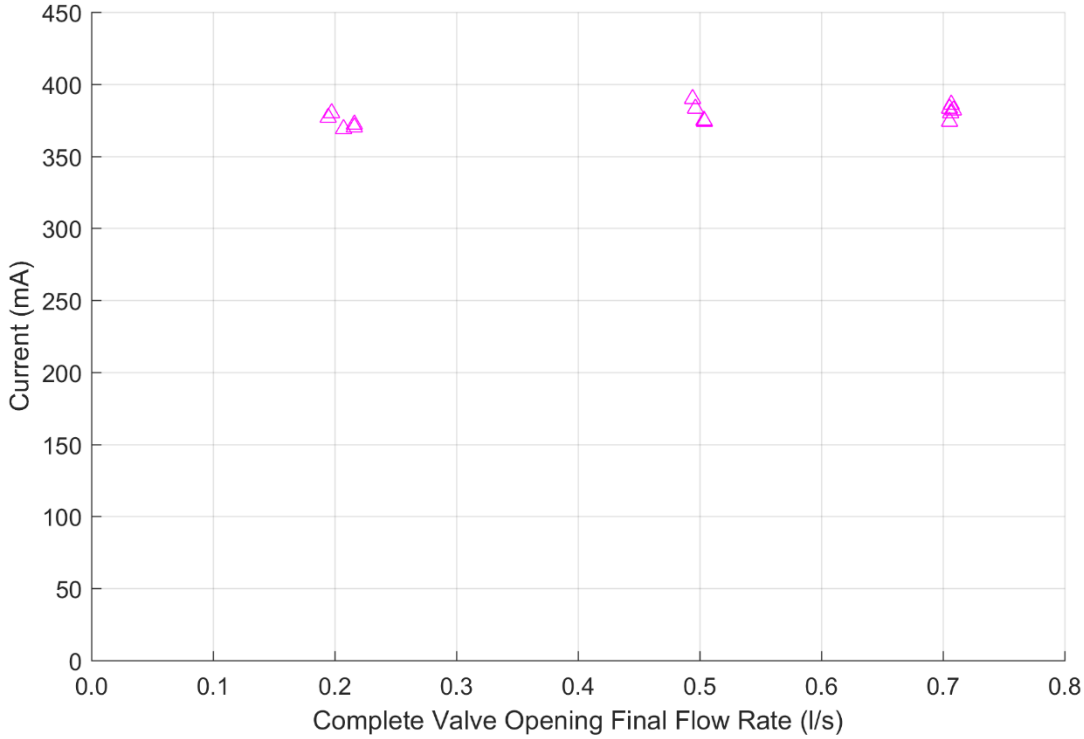


**Figure 6.10.** Currents at which mobilisation occurred for ball bearings mobilised by complete valve opening transients set two. The transients transitioned from zero initial flow rates to varying final flow rates, with initial pressure fixed at approximately 45 m.

Complete valve opening transients tested produced similar currents at which mobilisation occurred (Figure 6.10). The standard deviation of across all these values (6.73 mA) was equivalent to standard deviations between repeats during other valve opening experiments (5.59 mA to 9.30 mA), i.e. the different conditions tested could not be separated from experimental errors. This led to the conclusion that the final flow rate of valve opening transients does not relate to the current at which mobilisation occurred. Other data sets were analysed with respect to the currents at which mobilisation occurred and found that no trend exists between final flow rate and transient mobilisation behaviour. As a consequence of this finding, valve opening results presented for the remainder of section 6.2 will be given with regard to the transients' initial flow rate.

### 6.2.3 Effect of Initial Pressure Conditions

Transients are associated with pressure events, therefore initial pressure could be a crucial parameter for mobilisation. This would be more pronounced for valve opening transients where the higher upstream pressure released could act like a dam break.

Figure 6.11 presents the currents at which mobilisation occurred plotted against valve closing initial pressures. This figure shows a quadratic curve correlating the two parameters

together – squared term coefficient -44.13 mA per $(l/s)^2$, linear term coefficient 3798.40 mA per l/s, offset -81325.14 mA, coefficient of determination 0.987. The range of initial pressures tested for complete valve closing transients was very narrow (43.57 m to 46.08 m, only 2.51 m), especially when compared to the more significant changes in initial flow rates. Furthermore this range of initial pressures was not significantly greater than the level of experimental repeatability for the system. Any correlation between initial pressure and current is, therefore, inconclusive.

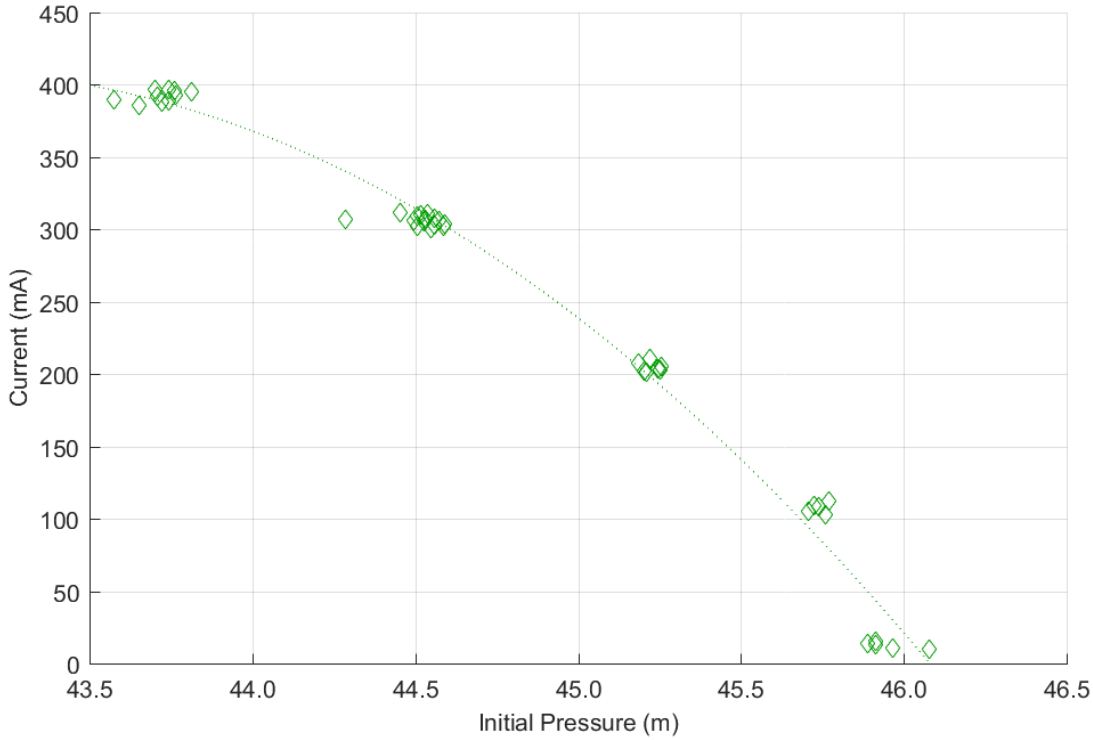


**Figure 6.11.** Currents at which mobilisation occurred for complete valve closing transients using ball bearings, against initial pressure.

Figure 6.12 presents the currents at which mobilisation occurred plotted against valve opening initial pressures. It shows that, within each data set tested, as the initial pressure increased the current at which mobilisation occurred also increased. However, this relationship is not consistent across the full set of results and cannot be used as the sole parameter to predict currents at which mobilisation occurred. For example, an initial pressure of 45 m for complete valve opening set one transients (zero initial flow rate) mobilised the ball bearing at an average current of 366 mA. Yet for partial valve opening set two transients (initial flow rate of 0.31 l/s) with the same initial pressure, the average current at which mobilisation occurred was 241 mA, approximately two thirds of the previous value. This led to the conclusion that there is a relationship between initial pressure and current at which mobilisation occurred, but initial pressure is not the sole indicator of mobilisation.

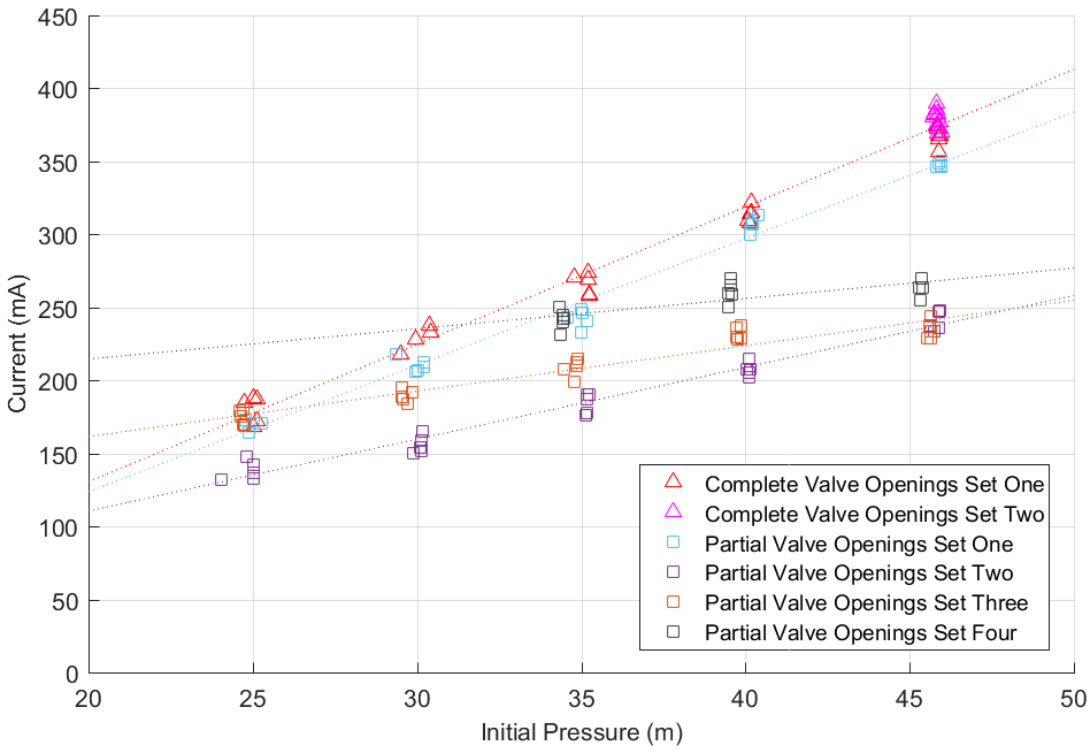


**Figure 6.12.** Currents at which mobilisation occurred for all valve opening transients using ball bearings, against initial pressure.

### 6.2.4 Effect of Final Pressure Conditions

Final pressure is understood not to be a strong descriptor of transients, so it was not expected to correlate with mobilisation. Yet the effect of final pressure conditions on the currents at which mobilisation occurred was still investigated here to be comprehensive.

The range of final pressures quantified during complete valve closing transients was 0.78 m. This was even narrower than the range of corresponding initial pressures as the system was in a no flow condition. Moreover, the variability in values was similar to the level of experimental repeatability for the system. Any potential relationship between final pressure and currents at which mobilisation occurred for complete valve closing transients was indistinguishable from experimental repeatability.

Conversely, valve opening transients produced a much larger range of final pressures. Figure 6.13 presents the currents at which mobilisation occurred plotted against valve opening final pressures. Results are found to be similar to initial pressure results presented in Figure 6.12; within each data set tested, as the initial pressure increased the current at which mobilisation occurred also increased, but values of final pressure can relate to ranges of current. This led to the conclusion that there is a relationship between final pressure and current at which mobilisation occurred, but final pressure is not the sole indicator of mobilisation.

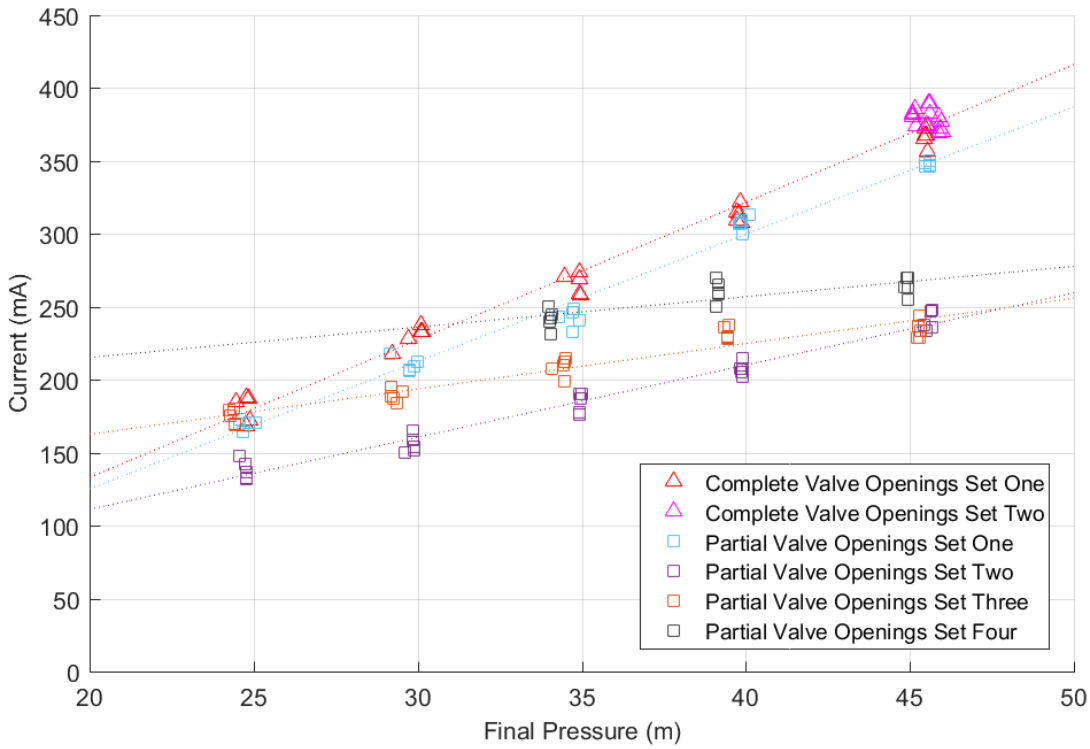


**Figure 6.13.** Currents at which mobilisation occurred for all valve opening transients using ball bearings, against final pressure.

### 6.2.5 Effect of the Change in Flow Rate

One of the common ways to characterise transients is the rapid change in flow rate from one steady state to another (Gally et al., 1979; Zhang et al., 2008). For a valve closing transient, this is a decrease in flow; for a valve opening transient, this is an increase in flow. This parameter was quantified and compared to currents at which mobilisation occurred to determine if this parameter related to mobilisation of the ball bearings.

Initial flow rates of the complete valve closing transients transitioned to zero final flow rate, therefore, any change in flow rate was equal to the initial flow rate. An analysis of changing flow rate would be identical to the initial flow rate results presented in Figure 5.4.

Valve opening transients tested provided a large variety of initial and final flow conditions to compare the change in flow rate. For example, valve opening transients were performed with an approximate 0.2 l/s change in flow rate for initial conditions of zero flow rate, 0.3 l/s, 0.5 l/s and 0.7 l/s. Figure 6.14 presents the currents at which mobilisation occurred against valve opening change in flow rates. It shows that the aforementioned transients (0.2 l/s change in flow rate) produced a large range of currents at which mobilisation occurred (132 mA to 380 mA). Furthermore, any value of current corresponded

with multiple changes in flow rate. This led to the conclusion that the change in flow rate for valve opening transients does not relate to the current at which mobilisation occurred.

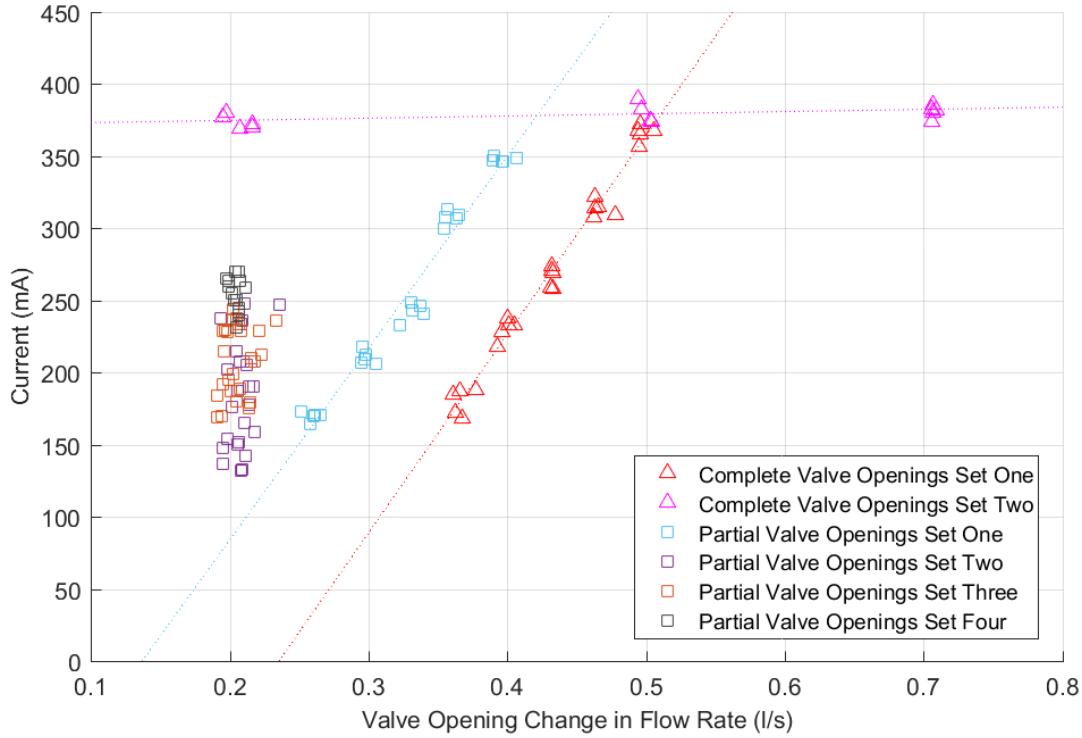


**Figure 6.14.** Currents at which mobilisation occurred for ball bearings, against valve opening change in flow rates.

### 6.2.6 Effect of the Change in Pressure

A rapid change in pressure will generate a transient, even when there is no bulk change in flow conditions, for example when there is a pressure differential across a valve in a closed system (Collins et al., 2012). To investigate the effect of the change in pressure (between initial and final conditions) on currents at which mobilisation occurred, these values were calculated for valve closing and valve opening transients.

Valve closing transients were not explored in this analysis. The previous sections showed an inconclusive correlation between initial pressure and current (section 6.2.3), and an indistinguishable correlation between final pressure and current (section 6.2.4). Any potential correlation between changes in pressure and current would be accordingly inconclusive and hence there is no value in presenting it.

Valve opening transients, on the other hand, exhibited relationships between initial pressure and currents at which mobilisation occurred, as well as between final pressure and currents at which mobilisation occurred. Figure 6.15 presents the currents at which mobilisation occurred plotted against valve opening changes in pressure. The pressure changes were negative values as pressure decreased, but absolute values are plotted for ease

of comparison. This figure shows that the absolute change in pressure does not relate to the currents at which mobilisation occurred. This is strongly indicated by the complete valve opening set two transients. The currents are inseparable from experimental repeatability (discussed in section 6.2.2); however, the changes in pressure exist at either end of the spectrum (0.003 m to 0.664 m). Moreover the range of changes in pressure was significantly narrow and equivalent to experimental repeatability.

**Figure 6.15.** Currents at which mobilisation occurred for valve opening transients using ball bearings, against the absolute change in pressure between initial and final conditions.

### 6.2.7 Summary of the Effect of Initial and Final Steady State Conditions on Mobilisation

An objective of this work was to identify parameters describing the transient that relate to mobilisation behaviour. Flow rate and pressure parameters relating to the steady state conditions pre and post transient have been evaluated in this section to determine if they correlate to currents at which mobilisation occurred.

Correlations, or lack thereof, found for complete valve closing transients are summarised here:

- A linear correlation exists between initial flow rate and current at which mobilisation occurred. Thus, initial flow is likely to be good descriptor.
- Final flow rate was not examined as these values were constant, so could not relate to varying currents. Similarly, change in flow rate was equivalent to initial flow rate, so also not examined.

- Initial, final and changes in pressure were not significantly greater than the level of experimental repeatability for the system. Any correlation between these pressures and current are, therefore, inconclusive.

Correlations found for valve opening transients are summarised here:

- An inverse quadratic correlation exists between initial flow rate and current at which mobilisation occurred, but it has been shown not be the sole parameter describing mobilisation.
- Final flow rates, changes in flow rate and changes in pressure were shown not to relate to currents at which mobilisation occurred.
- Initial pressure was shown to have a linear correlation with current across each data set, but not for the whole data set. Therefore, initial pressure plays a role in describing mobilisation behaviour but is not the only dependent factor.
- Final pressure was shown to have a linear correlation with current at which mobilisation occurred. However, this correlation is likely to be a consequence of the initial pressure. As final flow rate was shown not to play a role in mobilisation, it is unlikely that final pressure would.

The conclusion of section 6.2 is that initial flow rate and initial pressure both play a role in transient mobilisation.

## 6.3 Effect of Short-Term Conditions

Parameters used to describe the transients have been steady state conditions of flow and pressure. These robust parameters have not completely explained mobilisation behaviour. This section, therefore, aims to identify and investigate potential short-term (dynamic) parameters that occur between the steady state initial and final conditions.

### 6.3.1 When Mobilisation Was Initiated

To identify potential dynamic parameters, the first step taken was to determine when in the transient the particles began to mobilise. This would indicate possible parameters to investigate as only parameters that occur before mobilisation is initiated could cause this movement. To achieve this, hydraulic time series data was synced with the ball bearing location data collected by the high speed camera. The flow meter recorded at insufficient resolution (3Hz) to be effectively compared to the high speed camera (393 fps). Therefore, the hydraulic time series data utilised was the high speed pressure data collected by the pressure transducers.

6.3.1.1 Method: Synchronisation of Pressure Sensors and Camera

During the experiments, the camera was activated with an external trigger. This trigger was connected to the data acquisition device (Table 4.1) so that a simultaneous electric pulse was recorded on the DAQ. The rising limb of this pulse was used as a datum for both time series (pressure and camera), illustrated in Figure 6.16.

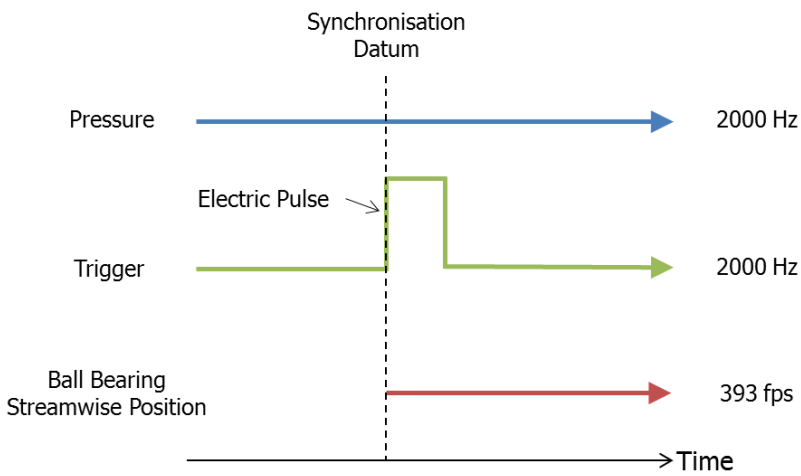


**Figure 6.16.** Illustration showing the synchronisation datum linking the pressure transducer time series and the camera time series, via the trigger electric pulse.

The pressure transducers and camera were recording at different frequencies, 2000 Hz and 393 fps, respectively. Consequently, each frame corresponded to ~ 5.09 pressure samples (2000 Hz divided by 393 fps). Whilst an ideal situation would be 1:1 when comparing data recording devices, this ratio is an improvement on other studies. For example Brunone and Berni (2010) used ultrasonic Doppler velocimetry equipment at a recording frequency of 60 Hz, and pressure transducers at 1024 Hz. This gives a ratio of ~ 1:17.07.

Initiation of mobilisation was resolved to two consecutive frames. In simple terms, in frame A the ball bearing was in initial position y and in the consecutive frame B the bearing was in position y + Δy. Initiation of mobilisation was considered where the continuation of the Δy movement led to mobilisation over the threshold and the Δy movement was dissimilar to previous steady state movements. It is important to note that by the time the particle had crossed the mobilisation threshold, it had already begun to mobilise. Therefore, initiation of mobilisation must have been prior to this.

The consecutive frames equated to pressure samples approximately captured ~ 5.09 pressure samples (rounded to the nearest discrete sample) or ~ 0.0025 s later. Initial movement must have occurred in between these two time points, thus it will be referred to in this work as the mobilisation time window. Figure 6.18 presents the streamwise tracking

example of a ball bearing during a complete valve closing transient that transitioned from 1.00 l/s initial flow rate to zero final flow rate. The mobilisation time window is indicated.

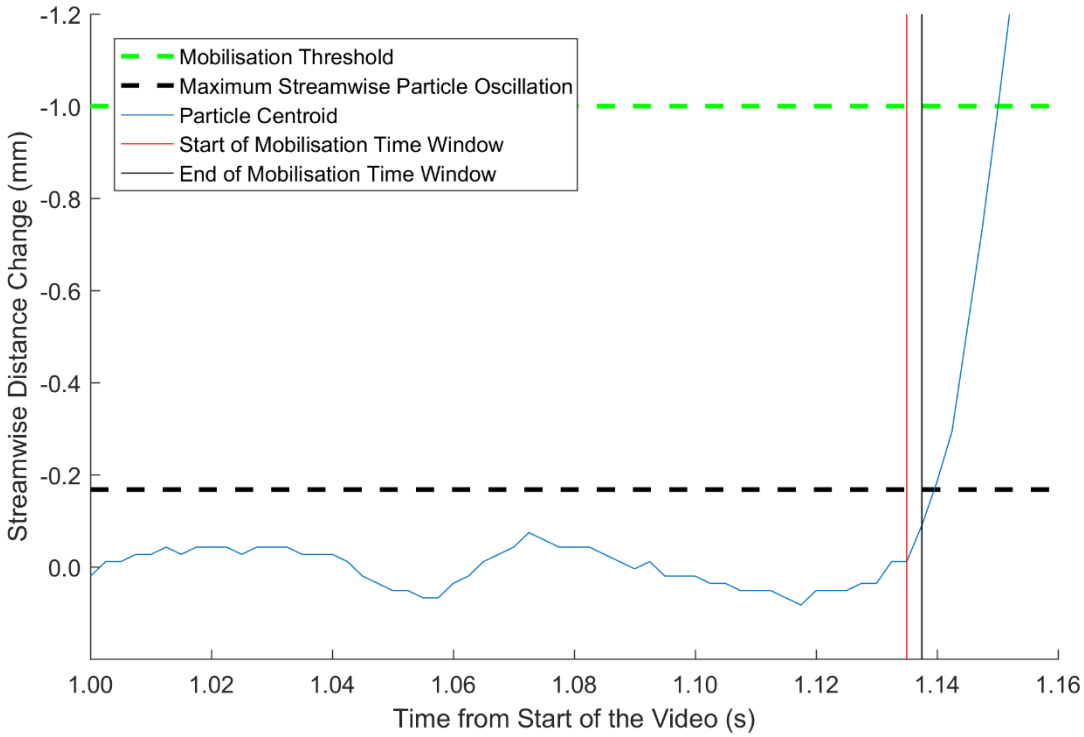


**Figure 6.17.** Example of selecting the mobilisation time window using the frames captured by the camera during a complete valve closing transient, which transitioned from 1.00 l/s initial flow rate to zero final flow rate.

The mobilisation time window was determined for all transient results where the ball bearing was mobilised. These windows were then synchronised with the respective pressure data collected. Figure 6.18 shows the mobilisation time window synchronized with pressure data for the example case presented in Figure 6.17. Here the mobilisation time window occurred 0.0860 s to 0.0885 s after the start of the transient (first change in pressure). Likewise, Figure 6.19 shows the mobilisation time window synchronized with pressure data for a complete valve opening transient, which transitioned from zero initial flow rate to 0.51 l/s at an initial pressure of 45 m. This opening transient had a similar mobilisation time window of 0.0850 s to 0.0875 s. From here on in, the time between the start of the transient and the start of the mobilisation time window will be called $\Delta t$.

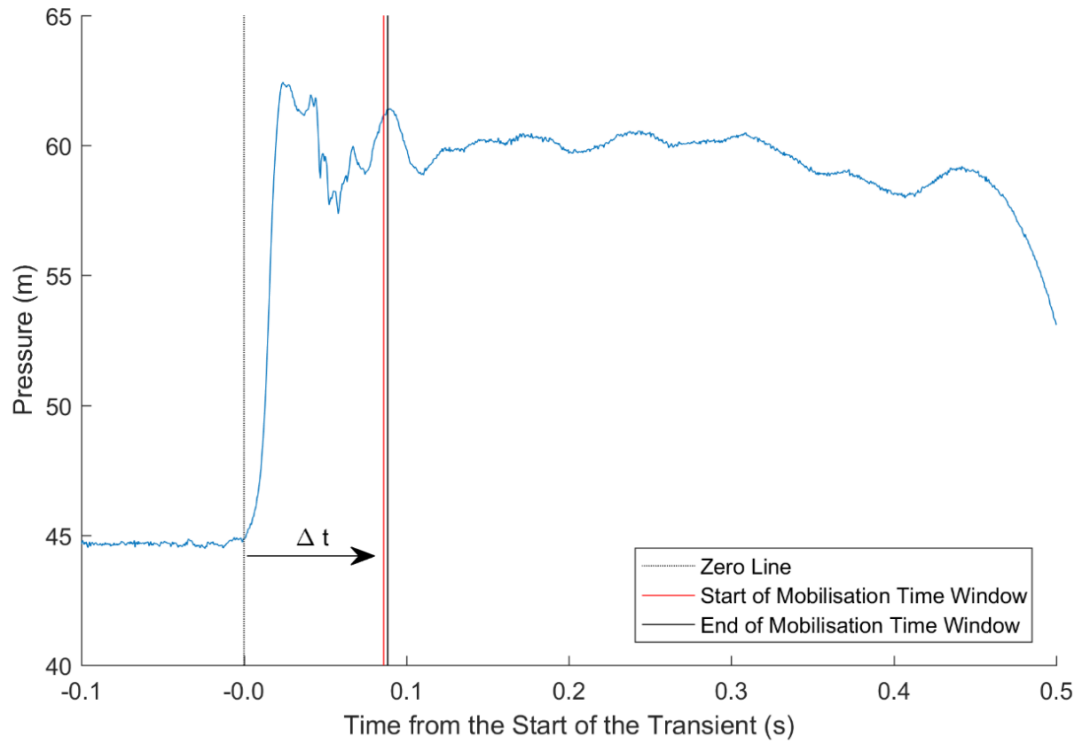


**Figure 6.18.** Pressure trace of an example complete valve closing transient, which transitioned from 1.00 l/s to zero final flow rate, synchronized with the mobilisation time window.

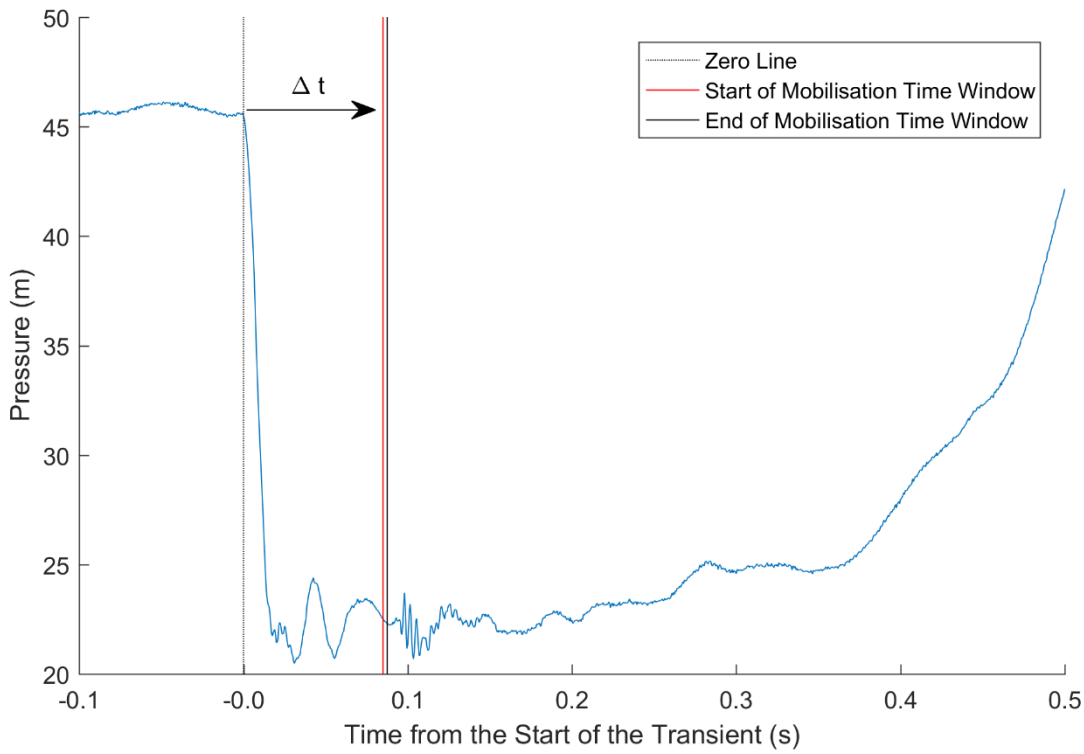


**Figure 6.19.** Pressure trace of an example complete valve opening transient, which transitioned from a zero initial flow rate to 0.50 l/s, synchronized with the mobilisation time window.

6.3.1.2 Exploring $\Delta t$

To understand how this time changes with different transient conditions, Figures 6.20 and 6.21 present delta t plotted against initial flow rate for valve closing and valve opening transients, respectively. Both types of transients have shown that initial flow rate correlates with mobilisation. Therefore it is used as the parameter for comparison here.

Figure 6.20 shows, for complete valve closing transients, $\Delta t$ times were between 0.08 s and 0.15 s. There is no relationship between initial flow rate and $\Delta t$ times, beyond experimental repeatability. The $\Delta t$ values for complete valve closing transients initially in the transitional flow regime (initial flow rate of 0.1 l/s) are similar to those in the turbulent regime. Within each set of conditions tested, the range of $\Delta t$ values did not correlate with initial pressure, or any other initial or final condition.

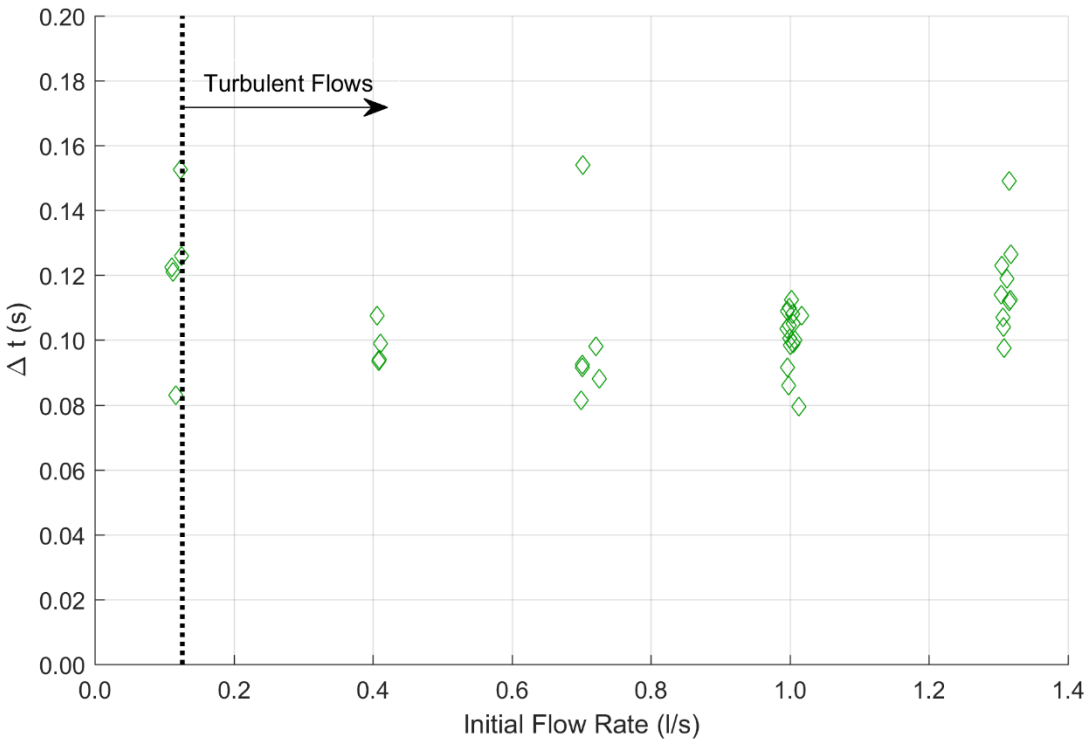


**Figure 6.20.** $\Delta t$ values for valve closing transients plotted against initial flow rate.

Figure 6.21 shows, for complete valve opening transients and partial valve opening transients with initial flow rate of 0.1 l/s, $\Delta t$ times were between 0.05 s and 0.16 s. In contrast, for partial valve opening transients with initial flow rates of 0.3 l/s, 0.5 l/s and 0.7 l/s, $\Delta t$ times were determined to be between 0.22 s and 0.48 s, bar three outlying points. These three points were examined in detail and nothing observable to explain these outliers were found. Within each set of conditions tested, the range of $\Delta t$ values seen did not correlate with initial pressure, or any other initial or final condition.

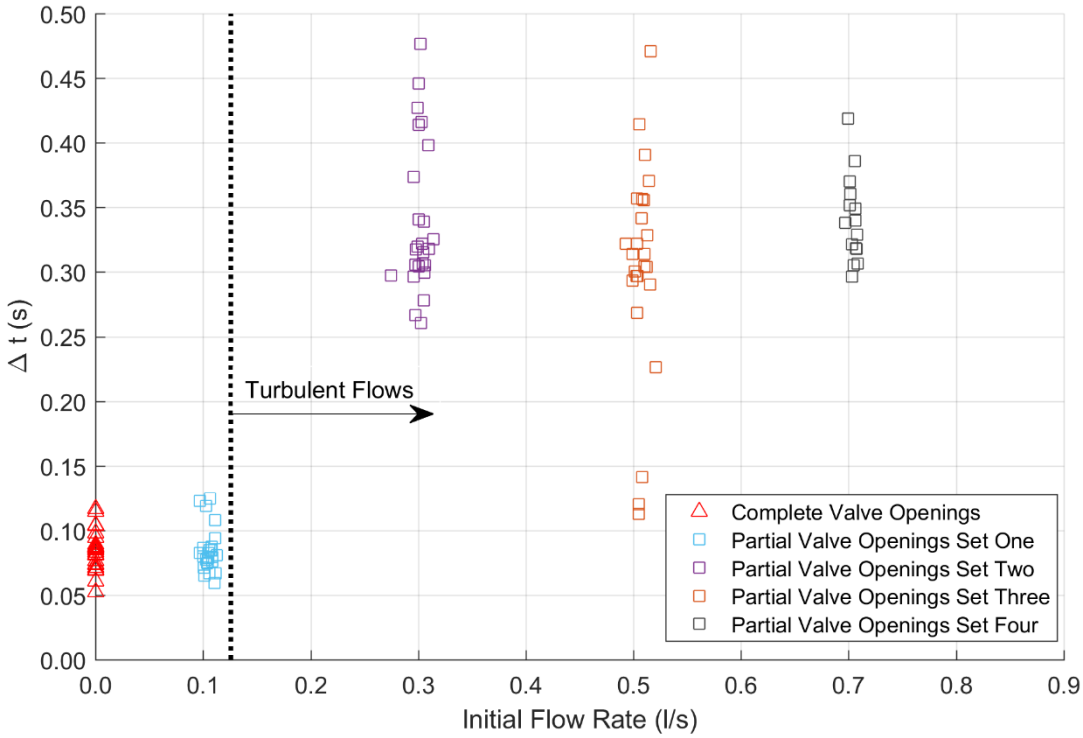


**Figure 6.21.** $\Delta t$ values for valve opening transients plotted against initial flow rate.

The $\Delta t$ values would suggest that there is a distinction between initially zero/transitional valve opening transients and turbulent valve opening transients. This change in behaviour echoes the variation in streamwise particle movements observed in section 6.2.1.4. Moreover, it is interesting to note that the $\Delta t$ values for the turbulent valve openings do not correspond to the $\Delta t$ values for the turbulent valve closings. For example Figure 6.20 shows, for initial flow rate of 0.7 l/s, the complete valve closing transients produce $\Delta t$ values between 0.08 s and 0.15 s. Whereas, Figure 6.21 shows, for the same initial flow rate, the partial valve opening transients produce $\Delta t$ values between 0.30 s and 0.42 s.

Irrespective of the initial flow rate, the largest observed $\Delta t$ time was 0.477 s. As a further observation, this $\Delta t$ time was within the first third of the first pipeline period (0 to 1.43 s) where the dynamic effects were greatest (section 2.3.6.1). Figure 6.22 presents the transient pressure trace, synchronized with the mobilisation time window, of the transient with this largest value of $\Delta t$; a partial valve opening transient transitioning from 0.30 l/s to 0.52 l/s.

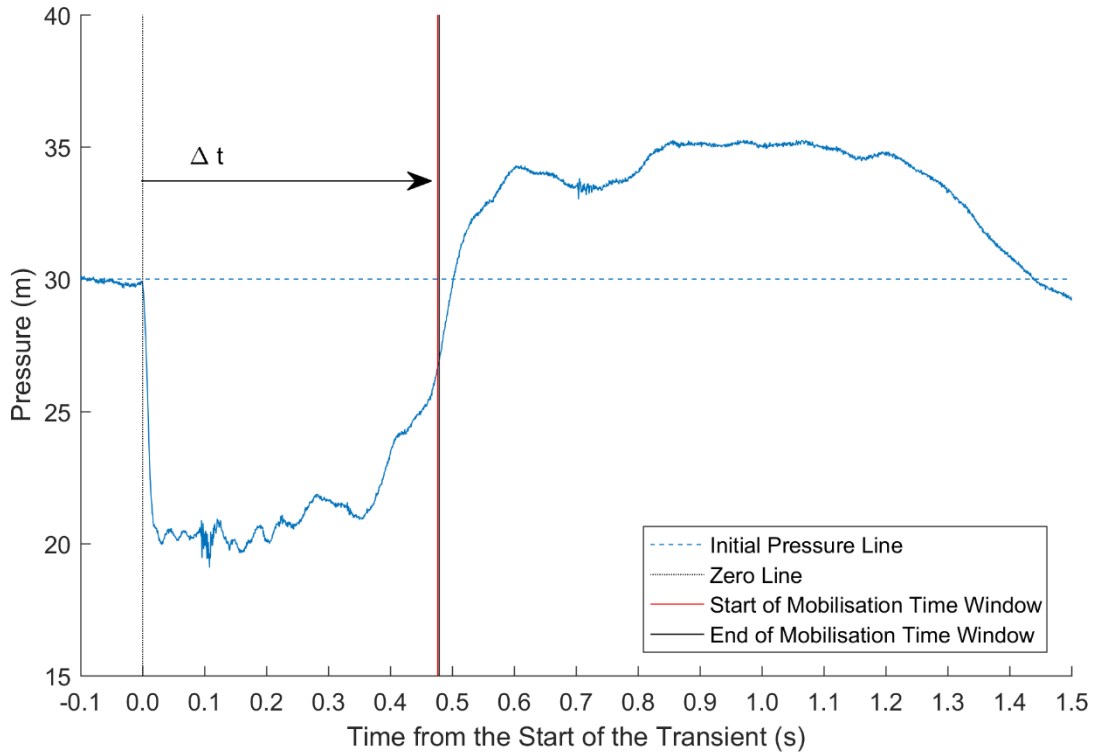


**Figure 6.22.** Pressure trace of an example partial valve opening transient, which transitioned from 0.30 l/s to 0.52 l/s, synchronized with the mobilisation time window. Initiation of mobilisation of the ball bearing must have occurred during this time period. This transient had the largest $\Delta t$ time observed of all experiments.

Figures 6.20 to 6.22 present evidence that the transient initiates mobilisation during the first dynamic change, or surge, of the transient, irrespective of whether the transient is generated by a valve closing or a valve opening. Accordingly, short-term or dynamic parameters investigated were related to this dynamic surge; its magnitude and temporal rate of change.

The low resolution flow meter used in the laboratory facility was limited to steady state flows, so could not capture the dynamic changes occurring during the transients. Alternatively pressure data collected during the experiments was recording at a significantly high rate (2000 Hz), so could be representative of the dynamic surge. Therefore, the time series pressure data recorded will be used in the following analysis.

### 6.3.2 Exploring Dynamic Surge Properties

The results chapter presented examples of transients that caused mobilisation of the ball bearings; complete valve closings, Figure 5.3; complete valve openings, Figures 5.6 and 5.7; and partial valve openings in Figures 5.9 to 5.12. These figures showed that as the initial and final conditions increased, the absolute magnitude of the surge also increased.

Furthermore, these transients appeared to show instantaneous changes in pressure, irrespective of the type of transient generated and the initial and final conditions. This effect was due to the time axis range showing the entire transient. When the transients are scaled to just the first surge, disparity in the gradient of the first pressure surge becomes evident. Figure 6.23 demonstrates this effect using partial valve opening set one transients, originally presented in Figure 5.8, wherein part a) the time axis ranges between -2 s and 10 s, and in part b) the time axis ranges between -0.05 s and 0.025 s.

This section aimed to quantify the magnitude and temporal rate of change (i.e. gradient) of the first pressure surge. These values were determined for all transients and compared to each other to understand how transient dynamics varied. From here on in, the magnitude of the first pressure surge will be called $\Delta P$ and temporal rate of change will be called $dP/dt$ (the gradient of pressure with respect to time).

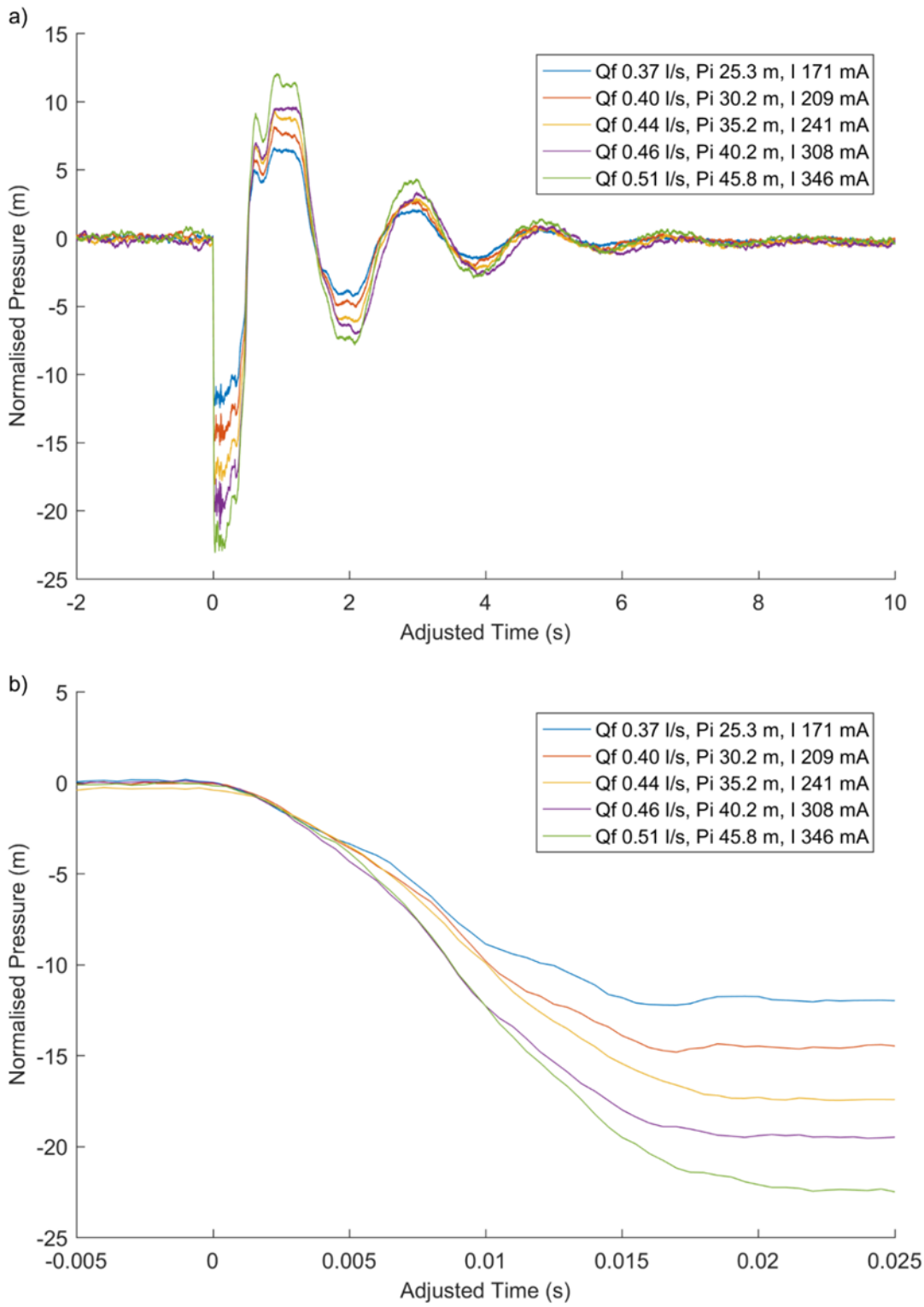


**Figure 6.23.** Pressure traces of partial valve opening transients set one that caused mobilisation of the ball bearings. Traces are normalised by subtracting initial pressure and adjusted so that the first surge commences at time zero. Part a) the time axis ranges between -2 s and 10 s to show the entire transient. Part b) the time axis ranges between -0.050 s and 0.025 s to highlight the varying gradients of the initial surge.

6.3.2.1 Method: $\Delta P$ Quantification

Surge magnitude can be determined by Equation 6.1 where $\Delta P$ is the magnitude of the short-term primary pressure surge, $P_I$ is the initial pressure, and $P_S$ is the pressure to which the surge changes:

$$\Delta P = P_I - P_S \qquad \text{Equ. 6.1}$$

This third term, $P_S$, is not necessarily the maximum or minimum pressure observed during the entire transient. The maximum or minimum pressure may be due to line packing effects (section 2.3.6.2) in addition to the primary surge. Figure 6.24 illustrates this using an idealised transient.

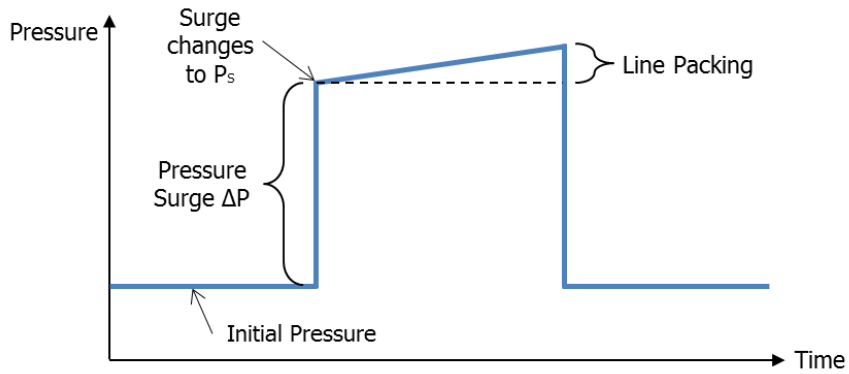


**Figure 6.24.** Schematic of an idealised transient signifying line packing effects. Highlighted points indicate the initial pressure, magnitude of the primary pressure surge $\Delta P$ and the pressure to which the surge changes to $P_S$.

Due to the variable nature of the transients generated within this system, automatic identification of the pressure to which the surge changes, $P_S$, would have been highly complex. For consistency during this work, a manual identification process was therefore adopted. This process involved zooming in on the surge and selecting the first significant peak (valve closing transients) or trough (valve opening transients) after the pressure surge. Small noise variations in the pressure, on the order of one or two data samples, were ignored. This process was refined during initial work involving thousands of generated transients. The error in selecting these points was estimated as 0.20 m. This value was greater than the instrument error but less than the average variability across repeats.

Figure 6.25 presents an example complete valve opening transient, which transitioned from zero initial flow rate to 0.51 l/s, with the selected $P_S$ value highlighted. Values of $P_I$ and $P_S$ were 46.28 m and 21.65 m, respectively. Therefore, $\Delta P$ was calculated as 24.63 m.

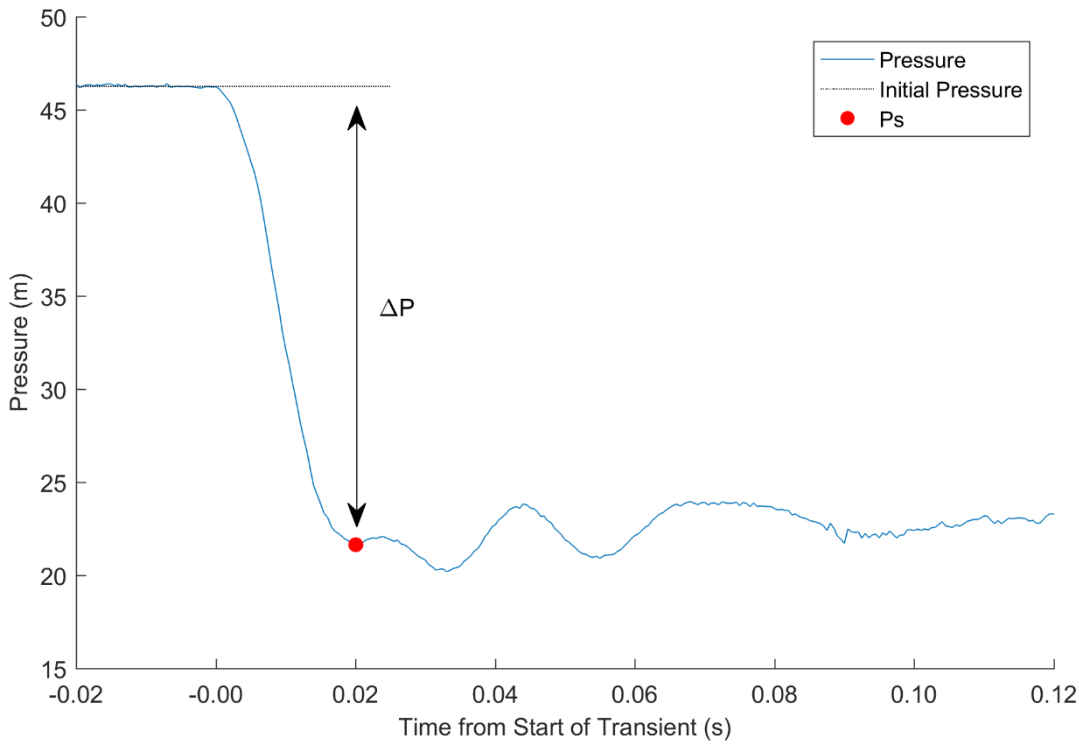


**Figure 6.25.** Pressure trace of an example complete valve opening transient, which transitioned from zero initial flow rate to 0.51 l/s, with the $P_S$ value highlighted.

6.3.2.2 Method: $dP/dt$ Quantification

To quantify $dP/dt$ for all pressure transients collected, a simplistic approach would have been to calculate the pressure difference in consecutive pressure samples and divide by one transducer time step of 0.0005 s (transducer recording frequency of 2000 Hz). However, using a consecutive pair of pressure samples would have been highly influenced by measurement errors and potentially produce extreme values, which are non-representative of the entire surge.

An alternative method was used. A linear regression gradient (least-squares fit) was calculated for a "bin" of 20 samples, $(t_i, P_i)$ to $(t_{i+19}, P_{i+19})$. This bin size was chosen via a trial-and-error approach to produce gradient values more representative of the pressure measured (improved accuracy) whilst limiting noise effects. The calculation was repeated for $i = 1, 2, 3, \ldots n$ where $n$ equalled the length of the pressure data minus 19. The largest of these gradients then became the magnitude of $dP/dt$ for that transient surge. All $dP/dt$ values were calculated as absolute values, as only the magnitude of the gradient was relevant. Positive or negative gradients only informed if the transient had a primary upsurge or downsurge.

Table 6.1 presents $dP/dt$ values calculated for the partial valve opening transients shown in Figure 6.23. The higher the final flow rate and initial pressure conditions, the greater the $dP/dt$ values. Root mean square errors (RMSE) are also given, calculated

between the pressure data and the respective linear regression lines. Lower RMSE values indicate better quality of fit. These RMSE values are negligible compared to the $dP/dt$ values, less than 0.05 %.

**Table 6.1.** $dP/dt$ and corresponding RMSE values calculated for partial valve opening transients (Set One).

| Final Flow Rate (l/s) | Initial Pressure (m) | $\frac{dP}{dt}$ (m/s) | RMSE (m/s) |
|---|---|---|---|
| 0.37 | 25.3 | 859.6 | 0.40 |
| 0.40 | 30.2 | 1040.6 | 0.45 |
| 0.44 | 35.2 | 1154.3 | 0.46 |
| 0.46 | 40.2 | 1348.8 | 0.54 |
| 0.51 | 45.8 | 1490.9 | 0.54 |

6.3.2.3 Dynamic Surge Properties Comparison

Using the two methods described in sections 6.3.2.1 and 6.3.2.2, $\Delta P$ and $dP/dt$ were calculated for all transients. Both methods were applied systematically and produced small errors. The values calculated were then compared for valve closing transients and valve openings transients to understand the dynamic surges induced. Figure 6.26 presents the relationship between $dP/dt$ and $\Delta P$ of the first surge for valve closing transients. The regression line shows a positive linear relationship – gradient of 77.76 $s^{-1}$, offset 81.52 m/s per m, coefficient of determination 0.995. Each method produced error bars too small to be seen in the figure, i.e. on the order of graph point size, thus have not been included.

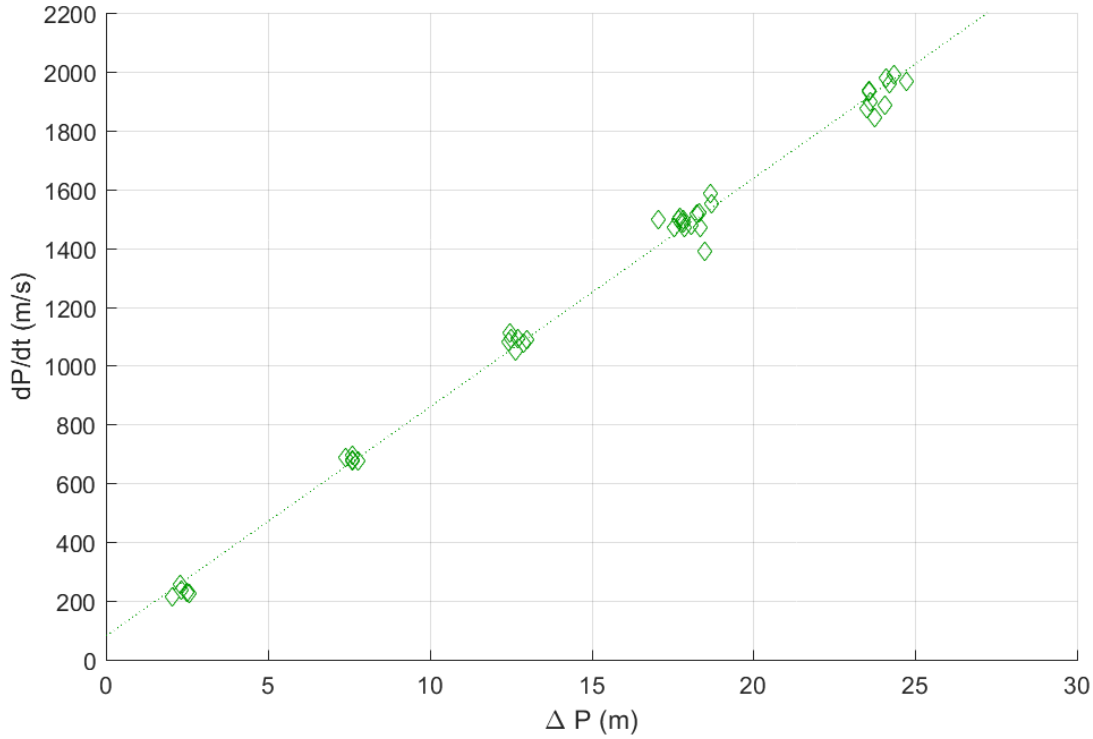


**Figure 6.26.** $dP/dt$ and $\Delta P$ values calculated for complete valve closing transients.

Figure 6.27 presents the relationship between $dP/dt$ and $\Delta P$ of the first surge for valve opening transients (complete and partial). Regression analysis showed that each of the partial valve opening relationships were statistically similar to the complete valve opening relationship (p-values > 0.05). Therefore, the positive linear regression line given in Figure 6.27 was determined for all valve opening results as one entity – gradient of 70.64 $s^{-1}$, offset 6.63 m/s per m, coefficient of determination 0.992.

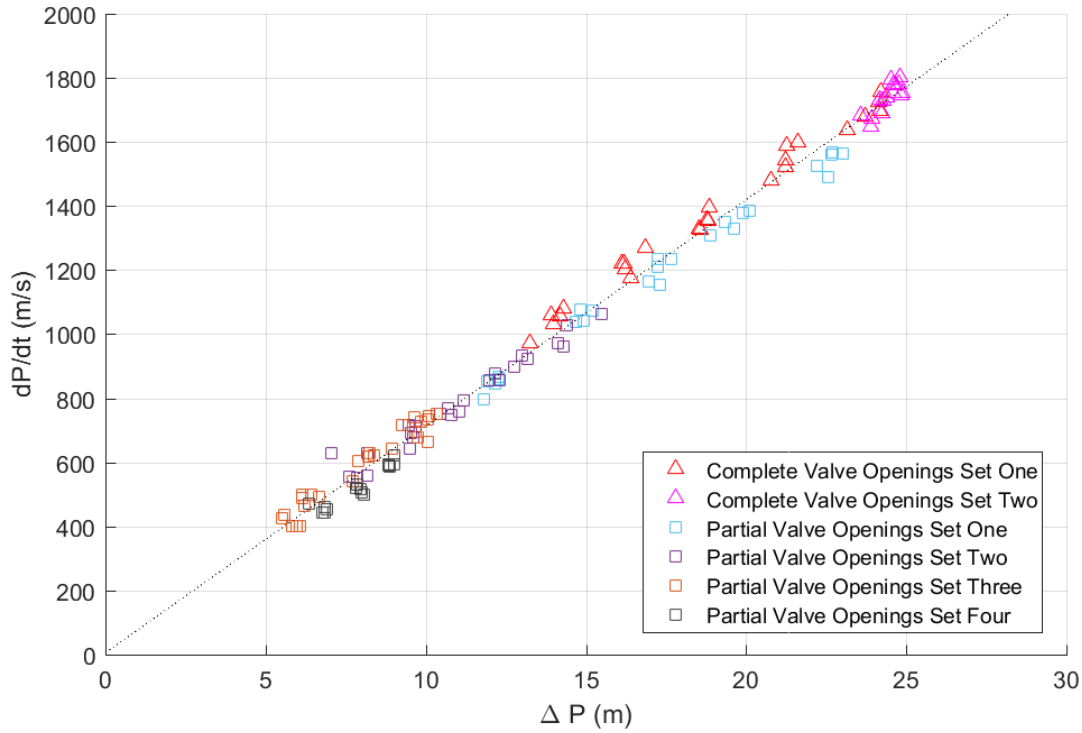


**Figure 6.27.** $dP/dt$ and $\Delta P$ values calculated for all valve opening transients. All sets of partial valve opening transients are statistically similar to the complete valve opening relationship, therefore the linear regression line given was determined for all valve openings.

Figures 6.26 and 6.27 demonstrate that the surge properties of magnitude and temporal rate of change are equivalent; a simple linear transformation exists between the two properties. However, the transformation parameters (regression line gradient and offset) are not equal for valve closing and valve opening transients, i.e. the regression lines are statistically different (p-value < 0.05). The rigorous $dP/dt$ method is statistically equivalent to the $\Delta P$ method, which implies that the selection of the $P_S$ values was also robust.

### 6.3.3 Exploring $\Delta P$

The aim of this section was to understand and interpret the relationship between the surge and the currents at which mobilisation occurs. This would lead to an understanding of the dynamic forces induced during the surge as a cause of mobilisation. The magnitude, $\Delta P$, and the temporal rate of change, $dP/dt$, of the surge were synonymous. Here, $\Delta P$ was chosen as the surge descriptor due to $\Delta P$ being conceptually more meaningful and it can potentially be used in the Joukowski equation.

To determine if $\Delta P$ related to mobilisation of the ball bearings, the $\Delta P$ values calculated for Figures 6.26 and 6.27 were compared to the currents at which mobilisation occurred. Figure 6.28 reveals a clear positive linear relationship between $\Delta P$ and current at which mobilisation occurred, for complete valve closing transients. Relationships for valve opening

transients, Figure 6.29, appear to be more intricate but there is a general increase in current as $\Delta P$ increases. The extrapolated relationships for the individual sets of transients appear to converge at approximate values of 31 m and 500 mA. There is not a clear immediate reason for these specific values and they cannot be tested due to the limits of the electromagnet.

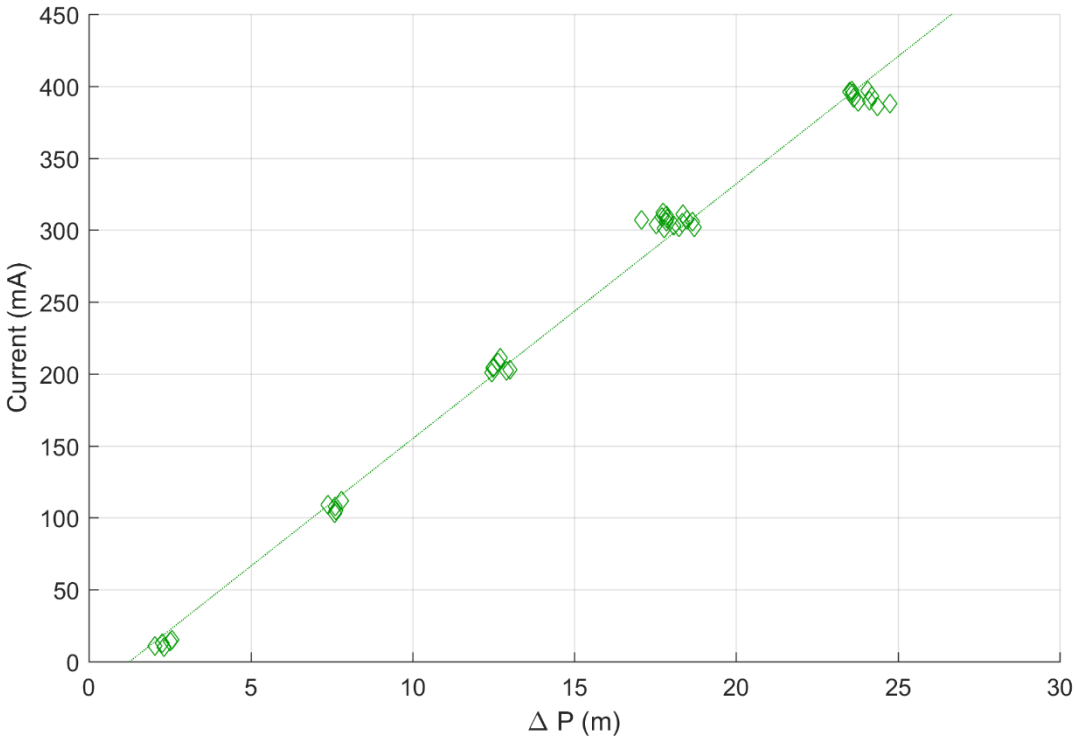


**Figure 6.28.** Relationship between the current at which mobilisation occurred for ball bearings, and $\Delta P$ values for complete valve closing transients.

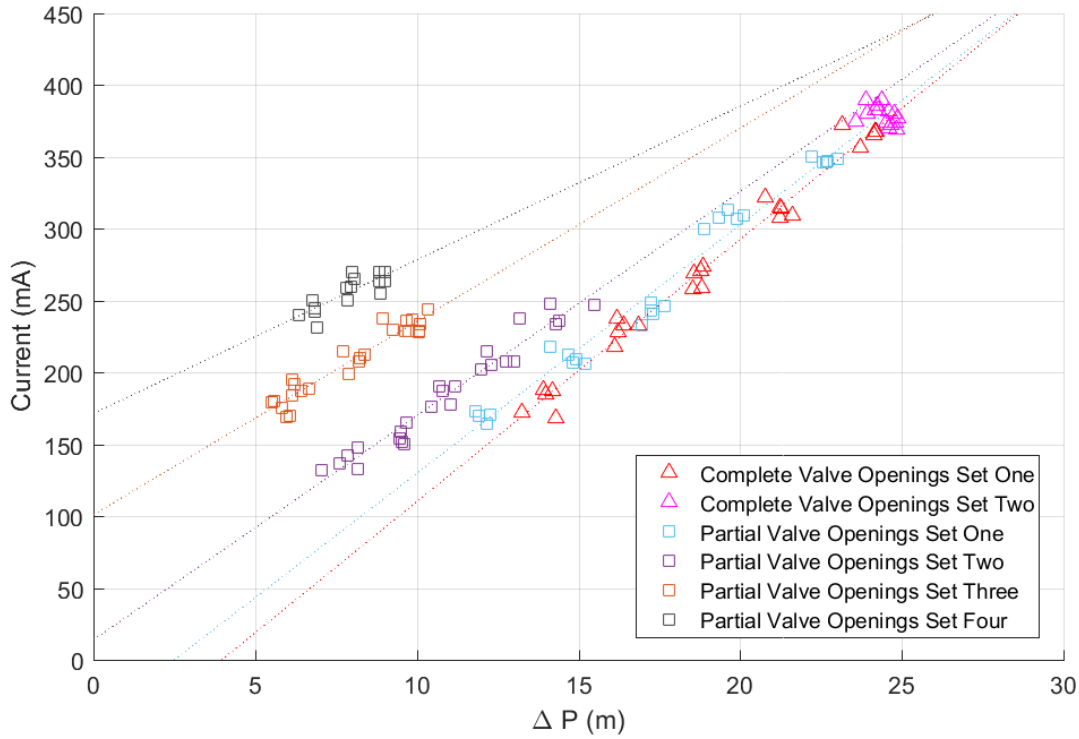


**Figure 6.29.** Relationships between the current at which mobilisation occurred for ball bearings, and $\Delta P$ values for valve opening transients.

### 6.3.4 Evaluating $\Delta P$

Figures 6.28 and 6.29 demonstrate clear relationships between transients' $\Delta P$ parameter, which quantifies the pseudo instantaneous magnitude of the first pressure surge, and the currents at which the ball bearing particles mobilised. The first major section of this chapter (section 6.2) has shown that initial flow rate ($Q_I$) and initial pressure ($P_I$) correlate to mobilisation. Therefore, the goal here is to examine if $\Delta P$ relates to these two initial parameters. If they do, it would suggest that $\Delta P$ correlates to mobilisation potentially due to links with $Q_I$ and $P_I$. Whereas, if they do not, it would suggest that $\Delta P$ correlates to mobilisation in addition to $Q_I$ and $P_I$, i.e. as an additional parameter.

Section 6.2.3 indicated that any correlation between initial pressure and currents at which mobilisation occurred would be inconclusive for complete valve closing transients. Therefore, only initial flow rate was compared to $\Delta P$. Figure 6.30 presents $\Delta P$ values induced for complete valve opening transients with varying initial flow rates. A clear linear relationship can be observed. Overall, linear relationships have been shown to exist between: initial flow rate and current (Figure 6.1), $\Delta P$ and current (Figure 6.28), and initial flow rate and $\Delta P$ values (Figure 6.30). The greater the initial flow, the greater the dynamic transient surge, and the greater the current.

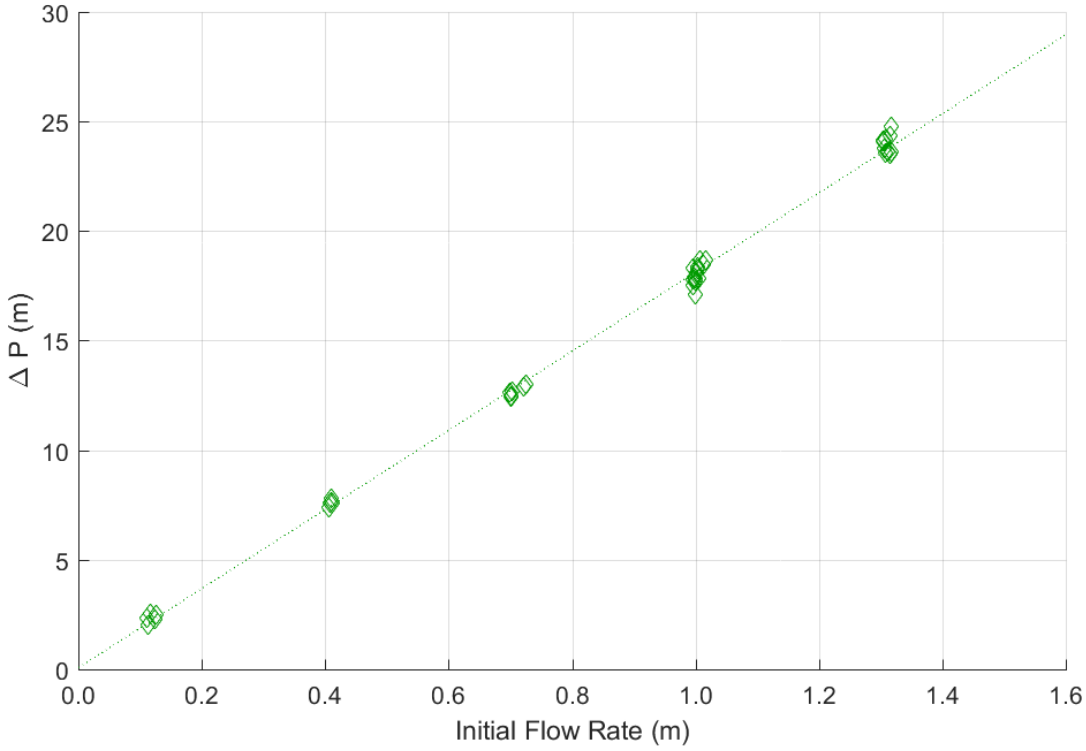


**Figure 6.30.** Relationship between the $\Delta P$ values and complete valve closing initial flow rate, for ball bearings.

Figures 6.31 and 6.32 present $\Delta P$ values induced for complete and partial valve opening transients with varying initial flow rates and initial pressures, respectively. These figures reveal that $\Delta P$ has an inverse quadratic relationship with initial flow rate, and a positive linear relationship with initial pressure. Consequently, it is believed that for valve openings the initial conditions of flow rate and initial pressure couple together in a complex manner to influence the dynamic surge, which initiates mobilisation of the particles.

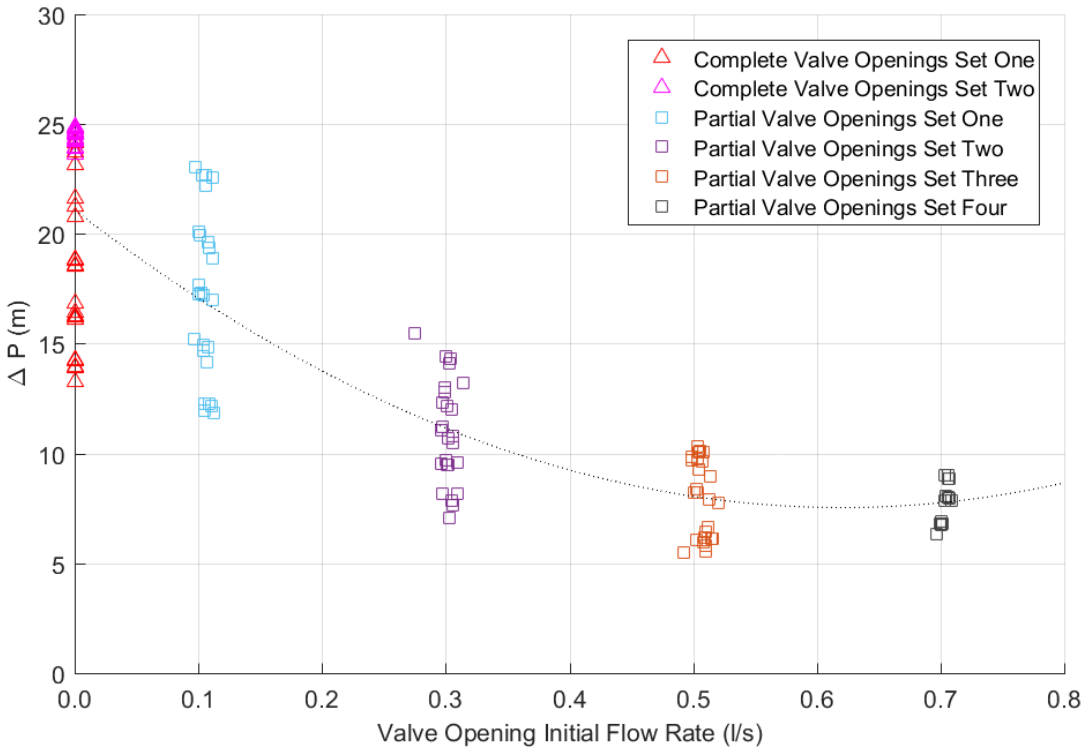


**Figure 6.31.** Relationship between the $\Delta P$ values and valve opening initial flow rate, for ball bearings.

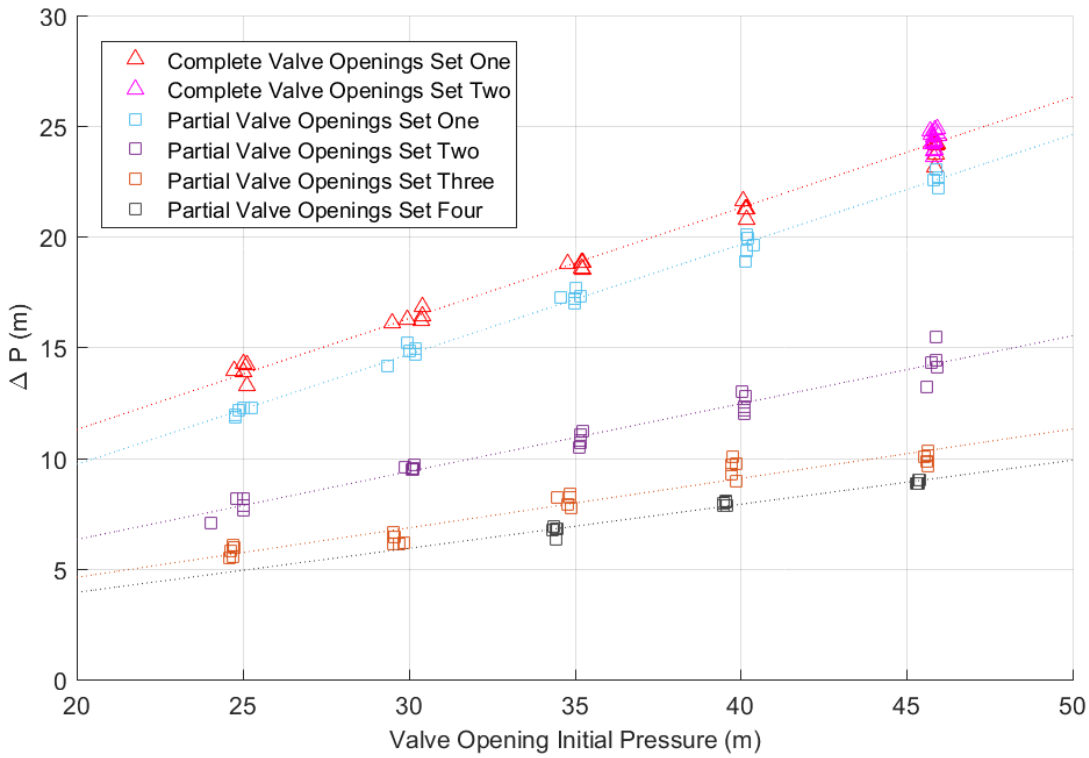


**Figure 6.32.** Relationship between the $\Delta P$ values and valve opening initial pressure, for ball bearings.

## 6.4 Development of a Transient Mobilisation Behaviour Function

The short-term dynamic parameter of $\Delta P$ has been shown to correlate with current at which mobilisation occurs for the ball bearings. Transient mobilisation behaviour may be dominated by this first pseudo instantaneous pressure surge ($\Delta P$), which has been shown to be affected by steady state initial conditions of flow ($Q_I$) and pressure ($P_I$). The aim of this section was to develop an encompassing function of these parameters to describe transient mobilisation behaviour, and then compare this function to steady state mobilisation behaviour. If the two aligned, then transients must cause mobilisation by creating as much dynamic force as the steady state equivalent force.

It is important to note that the focus of this work is now on the peak force generated, as it is believed that the peak force will cause mobilisation for both transients and steady state. From here on in, the steady state mobilisation force relationship developed previously will not be compared with the transient initial or final steady state conditions. Rather it should be compared to the peak transient force. Figure 6.33 illustrates this concept, adapted from the schematic presented in Figure 3.1.

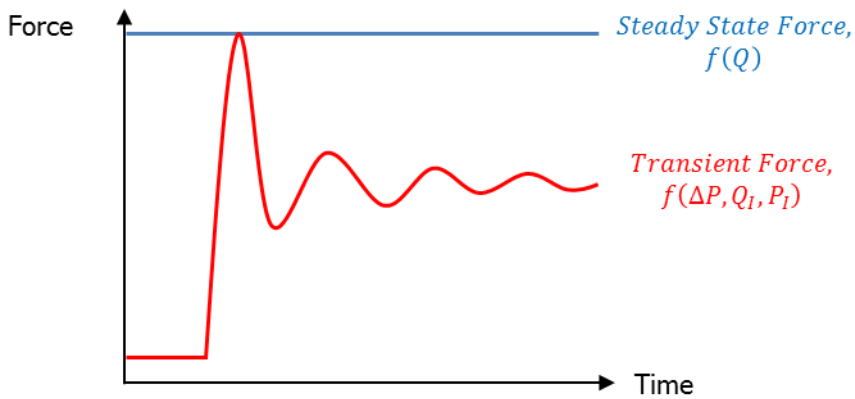


**Figure 6.33.** Idealised force schematic for steady state and a partial valve opening transient. Parameters relating to these forces are indicated. $\Delta P$ pseudo instantaneous change in pressure, $Q_I$ initial flow rate, $P_I$ initial pressure, $Q$ flow rate.

It is well established that the steady state force for mobilisation is related to the steady state shear stress, and consequently bulk flow rate (section 2.4.6). For direct comparison, a bulk flow rate basis is also required for the transient mobilisation function. Therefore, transient forces will attempted to be captured using bulk flow rates. The first step in addressing this aim was to select a method for converting a pressure parameter into a flow parameter. This method is outlined, including assumptions made and calculated errors (section 6.4.1), and applied to the data (section 6.4.2). An overall function to describe transient mobilisation behaviour is then given and compared to steady state (section 6.4.3).

### 6.4.1 Method: Converting $\Delta P$ into $\Delta Q$

Within the first surge, the Joukowski or impulse equation relates $\Delta P$ to bulk pseudo instantaneous change in velocity $\Delta V$. The Joukowski equation, like most models, has limitations (described in section 2.3.5.3), but when applied to the first dynamic pressure surge produced an indication of the dynamic flow changes occurring across the pipe. The equation, outlined in Equation 6.2, states that during the first surge of a transient, velocity and pressure are linearly related.

$$\Delta V = \pm \frac{g}{c} \Delta P \qquad \text{Equ. 6.2}$$

Where $\Delta V$ is the pseudo instantaneous bulk change in velocity, $g$ is the gravitational constant, $c$ is wavespeed, and $\Delta P$ is the pseudo instantaneous change in pressure. In this work, velocity and flow rate are equivalent. The diameter of the pipeline was kept constant and transients were performed with the pipeline at maximum strain to minimise any potential cross-sectional area changes. Consequently $\Delta V$ can be converted to $\Delta Q$ using an adapted Joukowski equation, Equation 6.3.

$$\Delta Q = \pm \frac{gA}{c} \Delta P \qquad \text{Equ. 6.3}$$

Where $\Delta Q$ is the pseudo instantaneous bulk change in flow rate, and $A$ is the constant pipe cross-sectional area.

#### 6.4.1.1 Determining Wavespeed

A value for wavespeed is required for the Joukowski equation. An assumption made in this work is that the wavespeeds for valve closings were comparable to the wavespeeds for valve opening transients, i.e. wavespeed values are irrespective of the direction of propagation. Direct measurements of wavespeed were not possible during this work. Therefore, a bespoke method for determining values of wavespeed is used.

An assumption made is that complete valve closing initial flow rates instantaneously transfer to zero. Therefore, $\Delta Q$ becomes equal to the initial flow rate. If $\Delta P$ is calculated from the pressure transient data as described in section 6.3.2.1, these two parameters come together in the Joukowski equation to produce a wavespeed for the complete valve closing transient. This wavespeed is then transferred to the valve opening transient with the same initial conditions and combined with those $\Delta P$ values (also calculation via the method described in section 6.3.2.1), to produce $\Delta Q$ values. This is summarised as a simple flow diagram in Figure 6.34.

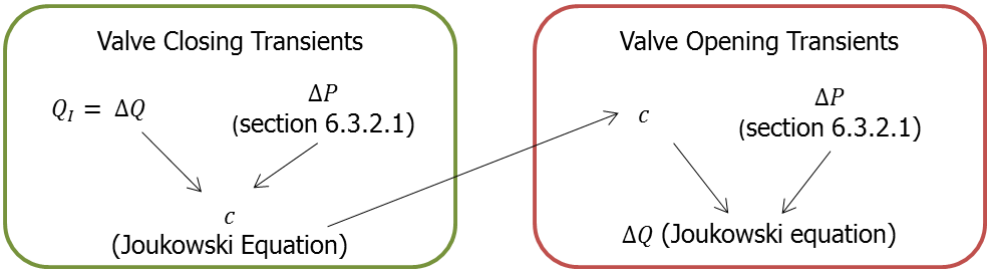


**Figure 6.34.** Flow diagram of the method utilised to determine $\Delta Q$ for both valve closing and valve opening transients. The wavespeed from the closings is transferred to the openings.

A separate set of complete valve closing transients were induced without the ball bearings (120 transients). This data set was used to calculate wavespeed (the left hand side of Figure 6.34), for varying initial flow rates and initial pressures, effectively producing a lookup table for wavespeed (Table 6.2). The initial conditions of this additional data set ranged across values used in the main body of experiments, except for zero initial flow rate for obvious reasons. Any combination of initial conditions not directly tested in this manner was interpolated. Valve opening transients utilised this wavespeed table to determine $\Delta Q$ values (the right hand side of Figure 6.34).

**Table 6.2.** Wavespeed lookup table calculated using the separate set of complete valve closing transients. Average wavespeeds (units m/s) are presented with standard deviations across ten repeats.

| | | **Initial Flow Rate (l/s)** | | | |
|---|---|---|---|---|---|
| | | **0.1** | **0.3** | **0.5** | **0.7** |
| Initial Pressure (m) | 25 | 383.0 ± 26.0 | 359.0 ± 7.7 | 342.7 ± 5.6 | |
| | 35 | 407.6 ± 27.1 | 356.4 ± 10.0 | 340.1 ± 4.4 | 345.7 ± 4.1 |
| | 40 | | | | 347.4 ± 5.6 |
| | 45 | 391.6 ± 27.6 | 361.4 ± 17.6 | 341.4 ± 4.9 | 342.2 ± 6.3 |

Table 6.2 demonstrates no correlation between initial pressure and wavespeed (beyond experimental repeatability), but wavespeed does appear to decrease as initial flow rate increases. Complete valve closing transients were performed by Covas et al. (2005) in a system consisting of polyethylene pipe with the same nominal diameter as the laboratory facility used in this work. Those transients appear to also show a relationship between initial flow rate and wavespeed. Therefore, the wavespeeds calculated from this separate data set were accepted.

#### 6.4.1.2 Errors in Valve Opening $\Delta Q$

Equation 6.3 showed that pseudo instantaneous bulk change in flow rate, $\Delta Q$, is related to wavespeed and $\Delta P$. Accordingly, $\Delta Q$ errors must also be related to the errors in determining $\Delta P$ and wavespeed. Applying propagation of errors theory (Harvard University, 2007) to Equation 6.3 led to Equation 6.4 for calculating $\Delta Q$ errors:

$$\Delta Q_{error} = \Delta Q \sqrt{\left(\frac{\Delta P_{error}}{\Delta P}\right)^2 + \left(\frac{c_{error}}{c}\right)^2} \qquad \text{Equ. 6.4}$$

Variability across experimental repeats was used here to quantify errors, as measurement errors were considerably smaller and more likely to be systematic. For $\Delta P_{error}$, the standard deviation across a set of repeats taken from the main body of experiments. For $c_{error}$, the maximum standard deviation across wavespeed tests (Table 6.2) was taken for each initial flow rate. Using the maximum standard deviation was deemed to be the most conservative option. So for partial valve opening transients with initial flow rates of 0.1 l/s, 0.3 l/s, 0.5 l/s, and 0.7 l/s, the corresponding $c_{error}$ values were 27.6 m/s, 17.6 m/s, 5.6 m/s, and 6.3 m/s, respectively. Complete valve opening transients used a $c_{error}$ value of 27.6 m/s as 0.1 l/s was the closest initial flow rate to zero.

Other parameters were individualised to each particular test performed. Values used for a partial valve opening transient with initial conditions of 0.5 l/s and 35 m (Repeat 2) are included in Equation 6.5 as an example.

$$\Delta Q_{error} = 0.463 \sqrt{\left(\frac{0.355}{26.692}\right)^2 + \left(\frac{5.588}{340.104}\right)^2} = 0.010\ l/s \qquad \text{Equ. 6.5}$$

### 6.4.2 Exploring $\Delta Q$

Valve closing transients were not relevant in this analysis. The assumption made was that initial flow rates for these transients instantaneously transferred to zero. Therefore, $\Delta Q$ became equal to the initial flow rate and an analysis of $\Delta Q$ would be identical to the initial flow rate results given in Figure 5.4.

For valve opening transients, $\Delta P$ was previously shown to correlate with initial conditions of flow rate (Figure 6.31) and pressure (Figure 6.32). As $\Delta Q$ is linearly proportional to $\Delta P$ (Equation 6.3), it would follow that the same correlations exist for $\Delta Q$. Analysis revealed that this was the case: $\Delta Q$ and initial flow rate exhibited a negative quadratic relationship, and $\Delta Q$ and initial pressure exhibited a positive linear relationship. These relationships are not included here as they are identical to Figures 6.31 and 6.32.

Figure 6.35 presents the $\Delta Q$ values calculated plotted against currents at which mobilisation occurred. The steady state mobilisation results, including the corresponding

regression line, are included for comparison. Errors in the $\Delta Q$ values are drawn on the figure as error bars. Generally, these errors increased with increasing pressure but decreased with increasing initial flow rate. The parameters couple together in a complex relationship.

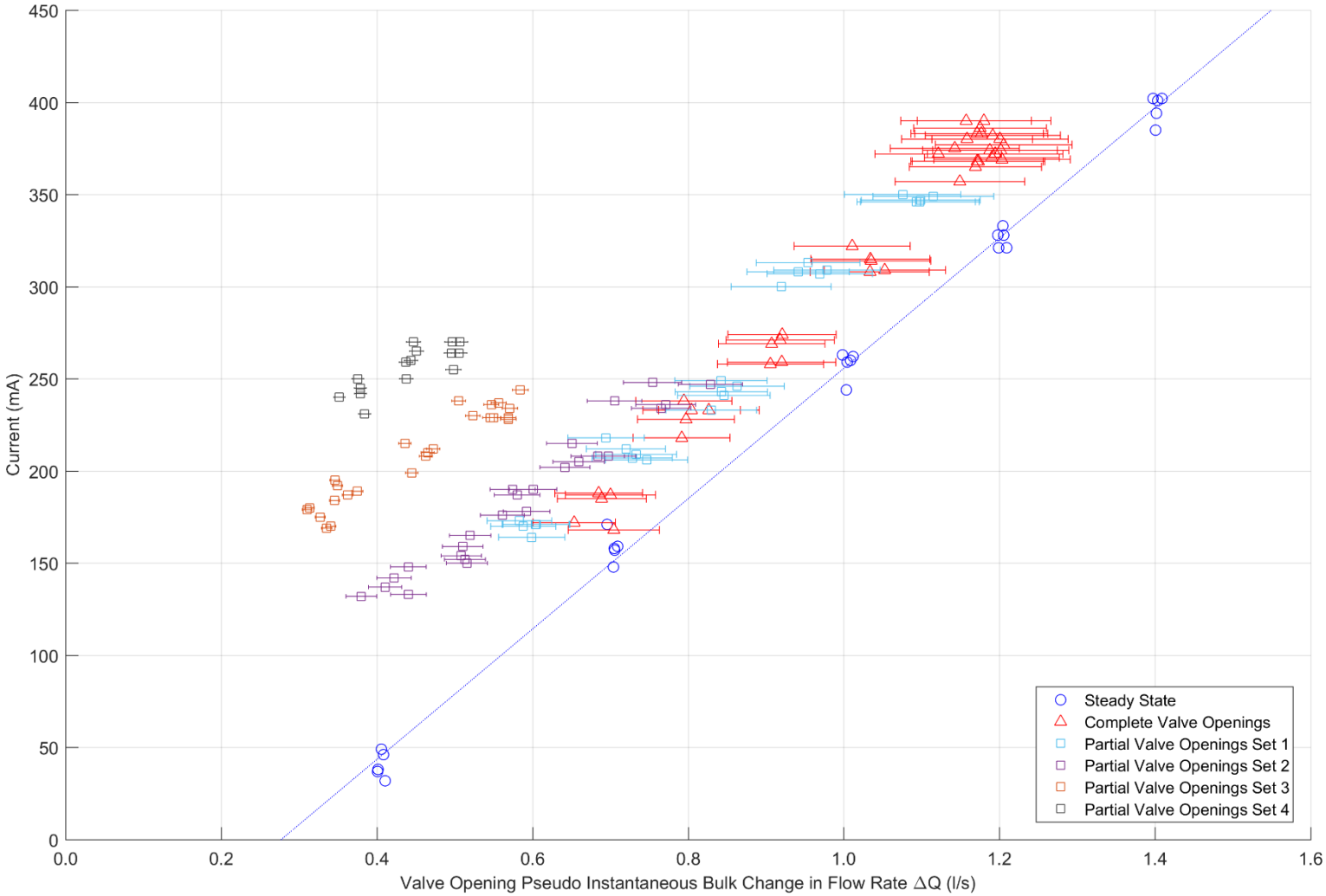


**Figure 6.35.** Currents at which mobilisation occurred for ball bearings, against valve opening $\Delta Q$ values. Error bars in $\Delta Q$ are included as well as the steady state mobilisation force relationship for comparison.

The transient pseudo instantaneous bulk change in flow rate, $\Delta Q$, parameter informs the magnitude of the dynamic flow change. If the transient mobilisation behaviour function only contained this parameter, the transient $\Delta Q$ relationships would ideally align with the steady state relationship. Figure 6.35 shows that these relationships sit near but still left of the steady state relationship. Therefore, whilst the $\Delta Q$ parameter must be significant in describing the peak mobilising force, it must not be the only component in the transient mobilisation behaviour function. For example, partial valve openings set four that transition between 0.7 l/s and 0.9 l/s exhibit $\Delta Q$ values between 0.35 l/s and 0.51 l/s, yet the ball bearing must have been able to resist the initial larger flow. Figure 6.35 revealed the further the transient $\Delta Q$ relationships were from the steady state relationship, the higher the initial flow rates of the transients were. Therefore, initial flow rate must play a more substantial role in transient mobilisation.

### 6.4.3 Peak Dynamic Force

A new function is proposed to determine the peak transient force to describe mobilisation behaviour of valve opening transients. This function is termed the 'Peak Dynamic Force' (PDF) and combined the initial flow rate with the transient-induced flow rate $\Delta Q$. This function is outlined in Equation 6.6 and illustrated for a partial valve opening transient in Figure 6.36.

$$Peak\ Dynamic\ Force = |Q_I + \Delta Q| \qquad \text{Equ. 6.6}$$

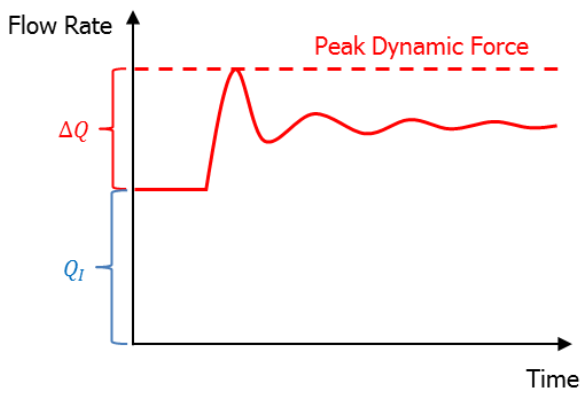


**Figure 6.36.** Idealised flow rate schematic for a partial valve opening transient showing the peak dynamic force as a sum of the initial steady state flow rate, $Q_I$, and the pseudo instantaneous change in flow rate, $\Delta Q$.

The $\Delta Q$ values necessitated a directional sign to indicate whether the transient force acted upstream or downstream. This can originate from an increase or decrease in pressure. Therefore, the PDF equation holds when $+\Delta Q = -k\Delta P$. A decrease in pressure (valve

opening) corresponds to an increase in dynamic flow rate and a dynamic upstream force. Similarly, an increase in pressure (valve closing) corresponds to a decrease in dynamic flow rate and a dynamic downstream force.

For complete valve closing transients the force must exceed initial flow rate in the same manner, otherwise the particles would not have been able to mobilise due to the transient. Therefore, conceptually this function would apply to closing transients as well. However, the assumption made for the $\Delta Q$ analysis was that the complete valve closing initial flow rate instantaneously transferred to zero (section 6.4.1.1). As this meant that $\Delta Q$ was equal to $Q_I$, the same method cannot be used to establish a $\Delta Q$ value greater than $Q_I$.

The PDF function was consequently only examined here for valve opening transients. Figure 6.37 presents the PDF values calculated plotted against currents at which mobilisation occurred for valve opening transients. The steady state mobilisation results, including the corresponding regression line, are included for comparison. Errors in the PDF values are drawn on the figure as error bars.

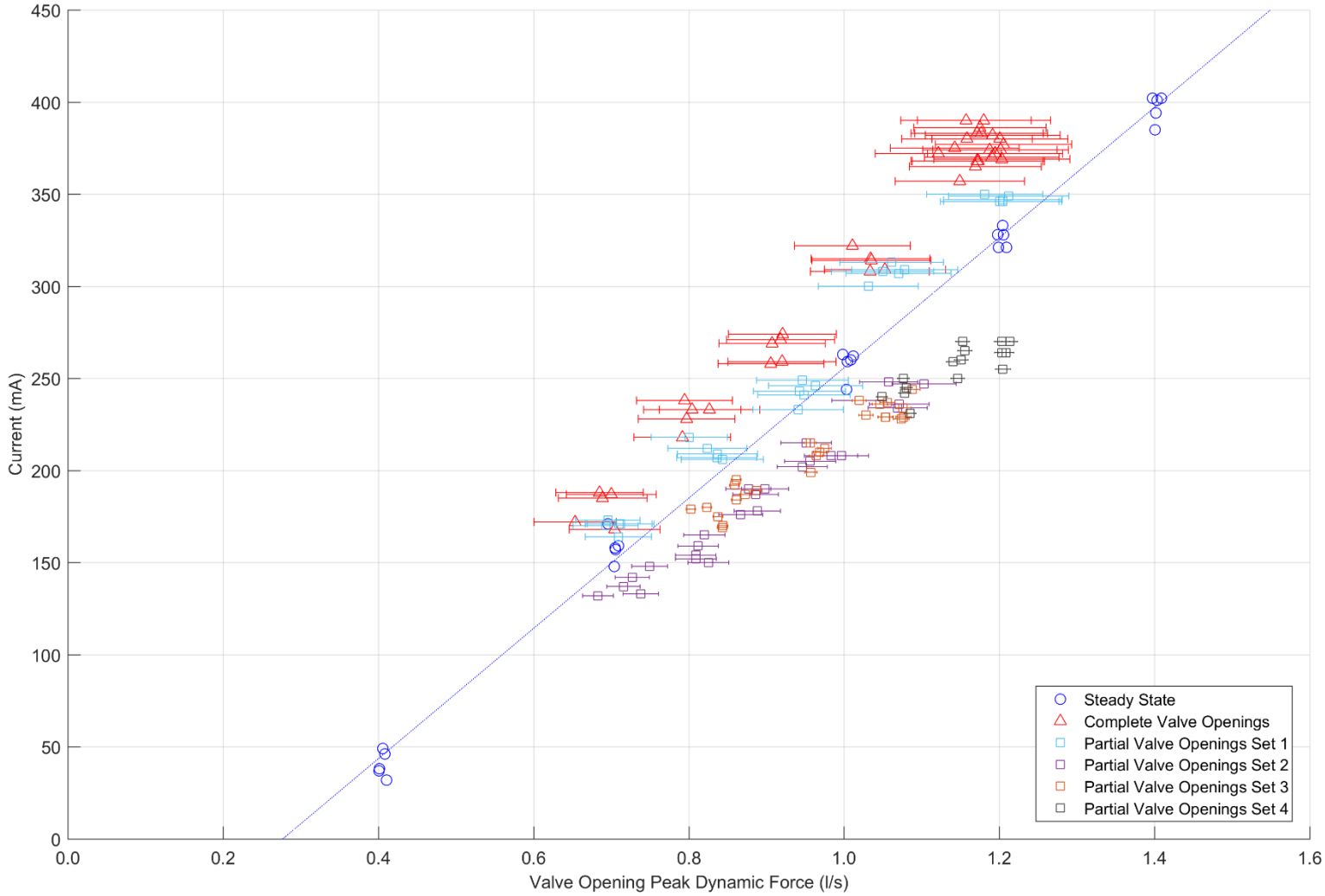


**Figure 6.37.** Currents at which mobilisation occurred for ball bearings, against valve opening PDF values. Error bars in PDF are included as well as the steady state mobilisation force relationship for comparison.

If the transient PDF function perfectly described transient mobilisation behaviour, the PDF relationships with current would align with the steady state relationship, i.e. the relationships will all be on top of each other producing a single trend. Figure 6.37 shows PDF values for valve opening transients sit broadly around the steady state mobilisation relationship. Therefore, the proposed PDF function is close to being representative of transient mobilisation behaviour.

Further analysis of the data sets revealed connections between them (statistically similar if p-value > 0.05, but statistically different if p-value < 0.05):

- Complete valve opening transients sit above the steady state relationship and the two data sets are statistically different.
- Partial valve opening transients set one are statistically similar to the steady state data set.
- Partial valve opening transients sets two, three and four sit below the steady state relationship and are statistically different from the steady state data set.
- Partial valve opening transients set two is statistically different to sets three and four.
- Partial valve opening transients set three is statistically similar to set four.

There is a behaviour change in valve opening transients where those with zero or transitional initial flow sit on or above the steady state relationship, and those with turbulent initial flow sit below the steady state relationship. Simply put, valve opening transients with no initial flow 'undershoot' PDF values, and valve opening transients with turbulent initial flow 'overshoot' PDF values.

#### 6.4.3.1 PDF Variation Due To Wavespeed

The PDF function relies on a method for determining wavespeed, as described in section 6.4.1.1. If this method (a function of $Q_I$) is imperfect, it could impose a change in behaviour due to turbulent flow rates on to wavespeed values. This behaviour change could then propagate to PDF and cause the variation seen in Figure 6.37.

The goal of this section is to determine if an error in wavespeed could explain the lack of a single trend in PDF values. This is achieved by calculating what constant value of wavespeed would make each data set statistically similar to the steady state mobilisation results. These values are then compared to the previous values used to see if the PDF variation could be attributed to the wavespeed method.

Table 6.3 presents, for each valve opening data set, the previous wavespeeds used (averaged across initial pressure) and the range of wavespeeds that produce statistically similar PDF results to steady state. These values apply to ball bearing results. Several observations can be made from this data. Firstly, comparison of the previous wavespeeds shows higher wavespeeds for zero and transitional initial flow rates, than for turbulent initial

flow rates. Thus confirming a change in wavespeed behaviour due to initial flow rate. This could be due to where the points lie on the inverse 2nd order polynomial relationship between initial flow rate and wavespeed. Secondly, where the previous wavespeeds decreased with increasing flow rate, the wavespeeds that produce statistically similar results to steady state increase with increasing flow rate.

**Table 6.3.** Previous values of wavespeed and constant wavespeeds required for valve opening PDF values to be statistically similar to the steady state relationship. These values apply to ball bearing results.

| Valve Opening Data Set Name | Initial Flow Rate (l/s) and Regime | Previous Average Wavespeed (m/s) | Wavespeeds that Produce Statistically Similar Results to Steady State |
|---|---|---|---|
| Completes | 0 | 394.14 | 346.64 to 384.90 |
| Partials Set One | 0.1, Transitional | 394.14 | 365.27 to 420.14 |
| Partials Set Two | 0.3, Turbulent | 358.98 | 390.88 to 464.33 |
| Partials Three | 0.5, Turbulent | 341.42 | 439.71 to 564.01 |
| Partials Set Four | 0.7, Turbulent | 345.14 | 489.85 to 1244.92 |

Comparing the previous wavespeeds with the wavespeeds that produce statistically similar results to steady state for each data set in turn reveals the following information:

- Previous wavespeed for complete valve opening transients is only slightly higher than the suggested range for PDF values to align with steady state, and within typical wavespeeds for polyethylene pipes, 240 m/s to 425 m/s (Grann-Meyer, 2005).
- Previous wavespeed for partial valve opening set one transients fits within the suggested range as expected.
- Previous wavespeed for partial valve opening set two transients is lower than the suggested range. Furthermore the suggested range is on the upper end of typical wavespeeds.
- Previous wavespeeds for partial valve opening sets three and four transients are considerably lower than the suggested ranges. These ranges are substantially higher than typical values.

Complete valve opening transients produce values of PDF that 'undershoot' the steady state relationship. This could be attributed to experimental error in determining wavespeed and the 'undershooting' is likely to be caused by this minor disparity. In contrast, the partial valve opening transients with turbulent initial flow rates produce values of PDF that 'overshoot' the steady state relationship. Wavespeeds that could correct this variation are

beyond typical values for polyethylene pipes. That is to say the waves would have had to have been travelling exceptionally fast for the PDF values to be statistically similar to steady state.

To summarise, an imperfect method in determining wavespeed is unlikely to cause the variation between turbulent partial valve opening transient PDF values and the steady state mobilisation relationship. This change in behaviour echoes the variation in streamwise particle movements observed in section 6.2.1.4 and the $\Delta t$ times shown in section 6.3.1.2. Another physical and currently unaccounted effect must be occurring during these turbulent valve opening transients, which distinguishes them from the other valve opening transients.

6.4.3.2 Applying PDF to Complete Valve Closing Transients

It was previously stated that PDF analysis, as detailed here, could not be applied to the complete valve closing results; the wavespeed method described in section 6.4.1.1 would create a circular argument. However, conceptually this function would apply to closing transients as well. Figure 6.38 illustrates the PDF function for a complete valve closing transient.

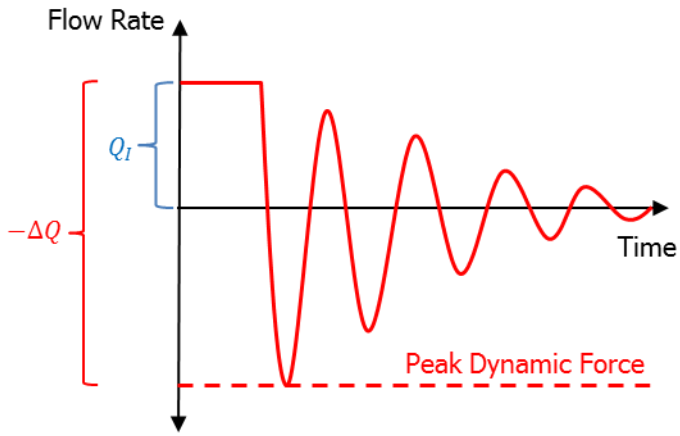


**Figure 6.38.** Idealised flow rate schematic for a complete valve closing transient showing the peak dynamic force as a sum of the initial steady state flow rate, $Q_I$, and the pseudo instantaneous change in flow rate, $-\Delta Q$.

The analysis presented here aimed to demonstrate what ideal value of wavespeed would produce a single trend for complete valve closing PDF values and steady state mobilisation values. Consequently, separate values of wavespeed were determined for each initial flow rate of the complete valve closing transients. Table 6.4 presents these values.

**Table 6.4.** Wavespeeds required for complete valve closing PDF values to be equal to the steady state relationship. These values apply to ball bearing results.

| Initial Flow Rate (l/s) and Regime | Wavespeed (m/s) |
|---|---|
| 0.1, Transitional | 104.89 ± 7.87 |
| 0.4, Turbulent | 148.06 ± 2.60 |
| 0.7, Turbulent | 156.08 ± 1.85 |
| 1.0, Turbulent | 161.77 ± 3.93 |
| 1.3, Turbulent | 171.12 ± 3.38 |

Two observations can be made from the wavespeeds given in Table 6.4. Firstly, the wavespeed values increase with initial flow rate. A similar trend was seen with the valve opening transients (Table 6.3). Secondly, the necessary wavespeeds for complete valve closings are considered significantly low when compared to typical wavespeeds for polyethylene pipes (240 m/s to 425 m/s). It is unlikely that the wavespeeds were this low during the ball bearing experiments. Therefore, another physical and currently unaccounted effect must be occurring during these turbulent complete valve closing transients.

## 6.5 Applying Peak Dynamic Force to Powder Results

The aim of this section is to apply the transient mobilisation behaviour function achieved in section 6.4 to the powder results. This will determine if the PDF function also applies in the same manner to the powder material.

To review, the experimental tests performed with the powder included steady state, complete valve opening transients (equivalent to the ball bearing complete valve opening set one transients), and partial valve opening transients (equivalent to the ball bearing partial valve opening set three transients). The partial valve opening transients commenced at an initial flow rate of 0.5 l/s and transitioned to 0.7 l/s. The final powder results were presented in Figure 5.25.

To analyse the powder experiments, the $\Delta t$ values were first determined. These times confirm that a dynamic force during the transient related to initiation of mobilisation (Figure 6.39). The method of converting $\Delta P$ to $\Delta Q$ was then applied in the same way as for the ball bearing particles, including the wavespeed method described in section 6.4.1.1. There were not enough data points for the powder analysis to conclusively demonstrate relationships between initial conditions and the $\Delta P$, and $\Delta Q$ values. Once the pressure surge was converted to a flow surge, the initial steady state flow was added to produce a PDF value. Figure 6.40 presents the PDF values calculated for powder tests performed that caused mobilisation.

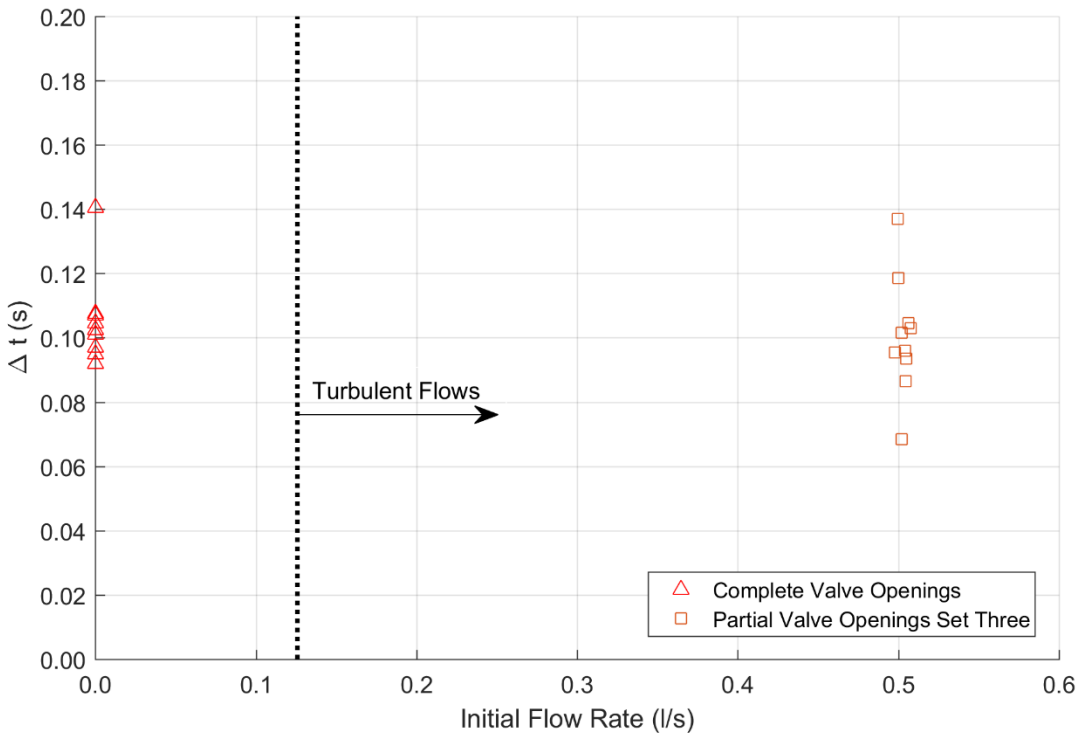


**Figure 6.39.** $\Delta t$ values for valve opening transients tested with the powder plotted against initial flow rate.

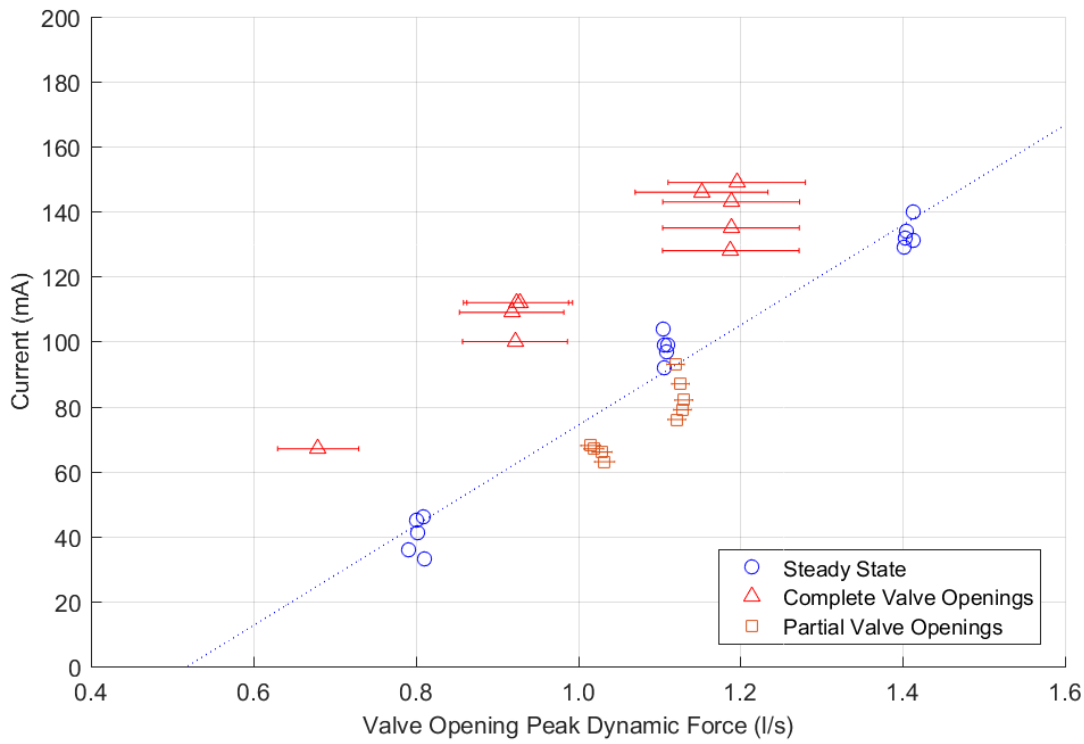


**Figure 6.40.** Currents at which mobilisation occurred for powder, against valve opening PDF values. Error bars in PDF are included as well as the steady state mobilisation force relationship for comparison.

Figure 6.40 reveals that the complete valve opening and partial valve opening transient values of PDF appear to sit above and below the steady state line, respectively. Yet, statistically, both transient data sets are similar to the steady state data set, i.e. they are statistically one single trend. The wavespeeds used from the previous method (section 6.4.1.1) are within the necessary range for statistical similarity and are reasonable values. Overall, the PDF function appears to act in same manner for the powder material as it did for the ball bearing valve opening results.

## 6.6 Summary

An objective of this work was to determine how transients, tested experimentally, caused mobilisation. This chapter performed observationally driven analysis on a range of transient parameters to examine how, or if, they correlated to the currents at which mobilisation occurred. The key parameter found to correlate for complete valve closing transients was initial flow rate. Conversely, initial flow rate and initial pressure couple together to affect mobilisation for valve opening transients.

A unique function was developed that aimed to describe the highest force generated during the transients. Synchronisation of the pressure time series data and the

videos captured by the camera revealed that the first dynamic surge of the transients initiated mobilisation. The dynamic force during this surge was consequently quantified using the parameter $\Delta Q$ and added to the initial steady state force to produce a function termed the Peak Dynamic Force. If the peak dynamic force causing mobilisation is absolute (i.e. non-directional), then this function can be applied to both valve closing and valve opening transients indiscriminately.

The resulting PDF values for complete valve opening transients and partial valve opening set one transients, aligned well with the steady state mobilisation relationship, if reasonable wavespeed values were used (347 m/s to 420 m/s). This implies that these transients cause mobilisation by producing the same peak forces as for steady state mobilisation. However, partial valve opening transients with turbulent initial flow rates appear to overestimate the PDF values. Another physical and currently unaccounted for effect must be occurring that distinguishes these transients from the other valve opening transients. Analysis of complete valve closing transients showed that significantly lower wavespeeds can equate transients to the steady state mobilisation relationship. Similar to the turbulent valve opening transients, the PDF function does not account for all physical effects in these cases.

# Chapter Seven

# Discussion

## 7.1 Introduction

This chapter discusses the work presented in this thesis. It is structured by the objectives outlined in Chapter Three. Each section addresses one of the four project objectives in turn and commences with a restatement of the relevant objective. The final section then proposes possible impacts of this work, and future research stemming from the main findings in this thesis.

## 7.2 Objective One

*"To develop an investigative technique in order to address the aim of this research. This technique would necessitate control, repeatability and reliability."*

### 7.2.1 Replication of Adhered Material

The novel experimental programme developed in this work required replicating key properties of pipe-wall adherence, variable adherence strength and material structure. An innovative analogue was designed and developed using an electromagnet with ferritic particles placed inside the pipe. The experiments were consistently performed where the particles experienced a magnetic adherence force in addition to their self-weight. This meant that adhered material strength was the only parameter being investigated. Current through the electromagnet was utilised as a repeatable and controllable measure of adherence force. Whilst current is not a typical metric of material strength, unlike elastic modulus, it was used as an effective tool to represent adhered material strength in pipeline systems and facilitate comparison between the effects of different hydraulic forces. These effects could then be compared to other literature and practical observations. For example, steady state results produced a linear mobilisation relationship between material strength (current) and bulk flow rate. This was expected based on existing understanding of material behaviour, discussed in section 2.4.6.

The combination of the electromagnet, curvature of the pipe and flow structures meant that the particles were observed during steady state flow to continuously move and return to the same initial location. It could be argued that this action is broadly analogous to elastic behaviour where organic material can extend and return (Stoodley et al., 1999). However, the speed and scale of this action for the ball bearings is not comparable.

An alternative system was considered; applying paint of known shear strength along the inside of the pipe. Paint stripped by the hydraulic force could directly inform the shear stress generated. This technique would be akin to flow visualisation paint currently used in many industries from high-speed racing to scale building aerodynamics (Terzis et al., 2011). The amount of paint removed could be used to compare between transients and steady state conditions. Yet, the shear strength range of any potential paint was likely to be smaller, more discrete and less accurate than current through the electromagnet. The magnetic system was chosen as it was reliable, controllable, repeatable, and allowed for a greater range of testing conditions.

### 7.2.2 Location of the Electromagnet System

DWDS field studies have shown that material accumulates on the entire pipe circumference (Husband and Boxall, 2016). To replicate this and explore mobilisation from different wall positions, the electromagnet/particle system could have been placed anywhere around the pipe circumference. As long as the magnetic force was greater than the self-weight, the particles would have adhered to the pipe wall. The difference would be whether the self-weight force acts with, or against, the magnetic force, as illustrated in Figure 7.1. In the experiments performed in this work, the magnetic particles were placed in the pipe invert. This was done for ease of use. For example, only gravity was needed to insert the particles within the pipeline. If the particles were in the obvert, a more complex system would have been necessary.

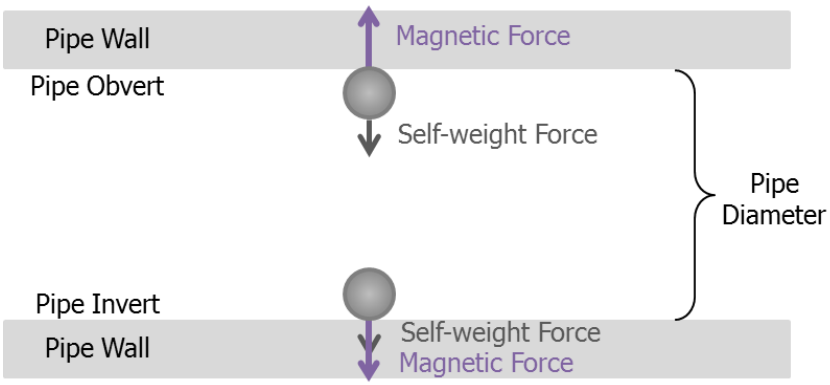


**Figure 7.1.** Illustration of the magnetic and self-weight forces on particles held against the pipe obvert and the pipe invert.

### 7.2.3 Particle Detachment

Detachment, in this work, was defined as the particles surpassing a distance-based threshold in the streamwise direction. To clearly show mobilisation had occurred, this

distance was taken as approximately twice the maximum of any initial particle movements (section 4.3.5). Conceptually, a "tailored" threshold could have been adapted for each transient so that the particle only just exceeded its initial movements. This might have produced slightly higher currents at which mobilisation occurred, and therefore an apparently higher mobilisation force. However, systematically applying a conservative and robust threshold distance was deemed the more objective and desired approach. A step-change in streamwise distance travelled by the ball bearing particles occurred at the currents recorded using this mobilisation criterion (Figures 4.15 and 4.16). Therefore, a consistent phenomenon was captured by this mobilisation detection process. Having a conservative threshold led to lower bound currents at which mobilisation occurred, closer to the steady state mobilisation force relationship, yet still clearly demonstrated transients can cause mobilisation where steady state cannot.

### 7.2.4 Evidencing Transient Events

Transients were measured via high temporal resolution pressure data, providing simultaneous evidence of transients and mobilisation. This is an improvement on previous literature as many of the previous DWDS studies have stated that a transient occurred, yet no direct data was presented to confirm this, e.g. Aisopou et al. (2012), Mustonen et al. (2008). Furthermore, the transients in this work were all pseudo instantaneous, so the forces induced were truly dynamic. Naser and Karney (2008) used field hydrant turbidity data drawn from Boxall et al. (2003) to attempt to validate their transient-water quality model. Yet, in that field work, it was most likely that the valve was not rapidly opened, so it is doubtful that the consequential hydraulic changes were truly dynamic. The transients produced in the experiments performed in this work were shown to be controlled, repeatable and consistently generated.

## 7.3 Objective Two

*"To determine, for sets of trials across a wide range of conditions, if transient induced forces can mobilise adhered material where steady state flow conditions cannot."*

### 7.3.1 Separating Transient and Steady State Forces

A critical aspect of this research was to separate transient forces from steady state forces at the equivalent initial or final flow rate, in order to differentiate and assess the ability of the dynamic forces to mobilise adhered material. This was achieved by comparing between

the established mobilisation force relationships for transient induced mobilisation and steady state induced mobilisation.

There is a lack of such comparisons in the literature. Often studies, such as the various biofilm studies introduced previously (section 2.5.2), report increased detachment (i.e. mobilisation) due to 'rapidly' increasing the rotation speed within reactors, and therefore 'rapidly' increasing shear stress. Yet, the experiments are not repeated with a gradual increase to the same resultant rotation speed to distinguish between the dynamic impact and the gradual change in flow rate impact.

Some rare examples of DWDS studies which begin to separate out the two types of forces are Karney and Brunone (1999), Mustonen et al. (2008) and Aisopou et al. (2012). In these three studies, there is initial flow before the respective valve closing transients are generated. This would imply that the additional mobilisation observed could only be due to the transients as the material resisted the initial steady state conditions. These particular studies, however, do not clearly state that this comparison between transient and steady state induced mobilisation was performed. In summary, the experiment presented here is unique in DWDS literature in that it clearly distinguishes the transient forces and their mobilisation ability.

### 7.3.2 Separating Accelerating and Decelerating Effects

To develop unique understanding of material mobilisation due to decelerating and accelerating flows, valve closing transients and valve opening transients were tested separately. This approach extended upon other studies where the two effects were coupled together. Within DWDS, Mustonen et al. (2008) performed complete valve closing events followed by complete valve openings five seconds later. Aisopou et al. (2012) similarly monitored a pump switch off and switch on, which can be equivalent to a valve closing transient followed by a valve opening transient. In both previous studies, the observed mobilised material cannot be specifically attributed to either type of transient. Potentially, the valve closing transients did not cause mobilisation and all material was mobilised due to the valve opening transients, or vice versa, or a combination of the two events. By isolating these transient forces, separate accelerating and decelerating effects were established.

A key novelty and substantial finding of this research was the confirmation that complete valve closing transients caused mobilisation of adhered material, where steady state could not (Figure 5.4). The particles were held by the magnetic adherence force during the initial steady state flow, then mobilised by the transient to beyond the distance threshold. This is significant as the steady state force reduces during the valve movement. Therefore, mobilisation must be due to forces generated by the transient.

Furthermore, this work has clearly demonstrated the ability of valve opening transients to cause mobilisation where the equivalent final steady state condition could not. This was evidenced in Figure 5.13 for the complete and partial opening transients tested, which transitioned between a variety of initial and final steady state flow rates.

In contrast, the partial valve closing transients tested did not cause mobilisation. Previous literature examining valve closing transients has only focused on 'complete' events where there is no final flow rate. Thus, there are no direct studies to compare this partial valve closing result to, making this study the first of its kind. This is a particularly interesting result as for the highest initial flow rate of 1.3 l/s tested, a rapid partial valve closing transient to 0.1 l/s final flow rate did not cause mobilisation; this equates to 92 % of a rapid complete valve closing transient to zero final flow rate, which did cause mobilisation. It was not possible to find the precise final flow rate at which behaviour transitioned from non-mobilisation to mobilisation in the facility available, due to the limitation of the measurement resolution in minimum flow rate. This minor sub-group of valve closing transients requires further study to find this transition value.

The experiments conducted in this research have advanced current hydraulic knowledge by distinguishing between mobilisation due to the dynamic forces induced during valve closing and valve opening transients.

### 7.3.3 Repeated and Different Conditions

To establish if a consistent mobilisation phenomenon was occurring, the experiments were performed across a wide variety of initial and final conditions. Furthermore, five repeats were executed at each combination of conditions (executed in a random order) to ensure any potential anomaly or bias did not take place. Findings from previous studies have been limited in this manner, commonly examining only one transient event and doing so at one combination of initial conditions. For example, Karney and Brunone (1999) attributed discoloured water reports to an induced valve closing transient. Similarly, Aisopou et al. (2012) linked increased bulk water material concentrations to one pump trip. The outcome of the experiments performed in this thesis conclusively prove what other works suggest from indirect observations and, furthermore, advances them by consistently and rigorously directly evidencing transient mobilisation due to a range of conditions.

### 7.3.4 Extension to Other Industries

Examination of the wider literature showed that the dynamic mobilisation principle explored here has been considered in other industries, including biofilm research, blood vessel trauma, colloidal material and whey protein layers in milk treatment (as set out in

sections 2.5.2 to 2.5.5). The findings of this work, in the DWDS context, broadly agree with the findings of these other industries. In particular, studies by Bode et al. (2007) and El-Farhan et al. (2000) also evidence increased mobilisation of material due to hydraulic halting of the respective fluids, greater than steady state initial conditions. These similarities imply that there might be a general behaviour of transients which is not greatly influenced by the context of the media being "adhered" and subsequently mobilised. The contributions made by the experiments performed here could extend to a wider community beyond DWDS. However, these links emphasise the need for consistently generated transients to facilitate such comparisons in the future.

## 7.4 Objective Three

*"To compare mobilisation of replicated adhered materials, becoming more representative of operational DWDS."*

### 7.4.1 Particle Structures

Two types of magnetic particles were used. The first were 500 μm ball bearings used individually to understand idealised behaviour. The second were 35 – 145 μm more irregular particles used as a powder to represent cohesive layers of material. Once in the magnetic field, the magnetic forces induced between the individual particles most likely acted with any other inter-particle forces, causing the powder to act like a variable aggregate. The powder was observed to form structures that elongated in the streamwise direction and varied in the steady flow (section 5.3.1). Parallels can be drawn between these structures and the 'streamers' described in Stoodley et al. (1998), which were also elongated towards the downstream direction.

### 7.4.2 Mobilisation Ability and Trends

Both types of particles were able to be mobilised due to steady state and transient hydraulic forces (Figures 5.13 and 5.25). The same global trend was exhibited: complete and partial valve opening transients caused mobilisation, where steady state did not. To directly compare between materials, the subset of the ball bearing results was selected that had identical hydraulic conditions to the powder results. For example, partial valve opening transients that transitioned from 0.5 l/s to 0.7 l/s were tested with the powder at initial pressures of 35 m and 45 m. The same flow transition was tested with the ball bearings at a wider variety of initial pressures but only tests with the same 35 m and 45 m initial pressure

were taken into the new subset for direct comparison. Figure 7.2 presents the mobilisation force relationships for this ball bearing subset in part a) and the powder results in part b).

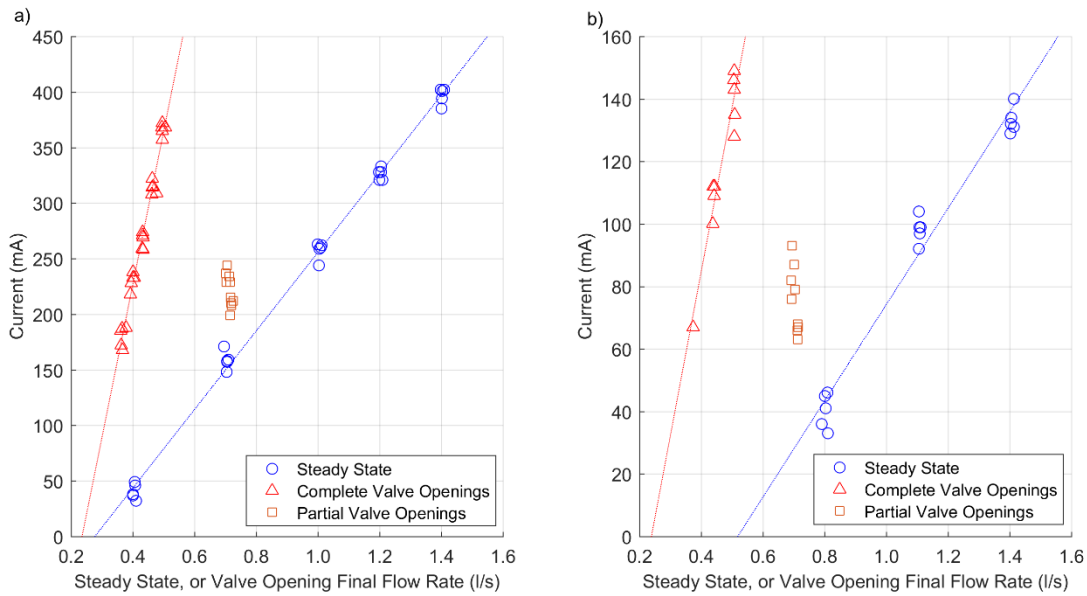


**Figure 7.2.** Mobilisation force relationships for steady state, complete valve opening and partial valve opening conditions for a) the ball bearings, and b) the powder. These results are for directly comparable hydraulic conditions. The current range is significantly smaller (0 mA to 160 mA) for the powder results than for the ball bearing results (0 mA to 450 mA).

The similarity in mobilisation trends suggests that the ball bearings and powder mobilised in the same manner. Therefore, the hydraulic processes involved in mobilisation act irrespective of the material being adhered.

### 7.4.3 Differences between the Materials

Figure 7.2 shows the same pattern of results for each of the two materials but at different values of flow rate and current at which mobilisation occurred. Extrapolating the steady state results showed that the minimum steady state flow rate necessary to mobilise a ball bearing without the magnet would be 0.28 l/s. The same parameter for powder would be 0.52 l/s, almost twice that of the ball bearing. Furthermore the currents at which mobilisation occurred were significantly lower for the powder than for the ball bearings, by up to a factor of three. For example, at the maximum steady state flow rate tested of 1.4 l/s, ball bearings were mobilised at 396.8 mA ± 7.4 mA and powder mobilised at 133.2 mA ± 4.4 mA.

#### 7.4.3.1 Material Resistive Forces

There are three proposed sources of material resistive forces that would be greater for the powder material than the ball bearings. Firstly, the total mass of SAF 2507 used per

hydraulic test was greater than the individual ball bearings by approximately one order of magnitude (section 4.3.4.4). This was established by weighing the powder prior to being placed inside the pipeline. During the powder testing process, some substructures were occasionally mobilised from the main body of material (section 5.3.1). Therefore, the aggregate powder would have a self-weight force up to an order of magnitude greater than each ball bearing. The greater self-weight, the greater the hydraulic force needed to overcome it. Secondly, the videos taken showed that the powder exhibited a larger plan area than the ball bearings (Figure 4.14). This suggests that the powder had more contact with the pipe surface, so increased friction resisting mobilisation. Thirdly, the magnetic forces between the powder particles, as well as any other inter-particle forces, meant the powder acted more like a single mass than individual particles (section 7.4.1). The aggregate, therefore, became polymorphic, i.e. able to change structure. It was able to reorganise and create the most streamlined structure. Where the ball bearings have a large frontal area and cannot deform, the powder is more flexible and can alter to resist motion.

For mobilisation to occur, the applied hydraulic force just exceeds the particles' resistive forces and adherence forces (quantified by current). The powder's resistive forces, due to the three factors discussed, could explain the significantly lower observed currents at which mobilisation occurred for the powder than for the ball bearings.

#### 7.4.3.2 Applied Hydraulic Force

Bulk flow rate in this work has been used to quantify the applied hydraulic force. Yet, the actual applied hydraulic force experienced by the two materials is likely to be different due to the intrusion of the particles into the initial steady state flow. The rigid ball bearings are likely to intrude higher into the flow than the more streamlined powder. The particles could, therefore, encroach into different boundary layers (described in section 2.3.3) and experience altered forces when the transient is generated.

The viscous sublayer and buffer layer thickness, calculated using standard 'law of the wall' calculations (Pope, 2000), vary with initial flow rate. Figure 7.3 presents these relationships for the range of initial flow rates tested in these experiments, as well as the constant height of the ball bearing particles (500 μm), and the height of the largest SAF 2507 particles (144 μm, Figure 4.11). As the camera was unable to resolve the powder in the radial direction, it is unknown what the maximum height of the powder structure was during the experiments and how it varied with initial steady state flow rate. Hence, the height of the largest SAF 2507 particles is taken as a lower bound.

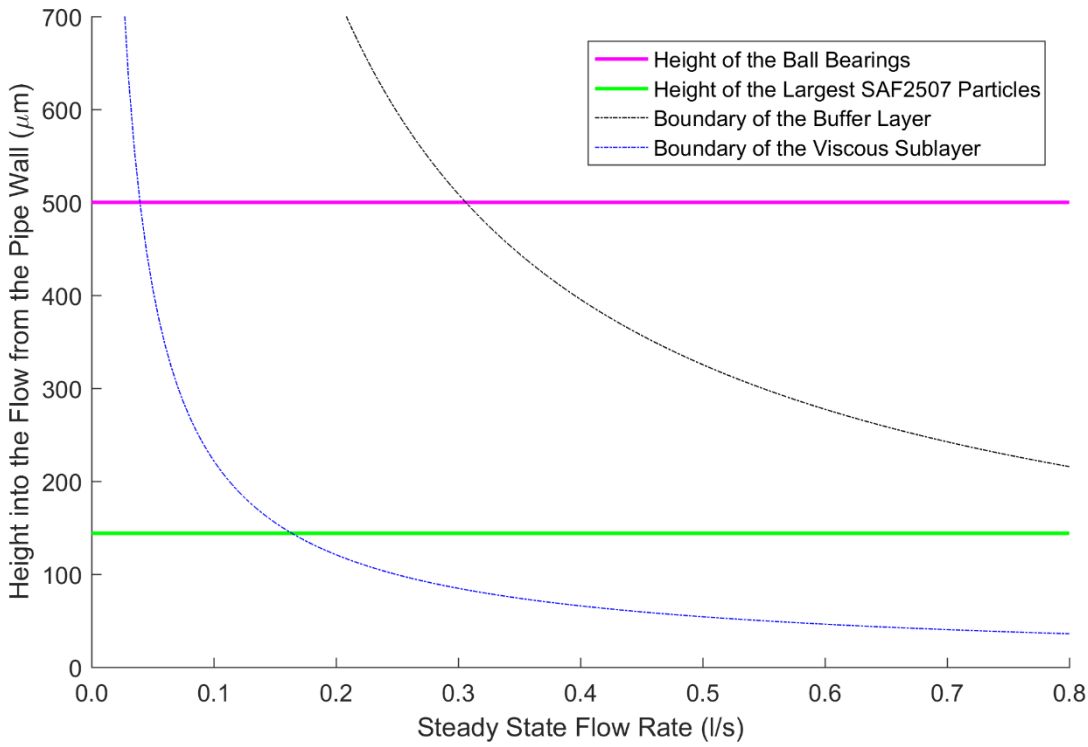


**Figure 7.3.** Height into the flow of the viscous sublayer, buffer layer, ball bearings and largest SAF 2507 particles, respectively. The viscous sublayer and buffer layer vary with initial flow rate, where the particles remain at a constant height.

Figure 7.3 shows that, for the initial flow rates tested with the powder material (0 l/s and 0.5 l/s), the powder was unlikely to have exceeded the buffer layer. Consequently, the powder will experience some turbulent forces but the flow is still dominated by viscous conditions even when the initial bulk flow rate is turbulent. On the other hand, the ball bearing protrudes above the buffer layer into the transition layer for initial flow rates of 0.3 l/s and above. Therefore, when the bulk flow rate is turbulent, the ball bearings also experience turbulent forces. These profiles do not explain the differences in minimum steady state flow rates necessary to mobilise the particles observed in Figure 7.2.

## 7.5 Objective Four

*"To understand and interpret the relative significance of transient forces that might contribute to material mobilisation."*

Chapter Six presented an observationally driven analysis that determined which transient parameters related to transient mobilisation behaviour, i.e. the currents at which mobilisation just occurred. From these parameters a function was developed that aimed to quantify the peak force induced during a transient event. This force was then compared to

the steady state mobilisation force relationship. If the two aligned, then transients were likely to cause mobilisation by creating as much dynamic force as the steady state equivalent force. Therefore, the PDF function would capture the dynamic forces leading to mobilisation.

### 7.5.1 Structure of the Peak Dynamic Force Function

Conventionally, it is assumed that steady state expressions, such as Darcy-Weisbach and Hazen-Williams, hold at every instant during a transient (Ghidaoui et al., 2005). Any discrepancy between the steady state condition and what happens during the transient is attributed to unsteady components. Therefore, transient analysis formulas frequently use the addition of a steady term to an unsteady term, such as for friction factors and wall shear stress, see Equation 7.1.

$$\tau_w(t) = \tau_{ws}(t) + \tau_{wu}(t) \qquad \text{Equ. 7.1}$$

Where $\tau_w$ is wall shear stress, $\tau_{ws}$ is quasi-steady wall shear stress, and $\tau_{wu}$ is unsteady wall shear stress. Different authors have attempted to formulate unsteady wall shear stresses in numerous ways, but overall this is the structure utilised by most (section 2.3.2).

With this in mind, it is reasonable for the function in this work to have a similar structure when derived from observations of transient behaviour. The pipeline is constant in this work (pipe diameter, roughness etc.) so bulk flow rate is analogous to shear stress. Therefore, the initial flow rate (steady term) was added to the dynamic flow rate (unsteady term), resulting from the transient pressure surge. Both these factors ($Q_I$ and $\Delta Q$) were shown individually to relate to currents at which mobilisation occurred, but best describe mobilisation when combined in this manner.

Daily et al. (1945) conducted laboratory experiments that found $\tau_{wu}$ to be positive for accelerating flows and negative for decelerating flows. This is widely accepted today. In the experiments performed in this work, bulk flow rate is used instead of wall shear stress but the same principle should apply; the unsteady component, $\Delta Q$, should be positive for accelerating flows and negative for decelerating flows.

Valve opening transients (accelerating flows) exhibited a decrease in pressure ($-\Delta P$). Therefore the PDF function became:

$$PDF = |Q_I - k * -\Delta P| = |Q_I + \Delta Q| \qquad \text{Equ. 7.2}$$

Similarly, valve closing transients (decelerating flows) exhibited an increase in pressure ($+\Delta P$). Therefore the PDF function became:

$$PDF = |Q_I - k * +\Delta P| = |Q_I - \Delta Q| \qquad \text{Equ. 7.3}$$

The summation of the steady and unsteady components is taken as an absolute value of force in this work. Whilst the flows have an upstream or downstream direction, the

resulting force is directionless. That is to say the force that mobilises the particles upstream is the same as the force that mobilises the particles downstream.

Overall, the structure of the PDF function has a basis in existing literature and performs as expected for valve opening transients with zero or transitional initial flow rates. Yet, valve opening transients with turbulent initial flow rates produced higher PDF values than for equivalent steady state values. Similarly, the PDF does not appear to explain complete valve closing results (a summary is given in section 6.6). Consequently, the PDF function requires further consideration.

### 7.5.2 Proposed Mechanisms for Mobilisation

The PDF function has been used to quantify the peak bulk force induced during a transient event. This section will examine how this force could be generated and explore physical effects that may or may not be accounted for in the existing PDF function. Two transient mechanisms for mobilisation are proposed that conceptually examine how transients could mobilise the particles. The first is driven by pressure, and the second by near wall velocity. Pressure and velocity are inherently coupled in the transient, therefore, conceptually cannot be truly separated (section 2.3.1). However, the mechanisms could produce mobilising forces in different ways. Understanding these mechanisms could contribute to understanding the observations seen in this work, including differences in the PDF function.

#### 7.5.2.1 Pressure Wave Front Mechanism

A key feature of transients is the generation of a pressure wave, which is driven by the pressure difference between zones of water (section 2.3.1). A significant pressure differential can exist across the wave front. It is proposed that this pressure differential will cause an imbalance of forces and could cause mobilisation as it passes the adhered material. The greater the pressure differential, the greater the mobilising force, and the higher the current at which mobilisation would just occur.

This mechanism is conceptually greatest in the first pass of the pressure wave, i.e. in the first pressure surge where the wave front is sharp, before resistive effects disperse the waveform (section 2.3.4.3). Figure 7.4 presents an illustration of this mechanism, for a simple adhered shape and a sharp vertical wave front. Only streamwise pressures are included as this mechanism does not impose radial pressure.

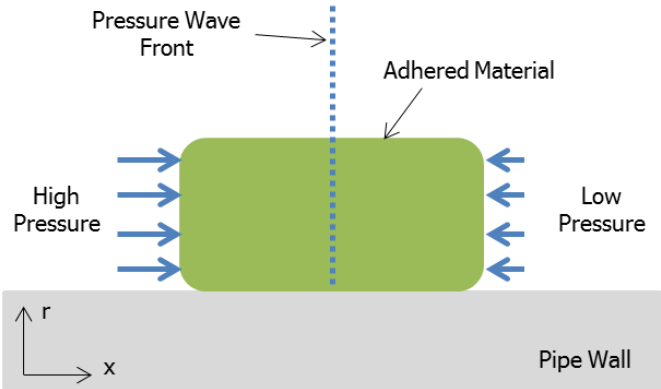


**Figure 7.4.** Illustration of the pressure wave front driven mechanism. The adhered material experiences high pressure forces on one side of the pressure wave front, and low pressure forces on the other. This imbalance of force across the wave front could lead to mobilisation. The indicated directions are streamwise along the pipe ($x$) and radial ($r$).

7.5.2.2 Velocity Profile Mechanism

A key feature of most transients is the generation of accelerating and decelerating flows. Complex near wall velocity profiles are induced that can create shallower profiles in rapidly accelerating flows and inverted profiles in rapidly decelerating flows (section 2.3.2). It has been established that these profiles can prompt additional unsteady shear stresses (section 2.3.2). If the near wall velocity profile surpasses the initial profile (in either direction), the excess unsteady shear stresses could contribute to mobilisation. The shallower the gradient of the near wall velocity profile, the greater the hydraulic force, and most likely the higher the current at which mobilisation could occur. Figure 7.5 presents an illustration of this mechanism, for a simple adhered shape and three velocity profiles. Interestingly for valve closing transients, within the first pipeline period the bulk velocity can be lower than the initial steady state bulk velocity value, or even zero, but a shallow profile near the wall could still induce additional unsteady shear stresses (Brunone and Berni, 2010).

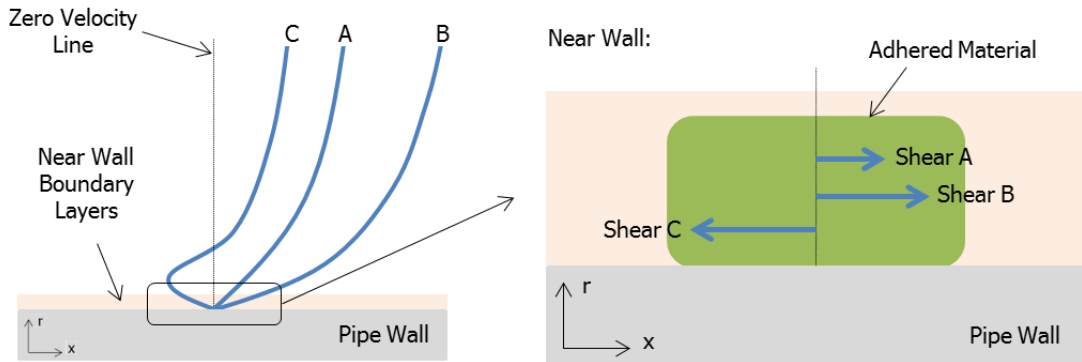


**Figure 7.5.** Illustration of the velocity driven mechanism. Velocity profiles are drawn for steady state (A), a rapidly accelerating transient (B), and a rapidly decelerating transient (C) that generates an inverted near wall profile. The highlighted near wall section shows the magnitude and direction of the corresponding shear forces induced on the adhered material. The indicated directions are streamwise along the pipe ($x$) and radial ($r$).

### 7.5.3 Applying the Pressure Wave Front Mechanism

Pressure differential across the wave front can be described as the change in pressure over a distance along the pipe ($dP/dx$). Riasi et al. (2009) attributed sudden rises in wall shear stress to peak $dP/dx$ values, i.e. passage of the pressure wave front. Kucienska (2004) has also shown that these sudden rises in wall shear stress are approximately proportional to the amplitude of the pressure wave. This $dP/dx$ parameter could not be directly measured in these experiments. Therefore, a transformation was applied based on the classic wave equation (Equation 7.4). This equation says that the spatial rate of change of pressure $dP/dx$ is proportional (via wavespeed $c$) to the temporal rate of change of pressure $dP/dt$ in the initial stages of the transient.

$$\frac{dP}{dt} = c\,\frac{dP}{dx} \qquad \text{Eq. 7.4}$$

In addition, Figure 6.28 showed that $dP/dt$ is linearly proportional to $\Delta P$. Combining these relationships together gives a transformation between $\Delta P$ and $dP/dx$, where $k$ is a coefficient.

$$\Delta P = c\,k\,\frac{dP}{dx} \qquad \text{Eq. 7.5}$$

The pressure driven mechanism is a 'bulk' factor, which is consistent with the one dimensional PDF function. As $\Delta P$ is utilised in the PDF function, the pressure wave front mechanism is already accounted for and cannot be the 'missing' effect described in sections 6.4.3.1 and 6.4.3.2.

Two further observations can be examined with regard to this pressure driven mechanism. Firstly, Figure 7.6 shows that the partial valve closing transients, which did not cause mobilisation, exhibited similar $\Delta P$ values as other transients that did cause mobilisation. This implies that mobilisation does not solely, if at all, depend on the magnitude of the pressure wave front force.

**Figure 7.6.** $\Delta P$ values calculated for all transients generated, separated into four categories: complete valve closing, partial valve closing, complete valve opening and partial valve opening. These transients are indicated, by colour, as causing mobilisation (green) or not causing mobilisation (red).

Secondly, pressure transducers were placed either side of the ball bearing, see Figure 4.6 e) and g). The time taken for the pressure surge to transmit from one transducer to the other is only up to 3.8 % of time taken for the ball bearing to commence mobilising, i.e. $\Delta t$ (Figures 6.20 and 6.21). This says that the pressure wave front has significantly transmitted past the ball bearing (minimum 20 m) before the ball bearing begins to mobilise. Moreover there is no correlation between $\Delta P$ values and step change in behaviour of the $\Delta t$ observed for the valve opening transients (Figure 6.20).

The PDF function is dominated by the $\Delta P$ parameter, yet these values do not correlate with the observed behaviour of the particles. This indicates that the pressure wave front mechanism does not dominate mobilisation ability; there may still be an imbalance of

forces due to the pressure wave front, i.e. the mechanism could still be happening, but it does not appear to be causing mobilisation.

### 7.5.4 Applying the Velocity Profile Mechanism

In contrast to the pressure wave front mechanism, the velocity driven mechanism requires a two dimensional approach to capture the varying velocity profiles induced during rapid transient events. The complex nature of the near wall velocity profile, and corresponding shear stresses, cannot be fully accounted for if only bulk flow rates (i.e. $\Delta Q$) are considered, as in the PDF function. The following subsections aim to describe the observations seen in this work, with respect to this mechanism and current literature.

#### 7.5.4.1 Valve Closing Transients

Experimental work in other studies has shown that valve closing transients are capable of producing inverted near wall velocity profiles (Brunone et al., 2000; Brunone and Berni, 2010; Riasi et al., 2009; Silva-Araya and Chaudhry, 1997; Zidouh, 2009). Those profiles were generated under rapid complete valve closing conditions. Therefore, it is reasonable to postulate that during the complete valve closing transients performed here, inverted profiles were also induced, as illustrated in Figure 7.5. These inverted profiles most likely produced greater magnitudes of absolute shear stresses than the initial velocity profiles, thus causing mobilisation of the ball bearing particles.

As the initial flow rate increased, the difference in currents at which mobilisation occurred between the steady state and complete valve closing transient results decreased (Figure 5.4). This finding implies that there is less inversion of the velocity profile for greater initial flow rates with more developed initial velocity profiles; consequently reducing the additional dynamic shear stress. Ariyaratne et al.'s (2010) numerical study showed a similar outcome for linearly decelerating flow (the closest study available for comparison); the higher the initial Reynolds number, the lower the magnitude of the unsteady wall shear stress. Theoretically at a higher flow rate than those tested in this work, the inverted profile induced might not be able to produce dynamic shear stresses greater than the initial steady state shear stresses. That is to say that the near wall velocity profile might not be able to invert sufficiently in the upstream direction to cause mobilisation. There is no data set in literature to compare this hypothesis against.

Conceptually, mobilisation did not occur for the partial valve closing transients tested in this study because the near wall velocity profiles were unable to generate sufficient dynamic additional shear stresses beyond the initial values; the near wall velocity profiles did not invert sufficiently. Other studies have only investigated velocity profiles of complete valve

closing transients so there is a gap regarding partial valve closing transients. Therefore, there are no other studies to directly compare these results to.

#### 7.5.4.2 Valve Opening Transients

Naser and Karney (2008) observed that literature studying velocity profiles during transient events was biased to valve closing events. In comparison, there are few studies focusing on near wall velocity profiles during valve opening events. Bergant et al. (2002) showed that the models for valve closing transients do not always transfer to valve opening transients. The existing, if narrow, research investigating valve opening transients agrees that the near wall profile is steeper at the beginning of the transient than the final velocity profile (Bergant et al., 2002; Naser and Karney, 2008; Zidouh and Elmaimouni, 2013). This could explain why mobilisation occurs during valve opening transients but not during steady state equivalent final flow rates.

#### 7.5.4.3 Initial Turbulence Effects

A further aspect of the velocity driven mechanism is turbulence. As stated in section 6.4.3.1, ball bearing valve opening transients with turbulent initial flow rates exhibit different behaviour to those with non-turbulent initial flow rates. This different behaviour occurred for $\Delta t$ times, streamwise motions and PDF values. It is postulated that the existing turbulence in the initial flow rate interacts somehow with the physical dynamic effects of the transient, causing the observed effects. This potential interaction, however, is not a straightforward process and there is little literature on the topic. In this subsection, $\Delta t$ times are explored across all results, and then the streamwise motions and PDF values are discussed for the valve opening transient tests performed with ball bearings.

Maruyama et al. (1976) showed that a rapid (0.05 s) valve opening from one turbulent steady state flow to another brings about a non-equilibrium state of turbulence, which changes with time and space. The turbulence intensity can quickly increase, surpassing the final steady values. He et al. (2011) went on to find linearly accelerating turbulent pipe flow causes a two stage turbulence response. In He et al.'s work (2011), the flow rates were ramped from one valve to another at an approximately constant rate for between five and ten seconds (non-rapid). This is not identical to a transient response, yet it is the closest approximation possible with current knowledge. He et al. (2011) found turbulence, in the first stage of the accelerating flow, is in a frozen state and the wall shear depends on the acceleration. The level of initial turbulence or indeed its existence is irrelevant. It is in the second stage that the turbulence starts to play a role, rapidly increasing the turbulent wall shear stress as Maruyama et al. (1976) described.

It is inferred from He et al's study (2011) that mobilisation in the experiment presented here occurs in stage one of the non-turbulent valve openings, but in stage two of

the turbulent valve openings. There is no direct evidence to show that this is the case, as there are no measurements of the duration of stage one to compare to from other literature. Though, if it is, the time difference between stage one and stage two could explain the step change in $\Delta t$ times for the ball bearings (Figure 6.21).

The powder, on the other hand, did not exhibit such a step change for the conditions tested. Valve opening transients tested with the powder at 0.5 l/s initial flow rate produced $\Delta t$ times of 0.101 s ± 0.018 s, which was equivalent to the complete valve opening transients (Figure 6.39). At this turbulent bulk initial flow rate of 0.5 l/s, the powder is likely to remain in the buffer layer (Figure 7.3), and consequently experiences less effects of turbulence than the ball bearings.

For valve closing transients, mobilisation of the ball bearing particles occurred within the first 0.16 s of all the closing transients being induced. This was shown by $\Delta t$ values in Figure 6.21. The time in which inversion acts appears to be irrespective of the initial flow rate, based on the resolution of this experiment. Perhaps this is because in the first stage of deceleration the turbulent structures already present in the flow have a delayed response to the initial dynamic effects (Ariyaratne et al., 2010). Mathur (2016) showed that near wall velocity profiles rapidly invert immediately following the start of transients, even when there are turbulent structures in the initial flow.

Expanding on the change in behaviour for $\Delta t$ times, for the ball bearing experiment, the $\Delta Q$ parameter could be capturing the acceleration effects for non-turbulent valve openings (the PDF parameter aligns with steady state). Yet, the $\Delta Q$ parameter could be missing the turbulent effects present in initially turbulent valve opening transients (the PDF parameter overestimates). If the powder does not experience turbulent forces even at turbulent bulk initial flow rates (due to not exceeding the buffer layer, Figure 7.3), this could explain why the PDF parameter for the powder aligns with steady state relationship where the equivalent ball bearing values overestimate.

The turbulence effects in stage two could affect the ball bearing streamwise movements seen during the transient, i.e. the stepped motions (Figure 6.7). Random turbulent forces could be generated (varying in time and magnitude), which could in turn cause the ball bearings to travel down the pipe in random motions. Whereas for the non-turbulent valve openings the acceleration effects dominate, which cause the ball bearings to only mobilise in one swift motion (Figure 6.8).

### 7.5.5 Objective Four Summary

Overall the PDF function appears to explain most but not all observed behaviour. The pressure wave front mechanism does not explain mobilisation, even though the $\Delta P$ parameter dominates the PDF function. In contrast, the observations seen in this work appear to be

consistent with existing understanding of velocity profiles induced during transient events. For example, lack of near wall velocity profile inversion could explain why the partial valve closing transients did not cause mobilisation. This implies that a velocity profile driven mechanism leads to mobilisation of the ball bearings and powder material. Consideration of the initial turbulence and material size with regard to the height of the boundary layers does explain the observed differences in $\Delta t$ for ball bearings and powder experiments. Therefore, the PDF function is a useful first approximation for mobilisation behaviour, but it is missing the physical effects of initial velocity profile and existing turbulence.

## 7.6 Significance of This Work

This final section raises possible theoretical and practical impacts of this work focusing on transients as a cause of water quality risk. Building upon the rigorous experiments performed, the following subsection proposes other future research stemming from the main findings in this thesis. Here, the phrase 'transient mobilisation' applies to the ability of transients to mobilise adhered material where steady state cannot.

### 7.6.1 Theoretical Impacts

Transient mobilisation of adhered material combines two traditionally separate areas of DWDS study: water quality, and transient behaviour. This combination may lead to a change in thinking for both fields, which may in turn develop into a new area of research.

Results of the experiments presented in this work propose that transients may create a water quality risk in operational networks by mobilising material that would otherwise remain adhered. This risk would need to be quantified, yet water quality issues not currently accounted for could be attributed to transient events. Long term, water quality management strategies that include transient analysis could be developed, which might help deliver safer drinking water in the future.

### 7.6.2 Practical Impacts

As a consequence of this work, the first practical implication would be increased monitoring of transient parameters using high temporal resolution equipment. High frequency pressure data in particular is necessary to evidence the short lived transient events. This would be a step change in data collection as currently pressure and turbidity are limited to low temporal resolution, i.e. 15 minutes. Such a data set could be used to relate areas of high transient activity to areas of increased turbidity, thus linking transients and water quality in operational networks. Moreover, data collected could validate any transient simulations added

to steady state DWDS numerical models. This monitoring, however, is likely to have an associated high cost due to increased high resolution equipment, operator time, and analyst processing time. This cost may be prohibitive for water companies.

Valve operations are a common source of transients (section 2.3.1). If these operations can be controlled so that only gradual changes in flow occur, transients can be mitigated and the risk of transient mobilisation of adhered material reduced. This is particularly pertinent for complete valve closing transients. There may be a tendency for valve operators to think that valve closing operations can only cause a decrease in hydraulic force, so operators may slam the valves closed. These operators should be trained to open and close valves slowly to reduce transient generation. Water companies should likewise encourage major water users, like industrial factories, to have slow start/stop pumps to also reduce the frequency of significant transients.

### 7.6.3 Future Research

Building upon the findings presented in this work, the following section recommends three further investigations. The first focuses on two dimensional velocity profiles through the boundary layers of valve closing and valve opening transients. The second focuses on organic material more representative of that found in operational networks. The final proposes an alternative perspective on the impact of transients on water quality. These future investigations should aim to continue on the same level of rigorous and control as presented here.

#### 7.6.3.1 Velocity Wall Profiles

The analysis performed here has highlighted the strong need for understanding two dimensional velocity profiles during valve closing and valve opening transients. Current studies have so far measured velocity across the pipe diameter (section 2.3.2). However, future work should focus on measurements with high radial and temporal resolution through the boundary layers to understand how the velocity profiles change during transients. Comparing profile changes between complete and partial valve closing transients, which in this work did and did not cause mobilisation, would be especially informative.

Described in section 2.3.3, the inner layer of the pipe wall exists up 200 wall units (a non-dimensional radial scale) and constitutes the following layers; viscous sublayer 0 to 5 wall units, buffer layer 5 to 30 wall units, and transition layer 30 to 200 wall units (Pope, 2000). A minimum of three velocity measurements should be taken within each layer to develop an understanding of the profiles generated. Ideally, a larger number, perhaps an order of magnitude greater, would be taken in the transition layer to account for the turbulent structures induced. Similarly, section 6.3.1.2 revealed that the largest observed $\Delta t$ time,

between the start of the transient and when mobilisation of the ball bearing was instigated, was 0.477 s. Thus, the velocity profile within the first 0.5 s is of greatest relevance. Data recording on the order of 100 Hz would give enough data points within this time period (approximately 50).

Experimental velocity profiles measured in this way could be used to validate current and future transient models of unsteady shear stress, and ultimately advance current hydraulic understanding of the transient forces generated. This work should be considered a high priority.

#### 7.6.3.2 Impact of Organic Material

The magnetic analogue proved invaluable due to its replication of pipe-wall material in a repeatable, controllable and quantifiable manner. It would also be desirable, however, to apply the methods used successfully here to organic material found in operational networks. This would determine how transients interact with thin, variable elastic material, which could deform prior to mobilisation. Complications in such an investigation would include time to grow the material, and quantifying whether mobilisation occurred. A new type of threshold would need to be derived, such as a change in bulk water cell count or change in turbidity. Nonetheless, evaluation of "real" DWDS material could evidence transient mobilisation beyond the material tested in these experiments. This would demonstrate the transferability of the physical phenomenon observed here.

#### 7.6.3.3 An Alternative Impact on Water Quality

As previously stated, results of the experiments presented in this work propose that transients may create water quality risk by mobilising material that would otherwise remain adhered. Consequently, this risk could be lessened if the presence of transients is reduced. A counter argument could be made for increasing the quantity of transients as a potential strategy for improving water quality. Relatively small transients frequently imposed in the system could prevent the accumulation of material on the pipe walls. Material in the bulk water would remain as low level 'background contamination', rather than accumulating and causing a significant water quality risk upon subsequent release. It may be that current valve operators are unknowingly generating such transients and accidentally aiding the system by 'cleaning pipes' in this manner. A future study could relate the frequency and magnitude of induced transients to the volume of material present in the bulk water, in order to observe whether transient mobilisation helps or hinders water quality.

# Chapter Eight
# Conclusions

## 8.1 Thesis Overview

This thesis has made a significant and novel contribution to the fields of transients and water quality by investigating transient mobilisation of pipe wall adhered material within a representative DWDS pipeline. The experiment presented within this work uniquely allowed transient forces to be isolated and their mobilisation ability quantified for a range of repeatable conditions. This dynamic ability has theoretical and practical implications, and could ultimately lead to the development of effective management strategies to control transients for improved drinking water quality.

## 8.2 Leading Conclusions

A key novelty and substantial finding of this research was the confirmation that complete valve closing transients caused mobilisation of adhered material, where steady state could not. This is a significant contribution as the steady state force reduces during the valve movement; therefore, mobilisation must be due to forces generated by the transient.

A second substantial finding was the demonstration of the ability of valve opening transients to cause mobilisation where the equivalent final steady state conditions could not. This was shown for the complete and partial opening transients tested, which transitioned between a variety of initial and final steady state flow rates. These outcomes support observations from previous literature and advance them by consistently and rigorously directly evidencing transient mobilisation throughout a range of conditions.

## 8.3 Further Conclusions

- A consistent and unique phenomenon of particle mobilisation was captured using the repeatable, rigorous and highly controllable methods developed here.
- The same general result was found for the ball bearing and powder material tested, whereby complete and partial valve opening transients caused mobilisation, where steady state did not. This commonality suggests that there is a general behaviour of transients that might not be dominated by the media being adhered and subsequently mobilised.

- Development and application of a function capturing the peak dynamic force of transient events that captures the significant mobilisation behaviour.
- Physical effects, such as complex velocity profiles, near wall boundary layers and initial turbulence, may contribute to mobilisation behaviour. These effects are not currently accounted for in the peak dynamic force function.
- The function is a good first approximation of the dynamic processes and forces induced during transients that cause mobilisation.

# Chapter Nine

# References


Ackers, J., Brandt, M.J., Powell, J., 2001. Hydraulic Characterisation of Deposits and Review of Sediment Modelling. UK Water Industry Research Limited.

Agolom, M.O., Lucas, G., Webilor, R.O., 2018. Measurement of Velocity Profiles in Transient Single and Multiphase Flows using Inductive Flow Tomography. Flow Meas. Instrum. 62, 246–254. https://doi.org/10.1016/j.flowmeasinst.2017.08.010

Aisopou, A., Stoianov, I., Graham, N.J.D., 2012. In-pipe Water Quality Monitoring in Water Supply Systems Under Steady and Unsteady State Flow Conditions: A Quantitative Assessment. Water Res. 46, 235–246. https://doi.org/10.1016/j.watres.2011.10.058

Aisopou, A., Stoianov, I., Graham, N.J.D., 2010. Modelling Discolouration in WDS Caused by Hydraulic Transient Events, in: Water Distribution Systems Analysis 2010. Tucson AZ, USA, pp. 522–534. https://doi.org/10.1061/41203(425)49

Allen, M., Clark, R.M., Cotruvo, J.A., Grigg, N.S., 2018. Drinking Water and Public Health in an Era of Aging Distribution Infrastructure. Public Work. Manag. Policy 23, 301–309. https://doi.org/10.1177/1087724X18788368

American Water Works Association, 2004. Steel Pipe: A Guide for Design and Installation, Manual M11, 4th Edition.

Ariyaratne, C., He, S., Vardy, A., 2010. Wall Friction and Turbulence Dynamics in Decelerating Pipe Flows. Hydraul. Res. 48, 810–821. https://doi.org/10.1080/00221686.2010.525372

Armand, H., Stoianov, I., Graham, N.J.D., 2015. A Holistic Assessment of Discolouration Processes in Water Distribution Networks. Urban Water J. 9006, 1–15. https://doi.org/10.1080/1573062X.2015.1111912

Atkin, E., 2017. How Can I Measure Turbidity? [WWW Document]. CamLab. URL http://camblab.info/wp/index.php/how-can-i-measure-turbidity/

Augustin, W., Bohnet, M., 1999. Influence of Pulsating Flow on Fouling Behaviour, in: Proceedings of the Engineering Foundation Conference on Mitigation of Heat Exchanger Fouling and Its Economic and Environmental Implications, Banff, Canada.

Bakke, R., 1986. Biofilm Detachment. Montana State University, U.S.A.

Bakke, R., Olsson, P.Q., 1986. Biofilm Thickness Measurements by Light Microscopy. Microbiol. Methods 5, 93–98. https://doi.org/10.1016/0167-7012(86)90005-9

Ballermann, B.J., Dardik, A., Eng, E., Liu, A., 1998. Shear Stress and the Endothelium. Kidney Int. 54, S100–S108. https://doi.org/10.1046/j.1523-1755.1998.06720.x

Bartram, J., Cairncross, S., 2010. Hygiene, Sanitation, and Water: Forgotten Foundations of Health. PLoS Med. 7, 1–9. https://doi.org/10.1371/journal.pmed.1000367

Batté, M., Appenzeller, B.M.R., Grandjean, D., Fass, S., Gauthier, V., Jorand, F., Mathieu, L.,

Boualam, M., Saby, S., Block, J.C., 2003. Biofilms in Drinking Water Distribution Systems. Rev. Environ. Sci. Bio/Technology 2, 147–168. https://doi.org/10.1023/B:RESB.0000040456.71537.29

Bergant, A., 2016. Principles of Water Hammer Interferometer. Energy Technol. 9, 11–20.

Bergant, A., Simpson, A.R., 2001. Developments in Unsteady Pipe Flow Friction Modelling. Hydraul. Eng. 39, 249–257. https://doi.org/10.1080/00221680109499828

Bergant, A., Simpson, A.R., Tijsseling, A.S., 2006. Water Hammer with Column Separation: A Historical Review. Fluids Struct. 22, 135–171. https://doi.org/10.1016/j.jfluidstructs.2005.08.008

Bergant, A., Vítkovský, J.P., Simpson, A.R., Lambert, M.F., 2002. Behaviour of Unsteady Pipe Flow Friction Models in the Case of Valve-Opening, in: 21st IAHR Symposium on Hydraulic Machinery and Systems, IAHR. Lausanne, Switzerland.

Besner, M.-C., Prevost, M., Lavoie, J., Payment, P., 2007. Distribution System Operation: Impact on Transient Pressures and Water Quality Variations, in: Computing and Control in the Water Industry. Leicester, UK, pp. 97–102.

Besner, M.-C., Prévost, M., Regli, S., Prevost, M., Regli, S., 2011. Assessing the Public Health Risk of Microbial Intrusion Events in Distribution Systems: Conceptual Model, Available Data, and Challenges. Water Res. 45, 961–979. https://doi.org/10.1016/j.watres.2010.10.035

Bhagyalakshmi, A., Berthiaume, F., Reich, K.M., Frangos, J.A., 1992. Fluid Shear Stress Stimulates Membrane Phospholipid Metabolism in Cultured Human Endothelial Cells. Vasc. Res. 29, 443–449.

Billings, N., Birjiniuk, A., Samad, T.S., Doyle, P.S., Ribbeck, K., 2016. Material Properties of Biofilms - Key Methods for Understanding Permeability and Mechanics. Reports Prog. Phys. 78, 036601. https://doi.org/10.1088/0034-4885/78/3/036601.Material

Blokker, E.J.M., Vreeburg, J.H.G., Schaap, P.G., van Dijk, J.C., 2010. The Self-Cleaning Velocity in Practice, in: Water Distribution Systems Analysis 2010. pp. 187–199. https://doi.org/10.1061/41203(425)19

Bode, K., Hooper, R.J., Paterson, W.R., Wilson, D.I., Augustin, W., Scholl, S., 2007. Pulsed Flow Cleaning of Whey Protein Fouling Layers. Heat Transf. Eng. 28, 202–209. https://doi.org/10.1080/01457630601064611

Bong, S.J., Karney, B.W., Boulos, P.F., Wood, D.J., 2007. The Need for Comprehensive Transient Analysis of Distribution Systems. Am. Water Work. Assoc. 99, 112–123.

Bosserman II, B.E., Hunt, W.A., Glover, R.C., Kroon, J.R., Merrill, M.S., Watters, G.Z., 2008. Chapter Six - Fundamentals of Hydraulic Transients, in: Pumping Station Design. Butterworth-Heinemann, p. 6.1-6.13. https://doi.org/doi.org/10.1016/B978-185617513-5.50013-5

Boulos, P.F., Karney, B.W., Wood, D.J., Lingireddy, S., 2005. Hydraulic Transient Guidelines for Protecting Water Distribution Systems. Am. Water Work. Assoc. 97, 111–124.

Boxall, J.B., Prince, R.A., 2006. Modelling Discolouration in a Melbourne (Australia) Potable Water Distribution System. Water Supply Res. Technol. 55, 207–219.

Boxall, J.B., Saul, A.J., 2005. Modeling Discoloration in Potable Water Distribution Systems. Environ.

Eng. 131, 716–725. https://doi.org/10.1061/(ASCE)0733-9372(2005)131:5(716)

Boxall, J.B., Skipworth, P.J., Saul, A.J., 2003. Aggressive Flushing For Discolouration Event Mitigation in Water Distribution Networks. Water Sci. Technol. Water Supply 3, 179–186.

Boxall, J.B., Skipworth, P.J., Saul, A.J., 2001. A Novel Approach to Modelling Sediment Movement in Distribution Mains Based on Particle Characteristics. Water Softw. Syst. 1, 263–273.

Boyd, G.R., Wang, H., Britton, M.D., Howie, D.C., Wood, D.J., Funk, J.E., Friedman, M.J., 2004. Intrusion within a Simulated Water Distribution System due to Hydraulic Transients. II: Volumetric Method and Comparison of Results. Environ. Eng. 130, 778–783. https://doi.org/10.1061/(ASCE)0733-9372(2004)130:7(778)

Branda, S.S., Vik, Å., Friedman, L., Kolter, R., 2005. Biofilms: The Matrix Revisited. Trends Microbiol. 13, 20–26. https://doi.org/10.1016/j.tim.2004.11.006

Brashear, K., 1998. Distribution Water Quality Problems Created by Upgraded Water Treatment Plants, in: Proc. 1998 AWWA WQTC, San Diego.

British Standard Institution, 2006. BS 6700:1997 - Design, Installation, Testing and Maintenance of Services Supplying Water for Domestic use Within Buildings and their Curtilages, British Standard Institution.

Brunone, B., Berni, A., 2010. Wall Shear Stress in Transient Turbulent Pipe Flow by Local Velocity Measurement. Hydraul. Eng. 136, 716–726. https://doi.org/10.1061/(ASCE)HY.1943-7900.0000234

Brunone, B., Golia, U.M., Greco, M., 1995. Effects of Two-Dimensionality on Pipe Transients Modeling. Hydraul. Eng. 121, 906–912.

Brunone, B., Karney, B.W., Mecarelli, M., Ferrante, M., 2000. Velocity Profiles and Unsteady Pipe Friction in Transient Flow. Water Resour. Plan. Manag. 126, 236–244. https://doi.org/10.1061/(ASCE)0733-9496(2000)126:4(236)

Caupin, F., Herbert, E., 2006. Cavitation in Water: a Review. Comptes Rendus Phys. 7, 1000–1017. https://doi.org/10.1016/j.crhy.2006.10.015

Centers for Disease Control and Prevention, 1994. Assessment of Inadequately Filtered Public Drinking Water --Washington, DC, December 1993., MMWR. Morbidity and mortality weekly report.

Chambers, K., Creasey, J., Forbes, L., 2004. Safe Piped Water: Managing Microbial Water Quality in Piped Distribution Systems. World Heal. Organ. IWA Publ. London, UK.

Chaudhry, M.H., 2014. Applied Hydraulic Transients, Third. ed. Springer.

Choi, Y.C., Morgenroth, E., 2003. Monitoring Biofilm Detachment Under Dynamic Changes in Shear Stress Using Laser-Based Particle Size Analysis and Mass Fractionation. Water Sci. Technol. 47, 69–76.

Chyzheuskaya, A., Cormican, M., Srivinas, R., O'Donovan, D., Prendergast, M., O'Donoghue, C., Morris, D., 2017. Economic Assessment of Waterborne Outbreak of Cryptosporidiosis. Emerg. Infect. Dis. 23, 1650–1656. https://doi.org/10.3201/eid2310.152037

Clark, R.M., Geldreich, E.E., Fox, K.R., Rice, E.W., Johnson, C.H., Goodrich, J.A., Barnick, J.A., Abdesaken, F., 1996. Tracking a Salmonella Serovar Typhimurium Outbreak in Gideon, Missouri: Role of Contaminant Propagation Modelling. Aqua 45, 171–183.

Clark, R.M., Goodrich, J.A., Wymer, L.J., 1993. Effect of the Distribution System on Drinking-Water Quality.

Collier, S.A., Stockman, L.J., Hicks, L.A., Garrison, L.E., Zhou, F.J., Beach, J., 2015. Direct Healthcare Costs of Selected Diseases Primarily or Partially Transmitted by Water. Epidemiol. Infect. 140, 2003–2013. https://doi.org/10.1017/S0950268811002858.Direct

Collins, R.P., Boxall, J.B., Karney, B.W., Brunone, B., Meniconi, S., 2012. How Severe Can Transients Be After a Sudden Depressurization? Am. Water Work. Assoc. 104, 67–68. https://doi.org/10.5942/jawwa.2012.104.0055

Cook, D.M., Boxall, J.B., 2011. Discoloration Material Accumulation in Water Distribution Systems. Pipeline Syst. Eng. Pract. 2, 113–122. https://doi.org/10.1061/(ASCE)PS.1949-1204.0000083

Covas, D., Stoianov, I., Ramos, H., Graham, N.J.D., Maksimovic, C., 2005. The Dynamic Effect of Pipe-Wall Viscoelasticity in Hydraulic Transients. Part II — Model Development, Calibration and Verification. Hydraul. Res. 43, 56–70. https://doi.org/10.1080/00221686.2004.9641221

Covas, D., Stoianov, I., Ramos, H., Graham, N.J.D., Maksimovic, C., 2004. The Dynamic Effect of Pipe-Wall Viscoelasticity in Hydraulic Transients. Part I — Experimental Analysis and Creep Characterization. Hydraul. Res. 42, 517–532. https://doi.org/10.1080/00221686.2004.9641221

Cowle, M.W., Babatunde, A.O., Rauen, W.B., Bockelmann-Evans, B.N., Barton, A.F., 2014. Biofilm Development in Water Distribution and Drainage Systems: Dynamics and Implications for Hydraulic Efficiency. Environ. Technol. Rev. 3, 31–47. https://doi.org/10.1080/09593330.2014.923517

Craun, G.F., Calderon, R.L., 2001. Waterborne Disease Outbreaks Caused by Distribution System Deficiencies. Am. Water Work. Assoc. 64–75.

Creasey, J., Garrow, D., 2011. Investigation of Instances of Low or Negative Pressures in UK Drinking Water Systems - Final Report, DEFRA8356.

Crouch, D.P., 1993. Water Management in Ancient Greek Cities. Oxford University Press.

Daily, J.M., Hankey Jr, W.L., Olive, R.W., Jordaan Jr, J.M., 1945. Resistance Coefficients for Accelerated and Decelerated Flows Through Smooth Tubes and Orifices. Science 102, 144–5. https://doi.org/10.1126/science.102.2641.144

Davidson, P.A., Belova, E.V., 2002. An Introduction to Magnetohydrodynamics. Am. J. Phys. 70, 781–781. https://doi.org/10.1119/1.1482065

Davies-Colley, R.J., Smith, D.G., 2001. Turbidity Suspended Sediment, and Water Clarity: a Review. Am. Water Resour. Assoc. 37, 1085–1101. https://doi.org/10.1111/j.1752-1688.2001.tb03624.x

De Beer, D., Stoodley, P., Roe, F., Lewandowski, Z., 1994. Effects of Biofilm Structures on Oxygen Distribution and Mass Transport. Biotechnol. Bioeng. 43, 1131–1138. https://doi.org/10.1002/bit.260431118

Douterelo, I., Husband, S., Loza, V., Boxall, J.B., 2016. Dynamics of Biofilm Regrowth in Drinking Water Distribution Systems. Appl. Environ. Microbiol. 82, 4155–4168. https://doi.org/10.1128/AEM.00109-16

Drinking Water Inspectorate, 2017a. Prosecutions Brought by the Drinking Water Inspectorate.

Drinking Water Inspectorate, 2017b. Guidance to Water Companies.

Drinking Water Inspectorate, 2015a. Significant, Serious and Major Drinking Water Quality Events, Drinking Water Inspectorate Annual Report.

Drinking Water Inspectorate, 2015b. Drinking Water Quality in England: The Position After 25 Years of Regulation. London.

Drinking Water Inspectorate, 2010. What are the Drinking Water Standards?, DWI Advice Leaflets.

Duan, H.F., 2017. Transient Wave Scattering and Its Influence on Transient Analysis and Leak Detection in Urban Water Supply Systems: Theoretical Analysis and Numerical Validation. Water (Switzerland) 9. https://doi.org/10.3390/w9100789

Duan, H.F., Lee, P.J., Che, T.C., Ghidaoui, M.S., Karney, B.W., Kolyshkin, A.A., 2017. The Influence of Non-Uniform Blockages on Transient Wave Behavior and Blockage Detection in Pressurized Water Pipelines. Hydro-Environment Res. 17, 1–7. https://doi.org/10.1016/j.jher.2017.08.002

Duan, H.F., Lee, P.J., Tuck, J., 2014. Experimental Investigation of Wave Scattering Effect of Pipe Blockages on Transient Analysis, in: Procedia Engineering. Elsevier B.V., Bari, Italy, pp. 1314–1320. https://doi.org/10.1016/j.proeng.2014.11.445

Durst, F., Kikura, H., Lekakis, I., Jovanovi, J., Ye, Q., 1996. Wall Shear Stress Determination from Near-Wall Mean Velocity Data in Turbulent Pipe and Channel Flows. Exp. Fluids 20, 417–428.

El-Farhan, Y.H., Denovio, N.M., Herman, J.S., Hornberger, G.M., 2000. Mobilization and Transport of Soil Particles during Infiltration Experiments in an Agricultural Field, Shenandoah Valley, Virginia. Environ. Sci. Technol. 34, 3555–3559. https://doi.org/10.1021/es991099g

Encyclopædia Britannica, 2018. Density of Seawater and Pressure [WWW Document]. Encycl. Br. inc. URL https://www.britannica.com/science/seawater/Density-of-seawater-and-pressure

Esrey, S.A., Potash, J.B., Roberts, L., Shiff, C., 1991. Effects of Improved Water Supply and Sanitation on Ascariasis, Diarrhoea, Dracunculiasis, Hookworm Infection, Schistosomiasis, and Trachoma. Bull. World Health Organ. 69, 609–21. https://doi.org/http://dx.doi.org/10.2147/IJWH.S77807

Ferriman, A., 2007. BMJ Readers Choose Sanitation as Greatest Medical Advance Since 1840. BMJ 334, 111. https://doi.org/10.1136/bmj.39098.461968.DB

Fish, K.E., Collins, R.P., Green, N.H., Sharpe, R.L., Douterelo, I., Osborn, A.M., Boxall, J.B., 2015. Characterisation of the Physical Composition and Microbial Community Structure of Biofilms within a Model Full-Scale Drinking Water Distribution System. PLoS One 10, 1–22. https://doi.org/10.1371/journal.pone.0115824

Fish, K.E., Osborn, A.M., Boxall, J.B., 2017. Biofilm Structures (EPS and Bacterial Communities) in Drinking Water Distribution Systems are Conditioned by Hydraulics and Influence Discolouration. Sci. Total Environ. 593–594, 571–580. https://doi.org/10.1016/j.scitotenv.2017.03.176

Fish, K.E., Osborn, A.M., Boxall, J.B., 2016. Characterising and Understanding the Impact of Microbial Biofilms and the Extracellular Polymeric Substance (EPS) Matrix in Drinking Water Distribution Systems. Environ. Sci. Water Res. Technol. 2, 614–630. https://doi.org/10.1039/C6EW00039H

Flemming, H.C., Percival, S.L., Walker, J.T., 2002. Contamination Potential of Biofilms in Water Distribution Systems. Water Sci. Technol. Water Supply 2, 271–280.

Flemming, H.C., Wingender, J., 2010. The Biofilm Matrix. Nat. Rev. Microbiol. 8, 623–633. https://doi.org/10.1080/0892701031000072190

Föste, H., Schöler, M., Majschak, J.P., Augustin, W., Scholl, S., 2011. Optimization of the Cleaning Efficiency by Pulsed Flow using an Experimentally Validated CFD Model, in: International Congress of Engineering in Food. Athens, Greece.

Fox, K.R., Lytle, D.A., 1996. Milwaukee's Crypto Outbreak: Investigations and Eecommendations. Am. Water Work. Assoc. 88, 87–94.

Fox, S., Shepherd, W., Collins, R.P., Boxall, J.B., 2014. Experimental Proof of Contaminant Ingress into a Leaking Pipe during a Transient Event, in: Procedia Engineering. Elsevier B.V., Perugia, Italy, pp. 668–677. https://doi.org/10.1016/j.proeng.2014.02.073

Friedman, M.J., Holt, D., 2003. Establishing Site-Specific Flushing Velocities. AWWA Research Foundation Denver.

Gaines, M., 2017. Southern Water Hit with £480K Fine. Water Wastewater Treat. Online.

Gally, M., Güney, M., Rieutord, E., 1979. An Investigation of Pressure Transients in Viscoelastic Pipes. Fluids Eng. 101, 495–499. https://doi.org/10.1115/1.3449017

Gauthier, V., Barbeau, B., Millette, R., Block, J.C., Prevost, M., 2001. Suspended Particles in the Drinking Water of Two Distribution Systems. Water Sci Technol Water Supply 1, 237–245.

Gauthier, V., Gérard, B., Portal, J.M., Block, J.C., Gatel, D., 1999. Organic Matter as Loose Deposits in a Drinking Water Distribution System. Water Res. 33, 1014–1026. https://doi.org/10.1016/S0043-1354(98)00300-5

Geiger, R.V., Berk, B.C., Alexander, R.W., Nerem, R.M., 1992. Flow-Induced Calcium Transients in Single Endothelial Cells: Spatial and Temporal Analysis. Physiology 262, C1411-7.

Ghidaoui, M.S., Zhao, M., McInnis, D.A., Axworthy, D.H., 2005. A Review of Water Hammer Theory and Practice. Appl. Mech. Rev. 58, 49. https://doi.org/10.1115/1.1828050

Gill, M., Dias, S., Hattori, K., Rivera, M.L., Hicklin, D., Witte, L., Girardi, L., Yurt, R., Himel, H., Rafii, S., 2001. Vascular Trauma Induces Rapid but Transient Mobilization of VEGFR2+AC133+ Endothelial Vascular Trauma Induces Rapid but Transient Mobilization of VEGFR2 Endothelial Precursor Cells. Circ. Res. 88, 167–174. https://doi.org/10.1161/01.RES.88.2.167

Gillham, C.R., Fryer, P.J., Hasting, A.P.M., Wilson, D.I., 2000. Enhanced Cleaning of Whey Protein Soils Using Pulsed Flows. Food Eng. 46, 199–209. https://doi.org/10.1016/S0260-8774(00)00083-2

Grann-Meyer, E., 2005. Polyethylene Pipes in Applied Engineering, Total Petrochemicals.

Grayman, W.M., Clark, R.M., Males, R.M., 1988. Modeling Distribution-System Water Quality:

Dynamic Approach. Water Resour. Plan. Manag. 114, 295–312. https://doi.org/10.1061/(ASCE)0733-9496(1988)114:3(295)

Grigg, N.S., 2005. Assessment and Renewal of Water Distribution Systems. Am. Water Work. Assoc. 97, 58–68.

Gullick, R.W., LeChevallier, M.W., Svindland, R.C., Friedman, M.J., 2004. Occurrence of Transient Low and Negative Pressures in Distribution Systems. Am. Water Work. Assoc. 96, 52–66.

Halliwell, A.R., 1963. Velocity of a Water-Hammer Wave in an Elastic Pipe. Hydraul. Div. 89, 1–21.

Halonen, J.I., Kivimäki, M., Oksanen, T., Virtanen, P., Virtanen, M.J., Pentti, J., Vahtera, J., 2012. Waterborne Outbreak of Gastroenteritis: Effects on Sick Leaves and Cost of Lost Workdays. PLoS One 7, 1–5. https://doi.org/10.1371/journal.pone.0033307

Hanratty, T.J., Campbell, J.A., 1983. Measurement of Wall Shear Stress, in: Goldstein, J.R. (Ed.), Fluid Mechanics Measurements.

Harvard University, 2007. A Summary of Error Propagation.

He, S., Ariyaratne, C., Vardy, A., 2011. Wall Shear Stress in Accelerating Turbulent Pipe Flow. Fluid Mech. 685, 440–460. https://doi.org/10.1017/jfm.2011.328

Howe, A.D., Forster, S., Morton, S., Marshall, R., Osborn, K.S., Wright, P., Hunter, P.R., 2002. Cryptosporidium Oocysts in a Water Supply Associated with a Cryptosporidiosis Outbreak. Emerg. Infect. Dis. 8, 619–624.

Hrudey, S.E., Hrudey, E.J., 2007. Published Case Studies of Waterborne Disease Outbreaks—Evidence of a Recurrent Threat. Water Environ. Res. 79, 233–245. https://doi.org/10.2175/106143006X95483

Hrudey, S.E., Payment, P., Huck, P.M., Gillham, R.W., Hrudey, E.J., 2003. A Fatal Waterborne Disease Epidemic in Walkerton, Ontario: Comparison with other waterborne outbreaks in the developed world. Water Sci. Technol. 47, 7–14.

Hunter, P.R., Chalmers, R.M., Hughes, S., Syed, Q., 2005. Self-Reported Diarrhea in a Control Group: a Strong Association with Reporting of Low-Pressure Events in Tap Water. Clin. Infect. Dis. 40, 32–34. https://doi.org/10.1086/427750

Husband, S., Boxall, J.B., 2016. Understanding and Managing Discolouration Risk in Trunk Mains. Water Res. 107, 127–140. https://doi.org/10.1016/j.watres.2016.10.049

Husband, S., Boxall, J.B., 2010. Field Studies of Discoloration in Water Distribution Systems: Model Verification and Practical Implications. Environ. Eng. 136, 86–94. https://doi.org/10.1061/(ASCE)EE.1943-7870.0000115

Husband, S., Boxall, J.B., Saul, A.J., 2008. Laboratory Studies Investigating the Processes Leading to Discolouration in Water Distribution Networks. Water Res. 42, 4309–4318. https://doi.org/10.1016/j.watres.2008.07.026

Husband, S., Fish, K.E., Douterelo, I., Boxall, J.B., 2016. Linking Discolouration Modelling and Biofilm Behaviour Within Drinking Water Distribution Systems. Water Sci. Technol. Water Supply 16, 942–950. https://doi.org/10.2166/ws.2016.045

International Organisation for Standardization, 2006. ISO 19458:2006 Water Quality - Sampling for Microbiological Analysis.

Janson, L.E., 1995. Plastics Pipes for Water Supply and Sewage Disposal. Borealis.

Jones, S.L., Shepherd, W., Collins, R.P., Boxall, J.B., 2019. Experimental Quantification of Intrusion Volumes due to Transients in Drinking Water Distribution Systems. Pipeline Syst. Eng. Pract. 10. https://doi.org/10.1061/(ASCE)PS.1949-1204.0000348

Joukowsky, N., 1904. Waterhammer. Proc. Am. Water Work. Assoc. 24, 341–424.

Karney, B.W., Brunone, B., 1999. Water Hammer in Pipe Network: Two Case Studies, in: Water Industry Systems: Modelling and Optimization Applications. pp. 363–376.

Karney, B.W., McInnis, D.A., 1992. Efficient Calculation of Transient Flow in Simple Pipe Networks. Hydraul. Eng. 118, 1014–1030. https://doi.org/10.1061/(Asce)0733-9429(1992)118:7(1014)

Karney, B.W., Ruus, E., 1985. Charts for Water Hammer in Pipelines Resulting from Valve Closure from Full Opening Only. Can. J. Civ. Eng. 12, 241–264. https://doi.org/10.1103/PhysRevA.71.020303

Kent, G.P., Greenspan, J.R., Herndon, J.L., Mofenson, L.M., Harris, J.A.S., Eng, T.R., Waskin, H.A., 1988. Epidemic Giardiasis Caused by a Contaminated Public Water Supply. Am. J. Public Health 78, 139–143. https://doi.org/10.2105/ajph.78.2.139

Körstgens, V., Flemming, H.C., Wingender, J., Borchard, W., 2001. Uniaxial Compression Measurement Device for Investigation of the Mechanical Stability of Biofilms. Microbiol. Methods 46, 9–17. https://doi.org/10.1016/S0167-7012(01)00248-2

Kucienska, B., 2004. Friction Relaxation Model for Fast Transient Flows. University of Catholique de Louvain, Belgium.

Lau, H.Y., Ashbolt, N.J., 2009. The Role of Biofilms and Protozoa in Legionella Pathogenesis: Implications for Drinking Water. Appl. Microbiol. 107, 368–378. https://doi.org/10.1111/j.1365-2672.2009.04208.x

Laursen, E., Mygind, O., Rasmussen, B., Ronne, T., 1994. Gastroenteritis: a Waterborne Outbreak Affecting 1600 People in a Small Danish Town. Epidemiol Community Heal. 48, 453–458. https://doi.org/10.1136/jech.48.5.453

LeChevallier, M.W., Gullick, R.W., Karim, M.R., Friedman, M.J., Funk, J.E., 2003. The Potential for Health Risks from Intrusion of Contaminants into th Distribution System from Pressure Transients. Water Heal. 01, 3–14.

Lee, T.S., 1998. Fluid Pressure Transients with Air Entrainment, in: Australasian Fluid Mechanics Conference. Melbourne, Australia.

Lee, T.S., Pejovic, S., 1996. Air Influence on Similarity of Hydraulic Transients and Vibrations. Fluids Eng. Asme. https://doi.org/10.1115/1.2835499

Levy, D.A., Bens, M.S., Craun, G.F., Calderon, R.L., Herwaldt, B.L., 1998. Surveillance for Waterborne-Disease Outbreaks — United States , 1995 – 1996, MMWR. Morbidity and mortality weekly report.

Lindley, T.R., Buchberger, S.G., 2002. Assessing Intrusion Susceptibility in Distribution Systems. Am. Water Work. Assoc. 94, 66–69.

Mac Kenzie, W.R., Hoxie, N.J., Proctor, M.E., Gradus, M.S., Blair, K.A., Peterson, D.E., Kazmierczak, J.J., Addiss, D.G., Fox, K.R., Rose, J.B., Davis, J.P., 1994. A Massive Outbreak in Milwaukee of Cryptosporidium Infection Transmitted Through the Public Water Supply. N. Engl. J. Med. 331, 161–167.

Mac Kenzie, W.R., Schell, W.L., Blair, K.A., Addiss, D.G., Peterson, D.E., Hoxie, N.J., Kazmierczak, J.J., Davis, J.P., 1995. Massive Outbreak of Waterborne Cryptosporidium Infection in Milwaukee, Wisconsin: Recurrence of Illness and Risk of Secondary Transmission. Clin. Infect. Dis. 21, 57–62. https://doi.org/10.1093/clinids/21.1.57

Malvern Instruments Limited, 2013. Mastersizer 3000. https://doi.org/10.1007/SpringerReference_28001

Mann, A.G., Tam, C.C., Higgins, C.D., Rodrigues, L.C., 2007. The Association between Drinking Water Turbidity and Gastrointestinal Illness: a Systematic Review. BMC Public Health 7, 256–262. https://doi.org/10.1186/1471-2458-7-256

Margevicius, A., 2012. Discussion of "Probability of Failure Analysis due to Internal Corrosion in Cast-Iron Pipes" by Hamid Yamini and Barbara J. Lence. Infrastruct. Syst. 18, 226–227. https://doi.org/10.1061/(ASCE)1076-0342(2010)16

Maruyama, T., Kuribayashi, T., Mizushina, T., 1976. The Structure of Turbulence in Transient Pipe Flows. Chem. Eng. Japan 9, 431–439. https://doi.org/10.1007/BF02970963

Mathieu, L., Bertrand, I., Abe, Y., Angel, E., Block, J.C., Skali-Lami, S., Francius, G., 2014. Drinking Water Biofilm Cohesiveness Changes Under Chlorination or Hydrodynamic Stress. Water Res. 55, 175–184. https://doi.org/10.1016/j.watres.2014.01.054

Mathur, A., 2016. Study of Accelerating and Decelerating Turbulent Flows in a Channel. University of Sheffield, UK.

MathWorks, 2016. MATLAB Software.

Mays, L.W., 2000. Water Distribution Systems Handbook. McGraw-Hill, New York.

Mega Speed, 2017. Camera Control Software.

Mehta, A.J., Lee, S.-C., 1994. Problems in Linking the Threshold Condition for the Transport of Cohesionless and Cohesive Sediment Grain. Coast. Res. 10, 170–177.

Menaia, J., Mesquita, E., 2004. Drinking Water Pipe Biofilm: Present Knowledge, Concepts and Significance. Water Sci. Technol. Water Supply 4, 115–124.

Minsier, V., Proost, J., 2008. Shock Wave Emission Upon Spherical Bubble Collapse During Cavitation-Induced Megasonic Surface Cleaning. Ultrason. Sonochem. 15, 598–604. https://doi.org/10.1016/j.ultsonch.2007.06.004

Misiunas, D., Vítkovský, J.P., Olsson, G., Simpson, A.R., Lambert, M.F., 2005. Pipeline Break Detection Using Pressure Transient Monitoring. Water Resour. Plan. Manag. 131, 316–325. https://doi.org/10.1061/(ASCE)0733-9496(2005)131:4(316)

Morgenroth, E., Wilderer, P.A., 2000. Influence of Detachment Mechanisms on Competition in Biofilms. Water Res. 34, 417–426.

Morris, R.D., Naumova, E.N., Levin, R., Munasinghe, R.L., 1996. Temporal Variation in Drinking Water Turbidity and Diagnosed Gastroenteritis in Milwaukee. Am. J. Public Health 86, 237–239. https://doi.org/10.2105/AJPH.86.2.237

Mustonen, S.M., Tissari, S., Huikko, L., Kolehmainen, M., Lehtola, M.J., Hirvonen, A., 2008. Evaluating Online Data of Water Quality Changes in a Pilot Drinking Water Distribution System with Multivariate Data Exploration Methods. Water Res. 42, 2421–2430. https://doi.org/10.1016/j.watres.2008.01.015

Naser, G., Karney, B.W., 2008. A Transient 2-D Water Quality Model for Pipeline Systems. Hydraul. Res. 46, 516–525. https://doi.org/10.3826/jhr.2008.3015

Naser, G., Karney, B.W., Boxall, J.B., 2008. Red Water and Discoloration in a WDS: A Numerical Simulation, in: Water Distribution Systems Analysis Symposium 2006. American Society of Civil Engineers, Reston, VA, pp. 1–16. https://doi.org/10.1061/40941(247)152

National Instruments Corporation, 2015. LabVIEW.

National Research Council, 2006. Drinking Water Distribution Systems: Assessing and Reducing Risks. National Academies Press.

Nerella, R., Venkata Rathnam, E., 2015. Fluid Transients and Wave Propagation in Pressurized Conduits Due to Valve Closure, in: Procedia Engineering. Elsevier B.V., pp. 1158–1164. https://doi.org/10.1016/j.proeng.2015.11.454

Nowak, M., 2002. Wall Shear Stress Measurement in a Turbulent Pipe Flow using Ultrasound Doppler Velocimetry. Exp. Fluids 33, 249–255. https://doi.org/10.1007/s00348-002-0407-x

Ohashi, A., Harada, H., 1994. Characterization of Detachment Mode of Biofilm Developed in an Attached-Growth Reactor, in: Water Science and Technology.

Padfield, G.J., Tura-Ceide, O., Freyer, E., Barclay, G.R., Turner, M., Newby, D.E., Mills, N.L., 2014. Percutaneous Coronary Intervention Causes a Rapid but Transient Mobilisation of CD34(+)CD45(-) Cells. Open Hear. 1, 1–10. https://doi.org/10.1136/openhrt-2014-000047

Patnaik, P., 2003. Handbook of Inorganic Chemicals. McGraw-Hill.

Paul, E., Ochoa, J.C., Pechaud, Y., Liu, Y., Liné, A., 2012. Effect of Shear Stress and Growth Conditions on Detachment and Physical Properties of Biofilms. Water Res. 46, 5499–5508. https://doi.org/10.1016/j.watres.2012.07.029

Payment, P., Richardson, L., Siemiatycki, J., Edwardes, M., Franco, E., 1991. A Randomized Trial to Evaluate the Risk of Gastrointestinal Disease due to Consumption of Drinking Water Meeting Current Microbiological Standards. Am. J. Public Health 81, 703–708.

Payment, P., Siemiatycki, J., Richardson, L., Renaud, G., Franco, E., Prevost, M., 1997. A Prospective Epidemiological Study of Gastrointestinal Health Effects due to the Consumption of Drinking Water. Environ. Heal. Res. 7, 5–31. https://doi.org/10.1080/09603129773977

Pearsall, I.S., 1965. The Velocity of Water Hammer Waves. Proc. Inst. Mech. Eng.

https://doi.org/10.1243/PIME_CONF_1965_180_160_02

Peyton, B.M., 1996. Effects of Shear Stess and Substrate Loading Rate on Pseudomonas Aeruginosa Biofilm Thickness and Density. Water Resour. 30, 29–36.

Peyton, B.M., Characklis, W.G., 1992. A Statistical Analysis of the Effect of Substrate Utilization and Shear Stress on the Kinetics of Biofilm Detachment. Biotechnol. Bioeng. 41, 728–735. https://doi.org/10.1002/bit.260410707

Picioreanu, C., van Loosdrecht, M.C.M., Heijnen, J.J., 2001. Two-Dimensional Model of Biofilm Detachment Caused by Internal Stress from Liquid Flow. Biotechnol. Bioeng. 72, 205–18.

Polychronopolous, M., Dudley, K., Ryan, G., Hearn, J., 2003. Investigation of Factors Contributing to Dirty Water Events in Reticulation Systems and Evaluation of Flushing Methods to Remove Deposited Particles. Water Sci. Technol. Water Supply 3, 295–306.

Pope, S.B., 2000. Turbulent Flows. Cambridge University Press. https://doi.org/10.1088/0957-0233/12/11/705

Pothof, I.W.M., Blokker, E.J.M., 2012. Dynamic Hydraulic Models to Study Sedimentation in Drinking Water Networks in Detail. Drink. Water Eng. Sci. 5, 87–92. https://doi.org/10.5194/dwes-5-87-2012

Pothof, I.W.M., Karney, B.W., 2012. Guidelines for Transient Analysis in Water Transmission and Distribution Systems. Water Supply Syst. Anal. - Sel. Top. 1–22. https://doi.org/10.5772/53944

Prest, E.I., Hammes, F., van Loosdrecht, M.C.M., Vrouwenvelder, J.S., 2016. Biological Stability of Drinking water: Controlling Factors, Methods, and Challenges. Front. Microbiol. 7, 1–24. https://doi.org/10.3389/fmicb.2016.00045

Prince, R.A., Goulter, I., Ryan, G., 2003. What Causes Customer Complaints about Discoloured Drinking Water? Water (Australia) 30, 62–67.

Rathsack, U., 1997. Massenentwicklung von eisenorganismen in wasserversorgungssystemen. Neue DELIWA Zeitschrift 5, 195–198.

Rezaei, H., Ryan, B., Stoianov, I., 2015. Pipe Failure Analysis and Impact of Dynamic Hydraulic Conditions in Water Supply Networks, in: Procedia Engineering. Elsevier B.V., pp. 253–262. https://doi.org/10.1016/j.proeng.2015.08.883

Riasi, A., Nourbakhsh, A., Raisee, M., 2009. Unsteady Velocity Profiles in Laminar and Turbulent Water Hammer Flows. Fluids Eng. 131, 121202. https://doi.org/10.1115/1.4000557

Roberts, J.A., Cumberland, P., Sockett, P.N., Wheeler, J., Rodrigues, L.C., Sethi, D., Roderick, P.J., 2003. The Study of Infectious Intestinal Disease in England: Socio-Economic Impact. Epidemiol. Infect. 130, 1–11. https://doi.org/10.1017/S0950268802007690

Saiers, J.E., Lenhart, J.J., 2003. Colloid Mobilization and Transport Within Unsaturated Porous Media Under Transient-Flow Conditions. Water Resour. Res. 39. https://doi.org/10.1029/2002WR001370

Sandvik, 2013. Sandvik SAF 2507.

Sanks, R.L., 2005. Water Transport section, in: Takahasi, Y. (Ed.), Water Storage, Transport, and

Distribution. Encyclopedia of Life Support Systems (www. eolss. net). Developed under the auspices of the UNESCO, EOLSS Publishers, Oxford, UK.

Schuster, C.J., Aramini, J., Ellis, A.G., Marshall, B.J., Robertson, W.J., Medeiros, D.T., Charron, D.F., 2005. Infectious Disease Outbreaks Related to Drinking Water in Canada, 1974-2001. Can. J. Public Heal. 96, 254–258.

Schwartz, J., Levin, R., Hodge, K., 1997. Drinking Water Turbidity and Pediatric Hospital Use for Gastrointestinal Illness in Philadelphia. Epidemiology 8, 615–20. https://doi.org/10.1097/00001648-199711000-00005

Seth, A., Bachmann, R.T., Boxall, J.B., Saul, A.J., Edyvean, R.G.J., 2004. Characterisation of Materials Causing Discolouration in Potable Water Systems. Water Sci. Technol. 49, 27–32.

Shang, J., Flury, M., Chen, G., Zhuang, J., 2008. Impact of Flow Rate, Water Content, and Capillary Forces on In Situ Colloid Mobilization During Infiltration in Unsaturated Sediments. Water Resour. Res. 44, 1–12. https://doi.org/10.1029/2007WR006516

Shen, Y., Monroy, G.L., Derlon, N., Janjaroen, D., Huang, C., Morgenroth, E., Boppart, S.A., Ashbolt, N.J., Liu, W.T., Nguyen, T.H., 2015. Role of Biofilm Roughness and Hydrodynamic Conditions in Legionella Pneumophila Adhesion to and Detachment from Simulated Drinking Water Biofilms. Environ. Sci. Technol. 49, 4274–4282. https://doi.org/10.1021/es505842v

Silva-Araya, W.F., Chaudhry, M.H., 1997. Computation of Energy Dissipation in Transient Flow. Hydraul. Eng. 123, 108–115.

Simply Bearings, 2015. AISI 52100 Chrome Steel Data Sheet 1.

Sinclair, M.I., Fairley, C.K., 2000. Drinking Water and Endemic Gastrointestinal Illness. Epidemiol. Community Health 54, 729–730. https://doi.org/10.1136/jech.54.10.729 [doi]

Slaats, L.P.M., Rosenthal, L.P.M., Siegers, W.G., van den Boomen, M., Beuken, R.H.S., Vreeburg, J.H.G., 2003. Processes Involved in the Generation of Discolored Water. AWWA Research Foundation and Kiwa Water Research.

Sly, L.I., Hodgkinson, M.C., Arunpairojana, V., 1990. Deposition of Manganese in a Drinking Water Distribution System. Appl. Environ. Microbiol. 56, 628–639.

Snow, J., 1857. Cholera, and the Water Supply in the South Districts of London. Br. Med. J. October, 864–865. https://doi.org/10.1136/bmj.s4-1.42.864

Soulsby, R., 1997. Dynamics of Marine Sands: A Manual for Practical Applications. Thomas Telford, London.

Starczewska, D., Collins, R.P., Boxall, J.B., 2015. Occurrence of Transients in Water Distribution Networks, in: Procedia Engineering. Elsevier B.V., pp. 1473–1482. https://doi.org/10.1016/j.proeng.2016.01.001

Stewart, P.S., 1993. A Model of Biofilm Detachment. Biotechnol. Bioeng. 41, 111–117. https://doi.org/10.1002/bit.260410115

Stirling, R., Aramini, J., Ellis, A.G., Lim, G., Meyers, R., Fleury, M., Werker, D., 2001. Waterborne Cryptosporidiosis Outbreak, North Battleford, Saskatchewan, April 2001, Public Health.

Stoodley, P., Boyle, J.D., Lappin-Scott, H.M., 1999a. Influence of Flow on the Structure of Bacterial Biofilms, in: Microbial Biosystems: New Frontiers, Proceedings of the 8th International Symposium on Microbial Ecology. Halifax, Canada.

Stoodley, P., Dodds, I., Boyle, J.D., Lappin-Scott, H.M., 1998. Influence of Hydrodynamics and Nutrients on Biofilm Structure. Appl. Microbiol. 85, 19S–28S. https://doi.org/10.1111/j.1365-2672.1998.tb05279.x

Stoodley, P., Hall-Stoodley, L., Lappin-Scott, H.M., 2001. Detachment, Surface Migration, and Other Dynamic Behavior in Bacterial Biofilms Revealed By Digital Time-lapse Imaging. Methods Enzymol. 337, 306–319. https://doi.org/10.1016/S0076-6879(01)37023-4

Stoodley, P., Lewandowski, Z., Boyle, J.D., Lappin-Scott, H.M., 1999b. Structural Deformation of Bacterial Biofilms Caused by Short-Term Fluctuations in Fluid Shear: an In Situ Investigation of Biofilm Rheology. Biotechnol. Bioeng. 65, 83–92. https://doi.org/10.1002/(SICI)1097-0290(19991005)65:1<83::AID-BIT10>3.0.CO;2-B

Sundstrom, L.R.., Cervantes, M.J., 2017. Transient Wall Shear Stress Measurements and Estimates at High Reynolds Numbers. Flow Meas. Instrum. 58, 112–119. https://doi.org/10.1016/j.flowmeasinst.2017.10.003

Suo, L., Wylie, E.B., 1990. Complex Wavespeed and Hydraulic Transients in Viscoelastic Pipes. Fluids Eng. 112, 496. https://doi.org/10.1115/1.2909434

Szewzyk, U., Szewzyk, R., Manz, W., Schleifer, K.-H., 2000. Microbiological Safety of Drinking Water. Annu. Rev. Microbiol. 54, 81–127.

Telgmann, U., Horn, H., Morgenroth, E., 2004. Influence of Growth History on Sloughing and Erosion from Biofilms. Water Res. 38, 3671–84. https://doi.org/10.1016/j.watres.2004.05.020

Temple Water, 2015. What About The Manganese? [WWW Document]. URL https://templewater.co.nz/what-about-the-manganese/

Terzis, A., Zachos, P.K., Charnley, B., Kalfas, A.I., 2011. On the Applicability of Oil and Dye Flow Visualization Technique During the Design Phase and Operation of Experimental Rigs. Flow Vis. Image Process. https://doi.org/10.1615/JFlowVisImageProc.2011002885

Thienen, P. Van, Vreeburg, J.H.G., Blokker, E.J.M., 2010. Radial Transport Processes as a Precursor to Particle Deposition in Drinking Water Distribution Systems. Water Res. 45, 1807–1817. https://doi.org/10.1016/j.watres.2010.11.034

Tijsseling, A.S., Lambert, M.F., Simpson, A.R., Stephens, M.L., Vitkovsky, J., Bergant, A., 2006. Wave Front Dispersion due to Fluid-Structure Interaction in Long Liquid-Filled Pipelines.

Tijsseling, A.S., Lambert, M.F., Simpson, A.R., Stephens, M.L., Vítkovský, J.P., Bergant, A., 2008. Skalak's Extended Theory of Water Hammer. Sound Vib. 310, 718–728. https://doi.org/10.1016/j.jsv.2007.10.037

Tinker, S.C., Moe, C.L., Klein, M., Flanders, W.D., Uber, J.G., Amirtharajah, A., Singer, P., Tolbert, P.E., 2009. Drinking Water Residence Time in Distribution Networks and Emergency Department Visits for Gastrointestinal Illness in Metro Atlanta, Georgia. Water Heal. 7, 332–343.

https://doi.org/10.2166/wh.2009.022

Twort, A.C., Ratnayaka, D.D., Brandt, M.J., Johnson, K.M., 2000. Water Supply. Butterworth-Heinemann.

Twyman, J., 2016. Wave Speed Calculation for Water Hammer Analysis. Obras y Proy. 20, 86–92.

UKWIR, 2003. National Database of Mains Failures (No. 23/3G/05/7).

Uni-Bell PVC Pipe Association, 2001. Handbook of PVC Pipe, Second. ed, Design and Construction. Dallas, Texas, USA.

Vallance, P., Channon, K., 2010. Blood Vessels and the Endothelium, in: Warrell, D.A., Cox, T.M., Firth, J.D. (Eds.), Oxford Textbook of Medicine. Oxford University Press, pp. 1–31. https://doi.org/10.1093/med/9780199204854.001.1

van den Boomen, M., Vreeburg, J.H.G., 1999. Nieuwe Ontwerprichtlijnen Voor Distributienetten (New Design Rules for Distribution Networks). Nieuwegein, Netherlands, Netherlands.

Vardy, A., Brown, J., 2004. Transient Turbulent Friction in Fully Rough Pipe Flows. Sound Vib. 270, 233–257. https://doi.org/10.1016/S0022-460X(03)00492-9

Vardy, A., Brown, J., 2003. Transient Turbulent Friction in Smooth Pipe Flows. Sound Vib. 259, 1011–1036. https://doi.org/10.1006/jsvi.2002.5160

Vardy, A., Brown, J., 1995. Transient, Turbulent, Smooth Pipe Friction. Hydraul. Res. 33, 435–456. https://doi.org/10.1080/00221689509498654

Vreeburg, J.H.G., 2007. Discolouration in Drinking Water Systems: A Particular Approach. Technische Universiteit Delft.

Vreeburg, J.H.G., Blokker, E.J.M., Horst, P., van Dijk, J.C., 2009. Velocity-Based Self-Cleaning Residential Drinking Water Distribution Systems. Water Sci. Technol. Water Supply 9, 635–641. https://doi.org/10.2166/ws.2009.689

Vreeburg, J.H.G., Boxall, J.B., 2007. Discolouration in Potable Water Distribution Systems: A Review. Water Res. 41, 519–29. https://doi.org/10.1016/j.watres.2006.09.028

Vreeburg, J.H.G., Schaap, P.G., van Dijk, J.C., 2004. Particles in the Drinking Water System: From Source to Discolouration. Water Sci. Technol. Water Supply 4, 431–438.

Wagner, I., 1994. International Report: Internal Corrosion of Pipes in Public Water Distribution Networks, Water Supply.

Walski, T.M., 2006. A History of Water Distribution. Am. Water Work. Assoc. 96, 110–121.

Walski, T.M., 1991. Understanding Solids Transport in Water Distribution Systems. Water Qual. Model. Distrib. Syst. USA 305–309.

Walski, T.M., Lutes, T.L., 1994. Hydraulic Transients cause Low-Pressure Problems. Am. Water Work. Assoc. 86, p24-32.

Walters, T.W., Leishear, R.A., 2018. When the Joukowsky Equation Does Not Predict Maximum Water Hammer Pressures, in: ASME Pressure Vessels and Piping Conference. Prague, Czech Republic, pp. 1–10.

Water Quality and Health Council, 2010. Waterborne Diseases Cost US $500 Million A Year [WWW

Document]. URL https://waterandhealth.org/safe-drinking-water/drinking-water/waterborne-diseases-cost-us-500-million-a-year/

Wazny, A., 2013. Repairs Could Temporarily Cause Discoloured Water, City Warns. Winnipeg Free Press.

Wingender, J., Flemming, H.C., 2011. Biofilms in Drinking Water and Their Role as Reservoir for Pathogens. Int. J. Hyg. Environ. Health 214, 417–23. https://doi.org/10.1016/j.ijheh.2011.05.009

Wood, D.J., Lingireddy, S., Boulos, P.F., Karney, B.W., McPherson, D.L., 2005. Numerical Methods for Modeling Transient Flow in Distribution Systems. Am. Water Work. Assoc. 97, 104–115.

Wylie, E.B., Streeter, V.L., 1978. Fluid Transients. McGraw-Hill International Book Co., New York.

Zarzycki, Z., Kudzma, S., Urbanowicz, K., 2011. Improved Method for Simulating Transients of Turbulent Pipe Flow. Theor. Appl. Mech. 49, 135–158.

Zhang, K.Q., Karney, B.W., McPherson, D.L., 2008. Pressure-Relief Valve Selection and Transient Pressure Control. Am. Water Work. Assoc. 100. https://doi.org/10.1002/j.1551-8833.2008.tb09700.x

Zhang, T.C., Bishop, P.L., 1994. Density, Porosity, and Pore Structure of Biofilms. Water Res. 28, 2267–2277. https://doi.org/10.1016/0043-1354(94)90042-6

Zhuang, J., McCarthy, J.F., Tyner, J.S., Perfect, E., Flury, M., 2007. In Situ Colloid Mobilization in Hanford Sediments under Unsaturated Transient Flow Conditions: Effect of Irrigation Pattern. Environ. Sci. Technol. 41, 3199–3204. https://doi.org/10.1021/es062757h

Zidouh, H., 2009. Velocity Profiles and Wall Shear Stress in Turbulent Transient Pipe Flow. Int. J. Dyn. Fluids 5, 61–83.

Zidouh, H., Elmaimouni, L., 2013. Wall Shear Stress in Transient Turbulent Pipe Flow, in: Renewable and Sustainable Energy Conference (IRSEC), 2013 International.

Zielke, W., 1968. Frequency-Dependent Friction in Transient Pipe Flow. Fluids Eng. 109–115.

# Appendix

# Summary of Experiments Performed

Testing conditions are given for the steady state and transient experiments performed, for ball bearings and powder particles, respectively. Every test was performed multiple times to produce five repeats, of which the average and standard deviation of results is given.

**Table A1.** Steady State Experiments Performed Using Ball Bearings as Adhered Particles.

| Flow Rate (l/s) | Pressure (m) |
|---|---|
| 0.405 ± 0.004 | 45.763 ± 0.070 |
| 0.704 ± 0.005 | 45.227 ± 0.051 |
| 1.005 ± 0.005 | 44.569 ± 0.080 |
| 1.203 ± 0.005 | 44.023 ± 0.080 |
| 1.403 ± 0.005 | 43.525 ± 0.073 |

**Table A2.** Transient Experiments Performed Using Ball Bearings as Adhered Particles.

| Transient Type | 'Complete' or 'Partial' Tests and Set Number | Initial Flow Rate (l/s) | Initial Pressure (m) | Final Flow Rate (l/s) |
|---|---|---|---|---|
| Valve Closing | Complete | 0.117 ± 0.007 | 45.953 ± 0.075 | 0.000 |
| | | 0.409 ± 0.002 | 45.740 ± 0.025 | 0.000 |
| | | 0.708 ± 0.011 | 45.224 ± 0.027 | 0.000 |
| | | 1.003 ± 0.006 | 44.518 ± 0.074 | 0.000 |
| | | 1.311 ± 0.005 | 43.718 ± 0.067 | 0.000 |
| Valve Opening | Complete Set One | 0.000 | 25.002 ± 0.167 | 0.367 ± 0.006 |
| | | 0.000 | 30.129 ± 0.391 | 0.399 ± 0.005 |
| | | 0.000 | 35.137 ± 0.201 | 0.432 ± 0.001 |
| | | 0.000 | 40.147 ± 0.009 | 0.466 ± 0.007 |
| | | 0.000 | 45.887 ± 0.023 | 0.497 ± 0.005 |
| | Complete Set Two | 0.000 | 45.910 ± 0.051 | 0.206 ± 0.010 |
| | | 0.000 | 45.832 ± 0.017 | 0.498 ± 0.005 |
| | | 0.000 | 45.767 ± 0.045 | 0.707 ± 0.001 |
| | Partial Set One | 0.108 ± 0.003 | 24.944 ± 0.214 | 0.368 ± 0.003 |
| | | 0.104 ± 0.004 | 29.952 ± 0.340 | 0.403 ± 0.003 |
| | | 0.104 ± 0.005 | 34.957 ± 0.226 | 0.435 ± 0.002 |
| | | 0.106 ± 0.005 | 40.233 ± 0.105 | 0.465 ± 0.001 |
| | | 0.105 ± 0.005 | 45.911 ± 0.061 | 0.500 ± 0.005 |
| | Partial Set Two | 0.304 ± 0.004 | 24.781 ± 0.432 | 0.508 ± 0.006 |
| | | 0.302 ± 0.005 | 30.079 ± 0.109 | 0.509 ± 0.009 |
| | | 0.302 ± 0.005 | 35.182 ± 0.038 | 0.512 ± 0.004 |
| | | 0.300 ± 0.003 | 40.106 ± 0.037 | 0.508 ± 0.004 |
| | | 0.299 ± 0.015 | 45.821 ± 0.134 | 0.510 ± 0.002 |
| | Partial Set Three | 0.505 ± 0.007 | 24.676 ± 0.064 | 0.708 ± 0.011 |
| | | 0.513 ± 0.003 | 29.635 ± 0.143 | 0.711 ± 0.006 |
| | | 0.508 ± 0.008 | 34.778 ± 0.179 | 0.719 ± 0.004 |

| | | | |
|---|---|---|---|
| | 0.505 ± 0.006 | 39.795 ± 0.076 | 0.721 ± 0.008 |
| | 0.505 ± 0.004 | 45.623 ± 0.040 | 0.708 ± 0.006 |
| | 0.700 ± 0.002 | 34.415 ± 0.048 | 0.906 ± 0.002 |
| Partial Set Four | 0.706 ± 0.002 | 39.527 ± 0.047 | 0.910 ± 0.005 |
| | 0.706 ± 0.002 | 45.351 ± 0.043 | 0.909 ± 0.002 |

**Table A3.** Steady State Experiments Performed Using Powder as Adhered Particles.

| Flow Rate (l/s) | Pressure (m) |
|---|---|
| 0.803 ± 0.008 | 45.083 ± 0.032 |
| 1.108 ± 0.002 | 44.270 ± 0.049 |
| 1.407 ± 0.006 | 43.558 ± 0.089 |

**Table A4.** Valve Opening Transient Experiments Performed Using Powder as Adhered Particles.

| 'Complete' or 'Partial' Tests and Set Number | Initial Flow Rate (l/s) | Initial Pressure (m) | Final Flow Rate (l/s) |
|---|---|---|---|
| Complete Set One | 0.000 | 25.092 ± 0.087 | 0.374 ± 0.001 |
| | 0.000 | 35.174 ± 0.072 | 0.441 ± 0.002 |
| | 0.000 | 46.040 ± 0.022 | 0.507 ± 0.001 |
| Partial Set One | 0.500 ± 0.002 | 34.960 ± 0.020 | 0.713 ± 0.001 |
| | 0.506 ± 0.001 | 45.671 ± 0.019 | 0.697 ± 0.006 |